UNIVERSITÉ DE SHERBROOKE
Faculté de génie
Département de génie civil

NUMERICAL SIMULATION OF FRESH SCC FLOW IN WALL AND BEAM ELEMENTS USING FLOW DYNAMICS MODELS

Simulation numérique de l'écoulement du BAP dans des éléments de mur et de poutre en utilisant des modèles dynamiques d'écoulement

Thèse de doctorat
Spécialité : génie civil

Masoud HOSSEINPOOR

Jury : Kamal H. KHAYAT (directeur)
Ammar YAHIA (co-directeur)
Jay LACEY (rapporteur)
Olafur H. WALLEVIK (évaluateur)
Pierre PROULX (évaluateur)

Sherbrooke (Québec) Canada Septembre 2016

À ma mère, à mon père

ABSTRACT

Recently, there is a great interest to study the flow characteristics of suspensions in different environmental and industrial applications, such as snow avalanches, debris flows, hydrotransport systems, and material casting processes. Regarding rheological aspects, the majority of these suspensions, such as fresh concrete, behave mostly as non-Newtonian fluids.

Concrete is the most widely used construction material in the world. Due to the limitations that exist in terms of workability and formwork filling abilities of normal concrete, a new class of concrete that is able to flow under its own weight, especially through narrow gaps in the congested areas of the formwork was developed. Accordingly, self-consolidating concrete (SCC) is a novel construction material that is gaining market acceptance in various applications. Higher fluidity characteristics of SCC enable it to be used in a number of special applications, such as densely reinforced sections. However, higher flowability of SCC makes it more sensitive to segregation of coarse particles during flow (i.e., dynamic segregation) and thereafter at rest (i.e., static segregation). Dynamic segregation can increase when SCC flows over a long distance or in the presence of obstacles. Therefore, there is always a need to establish a trade-off between the flowability, passing ability, and stability properties of SCC suspensions. This should be taken into consideration to design the casting process and the mixture proportioning of SCC. This is called "workability design" of SCC.

An efficient and non-expensive workability design approach consists of the prediction and optimization of the workability of the concrete mixtures for the selected construction processes, such as transportation, pumping, casting, compaction, and finishing. Indeed, the mixture proportioning of SCC should ensure the construction quality demands, such as demanded levels of flowability, passing ability, filling ability, and stability (dynamic and static). This is necessary to develop some theoretical tools to assess under what conditions the construction quality demands are satisfied. Accordingly, this thesis is dedicated to carry out analytical and numerical simulations to predict flow performance of SCC under different casting processes, such as pumping and tremie applications, or casting using buckets.

The L-Box and T-Box set-ups can evaluate flow performance properties of SCC (e.g., flowability, passing ability, filling ability, shear-induced and gravitational dynamic segregation) in casting process of wall and beam elements. The specific objective of the study consists of relating numerical results of flow simulation of SCC in L-Box and T-Box test set-ups, reported in this thesis, to the flow performance properties of SCC during casting. Accordingly, the SCC is modeled as a heterogeneous material. Furthermore, an analytical model is proposed to predict flow performance of SCC in L-Box set-up using the Dam Break Theory. On the other hand, results of the numerical simulation of SCC casting in a reinforced beam are verified by experimental free surface profiles. The results of numerical simulations of SCC casting (modeled as a single homogeneous fluid), are used to determine the critical zones corresponding to the higher risks of segregation and blocking. The effects of rheological parameters, density, particle contents, distribution of reinforcing bars, and particle-bar interactions on flow performance of SCC are evaluated using CFD simulations of SCC flow in L-Box and T-box test set-ups (modeled as a heterogeneous material). Two new approaches are proposed to classify

the SCC mixtures based on filling ability and performability properties, as a contribution of flowability, passing ability, and dynamic stability of SCC.

Keywords : Computational fluid dynamics, Dynamic stability, Flowability, Homogeneous and Heterogeneous analysis, Numerical simulation, Passing ability, Rheology, Segregation, Self-consolidating concrete.

RÉSUMÉ

Récemment, il y a un grand intérêt à étudier les caractéristiques d'écoulement des suspensions dans différentes applications environnementales et industrielles, telles que les avalanches des neiges, les coulées de débris, les systèmes de transport et les processus d'écoulement des matériaux. En ce qui concerne les aspects rhéologiques, la plupart des suspensions, comme le béton frais, se comportent comme un fluide non-Newtonien.

Le béton est le matériau de construction le plus largement utilisé dans le monde. En raison de limites qui caractérisent le béton normal en termes de maniabilité et de capacité de remplissage de coffrage, il était nécessaire de développer une nouvelle classe de béton qui peut couler sous son propre poids, en particulier à travers les zones congestionnées du coffrage. Par conséquent, le béton autoplaçant (BAP) est un nouveau matériau de construction qui est de plus en plus utilisé dans les différentes applications. Étant donné sa fluidité élevée de BAP peut être utilisé dans certaines applications particulières, notamment dans la section densément renforcée. Cependant, la fluidité élevée rend le béton plus sensible à la ségrégation des gros granulats pendant l'écoulement (la ségrégation dynamique) et ensuite au repos (ségrégation statique). La ségrégation dynamique peut augmenter lorsque le BAP est coulé sur une longue distance ou en présence d'obstacles. Par conséquent, il est toujours nécessaire d'établir un compromis entre la fluidité, la capacité de passage, et la stabilité du BAP. Ceci doit être pris en considération afin de concevoir le processus de coulée et dosage des mélanges du BAP. Ceci est appelé la conception d'ouvrabilité du BAP.

Une conception de maniabilité efficace et non coûteuse peut être achevée à travers la e prévision et l'optimisation de l'ouvrabilité des mélanges de béton pour les procédés de construction sélectionnés, notamment le transport, le pompage, la mise en place, le compactage, la finition, etc. En effet, les formulations de mélange doivent se confirmer à la qualité de la construction demandée, par exemple les niveaux exigés de fluidité, la capacité de passage, la capacité de remplissage, et la stabilité (statique et dynamique). Celui est nécessaire pour développer des outils théoriques afin d'évaluer dans quelles conditions les exigences de qualité de la construction sont satisfaites. Cette thèse est consacrée à la réaliser des simulations analytiques et numériques pour prédire la performance d'écoulement du BAP dans différents procédés de la mise en place du béton.

L'objectif spécifique de cette étude consiste à simuler l'écoulement du BAP dans essais empiriques, notamment la boite en L et la boite en T pour évaluer la performance du BAP pendent la mise en place (la fluidité, la capacité de passage, la capacité de remplissage, et la ségrégation dynamique induite par cisaillement ou par gravité). Par conséquent, le BAP est modélisé comme matériau hétérogène. En outre, un modèle analytique est proposé pour prédire la performance à l'écoulement du BAP dans la boite en L en utilisant la théorie de Dam Break. D'autre part, les résultats des simulations numériques de l'écoulement du BAP dans une poutre renforcée sont comparés aux résultats expérimentaux par des profils de surface libres. Les résultats des simulations numériques de BAP coulée (modélisée comme un fluide homogène unique), sont utilisés pour déterminer les zones critiques correspondant à des risques plus élevés de ségrégation et de blocage. Les effets des paramètres rhéologiques, la masse volumique, le contenu des particules, la distribution de barres d'armature, et les interactions particule-barres

sur les performances d'écoulement du BAP sont évaluées à l'aide de simulations MFN d'écoulement du BAP par les essais des L-Box et T-box (modélisée comme une matériau hétérogène). Deux nouvelles approches sont proposées pour classifier les mélanges du BAP sur la base de la capacité de remplissage, et les propriétés de *performabilité*, en fonction de la fluidité, la capacité de passage et de la stabilité dynamique du BAP.

Mots-clés : La mécanique des fluides numérique (MFN), La stabilité dynamique, La fluidité, L'analyse homogène et hétérogène, Le simulation numérique, La capacité de passage, Rhéologie, Ségrégation, Béton autoplaçant.

ACKNOWLEDGEMENTS

Firstly, I would like to express my sincere gratitude to my supervisor Professor Kamal H. Khayat for accepting me into his research group, for the continuous support of my Ph.D. study and related research, for his patience, motivation, and immense knowledge. His guidance helped me in all the time of research and writing of this thesis. I could not have imagined having a better advisor and mentor for my Ph.D. study.

My sincere thanks also goes to Professor Ammar Yahia who has been extremely helpful to me during the entire period of my studies in Université de Sherbrooke. As my advisor, he worked closely with me during the conduction of this research, the proposal writing and during the period of my dissertation. Without his helps and encouragement this dissertation would not have been written (or ever finished!).

I would like to thank all the professors of Civil Engineering Department and all the faculty staff I have interacted with. The kind cooperation of all the research assistants, technicians, and graduate students of the Cement and Concrete Research Group at the Université de Sherbrooke are also acknowledged. My special thanks goes to Mr. Behrouz Esmailkhanian for his friendly companionship during this memorable period of my life. I would also like to thanks Mr. Daddy Kabagire for his generous help to translate some parts of this thesis manuscript in French.

I am very much thankful to the members of the dissertation committee Professor Wallevik, Professor Proulx, and Professor Lacey for their valuable comments and advices.

I also wish to thank the financial support of the National Science and Engineering Research Council of Canada (NSERC) and the 16 industrial partners participating in the NSERC Chair on High Performance Flowable Concrete with Adapted Rheology, held by Professor Kamal H. Khayat of the Université de Sherbrooke.

Last but certainly not least, would like to acknowledge my family: My mother, Masoumeh, my father, Mahmoud, and my lovely sisters, Maryam and Marjan, who patiently encouraged and supported me spiritually over the period of my Ph.D. study and my life in general.

TABLE OF CONTENTS

LIST OF FIGURES

LIST OF TABLES

NOTATIONS

Symbol	Definition
$\dot{\gamma}_{max}$	Maximum shear rate
$\tilde{h}(\xi, t)$ and $\tilde{x}_f(t)$	Positive perturbation variables in Dam Break theory formulation
T_c^f	Characteristic flow time to indicate flowability
$T_c^{gravity}$	Characteristic flow time to indicate gravitational segregation
T_c^{shear}	Characteristic flow time to indicate shear-induced segregation
$\dot{\gamma}$	Shear rate
μ_∞	Viscosity at very high shear rate
τ_{app}^*	Apparent Bingham yield stress
μ_{app}	Apparent viscosity
μ_p	Bingham plastic viscosity
A	Surface area
A(t)	Cross-sectional area in the flow time t
B	Bingham number
CA_T and CA_B	Mass of coarse aggregate in the top and bottom sections of the column of segregation, respectively
D	Typical dimension of the flow
D1 and D2	Final diameters of the spread concrete in two perpendicular directions in slump flow test
d_2 and d_1	Final and initial reading of the probe head positions
$Displ_{max}(i)$	The maximum total displacement of the particle i
$Displ_X(i)$	Displacements of particle i in x direction
$Displ_Y(i)$	Displacements of particle i in y direction
$Displ_Z(i)$	Displacements of particle i in z direction
$E(\xi)$	Perturbation function
F	Force
g	Gravitational acceleration
G	Shear elasticity modulus
h	Fluid thickness
H	Characteristic fluid depth in the Dam Break Theory formulation
h(x,t)	Dimensionless profile thickness at dimensionless location x and flow time t
h_0	Maximum profile thickness at the casting point in LCPC Box
H_1 and H_2	Thickness of the final profile at the back wall and end of L-Box set-up, respectively
$H_{10\ cm}$	Depth of concrete at the entrance of the horizontal channel of L-Box
$h_\infty(x)$	Final profile function at static state
$h_{critical}$	The critical flow thickness of segregation
$h_{initial}$	Initial head in vertical compartment of L-Box
$H_{particles}$	Distance between two particles
H_{plates}	Distance between two parallel plates
i	Horizontal sampling part in L-Box
$I_{30\ cm}$	Initial average inertia stress in the first 30 cm in L-Box set-up
$I_{max}(i)$	Typical maximum values of inertial stress in the flow cycle (i) in T-Box test

j	Number of reinforcing bars in L-Box set-up
K	Consistency
k	Initial coarse particle content of modelled concrete suspension
K_i	The stiffness factor of spring i in Hooke's law
L	Fluid spread length in LCPC Box
L	Characteristic length in the Dam Break Theory formulation
l_0	Width of LCPC Box channel
L_{max}	The maximum flow distance in the horizontal leg of the L-Box
m	Mass
n	Power index
N	The number of measurements at different locations from the opening gate in L-Box test
P	Pressure
Pd	Penetration depth
Q(t)	Flow rate of the mixture in the flow time t
R and R'	Radius of the bottom surface before and after the slump test
R1 and R2	Heights of SCC in both columns of U-Box set-up
Re	Reynolds number
S	Static segregation, measured in column of segregation
Sf	Slump flow spread
Sl	Vertical slump value
t	Time
$T_{30\ cm}$	The flow time needed to the front of profile reaches 30 cm after the opening gate in L-Box test
$T_{40\ cm}$	Time values taken by the flow front to reach 40 cm after the sliding door in L-Box test
T_{50cm}	Flow time needed for the concrete to reach a spread value of 50 cm in slump flow test
U	Velocity scale toward the positive x' direction
V	Velocity
$V_{30\ cm}$	Average flow velocity of the mixtures in the first 30 cm in L-Box set-up
$V_f(t)$	Estimated velocity of the flow front at the end of each Δt = 1-s time step
V_i	Velocity made by the displacement of the spring i
$V_{initial}$	Initial velocity
V_{max}	Maximum flow velocity
$V_s(t)$	Estimated velocity of the flow surface at the vertical part, and at the end of each Δt = 1-s time step
W	SPH kernel function
w/p	Ratio of water to powder materials
x_a (t)	Active length
x_f (t)	Dimensionless front position of flow
x_f (t) and x_y (t)	Instantaneous positions of the front of the flow and yield point, respectively
$X_f(t)$	Horizontal positions of the flow front in the horizontal channel at the end of the 1-s time step after passing flow time t
$X_f(t-1)$	Horizontal positions of the flow front in the horizontal channel at beginning of the 1-s time step after passing flow time t
$x_{f\infty}$	The maximum flow distance in Dam Break Theory formulation

X_{front}	Front position of the flow
Z	Flow thickness
$Z_s(t)$	The vertical levels of the flow front in the horizontal channel at the end of the 1-s time step after passing flow time t
$Z_s(t-1)$	The vertical levels of the flow front in the horizontal channel at beginning of the 1-s time step after passing flow time t
γ	Shear strain
δ	Strain
Δx_i	Displacement of spring i
$\Delta\rho$	Density gradient between the particles and the suspending fluid
η	Newtonian viscosity
μ_0	Tangential viscosity of the suspending fluid in a given shear rate
ρ	Density
τ	Shear stress
τ_0	Bingham yield stress
τ_{app}	Apparent yield stress
τ_H	The maximum shear stress acting on the bottom surface of slump test
ϕ	Volume fraction of particles
Ω	Volume of fluid
$\omega(t)$	Angular velocity of T-Box apparatus in flow time t

LIST OF ABBREVIATIONS

Abbreviation	Definition
B.E.	Bar effect
B.I.	Blocking index
$B.I._{max}$	Maximum blocking index
CFD	Computational fluid dynamics
COV	Coefficient of variation
DEM	Discrete elements method
E.H.D.S.I.	Extremity horizontal dynamic segregation index
E.R.	Estimation ratio
FD	Finite difference
FEM	Finite elements method
FV	Finite volume
GMO	General moving object technique
H.D.S.I.	Horizontal dynamic segregation index
HRWR	High-range water-reducer
I.H.D.S.I. (i)	Individual horizontal dynamic segregation index, obtained in the horizontal sampling part i
MSA	Maximum size of aggregates
P.C.E.	Particle content effect
RMSE	Root-mean-square error
SCC	Self-consolidating concrete
SPH	Smoothed particles hydrodynamics
V.D.S.I.	Vertical dynamic segregation index
VEA	Viscosity enhancing admixture
VMA	Viscosity modifying agent
VOF	Volume of fluid method

CHAPTER 1 INTRODUCTION

1.1 Heterogeneous behavior of multiphase suspensions

Heterogeneous properties of multiphase suspensions have significant effects on their flow behavior in various domains, such as debris flows, snow avalanches, hydraulics and hydrology, wastewater engineering, polymers, casting, and other industrial applications [1-8]. On the other hand, separation of solid particles from the fluid part of the suspension has negative effects on quality and performance of the suspensions in the production and transportation procedures, and the destination where they are supposed to be transported or placed. Therefore, flow performance of suspension materials has a wide concern to study in environmental and industrial applications, as well as heterogeneous migration of solid phase through the fluid medium [9-13]. In macro scale, studying the evolution of flow profiles in a given application, from the flow origin till the desired destination such as a formwork to be cast, or environmental domains, can give an insight to modify the flow conditions, designing of the domain, selecting ingredients of the fluid, and optimizing the rheology and workability of the fluid materials. This can lead to save time and the energy needed to perform that application process. The problems in macro scale flowability of the materials can be effected by the potential problems in the micro scales interactions of different phases of the suspensions. For example, segregation of solid particles from the suspension, which is transported by a pipe, can change the rheology of the material, or lead to block the flow section in some local zones. This may affect the flowability of the suspension in macro scale, increase the flow time, and reduce the quality of the material in the destination.

Segregation of solid particles can be due to the gravitational and shear induced particle migrations. Gravitational segregation occurs when there is a gradient in gravitational forces between the coarse particles and the suspending fluid due to a difference of density of the materials [14]. On the other hand, shear-induced segregation is defined as the migration of particles from regions of higher shear rates to the regions of lower shear. This results in a decrease in the viscosity of suspensions after a given shearing period even though the viscosity

of the homogeneous suspending fluid remains constant under a given shear history applied on the suspension [9, 15-17]. Most of the common industrial and environmental suspensions behave as a non-Newtonian fluid. Recently, there is a great interest to study shear-induced migration and gravitational settlement of solid particles suspended in Non-Newtonian suspending fluids [18-21].

1.2 Workability of fresh conventional concrete

Fresh concrete is one of the most complex suspensions of solid particles (i.e., fine and coarse aggregates) in a non-Newtonian suspending fluid (i.e., cement paste or mortar matrix). Concrete is the most widely used construction material in the world [22]. Concrete is produced in over than 2 billion tons per year. By 2050, concrete use is expected to reach four times the volume of concrete produced in 1990 level. However, due to low flowability of conventional concrete, its use is limited in the case of special applications, such as high rise buildings, casting of thin and complicated shape sections in architectural applications, placing concrete in narrow gaps in highly dense reinforced zones in the formwork, repairing applications in the zones with difficult access, and under water concreting. Because of low fluidity properties of fresh conventional concrete, high amount of energy is needed to consolidate the concrete in the formwork. Application of vibrations can result in high noise pollution, construction period, and cost. Even in presence of vibrators, there is still high risks of segregation and blocking of the concrete during placement process. Therefore, due to the low stability and consequently low durability, long placement time, high number of labor needed to place the concrete, and expensive casting process of conventional concrete, a novel type of concrete with higher fluidity was necessary to be developed [23].

1.3 Self-consolidating concrete (SCC)

Self-consolidating concrete (SCC) is a novel type of concrete which can flow and consolidate into every corner of a formwork, purely by means of its own weight and without the need for vibration. SCC was developed in 1980s in Japan and then widely used in several applications, such as precast industry, high rise building constructions, casting tunnel linings, and under water

concreting. SCC has pushed back traditional limits concerning the casting of densely reinforced and complex structural elements in concrete construction. SCC can flow through narrow gaps in the formwork, between reinforcing bars obstacles or the formwork walls, which are not reachable for conventional concrete, while it maintains its homogeneity [23-26].

SCC behaves as a visco-elastoplastic material with yield stress. The existence of yield stress introduces a certain discontinuity between the flowing and stationary SCC. The evolution of the flow and the shape of free-surface profile are therefore dependent on the rheological behavior of SCC mixtures. In order to achieve higher flowability and passing ability, the rheological parameters of SCC, such as yield stress and plastic viscosity, should be significantly less than conventional concrete [27].

Higher fluidity of SCC (i.e., flowability) compared to the conventional concrete makes it more sensitive to segregation during flow (i.e., dynamic segregation) and thereafter at rest (i.e., static segregation) [28-30]. Dynamic segregation can be even more critical in presence of reinforcing bars obstacles, when concrete mixtures flows in narrow spaces between the bars (i.e., passing ability), especially for highly congested sections [30-32]. Therefore, there is always a need to establish a trade-off between flowability, passing ability, and stability properties of SCC given the mixture proportioning, formwork design, and configuration of casting procedure [24]. This is called workability design [33-35].

1.4 Workability design

An efficient and inexpensive workability design consists in predicting and optimizing the workability of the concrete mixtures for the selected construction processes, such as transportation, pumping, casting, compaction, finishing, etc [35]. Indeed, the mixture proportions should ensure the construction quality demands, such as demanded levels of flowability, passing ability, filling ability, and stability (dynamic and static). Therefore, the casting quality demands, construction conditions and methods, geometry of the formwork, and reinforcing bars configurations are the inputs of the workability design process. The workability of the mixtures should be examined experimentally or theoretically to confirm that the

demanded flow performance conditions are satisfied. Otherwise, the mixture proportions or the construction conditions should be optimized. The workability experimental tests are often carried out (i.e., empirical tools) to simulate experimentally the workability of the investigated SCC mixtures in a smaller scale to establish the workability design. For example, slump flow and V-Funnel tests can be used to examine flowability of SCC. L-Box and J-Ring tests can evaluate passing ability of SCC mixtures between reinforcing bars obstacles [23-25]. On the other hand, T-Box test set-up can be used to measure dynamic stability of fresh SCC [36-38]. However, experimental tests can be time consuming and inaccurate due to possible human errors. Therefore, theoretical tools can be used as an alternative to simulate flow performance of SCC in various empirical tests and casting processes and facilitate workability design process.

1.5 Theoretical flow analysis of SCC

Theoretical tools are useful to assess under what conditions the construction quality demands are satisfied. Accordingly, the analytical [39-41] and numerical models [29, 42-48] have been carried out to predict flow performance of SCC in workability tests and casting processes. Regarding the complexity of the SCC flow in the formworks, analytical models were mostly developed to predict the final profile of SCC in workability tests, such as slump flow and L-Box tests using dimensional analysis and 2^{nd} Newton's law. On the other hand, the numerical modeling of the flow of concrete presents a great challenge because of the necessity to take into account the complex interactions between the various solid particles in the system, solid obstacles and formwork walls, while simultaneously solving the Navier-Stokes equations for the incompressible liquid phase in which they are immersed. Therefore, it is necessary to consider some simplifying assumptions to convert the physical points, materials, and geometry information to the computational nodes, numbers, matrixes, and boundary conditions. According to the literature, the material and geometry can be discretized by the mesh cells or mesh-less particle based methods. On the other hand, the concrete mixture can be assumed as a single homogeneous fluid, discrete elements, or distinct particles. Recently, there is a great interest to carry out numerical simulations to predict flow characteristics of SCC as a homogeneous or heterogeneous material. An extensive comprehensive review regarding numerical simulation of fresh concrete flow can be found in [48].

1.6 Originality of this study

There is always an understanding conceptual gap between the theoretical predictions, which were obtained using computational simplifications, and physical/empirical results of workability of SCC mixtures. This is due to the lack in understanding the clear physical meaning of the numerical results. On the other hand, due to the limits in calculation capacity of the current computers, numerical simulation of whole casting process of SCC as a heterogeneous material in full size elements is impossible. Moreover, for the huge flow problems, plenty of simplifications and assumption can lead to accumulated computational errors. This can affect the accuracy of the predicting models to properly describe the physical phenomena.

Therefore, this research is dedicated to relate computational fluid dynamics (CFD) simulations of two main workability tests (i.e., L-Box and T-Box set-ups) of SCC, simulated as a heterogeneous material, to the construction quality demands, such as flowability, passing ability, filling ability, shear-induced and gravitational dynamic stability. On the other hand, the results of numerical simulations of SCC casting, where SCC is modeled as a single homogeneous fluid, are used to determine the critical zones corresponding to the higher risks of segregation and blocking. Moreover, the effects of rheological parameters, density, and particle contents of SCC, as well as configuration of reinforcing bars, and particle-bar interactions on flow performance of SCC are evaluated using CFD simulations.

The core of the study is statistic evaluation of the results obtained by numerical simulations of L-box and T-Box tests. The main novelty of the paper is the methodology of estimating the degree of segregation and blocking depending on the parameters under investigation, including particle content and number of reinforcing bars. On the other hand, a new analytical approach is proposed to predict flow surface profile of SCC as a homogeneous material, in a modified L-Box set-up, using Dam Break Theory, for Bingham and Herschel-Bulkley rheological models.

1.7 Outline of the thesis

According to the state of the art of the studies carried out on numerical simulations on the flow of SCC (presented in **Chapter 2**), the originality and objectives of this study are presented in **Chapter 3**. The Dam Break Theory and a CFD software (FLOW3D® using Volume of Fluid, VOF method) are employed in order to develop analytical and numerical simulations, respectively. The specifications of the applied theoretical models and methods are presented in **Chapter 4.** The main objectives and the remaining chapters of this thesis are as follows:

- **Chapter 5**: Analytical and numerical modeling of flow performance of self-consolidating concrete using the Dam Break Theory and CFD. In this chapter, a new analytical model is proposed to predict the evolution of free surface profile of various SCC mixtures in a modified L-Box set-up using the Dam Break Theory. The results of the analytical models are compared for both Bingham and Herschel-Bulkley rheological models. A CFD software (FLOW3D®) is also employed to simulate numerically the flow performance of SCC in the modified L-Box apparatus. The results of this chapter were submitted as a journal paper to the journal of "Computers and Concrete".

- **Chapter 6**: Homogeneous analysis of self-Consolidating Concrete (SCC) casting in reinforced beam using computational fluid dynamics (CFD). In this chapter, the flow is simulated to predict flow behavior of various SCC mixtures in a reinforced beam. The effect of rheological parameters on flow performance of the investigated mixtures are also evaluated using numerical results. The results of this chapter were submitted as a journal paper to the journal of "Construction and Building Materials".

- **Chapter 7**: Numerical simulation of self-consolidating concrete flow as a heterogeneous material in L-Box set-up - Effect of rheological parameters on flow performance. In this chapter, the effect of rheological parameters and density of suspending fluid of the concrete mixtures on flowability, passing ability, and dynamic stability of SCC in L-Box test are evaluated. SCC mixtures are simulated as heterogeneous materials. The results of

this chapter were submitted as a journal paper to the journal of "Cement and Concrete Composites".

- **Chapter 8**: Numerical Simulation of self-Consolidating concrete flow as a heterogeneous material in L-Box set-up - Coupled effect of reinforcing bars and aggregate content on flow characteristics: The interaction of different contents of coarse aggregate in presence of different configuration of reinforcing bar obstacles and their coupled effect on flow characteristics of SCC as a heterogeneous suspension are evaluated by CFD simulations in this chapter. The results of this chapter were submitted as a journal paper to the journal of "Materials and Structures".

- **Chapter 9**: Numerical simulation of dynamic segregation of self-consolidating concrete in T-Box set-up. The Effect of rheological parameters on flowability and dynamic stability of SCC in absence of reinforcing bars is simulated and analyzed using T-Box test set-up. The results of this chapter were submitted as a journal paper to the journal of "Computers and Concrete".

- **Chapter 10**: Comparison between flow performance of SCC as a heterogeneous material in L-Box and T-Box set-ups using numerical simulations. The effect of rheological parameters on flow behavior of SCC in L-Box and T-Box set-ups, i.e., in presence and in absence of reinforcing bars are simulated and the obtained results are compared.

According to each phase of this study, the main conclusions and recommendations for future researches are presented in **Chapters 11** and **12**, respectively.

CHAPTER 2 STATE OF THE ART

2.1 Rheology of non-Newtonian materials

Rheology is defined as the science of deformation and flow of matter. It describes the relationship between forces, deformations, and time. It is applied to more or less fluid materials, or materials that exhibit a time-dependent response to stress. An important issue of rheology is the definition and classification of materials [49-51]. The rheological behavior of fluids can be expressed by the shear stress-shear strain rate relationship. As can be observed in Fig. 2.1, a thin layer of a fluid contained between two parallel planes with a distance of h, having surface area of A, and subjected to a shear force F is considered. Applying this shear force can result in a relative displacement of the planes with a velocity of V_x, and consequently, displacements of δ and γ of the fluid, in the direction of the relative velocity V_x and angular rotation, respectively. Accordingly, corresponded shear stress, shear strain, and shear rate magnitudes can be calculated using Eq. 2.1, 2.2, and 2.3, respectively.

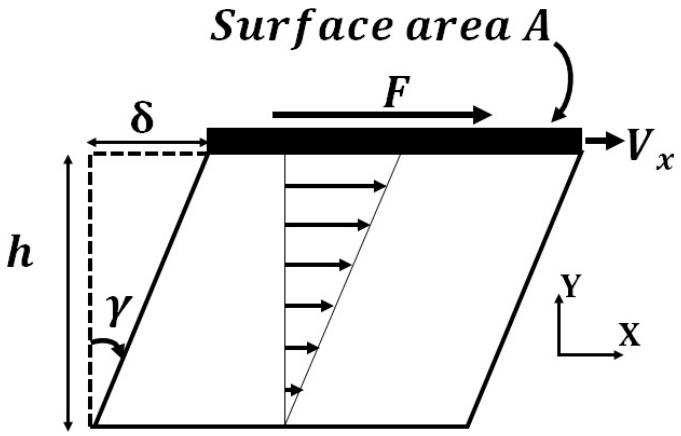

Figure 2. 1 Schematic of shearing flow

$$\tau = F/A \tag{2.1}$$

$$\gamma = \delta/h \tag{2.2}$$

$$\dot{\gamma} = V_x/h \tag{2.3}$$

where τ is the resulted shear stress due to the application of force F on the surface area of A, γ is the shear strain, h is the fluid layer thickness, and $\dot{\gamma}$ is the corresponding shear rate.

Correlating the values of shear stress to shear rate magnitudes (i.e., flow curve) can lead to classifying the materials based on their rheological behavior. Accordingly, the materials under steady shear flow conditions (equilibrium state), may exhibit certain behaviors over a limited range of shear rates. Additionally, some materials may exhibit more than one distinct behavior over different shear rate regions of the flow curve. Therefore, several types of behavior can be classified according to their characteristic shape (Fig. 2.2). The following classification system covers the most frequently encountered flow types, divided in terms of Newtonian, general non-Newtonian, and visco-elastoplastic non-Newtonian fluids. It must be noted that derivation of the fitted curves at each shear rate is called plastic viscosity (μ_p) as follows:

$$\mu_p = \frac{d\tau}{d\dot{\gamma}} \tag{2.4}$$

On the other hand, the apparent viscosity is defined by the ratio of the shear stress value to its corresponding shear rate, as follows:

$$\mu_{app} = \frac{\tau}{\dot{\gamma}} \tag{2.5}$$

According to the Fig. 2.2, four different rheological behaviors of the fluid can be observed:

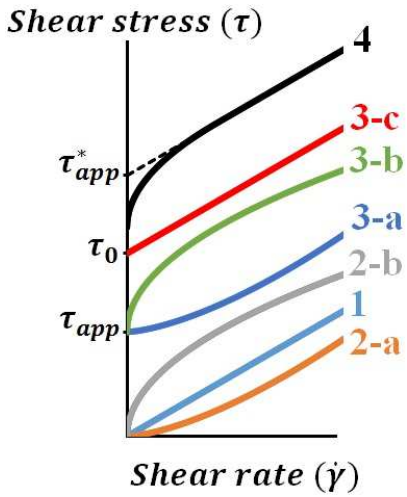

Figure 2. 2 Different rheological behaviors of the fluid

1. Newtonian fluid: In the simplest type of flow, termed Newtonian, the material's viscosity is constant and independent of the shear rate [49-51]. When shear stress (τ) is plotted against shear rate ($\dot{\gamma}$) at a given temperature, the plot shows a straight line with a constant slope (curve no. 1 in Fig. 2.2). This slope is called the Newtonian viscosity (η) of the fluid. On the other hand, no yield shear stress is necessary for the fluid to start the flow in plastic state (i.e., $when\ \dot{\gamma} = 0 \Rightarrow \tau = 0$). The simplest constitutive equation is Newton's law of viscosity:

$$\tau = \eta . \dot{\gamma} \tag{2.6}$$

In the case of this model, a single point measurement, with a corresponding pair of values of τ and $\dot{\gamma}$, would serve to rheologically define a Newtonian fluid. All gases and common liquids such as ethanol, water and most oils are Newtonian. Also, liquids and solutions of substances with low molecular weight materials in liquids, e.g. solutions of sugar or salt, are usually Newtonian.

2. General non-Newtonian: Any fluids that do not obey the Newtonian relationship between shear stress and shear rate are non-Newtonian. Rheology is generally devoted to the study the behavior of such fluids. Suspensions of fine particles are usually non-Newtonian [49-51]. In the case of general non-Newtonian fluids, the slope of the shear stress versus shear rate plot is not constant. In this case, the material shows a non-linear rheological behavior. However, the

material does not need any critical shear stress to initiate the flow. Two different types of non-Newtonian behavior include:

a) Shear-thickening: In this case, the plastic viscosity of the fluid increases continuously with shear rate.

b) Shear-thinning: This corresponds to the behavior where plastic viscosity decreases continuously with shear rate.

3. Visco-elastoplastic non-Newtonian fluids: In order to initiate the flow of a visco-elastoplastic material, the yield stress value is necessary to be exceeded. Therefore, before reaching this value of shear stress, the material behaves like an elastic solid. Once the applied shear stress exceeds the yield stress ($\tau > \tau_{app}$), the visco-elastoplastic fluid flows just like a normal fluid in the plastic state, as follows:

a, b) Shear-thickening and shear-thinning with yield-response: The plastic viscosity increases and decreases, respectively, with shear rate once the apparent yield stress (τ_{app}) has been exceeded.

c) Bingham plastic (ideal): Above the Bingham yield stress (τ_0) the plastic viscosity is constant and is called the Bingham plastic viscosity.

4. Bingham plastic (non-ideal): Above the apparent yield stress, the plastic viscosity decreases continuously and approaches a constant value with increasing shear rate. Extrapolation of the flow curve from the linear region (plastic region) to the stress axis gives the apparent Bingham yield stress (τ^*_{app}) and the plastic viscosity (μ_p).

2.2 Rheological models of cement based materials

By using a mathematical relationship, a fluid can be rheologically characterized by viscosity and yield stress. The models that are presented in this section are used to characterize the non-

Newtonian behavior of fluids in equilibrium, under steady shear flow conditions at constant pressure and temperature. Table 2.1 gives the most commonly used equations to describe the flow of cement based materials as a non-Newtonian fluid. The most frequently used fundamental models for cement based suspensions are Bingham and Herschel-Bulkley models.

2.2.1 Bingham model

Some materials exhibit an infinite viscosity until a sufficiently high stress is applied to initiate flow. Above this stress (i.e. yield stress) the material then shows simple Newtonian flow. The simplest model covering these types of viscoplastic fluids with a yield response is the ideal Bingham model, and is expressed by the following two-parameters model:

$$\tau = \tau_0 + \mu_p . \dot{\gamma} \tag{2.7}$$

Where, τ_0 and μ_p are the Bingham yield stress and plastic viscosity parameters, respectively. The Bingham model can describe the viscosity characteristics of a fluid with yield stress whose viscosity is independent of shear rate. Therefore, the Bingham plastic model does not have the ability to handle the shear-thinning characteristics of general non-Newtonian fluids. Many concentrated particle suspensions and colloidal systems, such as mortar and concrete, exhibit Bingham behavior at limited ranges of shear rate.

Table 2. 1 Equations relating shear stress and shear rate, proposed for cement based materials suspensions

Model	Analytical equation
Newtonian [52]	$\tau = \eta.\dot{\gamma}$ (2.6)
Bingham [53]	$\tau = \tau_0 + \mu_p.\dot{\gamma}$ (2.7)
Modified Bingham [54]	$\tau = \tau_0 + \mu.\dot{\gamma} + c.\dot{\gamma}^2$ (2.8)
Power law equations [55]	$\tau = A.\dot{\gamma}^n$ (2.9) $n = 1 \Rightarrow Newtonian\ fluid$ $n < 1 \Rightarrow Shear\ thinning$ $n > 1 \Rightarrow Shear\ thickening$
Herschel Bulkley [56]	$\tau = \tau_0 + K.\dot{\gamma}^n$ (2.10)
Vom Berg, and Ostwald-De Waele [57]	$\tau = \tau_0 + B\sinh^{-1}(\dot{\gamma}/C)$ (2.11)
Robertson-Stiff [58]	$\tau = a(\dot{\gamma} + C)^b$ (2.12)
Atzeni et al. [59]	$\dot{\gamma} = \alpha.\tau^2 + \beta.\tau + \delta$ (2.13)
Casson [60]	$\tau = \tau_0 + \mu_\infty.\dot{\gamma} + 2\sqrt{\tau_0.\mu_\infty}\sqrt{\dot{\gamma}}$ (2.14)
De Kee [54]	$\tau = \tau_0 + \mu_p.\dot{\gamma}.e^{-\alpha\dot{\gamma}}$ (2.15)
Yahia, and Khayat [61]	$\tau = \tau_0 + 2\sqrt{\tau_0.\mu_p}.\sqrt{\dot{\gamma}.e^{-\alpha_t\dot{\gamma}}}$ (2.16)
Variable definitions: $\tau : Shear\ stress$ $\tau_0 : Yield\ stress$ $\eta, \mu_p : Plastic\ viscosity$ $A, a, B, b, C, \alpha, \beta, \delta : Constant$	 $\dot{\gamma} : Shear\ rate$ $K : Consistency$ $\alpha_t : time - dependent\ parameter$ $\mu_\infty : viscosity\ at\ very\ high\ shear\ rate$

2.2.2 Herschel-Bulkley model

Herschel-Bulkley model is a three-parameters model used to describe viscoplastic materials exhibiting a yield response with a shear-thinning/shear-thickening behavior above the yield stress. It is a combination of Power-law and Bingham, and is expressed as:

$$\tau = \tau_0 + K.\dot{\gamma}^n \quad (2.10)$$

Where, K is the consistency and n index indicates the degree of non-Newtonian behavior of the material (the greater the departure from unity, the more pronounced the non-Newtonian properties of the material). When n = 1, Herschel-Bulkley is reduced to the equation for the Bingham. The Herschel-Bulkley model provides a more realistic prediction of flow over a wider range of conditions than the Bingham model. It is often applied to industrial fluids (e.g. biological fluids, food and cosmetics), where it is used for specifying conditions in the design of process plants.

2.3 Rheology of different cementitious materials

The satisfactory performance of cement-based materials depends on their facility to transport and cast in fresh state. The most important processes using cementitious materials are transportation, pumping, pouring, injection, spraying (shotcreteing), self-leveling, hand troweling, casting, consolidating, and finishing. All of these practical applications depend on the rheology of the mixtures, according to various aspects:

- Flowability on the surfaces, considering frictional resistance.
- Adhesion.
- Resistance against water bleeding, as a result of settlement of the coarser particles.
- Resistance against shear-induced heterogeneity of coarser particles during flow.
- Resistance against blocking of the coarse particles in narrow gaps of the formwork.
- Lower water contents, in order to obtain higher mechanical strength, as well as less porosity and, consequently, higher durability properties.
- Low lateral pressure exerted on the formwork.

Accordingly, this section discusses on the rheology of cement-based materials, including cement paste, mortar, and concrete in fresh state.

2.3.1 Rheology of cement paste

Cement paste is a highly concentrated suspension of cement and other powder particles in water. Particles of dry cement cover a wide range of size (1 to 100 μm) and different chemical and mineral components which react with water. These reactions may be very fast (such as the reactions of tricalcium aluminate and tricalcium alumino-ferrite), or take longer times. For example, tricalcium silicate and dicalcium silicates react over a few days and several months, respectively. The fresh concrete can be cast before the setting process, which consists of the growth and interlocking of needle-like crystals of calcium sulfoaluminate and calcium silicate hydrate. According to the presence of the hydration skin around the cement particles, the fresh properties of the cement paste are relatively insensitive to variations in the chemical composition of the cement clinker, while the water content has more significant effects. Accordingly, increasing water to cementitious materials ratio can lead to decrease the plastic viscosity and yield stress of the cement paste [62]. The other parameters affecting on the rheology of cement paste mixtures can be summarized as:

- Age and temperature, considering the breakdown of the internal structure [63-69].
- Cement composition and fineness [57, 63, 70].
- Supplementary materials, such as fly ash, silica fume, blast furnace slag, and metakaolin [71-73].
- Chemical admixtures, such as superplasticizers [74-75].

According to the literature, the Bingham rheological parameters of the cement paste mixtures can range from 10 to 100 Pa and from 0.01 to 1 Pa.s for yield stress and plastic viscosity values, respectively [76].

2.3.2 Rheology of cement mortar

Cement mortar is a suspension of fine aggregates (i.e. sand), with particle diameters less than 5 mm, in cement paste. According to the larger sizes of the particles in mortar matrix compared to the cement paste, the interlocking forces between the particles can increase the values of the

rheological parameters of the mixture. The effect of the presence of particles on rheology of the mortar matrixes is more dominant than the structural breakdown. The typical ranges of the Bingham yield stress and plastic viscosity of mortar is ranging from 80 to 400 Pa, and from 1 to 3 Pa.s, respectively [76].

2.3.3 Rheology of concrete

Concrete mixture is a suspension of coarse aggregates (larger than 5 mm) in the mortar matrix. Accordingly, it might be expected that the rheology of fresh concrete is more complex than cement paste and mortar, due to wider range of particle sizes, shapes, and compositions. Most of the studies on rheology of conventional concrete have been done on the effects of different constituents of the mixtures, such as cement, fly ash, silica fume, other filling powders, water to cementitious materials ratio, and other admixtures. For example, typical effect of different components of the mixture on the rheology of the fresh concrete is presented in Fig. 2.3.

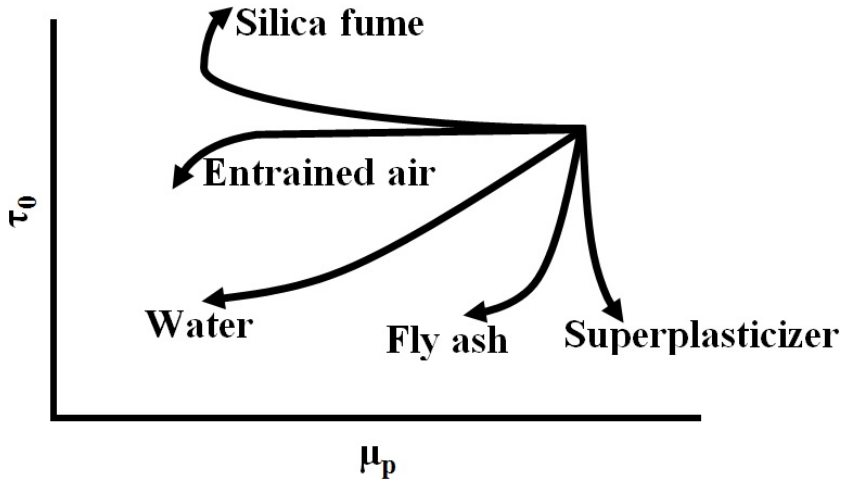

Figure 2. 3 The direction of the change in rheology of a typical concrete caused by an increase in the amount of the parameter noted is shown by the arrows [76]

As can be observed in Fig. 2.3, increasing water content can decrease significantly both yield stress and plastic viscosity values of the mixture. On the other hand, plastic viscosity can decrease significantly by increasing in silica fume content and entrained air, while keeping constant the yield stress values. Furthermore, increasing fly ash contents and superplasticizer

dosage decrease the yield stress values, but a small change of the plastic viscosity of the mixtures [76].

According to the literature, the rheological parameters of conventional concrete can vary from 500 to 2000 Pa and 50 to 100 Pa.s for yield stress and plastic viscosity values, respectively [76]. Rheological measurement can be used as a controlling tool for the quality of fresh concrete, which can also indicate the changes in the mix compositions. These changes can affect the properties of the hardened concrete and its structural performance and durability.

2.4 Self-consolidating concrete (SCC)

2.4.1 Rheology of SCC

Thanks to advances in chemical admixtures and superplasticizers, a novel type of high performance concrete, called self-consolidating concrete (SCC), was developed which can spread under its own weight. As a result of higher fluidity of SCC compared to the conventional concrete, this type of concrete can achieve good consolidation in the absence of vibration without exhibiting defects due to segregation and bleeding. The developments in the underwater concrete technology resulted in invention of self-consolidating concrete. SCC mixtures are proportioned to insure high fluidity as well as high resistance to bleeding and segregation [30].

The use of SCC has gained great interesting applications in Japan since the 1980s to cast densely reinforced structural members as well as the placement of concrete in restricted areas where consolidation may not be practical. SCC can improve the homogeneity of highly flowable concrete that is necessary to insure good bond development with reinforcing bars, adequate structural performance, and proper durability [30]. Therefore, there is a wide interest to use SCC for repairing applications in locations where are difficult to access or there are narrow gaps which cannot be filled with conventional concrete mixtures. On the other hand, SCC can be used in order to cast complex formworks or non-reinforced areas where proper consolidation by vibrators is difficult to be achieved. Higher fluidity of SCC can lead to reduce the construction

noises, casting time, removing formwork duration, labor requirement, finishing process, and consequently, the construction costs, as well as increasing the durability of the structure.

In order to reach these high levels of fluidity, proper rheological parameters are required compared to conventional concrete. SCC mixtures are usually proportioned with higher paste volume than conventional concrete. This can lead to lower yield stress and plastic viscosity values. According to the literature, the typical ranges of rheological parameters of SCC vary between 50 to 200 Pa and 20 to 100 Pa.s for yield stress and plastic viscosity values, respectively [76]. Also, the generally recommended values for rheological parameters of SCC in order to ensure good performance and workability is presented in Fig. 2.4 [76, 77]. As can be observed, for lower levels of viscosity, higher values of yield stress are recommended. On the other hand, for highly viscosity SCC mixtures, lower values of yield stress are suggested. This can be due to confirm different aspects of workability quality demands of SCC, which can be affected oppositely by different rheological parameters of the mixtures. In the next section the most important aspects of workability of SCC will be discussed.

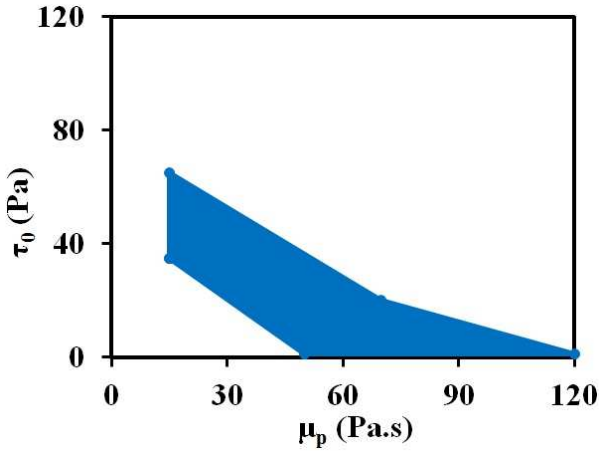

Figure 2. 4 Recommended rheograph: proposed limits of rheological values of SCC [77]

2.4.2 Workability of self-consolidating concrete

In order to achieve good performance properties from casting of SCC, the mixtures should show enough fluidity under its own weight to pass between the narrow gaps in the formwork, and through the congested areas with reinforcing bars, and at the same time keep their homogeneity

during flow and thereafter at rest. Workability describes the ease with which concrete can be mixed, placed, consolidated, and finished. It also describes the filling properties of fresh concrete in relation to the behavior of the concrete in the production process [23-27]. In this section, the main aspects of workability of SCC, consisting of flowability, passing ability, and stability, as well as the empirical measuring tools of each of these properties are described.

A) Flowability of SCC

The term of flowability was defined as the ability of fresh concrete to flow in confined or unconfined form of any shape, reinforced or not, under gravity and/or external forces, assuming the shape of its container [78]. In the case of SCC, the mixtures should flow under their own weight, without the need to any vibrations, showing higher fluidity compared to the conventional concrete. The term of fluidity was also defined as the ease by which fresh concrete flows under gravity [78].

Higher fluidity of SCC can decrease the casting duration. Indeed, it takes shorter time to cast a given volume of SCC compared to the conventional concrete. Since SCC flows under own weight, no vibrator is required for placement. Therefore, it needs lower placement energy compared to normal concrete mixtures, as well as lower labor forces to cast the concrete. On the other hand, higher flowability properties can lead to have various methods of pouring the concrete in horizontal and vertical applications. For example, there is a great interest to use SCC for high rise buildings, which needs that concrete gets pumped up to more than 500 m heights, which is much easier in the case of a highly flowable concrete than stiffer conventional ones. On the other hand, SCC can be used for tremie applications or casting of deep foundations which are not accessible with conventional concrete to be vibrated. Therefore, this can be concluded that flowability of SCC can reduce the construction costs corresponding to casting process compared to the conventional concrete.

Fluidity of the cement paste and mortar matrix play dominant role in flowability of the concrete mixture. Indeed, the flow energy required to transport the aggregates is provide by the deformable part of the suspension. Therefore, in order to increase the deformability of SCC,

higher paste volume is recommended, compared to the conventional concrete. On the other hand, in order to achieve higher flowability for SCC mixtures, the rheology of the fluid part of the suspensions should be modified. Accordingly, the mortar matrix and cement paste parts of the concrete mixtures should gain higher fluidity. Furthermore, increasing water to powder materials ratio, as well as using high-range water-reducer admixtures can lead to decrease the yield stress and plastic viscosity of the cement paste and mortar, and consequently, increase the flowability of the SCC mixture. For example, it is showed that increasing superplasticizer dosage from 0.2 % to 0.9%, by weight of cement, can decrease the thixotropic behaviour of the mixtures by 50% [79]. Thixotropic behaviour is the time dependent changes in rheological parameters of the cementitious materials as a result of the formation and breakdown of the internal structures of the cement paste under different shear rates.

On the other hand, presence of coarse particles can increase the shear rate of the cement paste on a local scale between the aggregates. This can have positive effects on breaking down the structure of cement paste, hence reducing the thixotropy effect. As can be observed in Fig. 2.5, flow of a monodisperse suspension, having spherical suspending particles, is considered under a shear flow between two parallel plates, separated by a distance of H_{plates}. The upper plate moves at a relative velocity V to the lower plate. As can be observed, due to the lower distance between the particles, $H_{particles}$, compared to distance of the plates, H_{plates} (i.e. $H_{particles} < H_{plates}$), the local shear rate in the matrix phase is higher than the general shear rate obtained by the velocity V between two plates (i.e., $\dot{\gamma}_{between\ particles} > \dot{\gamma}_{between\ plates}$).

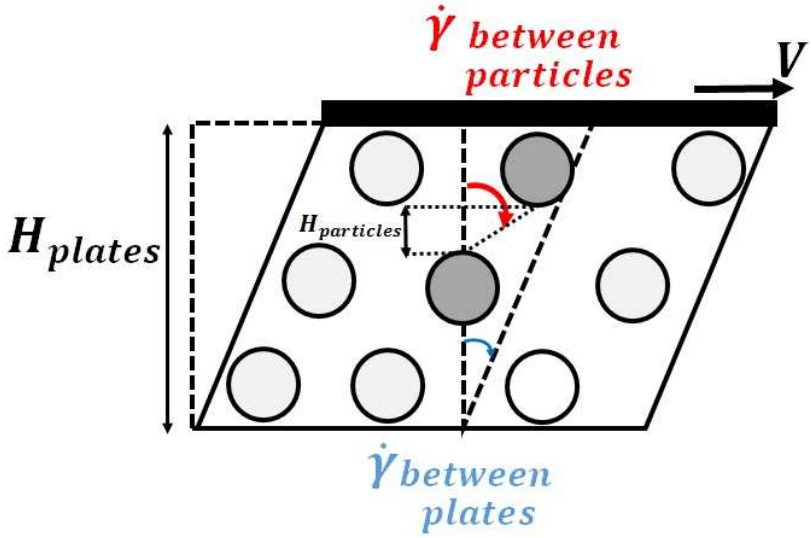

Figure 2. 5 Increasing effect of presence of aggregates on local shear rate values in the suspending matrix (cement paste or mortar) [29]

However, reducing the interaction between suspended aggregates can increase the flowability of the suspension. Accordingly, lower coarse aggregate volume is recommended for SCC, which means higher volume of mortar and paste. On the other hand, according to the literature [30], using continuously graded solid particles, including fine and coarse aggregates, and powder materials is recommended to decrease the particle-particle interactions. Using rounded aggregate instead of crushed ones can also improve flowability of SCC.

In order to evaluate the flowability properties of SCC, some empirical tests were developed. These tests measure the maximum flow distance traveled by a given volume of SCC, and also determine the concrete flow rate to assess the fluidity of the suspension. These tests consist of Slump-flow and V-funnel tests.

Slump flow test:

One of the most common tests for assessing flow performance of SCC is the slump flow test set-up [80]. This test uses the same Abrams slump cone [81]. Once approximately 6 L of concrete is poured in the cone, the cone is removed vertically with a constantly slow raising rate (around 5 cm/s) and allowed concrete to spread on the base. Whenever the flow of the mixture is stopped, the final diameters of the spread concrete in two perpendicular directions (D1 and

D2) are measured. The final slump flow spread diameter is reported as the average of those captured diameters as (D1+D2)/2. This value was shown to be depended on the yield stress value of the mixture. On the other hand, the flow time needed for the concrete to reach a spread value of 50 cm is reported as T_{50} to evaluate the viscosity dependent flowability properties of the mixtures. The schematics of the slump flow set-up is presented in Fig. 2.6.

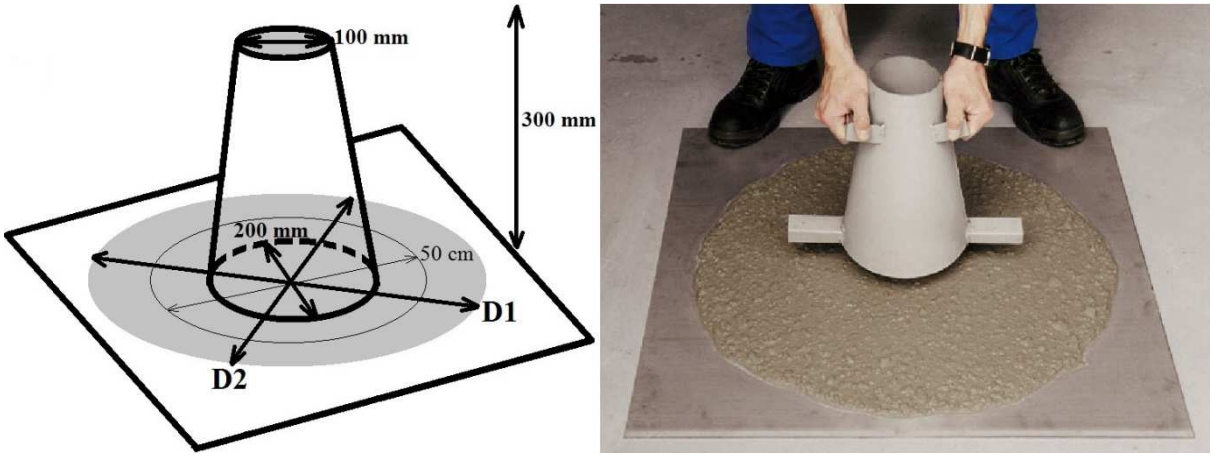

Figure 2. 6 Schematics of slump flow test for evaluating flowability of SCC [80]

The higher slump flow diameter values indicates higher flowability level. It means that the concrete mixture can travel higher distances under its own weight and fill the formwork. A minimum value of 650 mm is recommended for slump flow diameter to ensure the minimum flowability criteria of SCC. On the other hand, less T_{50} values indicates that SCC mixtures flow faster due to lower values of plastic viscosity. According to the results of the slump flow tests, Table 2.2 is proposed as a guidance to choose the initial targets of casting requirements [78]. Based on the application, the concrete producer rates the characteristics of an element as low, medium, or high. The dark areas are potential problem areas and should be avoided. For example, if the application presents a high level of reinforcement, SCC with a slump flow lower than 550 mm is not recommended. Initial targets should be chosen from the white areas.

Table 2. 2 Slump flow and T_{50} parameter determination, dark cells indicates risk of problem zones [78]

			Slump flow diameter (mm)			**$T_{50\,cm}$ (s)**		
			< 550	550-650	> 650	< 3	3-5	> 3
Member characteristics	Reinforcement level	Low						
		Medium	■			■		
		High	■			■		
	Element shape intricacy	Low						
		Medium	■					■
		High	■	■				■
	Element depth	Low						
		Medium						
		High				■		
	Surface finish importance	Low						
		Medium	■					■
		High	■	■				■
	Element length	Low						
		Medium	■					
		High	■	■		■		
	Wall thickness	Low	■	■				■
		Medium	■					
		High						
	Placement energy	Low	■	■				
		Medium	■					
		High				■		

V-funnel test set-up:

Flowability of SCC in vertical direction can be evaluated by the V-funnel test set-up [23-25, 78]. In order to perform this test, about 12 L of SCC are cast in a V-shaped funnel mold, then the gate is opened and the flow time taken for the concrete to flow through the apparatus is recorded. This test can measure the ease of SCC to flow in vertical direction, passing through the narrow gaps (i.e. outlet of the apparatus), considering the effect of different angles, section areas, and wall frictions. Shorter flow times indicate greater flowability, while higher flow times

are associated with low deformability due to high paste/mortar plastic viscosity, and high inter-particles interactions. A schematics of the V-funnel apparatus is presented in Fig. 2.7.

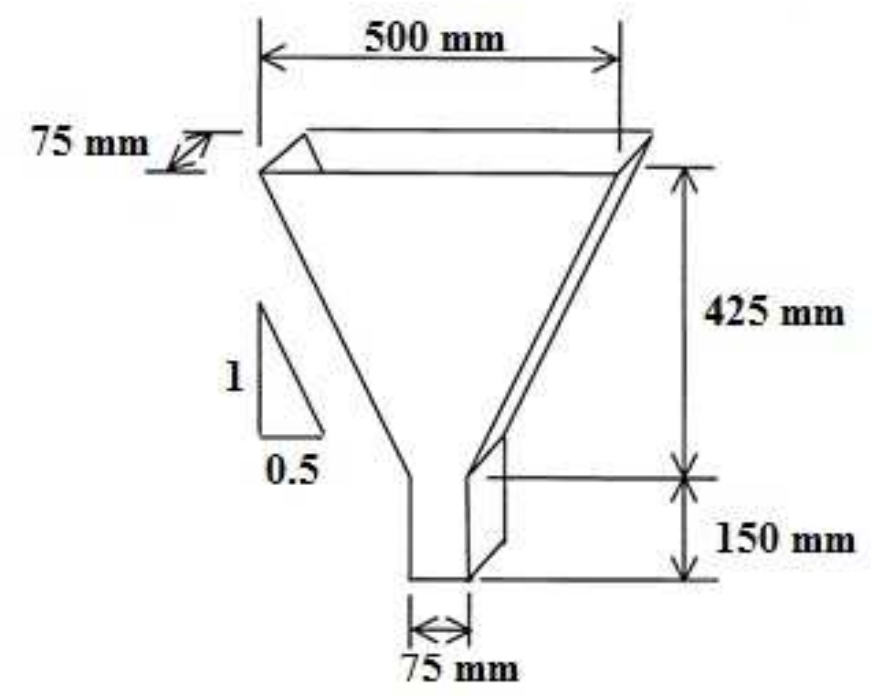

Figure 2. 7 Schematics of V-funnel test for evaluating flowability of SCC [23-25]

According to the proposed guidelines [78], as presented in Table 2.3, the V-funnel flow times between 6 and 10 s is recommended for SCC to ensure proper flowability properties. The dark areas are potential problem areas and should be avoided. For example, if the application presents a low wall thickness, SCC with a V-funnel time more than 10 s is not recommended. Initial targets should be chosen from the white areas.

Table 2. 3 V-funnel time parameter determination, dark cells indicates risk of problem zones [78]

			V-funnel time (s)		
			< 6	6-10	> 10
Member characteristics	Reinforcement level	Low			
		Medium	■		
		High	■		
	Element shape intricacy	Low			
		Medium			■
		High			■
	Element depth	Low			
		Medium			
		High	■		
	Surface finish importance	Low			
		Medium			■
		High			■
	Element length	Low			
		Medium			
		High	■		
	Wall thickness	Low			■
		Medium			
		High			
	Coarse aggregate content	Low			
		Medium			
		High			■
	Placement energy	Low			■
		Medium			
		High	■		

Passing ability of SCC

One of the main advantage of SCC is its ability to flow in narrow gaps of the formwork, including the restricted spaces between the reinforcing bars and walls of the formwork, that are

not accessible to ensure good consolidation using conventional concrete. This property is called passing ability. According to the published guidelines for SCC performance [26, 78], the terms of passing ability refers to the ability of SCC to flow through openings, such as the spaces between steel reinforcing bars, without segregation or aggregate blocking. As illustrated in Fig. 2.8, blocking is defined as accumulation of coarse aggregates behind the reinforcement bars and can result in honey combing and a poor form filling ability [29]. This can lead to increase the permeability of the concrete which results in decreasing its durability. On the other hand, it can reduce mechanical performance of the structures and bond strength between the reinforcing bars and concrete.

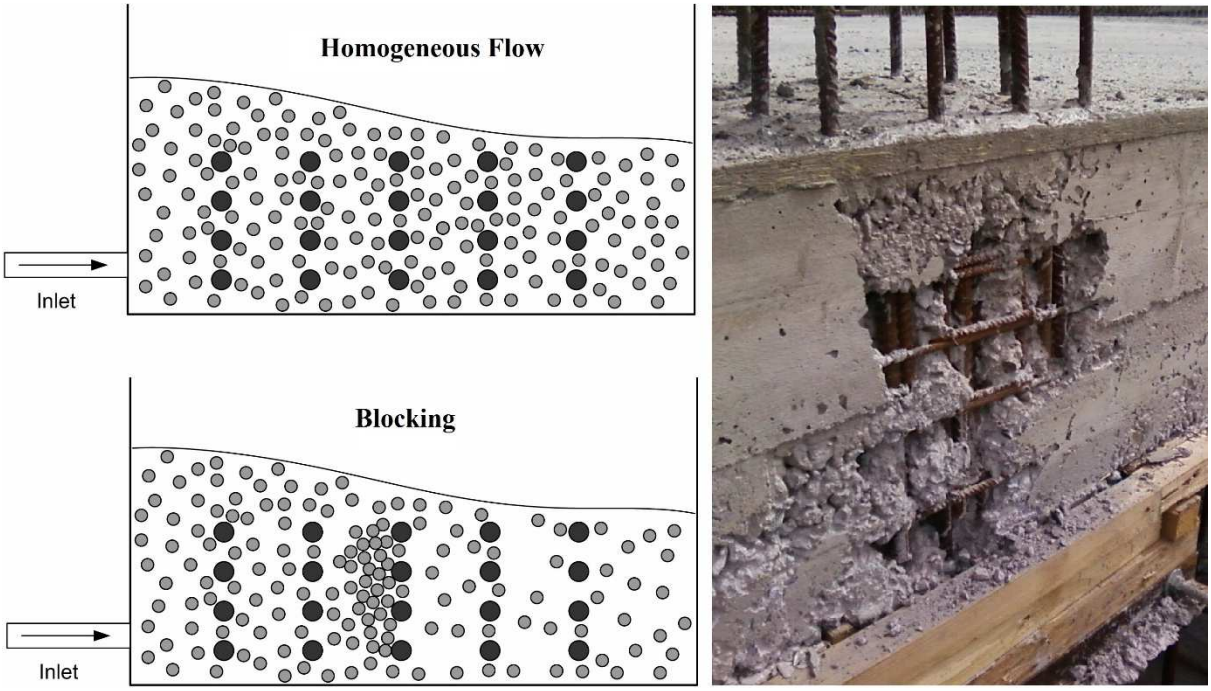

Figure 2. 8 Accumulation of coarse particles behind the obstacles (i.e. blocking) resulting in poor form filling and honey combing

In order to reduce the risk of blocking, it is recommended to lower the water content and/or to use viscosity modifying agents (VMA). These can lead to enhance cohesiveness of the cement paste and mortar matrix, and therefore decrease segregation of the coarse aggregate. On the other hand, clear spacing between reinforcement bars and coarse aggregate volume content as well as the maximum size of aggregates (MSA) should be compatible. Accordingly, lower coarse aggregate volume content and smaller MSA values are recommended [24]. Several

empirical tests were developed to evaluate the passing ability of SCC, such as J-Ring [82], U-Box, and L-box [23-25, 78] test set-ups. The properties of the final flow profiles are measured and compared at locations before and after the obstacles to quantify the blocking resistance of the concrete.

J-ring test: The J-ring test is used to determine the passing ability of SCC in presence of obstacles. The test consists of the same cone used in the slump flow test. J-ring test evaluates the flow performance of the concrete passing an apparatus consisting of rigid ring supported on sixteen 16-mm diameter rods equally spaced on a 300 mm diameter circle and 100 mm above a flat surface, as shown in Fig 2.9 [82]. In order to do the test, the Abrams cone is removed slowly and once the flow of concrete stopped, the diameter of the final spread is calculated as the average of the diameters measured in two perpendicular directions. The difference of the final spread of the J-ring test with the one obtained by slump flow test can determine the passing ability of the SCC mixture in presence of 16 reinforcing bars of the J-ring. According to [82], the blocking resistance of SCC is evaluated in three different criteria based on the results obtained by the difference between J-ring and slump flow tests (Table 2.4).

Table 2. 4 Blocking assessment, based on the difference between slump flow and J-ring flow [82]

Difference between slump flow and J-ring flow	Blocking assessment
< 25 mm	No visible blocking
25 to 50 mm	Minimal to noticeable blocking
> 50 mm	Noticeable to extreme blocking

Indeed, higher difference between the final spread diameter of SCC in slump flow and J-ring tests means that less amount of the mixtures was allowed to pass through the reinforcing bars and SCC exhibit less passing ability properties.

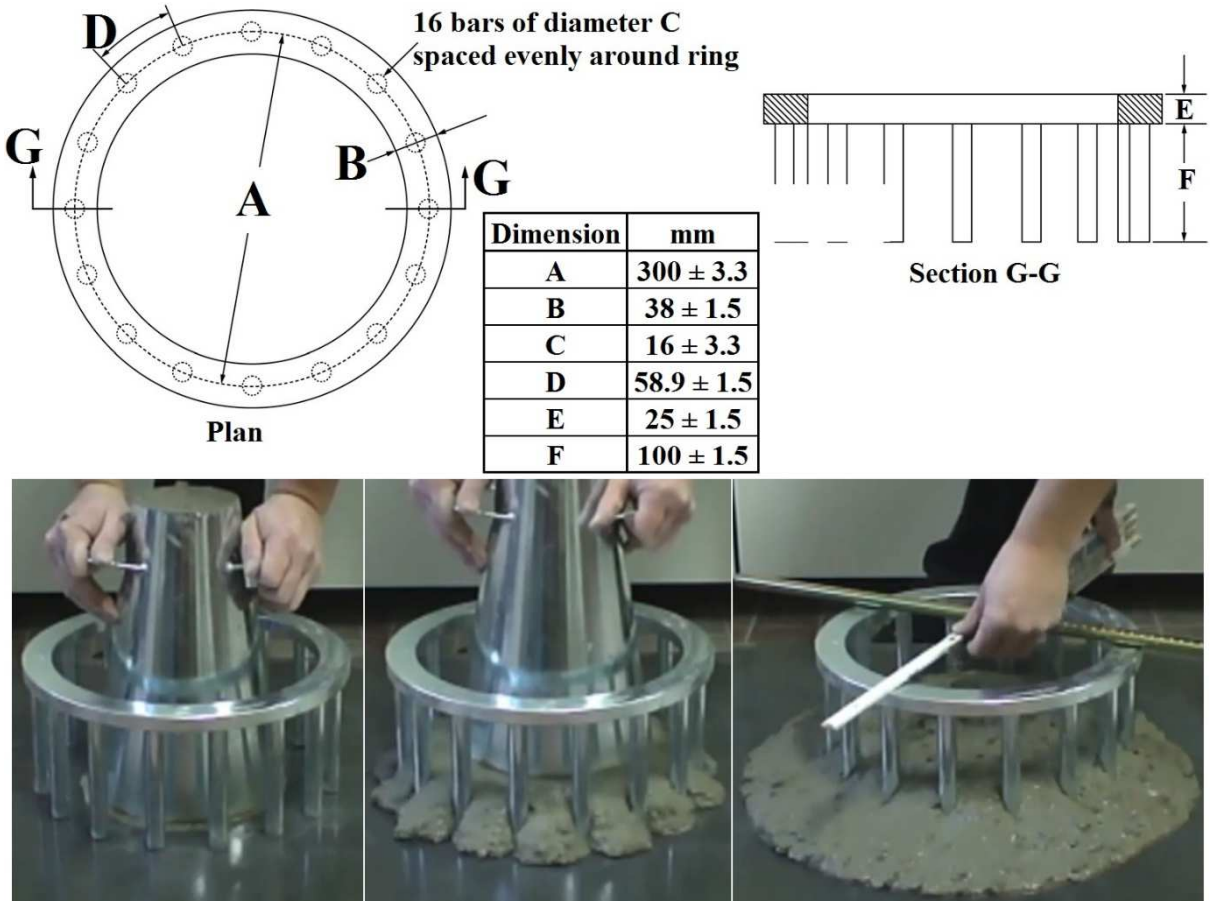

Dimension	mm
A	300 ± 3.3
B	38 ± 1.5
C	16 ± 3.3
D	58.9 ± 1.5
E	25 ± 1.5
F	100 ± 1.5

Figure 2. 9 Schematics of J-ring test for evaluating passing ability of SCC [82]

U-box test: The U-box test set-up consists of a U-shaped box, divided in the middle with a wall and sliding door. Reinforcing bars with nominal diameters of 13 mm are installed at the gate with center-to-center spacing of 50 mm. This creates a clear spacing of 35 mm between the bars. The left-hand section is filled with about 20 L of SCC then the gate is lifted and SCC flows upwards into the other section. Once the concrete flow is stopped, the height of the SCC in both sections are measured (R1 and R2). The difference between these two measurements can determine the passing ability of the SCC mixture. A schematics of the U-box test is presented in Fig. 2.10 [25].

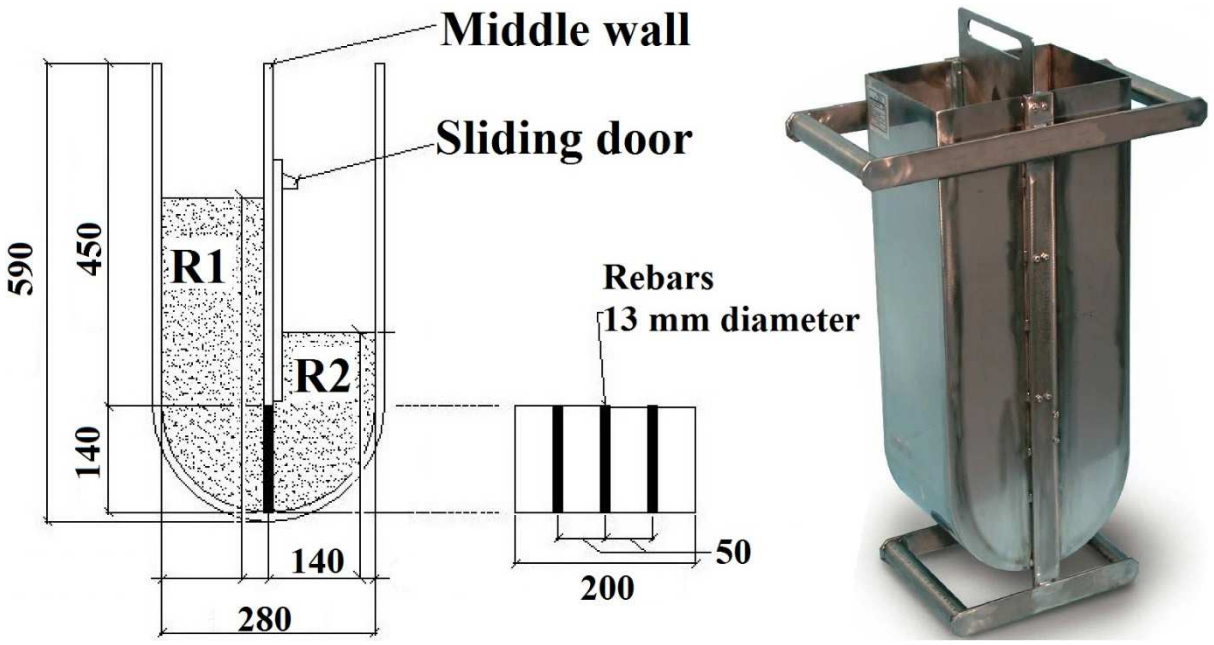

Figure 2. 10 Schematics of U-box test for evaluating passing ability of SCC. (all dimensions are in mm) [25]

L-box test: One of the main empirical tests for evaluating the passing ability of SCC is the L-Box test. The L-Box consists of vertical and horizontal compartments that are separated by a sliding door. Right after the gate there are three reinforcing bars with diameter of 12 mm and clear spacing of 41 mm. A concrete volume of 12 L is cast in the vertical compartment, and once the sliding door is opened, the concrete is gravitationally driven into the horizontal channel. After stoppage of the flow, the thickness of the final profile at the end of horizontal channel (H_2) and the back wall of the vertical compartment behind the bars (H_1) are recorded. Risk of blocking can be evaluated by the ratio of these flow depths (H_2/H_1). The ideal value of L-box blocking ratio can be 100 % and smaller values correspond to lower passing ability and higher blocking risks. Indeed, when the coarse particles accumulate behind the bars, lower amounts of concrete are able to spread in the horizontal channel, and they remain more in the vertical compartment of the L-box. Therefore, lower L-box ratio are obtained for lower passing ability mixtures. According to the proposed guidelines, a minimum L-box ratio of 75 % is recommended to ensure a good passing ability. The schematics of the L-box set-up is presented in Fig. 2.11 [23-25, 78].

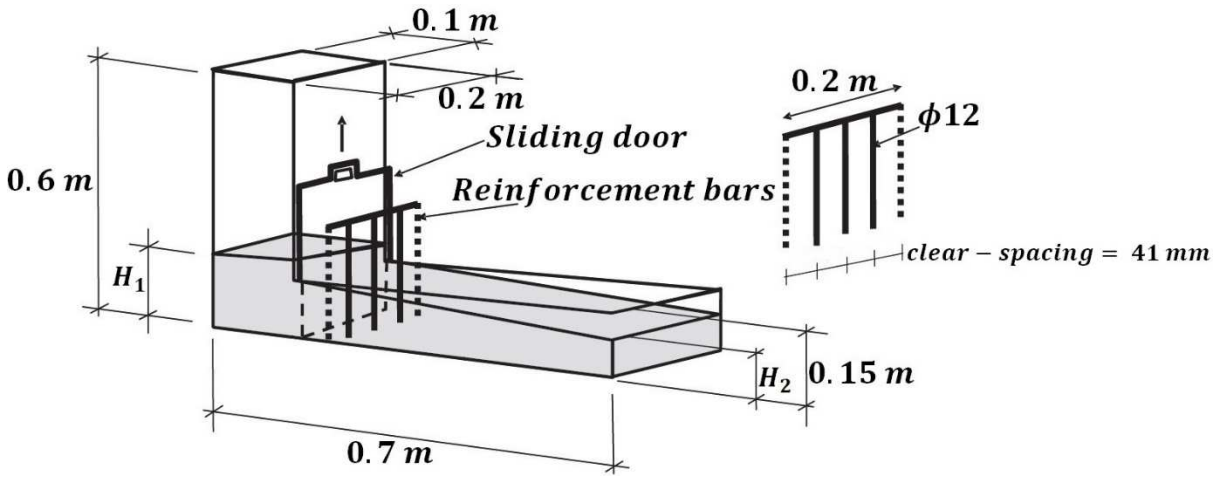

Figure 2. 11 Schematics of L-box test set-up and reinforcement bars details [23-25. 78]

Stability of SCC

Dispersion of suspended particles has a significant effect on flow behavior of materials in various domains, including debris flow [1], snow avalanche [2], conventional hydrotransport processes [3-5], and industrial applications [6-8]. On the other hand, separation of coarse particles from the suspending fluid has negative influence on the performance of suspensions and must be prevented in production processes. Therefore, there is a wide concern to study particle migration in granular flow motion and suspension dynamics transport [9-13]. Segregation of solid particles can be due to the gravitational and shear induced particle migration. Gravitational segregation occurs when there is a gradient in gravitational forces between the coarse particles and the suspending fluid due to a difference of density of the materials [14]. On the other hand, shear-induced segregation is defined as the migration of particles from regions of higher shear rates to the regions of lower shear. This results in a decrease in the suspensions viscosity after a given shearing period even though the viscosity of the homogeneous suspending fluid remains constant under a given shear history applied on the suspension [9, 15-17].

SCC has pushed back traditional limits concerning the casting of densely reinforced and complex structural elements in concrete construction [23]. SCC is a suspension of fine and coarse aggregates in a visco-elastoplastic cement paste. SCC is characterized by a relatively

high fluidity compared to conventional concrete, which makes it more sensitive to segregation during flow (i.e. dynamic segregation) and thereafter at rest (i.e. static segregation) [28-30, 84]. In this section, these two different types of segregation, as well as their measuring testing techniques are presented.

1. Static segregation

Static segregation occurs when the concrete is at rest, and aggregate particles can settle down given their higher density compared to the paste/mortar suspending fluid [83]. According to the low plastic viscosity of the mortar matrix in self-consolidating concrete, the drag forces exerted on the coarse particles is low and the mortar cannot keep the particles in their initial place and homogeneity of the suspensions is disturbed. Therefore, the concrete after the rest exhibit higher coarse particle content in the bottom layers, while higher mortar contents, including higher water bleeding, cement paste, and fine aggregate volume, are observed on the top layers (Fig. 2.12). This can lead to higher shrinkage in the surface of the structural members, which can affect negatively on durability of the concrete facing chloride and sulfate ions attacks.

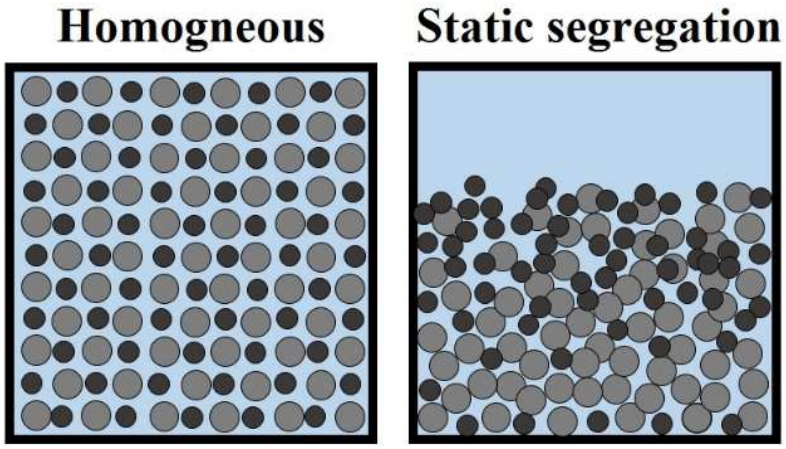

Figure 2. 12 Static segregation: migration of aggregates towards bottom layers

Accordingly, in order to improve the static stability of SCC, the fluid phase of the suspension (i.e. cement paste and mortar matrix) should be modified. For example, in order to minimize the bleeding of concrete, lower free water content and lower water to powder materials ratio are recommended. Furthermore, using fine filling powders, due to higher surface areas, and viscosity modifying agents can increase plastic viscosity of the suspending fluid part of the

mixture. This can increase the drag force exerted on the coarser particles and keep homogeneity of the suspension (static stability). On the other hand, limiting coarse particle content, and reducing the maximum size of aggregates can decrease static segregation of the SCC mixtures. Several experimental tests were developed to evaluate static stability of SCC. This includes the determination of coarse particle contents and different vertical layers [84, 85], electrical conductivity [86], penetration depth [87, 88], and image analysis techniques [89].

Column of segregation [84]:

The main empirical test to evaluate static stability of SCC is column test [84]. This test method covers the determination of static segregation of SCC by measuring the coarse aggregate content in the top and bottom portions of a cylindrical specimen (or column) with 200 mm diameter and 660 mm height. A sample of fresh SCC is placed in the column mold without any vibration. The mold is separated into three sections representing different levels of the cylindrical specimen (or column). The height of top, middle, and bottom layers are 165, 330, and 165 mm, respectively. The concrete is then allowed to stand undisturbed in the mold for 15 ± 1 min. Portions of concrete from the top and bottom section are washed on a 4.75 mm (No. 4) sieve, leaving the coarse aggregate on the sieve. The masses of coarse aggregate in the top and the bottom sections are determined and the percent static segregation is calculated as follows:

$$S = 2\left[\frac{(CA_B - CA_T)}{(CA_B + CA_T)}\right] \times 100\%, if\ CA_B\ >\ CA_T, and\ S = 0, if\ CA_B\ \leq\ CA_T \qquad (2.17)$$

Where S is the static segregation, in percent, and CA_T and CA_B are mass of coarse aggregate in the top and bottom sections of the column, respectively.

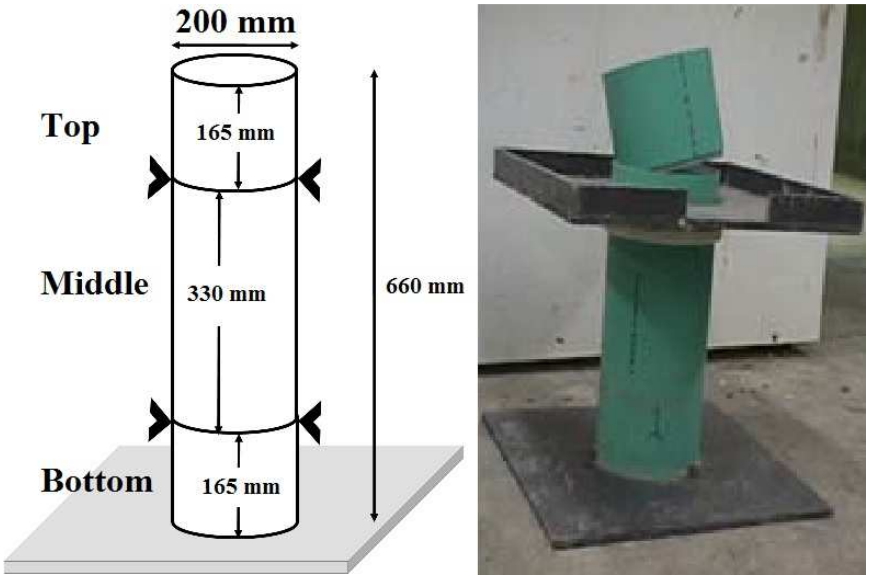

Figure 2. 13 Schematics of column of segregation test [84]

Penetration test [87]: This test evaluate the potential of static segregation by measuring the penetration of a 45 ± 1 gr probe in SCC, as presented in Fig. 2.14 [87]. In order to do the test, freshly mixed SCC cast in the inverted Abrams cone, then the probe will be placed slowly on the top surface of the concrete. Initial and final positions of the probe are recorded right when the concrete is cast and after 80 ± 1 s, respectively. The final penetration depth can be calculated as follows:

$$Pd = d_2 - d_1 \tag{2.18}$$

Where d_2 and d_1 are the final and initial reading of the probe head positions, and their difference corresponds to the final penetration depth of the probe. Higher penetration depth can indicate accumulation of higher amount of cement paste/mortar on the top surface of the sample, as well as higher migration of coarser particle towards bottom layers. This results in higher risk of static segregation.

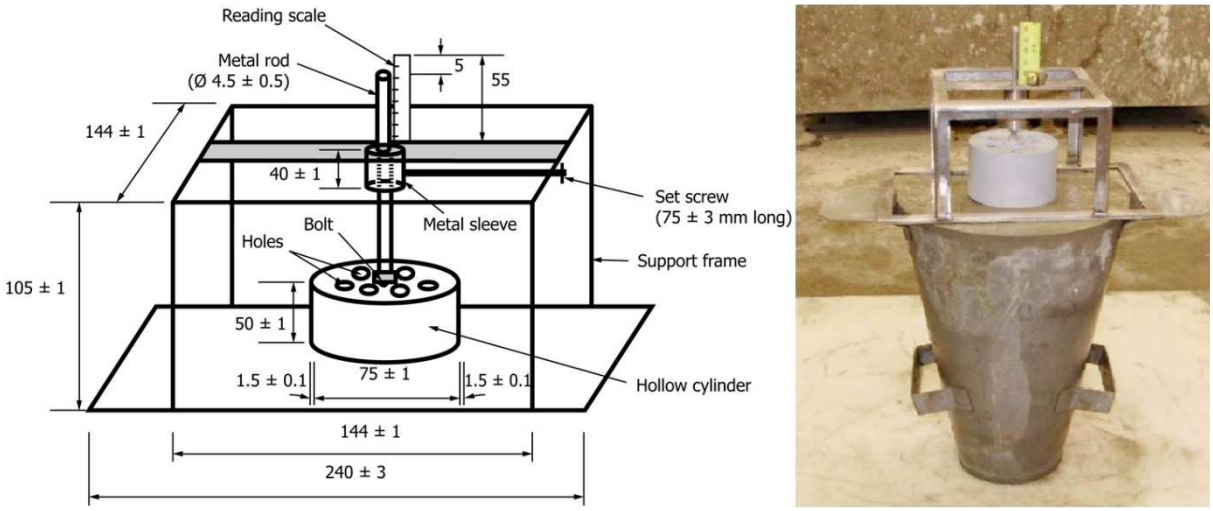

Figure 2. 14 Schematics of penetration test (all dimensions are in mm) [87]

Three criteria of static segregation resistance were developed based on the results of the penetration tests and presented in Table 2.5.

Table 2. 5 Degree of static segregation resistance [87]

Penetration depth (Pd)	Degree of static segregation resistance
Pd ≤ 10 mm	Resistant
10 mm < Pd < 25 mm	Moderately resistant
Pd ≥ 25 mm	Not resistant

2. Dynamic segregation

Dynamic segregation corresponds to the separation of coarse aggregates from mortar matrix during flow [29]. It can result in less aggregate content, as well as higher accumulation of cement paste in the top layers of the cast concrete, which is called vertical dynamic segregation (Fig. 2.15). This type of segregation is more important in the case of vertical applications, such as tremie concreting and casting of tall wall and column elements (Fig 2.15b). Indeed, the direction of gravitational forces are in contrary to the direction of the concrete flow in the formwork in vertical elements. Therefore, this can lead to decrease the displacement of the coarse particles compared to their adjacent cement paste/mortar matrix. This can be accelerated by gravitational

induced and static segregation, according to higher density of the coarse aggregate compared to the cement paste/mortar matrix [9, 14-16, 46-47].

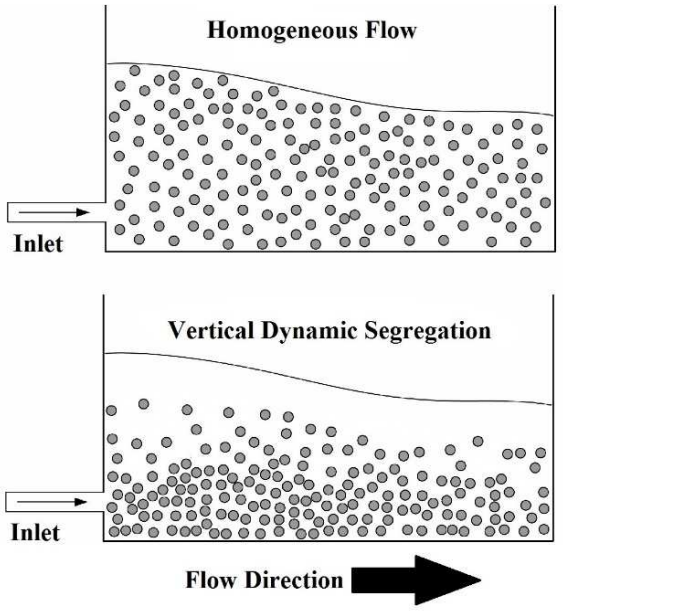

a) Horizontal flow

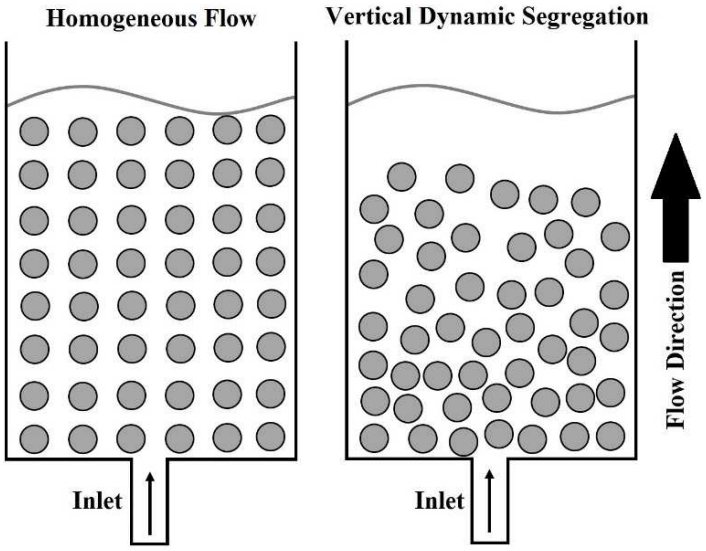

b) Vertical flow

Figure 2. 15 Homogeneous flow versus vertical dynamic segregation in a) horizontal flow, and b) vertical flow

On the other hand, increasing horizontal flow distance can result in less coarse aggregate content at flow front compared to the casting point and reference mixture, regardless of the effect of the obstacles and blocking resistance (Fig. 2.16). This is called horizontal dynamic segregation which is more concerned in horizontal applications, such as casting of long slabs, beams, and wall elements [26].

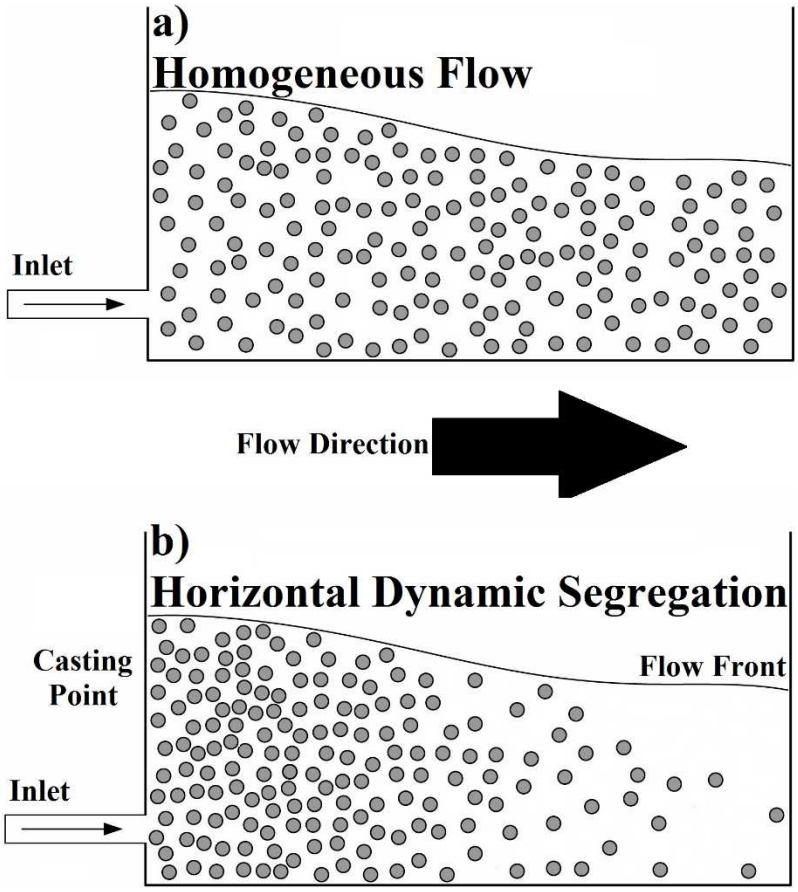

Figure 2. 16 Homogeneous flow versus horizontal dynamic segregation

Therefore, comparison between the properties of SCC at each horizontal or vertical levels and the casting point, i.e. the point where the concrete is dropped into the formwork, can lead to evaluate the dynamic stability of the mixtures on that level. Accordingly, new experimental tests are developed, including determination of coarse particle contents in different horizontal and vertical sections of a channel [45, 90], and penetration depth which measures the depth of the thickness of the cement mortar/paste accumulated above the settled aggregates [87, 88]. For example, SCC is allowed to flow in an inclined channel with 1.8 m length, 0.15 m × 0.15 m

cross section, and 7° angle of inclination, which was the smallest slope that allowed the SCC to flow to the lower end [45]. After the flow stoppage, particle content at the entrance and the end of the channel are compared to determine the horizontal dynamic segregation [91]. Shen et al. [91] showed that while coarse aggregate content decreased continuously along the channel, samples taken at the casting point could have up to 20% more coarse aggregate than the reference mixture.

Turgut et al. [92] developed a modified L-box set-up to evaluate the dynamic segregation of SCC in different locations in the horizontal direction. Accordingly, the particle content of concrete samples in three sections along the horizontal channel were measured after the L-box flow. The results of the horizontal dynamic segregation index values were correlated to slump flow results of the investigated mixtures to make a relation between dynamic segregation and flowability of SCC.

T-Box test:

The T-box test which resembles the non-restricted flow of the SCC by tilting motion of the box in different rotating cycles was developed (Fig. 2.17) [36, 37].

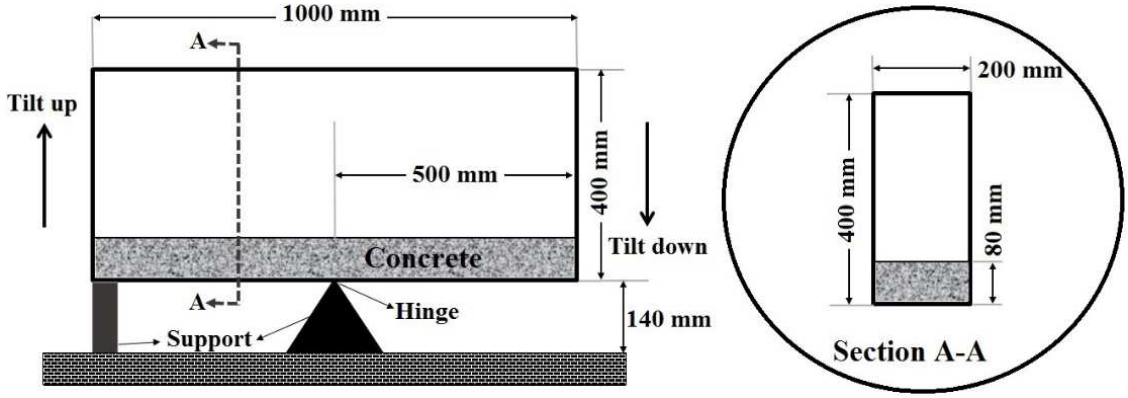

Figure 2. 17 Schematics of the T-Box test set-up [36-38]

As can be observed in Fig. 2.17, the proposed apparatus consists of a rectangular channel measuring 1 m in long, 0.2 m in width, and 0.4 m in height, hinged in the middle to a 140-mm height support. The rotating motion of the box is limited by another support beneath one end of

the channel. An amount of 16 L of SCC is required to be cast in the channel which provides an initial concrete thickness of 80 mm [36].

This test simulates the flow distance traveled by SCC in the formwork using a tilting motion of the box in given rotating cycles. Each single 2-s flow cycle is reached when the channel rotates from the initial horizontal position in the non-supported side till the box touches the floor in 1-s half cycle (i.e. titling down), and then moves back to the horizontal state in another 1 s (i.e. tilting up) in a continuous motion. Displacement of the mass-center of the concrete during tilting process can simulate the motion of concrete in the formwork in vertical and horizontal directions. Consequently, as the number of cycle increases, the coarse particles accumulate gradually in the tilt down section and at the same time this results in formation of a layer of mortar in the top surface of the concrete placed in the tilt up section. Vertical and horizontal dynamic segregation of SCC are then measured by determining the penetration depths and coarse aggregate contents at two sides of the box, respectively. Comparing the properties of the concrete in tilt down section to the one placed in tilt up section can lead to evaluate the dynamic stability of the investigated mixture in a given number of tilting cycles.

Esmaeilkhanian et al. [38] evaluated experimentally the effect of mix design parameters and rheological properties of SCC on the results obtained by T-box test. It was revealed that increasing yield stress and plastic viscosity can result in higher dynamic stability of SCC due to higher drag force exerted by the mortar matrix on coarse aggregates. Consequently, workability parameters of SCC have a significant effect on its dynamic stability. For example, decreasing slump flow from 700 to 640 mm and increasing V-funnel flow time from 5 to 25 s could result in increasing the dynamic stability of SCC up to 38 to 50%. This is due to higher plastic viscosity and yield stress of the mixture [36-38]. It was also concluded that ensuring a proper dynamic segregation is more stringent than static segregation [38].

2.5 Workability design

Regarding the different flow performance properties of SCC, presented in the previous sections, it can be concluded that it is always necessary to establish a trade-off between flowability and

stability properties of SCC. Indeed, the SCC mixtures having higher flowability, which corresponds to more flowability of the cement paste and mortar matrix, exhibit higher static and dynamic segregation. The higher segregations can be more critical in presence of obstacles and lead to higher risks of blocking. This can be explained by the lower values of plastic viscosity and yield stress of the corresponding cement paste and mortar matrix of higher flowable SCC mixtures. Lower values of rheological parameters can lead to lower cohesiveness between the fluid portion of the suspension and the solid particles, as well as decrease the drag forces exerted on coarse aggregates. Therefore, the cement paste and mortar matrix cannot transport the coarse particles with the same velocity. This can lead to higher segregation during flow (i.e., dynamic segregation). On the other hand fluid phase of the mixture cannot keep the solid particles in uniform distribution at rest and coarse aggregates settle down to bottom layers (i.e., static segregation). Accordingly, it seems to be important to take into consideration the desired workability and rheological performance of the mixture during mixture proportioning process.

Proportioning of concrete mixtures are usually designed only based on the desired structural properties of concrete in hardened state. These properties consist of compressive strength, modulus of elasticity, tensile strength, flexural strength, and bond with the reinforcing bars. On the other hand, the mix design can also be modified regarding durability aspects. For example, according to the environmental conditions, such as temperature, humidity, presence of sulfate and chloride ions attacks, and alkali reactions, proportioning of different components of concrete (e.g., different types of cement, aggregates, and admixtures) can be optimized to ensure higher durability of concrete in both early ages and longer ages of the life cycle of the concrete structure.

As explained earlier, an inappropriate rheological performance of concrete mixture in fresh state can negatively affect on structural and durability properties of concrete in hardened state. For example, poor formwork filling can lead to making honeycombing zones in the structural section, and consequently, higher permeability, less durability, and lower mechanical performance. Therefore, the rheological and workability aspects should also be considered in mixture proportioning design process. Accordingly, an efficient workability design corresponds to the prediction and optimization of the workability of the concrete mixtures for the selected

construction processes, such as transportation, casting, compaction, finishing, etc [33-35]. Indeed, the mixture components should be selected in order to ensure the construction quality demands, such as demanded levels of flowability, passing ability, filling ability, and stability (dynamic and static). Therefore, the quality demands are the inputs of the workability design process. On the other hand, the construction conditions, consisted of environment conditions (e.g., temperature and humidity), geometry of the formwork, reinforcement density, and the selected method of casting (e.g. pumping, cast in place by buckets, etc) can be assumed as the second group of the inputs. Accordingly, in order to reach the required levels of workability, the designed mixture should have proper set of rheological properties (i.e. yield stress, plastic viscosity, density, etc). The workability of the mixtures should be tested or analysed to confirm if the demanded flow performance conditions will be satisfied or not. If the rheological parameters of the mixtures, obtained by the chosen mixture proportions, could not reach the desired level of performance quality and workability, then the mixture proportions should be optimized, or if it is possible, the construction conditions can be even modified. This process can repeat to obtain the optimum, efficient, and inexpensive workability design. A schematics of the workability design process is presented in Fig. 2.18.

As can be observed, there is an essential necessary to develop some empirical and theoretical tools to evaluate the workability of the designed mixtures and compare the results with the construction demands. Empirical workability tests which were described in the previous sections, can simulate the behavior of the investigated mixture in a smaller scale comparing to the real size castings. For example slump flow and V-funnel tests can evaluate the horizontal and vertical flowability of SCC, respectively. On the other hand, J-ring and U-box tests can evaluate the horizontal and vertical passing ability of concrete, respectively. Moreover, according to the geometry of the L-Box test, this set-up can simulate the horizontal and vertical motion of SCC in presence of reinforcing bar obstacles. Therefore, the L-Box test is a proper workability test to evaluate passing ability and flowability of SCC in different directions. Since the particle contents along the horizontal channel of the T-Box set-up and the paste thickness on the top surface of the profile are measured, this set-up can also measure the non-restricted dynamic stability of the investigated SCC mixtures in the horizontal and vertical directions. The typical practical sheets, such as presented in Tables 2.2-2.5, which relate the experimental

workability test results to casting conditions can be used as empirical tools to ensure whether the designed mixture proportions can confirm the construction quality demands or not.

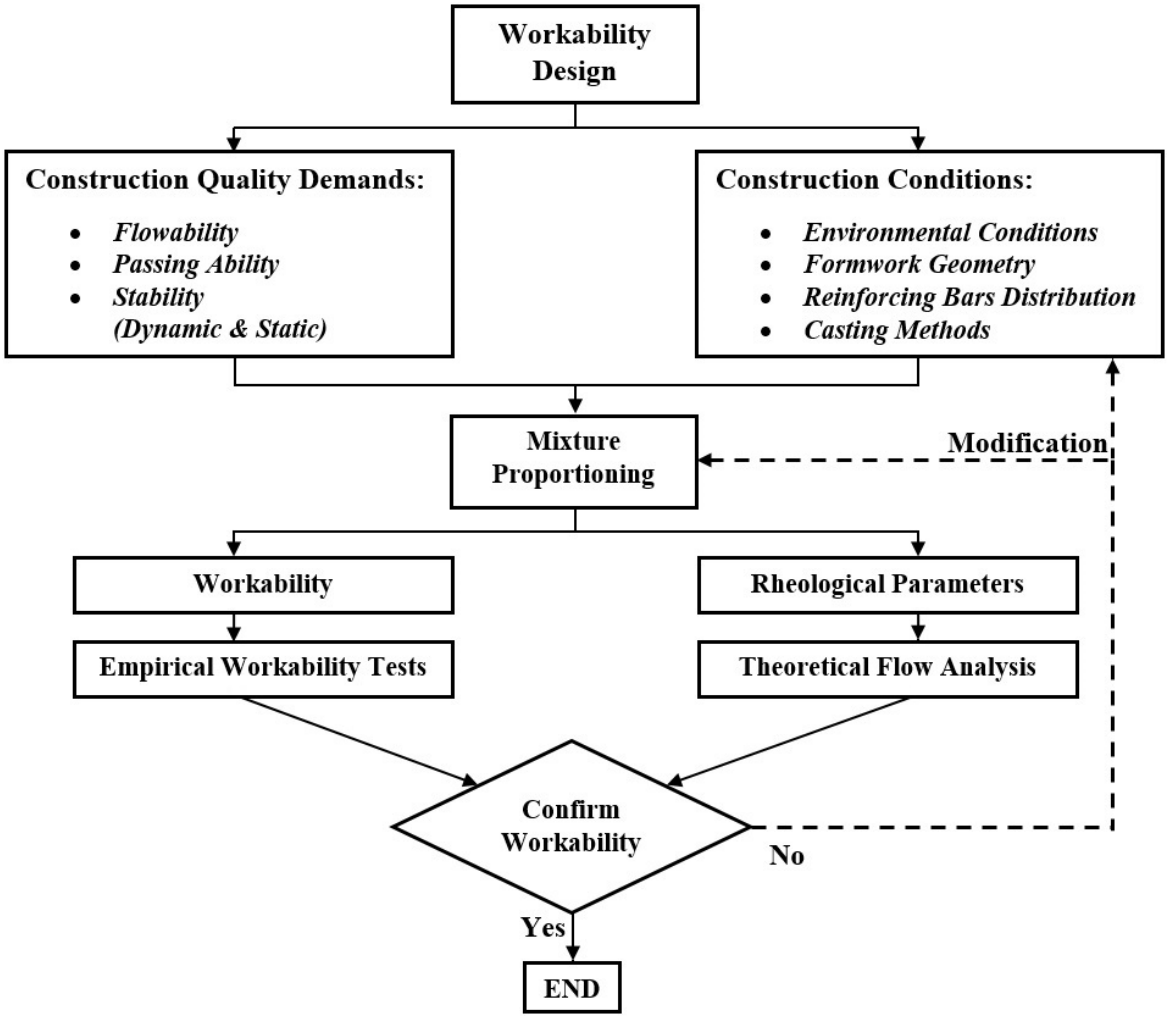

Figure 2. 18 Workability design procedure of SCC

The design and optimization of SCC is based largely on experience and empirical testing to tailor a given passing ability and filling capacity and achieve good material performance. A possible approach to understanding SCC flow and filling performance is to develop fundamental theoretical analyses [39-41] and numerical modeling [42, 44, 48, 93, 94]. Developing analytical and numerical simulations to predict flow characteristics of SCC during casting can improve the selection of mixture composition and ensure better planning of concrete placement to achieve successful filling of the formwork. However, it should be recognized that theoretical

analysis of SCC flow presents a great challenge because of the necessity of taking into account the complex interaction between the solid particles, reinforcing bar obstacles, and walls, while simultaneously solving the fluid dynamics equations for the liquid phase in which they are immersed [40].

This study is dedicated to the theoretical analysis of flow of SCC. In the next section, a review of the studies carried out on theoretical analysis of fresh concrete flow, including analytical and numerical simulations, are presented.

2.6 Theoretical flow analysis

Viscoplastic models are used typically to describe the flow behavior of liquid materials in manufacturing industrial processes [95-98], environmental phenomena [99-105], and granular and debris flow [106-108]. A viscoplastic material behaves as solid for shear stress lower than the yield stress and flows when the shear stress overcomes the yield stress. The motion of a viscoplastic material is eventually arrested when the gravitational forces are in equilibrium with the viscous forces [109-114]. Consequently, the shape of the free-surface profile is directly linked to the material yield stress and density. Accordingly, some laboratory tests are developed to feature viscoplastic flows with this kind of behavior, such as Bostwick consistometer for food industry [95]. Recently, there is also a great interest to develop analytical models [115-124] and numerical simulations [125-128] to link the free surface profile of viscoplastic materials and the rheological parameters.

SCC behaves as a viscoplastic material with yield stress. The existence of yield stress introduces a certain discontinuity between the flowing and stationary SCC. The evolution of the flow and the shape of free-surface profile are therefore dependent of the rheological behavior of SCC mixtures. Workability design should be carried out based on the information of flow profiles during cast, which is obtained from flow analyses or cast experiments of concrete under given structure and construction conditions. This section introduces the current state of the art in analytical flow analysis and numerical flow simulations of fresh concrete as the most basic tool of workability design.

2.6.1 Analytical flow analysis of fresh concrete

The studies presented in this section include analytical modelling of flow profile of fresh concrete based on non-Newtonian fluid dynamics and fluid mechanics equations. In general, the analytical models carried out on linking the flow profile in stoppage state to yield stress of the mixture, regardless of plastic viscosity values. The derived models considered several initial assumptions and conditions, as follows:

- The mixtures are assumed as a homogeneous Bingham non-Newtonian fluid
- The effects of fluid surface tension must be negligible.
- The flow must stop only when the shear stress is smaller than the yield stress of the material, regardless of the plastic viscosity values.
- The inertia effects must be negligible.
- The volume of the investigated mixture in the modelled test must be representative of the mixture.

The analytical models only studied the final profile of SCC in some laboratory tests such as slump flow and flow of SCC in a rectangular section channel, and are summarized in this section.

Analytical modellings of Slump Flow test

The analytical solutions for slump flow test are mostly presented by the final spread of concrete as a function of yield stress and density of the mixture. The solutions employed dimensional analysis, solving conversation of mass, and 2nd Newton's law. The equations are developed for two asymptotic situations of $R >> H$ and $R << H$ for slump flow and slump test, respectively. R and H are the representative spread radius and thickness of the flow profile, respectively. Accordingly, the governing flow equations can be simplified from three dimensional flow problem to one dimensional analysis. Therefore, the flow stops when shear stress in whole the modeled sample becomes less or equal the yield stress of the concrete.

Murata [129] was the first one who studied the deformation of concrete in a slump test analytically. It was assumed that concrete deforms into two yielded and non-yielded regions. The yielded region flows until the shear stress on the cross section is higher than the yield stress. When the shear stress equals the yield stress, the flow stops. Based on these assumptions, a relation was derived between the slump flow radius, yield stress, height, and density, as follows:

$$R' = \sqrt{\frac{\tau_H}{2\tau_0}}R \tag{2.19}$$

Where τ_H is the maximum shear stress acting on the bottom surface due to the dead weight of slump cone, τ_0 is the yield stress of the mixture, R and R' are the radius of the bottom surface before and after the test, respectively. Similar assumptions were applied by Christensen [130], Pashias et al. [118], Schowalter & Christensen [119], Clayton et al. [131], and Saak et al. [132]. It was also shown in [41], using a conic coordinate system, the final shape of the flow profile can be calculated by:

$$h(r) = \left(\frac{2\tau_0(R-r)}{\rho g}\right)^{1/2} \tag{2.20}$$

where R is the radius of the bottom surface (i.e., half of the slump flow diameter), r is the radial coordinate from the center of the bottom side of the cone, ρ is the density, and g is the gravity. Using Eq. (2.20), Roussel et al. [133] presented yield stress as a function of the final radius of profile (R) and volume of the sample (Ω), as follows:

$$\tau_0 = \frac{225\rho g\Omega^2}{128\pi^2 R^5} \tag{2.21}$$

The proposed analytical models expressing the relation between results of slump and slump flow tests and yield stress of the investigated mixture are summarized in the Tables 2.6 and 2.7. It must be noted that h_0 and R_0 are the initial height and bottom surface radius of slump cone, respectively, Sl is the vertical slump value, Sf is the slump flow spread, Ω is the volume of the specimen, and a and b are constant numbers which obtained empirically.

Table 2. 6 Analytical and empirical models relating yield stress, slump and slum flow spread

Type of models	Author	Equations (2.22-2.31)
Relation between slump and yield stress	Schowalter and Christensen [119]	$\tau_0 = \frac{\rho g(0.3 - h_0 - Sl)}{2ln\left(\frac{7}{\left(1+\frac{h_0}{0.3}\right)^3 - 1}\right)}$
	Chiadiac and Habibbeigi [134]	$\tau_0 = 0.3635\rho g(h_0 - Sl)$
	Roussel [93]	$Sl = 25.5 - 17.6\frac{\tau_0}{\rho}$
Empirical models	Murata and Kikukawa [135]	$\tau_0 = 715 - 474\log(10\ Sl)$
	Hu et al. [136]	$\tau_0 = \frac{\rho}{0.27}(0.3 - Sl)$
	Ferraris and De Larrard [137]	$\tau_0 = \frac{\rho(0.3 - Sl)}{0.347} - 212$
Relation between yield stress, Slump, and Slump flow	Kurokawa et al.[138]	$Sl = 0.3 - 0.012/Sf^2$
	Domone [139]	$Sl = 0.3 - \frac{0.021(Sf - 0.1)}{Sf^3 - 0.1^3}$
	Chidiac et al. [140]	$Sl = 0.3 - 0.01/Sf^2$
	Chidiac et al. [140]	$\tau_0 = \rho\left(1.85(0.3 - Sl) + \frac{0.0198}{Sf^2}\right)$

Table 2. 7 Analytical and empirical models relating yield stress and slump flow

Author	Equations (2.32-2.35)	Author	Equations (2.36-2.40)
Roussel and Coussot [41]	$\tau_0 = \frac{225\rho g\Omega^2}{128\pi^2 R^5}$	Kokado et al. [143]	$\tau_0 = \frac{225\rho g\Omega^2}{4\pi^2 Sf^5}$
Clayton [131]	$\tau_0 = \frac{\alpha}{6}\left[\beta - \frac{1}{\beta^2}\right]$ $\alpha = \frac{R_0}{R_f - R_0}, \beta = 1 + \frac{h_0}{\alpha}$	Helmuth et al. [144]	$\tau_0 = \frac{2\rho g\Omega}{\pi Sf^2}$
		Chidiac et al. [140]	$\tau_0 = 39.7 \times 10^{-3}\frac{\rho}{Sf^2}$
Murata and Shitayama [141]	$\tau_0 = \frac{2\rho g\Omega}{\pi Sf^5}$	Flatt et al. [39]	$\tau_0 = ae^{-bSf}$
Komura et al. [142]	$\tau_0 = \frac{4\rho g\Omega}{\sqrt{3}\pi Sf^2}$	Tregger et al. [145]	$\tau_0 = 2.75 \times 10^9 Sf^{-5.81}$

Analytical modellings of channel flow

Coussot and Ancey [146] showed that in order to be valid to consider the flow of a sample of a suspension as a homogeneous material, the thickness of the sample at flow stoppage should be at least five times the diameter of the maximum size of aggregates. According to the low thickness of the profile of the SCC spread in the slump flow test, this test cannot fulfill this condition. This is more critical for lower yield stress mixtures. For example, for a SCC mixture with maximum size of aggregate of 12 mm, a minimum thickness of the final profile of slump flow spread after stoppage of 60 mm is required. Hence, it needs at least 300 L of concrete for slump flow test to represent of the homogeneous rheological behavior of SCC, which is not realistic and practical in building sites. Accordingly, Roussel [147] proposed the LCPC Box as an alternative test method. This consisted of an open surface box, with 1.2 m length, 0.15 m thickness × 0.2 m width cross section (Fig. 2.19). The required sample volume in this test is same as the one used in the slump flow test (i.e., 6 L). The concrete is slowly poured in one of the ends of the channel. Once the flow stops, the maximum length of the spread of the flow along the channel, and the maximum thickness of the profile at the casting point are measured.

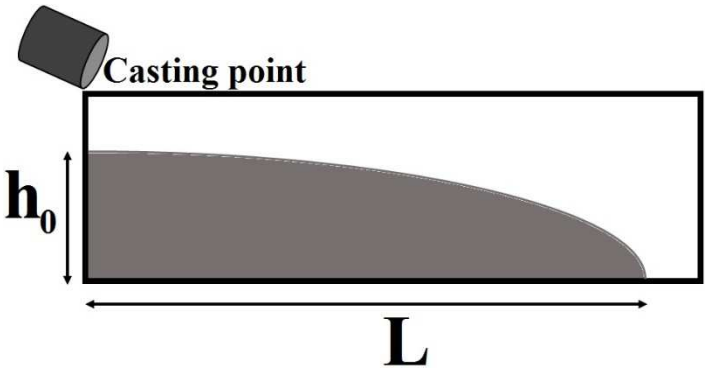

Figure 2. 19 Stoppage profile shape in LCPC-Box [147]

The analytical modelling of channel flow can be found in [40, 147]. The analysis takes into account the shear stress exerted on concrete at the side walls of the horizontal channel, as well as the bottom base wall. Applying conservation of mass, and volume (assuming incompressible fluid condition) can lead to the calculation of maximum spread length (L) as a function of the

yield stress of the mixture (τ_0) and the maximum profile thickness at the casting point (h_0), as follows:

$$L = \frac{h_0}{A} + \frac{l_0}{2A} LN\left(\frac{l_0}{l_0+2h_0}\right) \tag{2.41}$$

Where l_0 is the width of the channel, and $A=2\tau_0 / (\rho g l_0)$. Nguyen et al. [40] proposed a semi-empirical-semi analytical model for the L-box test based on the analytical solution presented in Eq. (2.41). The proposed models can predict the L-Box blocking ratios (H_2/H_1) as a function of density (ρ) and yield stress (τ_0) of the fresh SCC mixtures for the non-restricted L-box test set-ups, and also in presence of reinforcing bars, as follows:

$$\frac{H_2}{H_1} \cong \frac{\rho g - 84\tau_0}{\rho g + 84\tau_0} \qquad without\ bars \tag{2.42}$$

$$\frac{H_2}{H_1} \cong \frac{\rho g - 100\tau_0}{\rho g + 100\tau_0} \qquad with\ bars \tag{2.43}$$

2.6.2 Numerical flow simulations of fresh concrete

It is impossible for the most of concrete flow problems to be modelled by analytical solutions. This can be explained by the existing complexity of considering multiphase behavior of fresh concrete, presence of solid obstacles, interaction between solid particles, solid obstacles, and fluid medium, and various geometries of the casting set-ups. Therefore, numerical simulations can simplify these difficulties, solving different types of governing equations of motion. In order to do that, numerical simulations discretize the material and geometry to convert the physical domain to the computational nodes, vectors, and matrixes to become computable. Accordingly, several computational methods can be employed to solve the differential equations which were impossible using analytical methods. On the other hand, analytical models can be used as a verification tool for the numerical simulations to check whether the developed computational models provide logic and accurate predictions or not.

Numerical simulations need the results of the experimental tests, such as rheological parameters of concrete, as the input of the modellings to predict the flow performance of the investigated mixtures in a given application. Therefore, numerical simulation can make a link between the empirical tests and theoretical solutions. Accordingly, simulation of empirical workability/rheology tests can give an insight to the flow characteristics of concrete, such as flowability, stability, and passing ability, in the real size castings.

Numerical simulations are the fastest and less expensive way to predict the flow performance of concrete, compared to the experimental trial and error procedures. The main restriction of numerical methods corresponds to the calculation capacities of the current computers which are limited to consider vast range of particle numbers and sizing, as well as dimensions of the modelled geometry. Accordingly, it is necessary to optimize and modify the settings of the created models and choose proper assumptions to provide most accurate predictions. In order to perform any numerical simulation, the following items should be checked:

1. Risk of turbulence of the flow:

The dimensionless Reynolds number can indicate the risk of turbulence. Reynolds number is described as the ratio of the inertial forces (or kinetic energy) to the viscous forces (or viscous energy) and can be calculated for a Bingham material, having yield stress and plastic viscosity parameters, as follows:

$$R_e = \frac{\rho V^2 D}{D\tau_0 + \mu_p V} \tag{2.44}$$

Where ρ is the fluid density, V is the flow velocity, D is the typical dimension of the flow (for example width of a beam formwork), τ_0 and μ_p are the yield stress and plastic viscosity values of the investigated mixture, respectively. The laminar flows occur when the Reynolds number is below a critical values of 2,040, through the transition range is typically between 1,800 and 2,100, and the higher values of Re correspond to the turbulent flows. In the case of the most of the applications of fresh concrete, the flow types are laminar. Depending the rheological parameters and the method of castings, which affects on the initial flow rate and velocity of the flowing concrete, the turbulence effects can start to play a role (e.g., high flow rate pumping of

low viscosity SCC mixtures) [48]. For example, in the case of casting of a beam with 0.3m width, using a SCC mixture with density, plastic viscosity and yield stress values of 2300 kg/m3, 50 Pa.s, and 75 Pa, exhibiting an average flow velocity of 0.2 m/s corresponds to a Reynolds number of 1,656.

2. Time dependent properties of the flow:

Steady-state flow refers to the condition where the fluid properties at a point in the system do not change over time. Otherwise, flow is called unsteady (also called transient). The steady state occur in flow of concrete in viscometers or concrete pumping, while in the most of concrete flow situations (e.g., empirical tests and castings) monitoring of the changes in flow properties is interested to study (i.e., unsteady state).

3. Effect of surface tension:

According to [133], surface tension effects are mostly neglected in flow studies of the cement based materials due to the values lower than yield stress of the mixtures. However, in the case of very low yield stress and low plastic viscosity pastes (e.g., cement grouts) surface tension may lead to the stresses in order of yield stress (1 to 2 Pa) and has some dominant effects on the flow behaviour and stoppage of the material.

4. Flow surface condition:

Free surface is the interface between concrete surface and air. This affects the boundary conditions applied for the problem. Casting of the regular members, such as walls, beams, slabs, and workability tests are corresponded to the free surface flow, having zero pressure in the surface. On the other hand, flow of concrete in the pumping pipes are under effect of the wall of the tubes on shear stress and pressure exerted on the fluid, and consequently, is considered as a confined flow.

5. The rheological models:

The material behaviour law determines how shear rates evolves with increasing the shear stress exerted on the fluid. On the other hand, this is decisive to estimate of the viscosity and yield stress of the material which play the dominant roles in the flow motion equations. Therefore,

choosing whether Bingham or Herschel-Bulkley (or any other non-Newtonian models) can has a big effect on the calculation of the shear stresses and displacement of the flow.

6. Boundary conditions:

The boundary conditions include the filling conditions such as the flowrate of the pumping, assumptions for frictional stresses between the solid objects and the flowing parts (i.e., slip or no slip conditions), pressure and velocity gradients on the boundary of the formwork, and also the static of moving walls of the formwork boundary.

7. Simplification assumptions:

In order to simplify calculations and reduce running times of the developed simulations, there is necessary to consider several assumptions. These assumptions include neglecting the effects of temperature, thixotropic behavior of the material, and inertial effects, as well as using the maximum possibility of the existing symmetries in the system to reduce the calculation times.

8. Governing equations:

The main equations in fluid mechanics includes derivations from conservation of momentum (equation of motion), mass (continuity), and energy. In fluid dynamics, these equations are used to calculate the flow velocity, pressure, and density as a function of time and space. The equation of motion comes from Newton's second law (F = m dv/dt). The governing equations for non-Newtonian materials is called Cauchy equation of motion (Eq. 2.45) [148, 149], which is more complex than the governing equations of Newtonian flows (i.e., Navier-Stokes equations).

$$\rho\left[\frac{\partial v}{\partial t} + v.\nabla v\right] = \nabla.\sigma + \rho g \tag{2.45}$$

Where v is the three directional velocity, ρ is the density, t is the time, g is the gravity, and σ is the total stress tensor which is given by

$$\sigma = -p\mathrm{I} + \mathrm{T} \tag{2.46}$$

The stress tensor consists of isotropic pressure p, and extra stress tensor T and I is the unit dyadic. In computational fluid dynamics, the continuity equation used often to calculate pressure correction while solving Eq. (2.45). It writes as follows:

$$\frac{\partial p}{\partial t} = -(\nabla . \rho v) \tag{2.47}$$

In the case of incompressible fluids, such as cement based suspensions, it can be written as follows:

$$(\nabla . v) = 0 \tag{2.48}$$

On the other hand, in the case of cement based suspensions, the isothermal conditions are often assumed, and energy equation is often omitted.

9. Numerical solution methods:

In order to simulate a physical flow problem, it is necessary to convert the physical points of the material, space, and geometry to the computational points, nodes, elements, and matrixes to be able to calculate the equations of motions. Accordingly, there are several approaches to discretize the physical materials and space. Then, the numerical solution methods are employed to convert the partial differential equations of motions to the algebraic equations, which are solved in the discrete computational elements in space and during different time steps. This consists of mesh-based and meshless methods.

9-a. Mesh-based methods:

In the case of CFD, the discretization step is called meshing procedure. The mesh grids can be in different shapes, such as quadrilateral or triangle, and brick or tetrahedron in 2D and 3D, respectively. The meshing setting should be optimized in terms of number, size, and positions of the cells, and number of mesh blocks to obtain higher accuracy of predictions, and on the other hand, reduction of calculation times.

The main mesh-based numerical solutions include Finite Difference (FD), Finite Volume (FV), and Finite Element Methods (FEM) using Eulerian description of fluid motion. In Eulerian algorithms all the gird nodes and meshing cells are fixed in the space and do not move or change with time during the modelled flow period. The flow surface properties are defined by the position and filling fraction of the cells which contain the fluid. A basic layout of a 2D grid-based Eulerian fluid example is presented in Fig. 2.20. As can be observed, due to the coarse resolution of 6×6 sized grid, the whole fluid surface is contained in the same row, which is a common problem for visualization. In order to increase the accuracy of determination of the surface flow properties, a higher number of finer mesh cells is required.

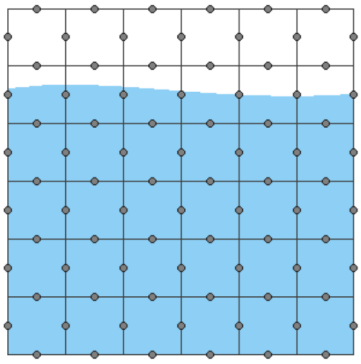

Figure 2. 20 Euler grid-based fluid structure in 2D

In the Eulerian description, large distortions in the continuum motion can be handled with using the Volume Of Fluid (VOF) technique, which is developed by Hirt and Nicols for the first time [150]. In the first step of VOF, in a given flow time step (t_n), the calculator algorithm computes the volumetric fluxes by geometrically reconstructing the interface using the values of the fluid fraction at the previous time steps (t_{n-1}) in and around a given control volume. The velocity field is then calculated by solving the Navier-Stokes (or Cauchy) equations for the time step t_n, considering incompressibility of the fluid. Consequently, fluid is advected by this new velocity and then local positions of the fraction of the fluid is updated. There are several CFD softwares which use VOF method to simulate the flow motions, such as FLOW3D©, ANSYS Fluent©, and OPENFOAM.

9-b. Meshless methods:

Another method of discretization of the flow problem corresponds to the meshless methods, such as Discrete Element Method (DEM) which convert the material and geometry to the discrete particles and boundary walls. This method was first developed to study flow behavior of granular materials. Recently, there is a great interest to employ DEM as a theoretical tool to simulate flow of fluids, such as fresh concrete. The forces acting on each individual particle are calculated according to the relevant laws of physics. Then, forces are added up to find the total force acting on the particles. An integration method is employed to compute new particle positions from applied forces according to Newton's laws of motion. The new positions are used to compute the forces for the next time-step, looping until the simulation ends. The most known softwares developed based on DEM method include PFC, EDEM, ELFEN, and LIGGHTS [48].

In summary, after discretization of the problem and choosing the numerical solution method, the initial and boundary conditions are defined. Non-linear governing equations of motion are then solved to calculate velocity and pressure in each time step. These equations must be solved iteratively using the substitutional methods such as Newton-Raphson, Modified Newton, Quasi-Newton, etc. The majority of calculation time of the numerical simulations corresponds mostly to this process.

In the case of fresh concrete, most of the numerical simulations assumed fresh concrete mixture as a homogeneous material. However, there are also a few studies which have considered the concrete mixtures as a heterogeneous suspension of coarse particles and suspending fluid (i.e., cement paste and mortar matrix). In the next section, the recent studies carried on numerical simulation of fresh concrete flow are presented in three different groups of homogeneous single fluid, particle based methods, and heterogeneous analysis of flow of fresh concrete suspension.

1. Numerical simulations of flow of fresh concrete as a homogeneous single fluid material

The studies presented in this section assume fresh concrete as a homogeneous non-Newtonian material interacting with solid obstacles and walls. Most of these predictions carried out on modelling of flow of fresh concrete in standard empirical workability test set-ups such as slump

flow and L-box test set-ups. However, there are some other examples of numerical simulations carried on modeling of casting of fresh concrete in full scale applications such as wall and beam castings. The studies carried out on numerical simulations of fresh cement based mixtures in workability test set-ups, as a single homogeneous fluid, using CFD are summarized in Table 2.8. In summary, these studies showed good correlations with experimental results, using the rheological parameters which were measured experimentally, as follows:

- A good correlation with analytical models predicting the final profile of the mixtures in stoppage state:
  This confirms that yield stress plays the dominant role on the final spread values in slump flow test, compared to the plastic viscosity, when the inertia effects was neglected in analytical solutions [29, 41, 93, 130, and 151-153]. However, in the case of the simulation of L-box test, plastic viscosity and kinetic energy are shown to have some effects on the final shape of the concrete profile [29 and 153-155].

- A good correlation between the free surface profiles [29, 41, 93, 130 and 151-155] and flow time [156-158], as well as a good agreement with the experimental data:
  This can explained by the true assumptions of boundary conditions, slip or non-slip conditions besides the walls, and laminar or turbulent assumptions. Although, most of the simulations consider laminar flow type and non-slip conditions, but however, the numerical simulations are able to consider the presence of friction and turbulent flow conditions.

Table 2. 8 Single fluid CFD numerical simulations of workability tests, software, and numerical methods used by the researchers

Researcher	Modelled test	Software	Method
Kurokawa [151]	Slump flow	-	VFEM
Christensen [130]	Slump flow	FIDAP	FEM
Roussel [41, 93]	Slump and Slump flow	FLOW3D	VOF
Thrane et al. [29, 152]	Slump flow	FIDAP	VOF
Tregger et al. [145]	Mini cone	POLYFLOW	VOF
Gram [153]	Slump flow and L-Box	OpenFOAM	VOF
Thrane et al. [29, 154]	L-Box	FIDAP	VOF
Uebachs and Brameshuber [155]	L-Box	FLUENT	VOF
Waarde [156]	Funnel test	FLUENT	VOF
Bras [157]	Marsh cone	FLUENT	VOF
Nguyen et al. [158]	Marsh cone	FLUENT	VOF

Single fluid casting simulations using CFD:

A few number of studies carried out on numerical simulation of full scale SCC castings in structural elements (Table 2.9). The results of these simulations were presented in terms of the free surface profile shapes [29, 156, 160, and 161], flow velocity [29], shear rates [29-153], flow rates, and formwork pressure [29 and 156] values versus the flow time, during the flow period, as well as the time needed for filling the formworks. Accordingly, the flowability and passing ability [29, 153, 159, 162] of the SCC mixtures were simulated. These studies showed that numerical simulations can predict qualitatively and quantitatively accurate the evolution of free surface profile of the fresh SCC in full size casting problems. The results of these simulations confirmed that the assumption of concrete mixture as a single homogeneous fluid can successfully work to simulate the flow performance of concrete interacting with reinforcing obstacles and wall boundaries. In order to evaluate the presence of reinforcing bars on flow behavior, finer mesh cells were selected around the obstacles, comparing to the ones corresponding to the regions including solid walls and moving boundaries, and material (concrete suspension) [29].

Table 2. 9 Numerical simulations of casting of SCC as a single fluid, homogeneous material

Researcher	Modelled casting problem	Numerical method/Software
Mori and Tanigawa [159]	Reinforced beam, and a reinforced wall (2 m high × 3 m long)	VDEM (Visco-plastic Divided Element)
Kitaoji et al. [160]	Non-reinforced formwork (1 m high × 2 m long)	VDEM
Thrane [29]	Non-reinforced wall (3 m long × 1.2 high × 0.3 m thickness)	FEM & VOF / FIDAP
Gram [153]	Reinforced wall (12.6 m long × 6.45 m high × 0.27 thickness)	VOF / OpenFOAM
Van Waarde [156]	Non-reinforced wall (6 m high × 6 m wide and various thicknesses)	VOF/ FLUENT
Ovarlez and Roussel [161]	Non-reinforced wall (1.5 m height)	VOF/FLOW3D
Roussel et al. [162]	13 m pre-cambered composite beam	VOF/FLOW3D
Roussel [163]	Multi-layer casting a 0.5 m long × 0.15 high beam	VOF/FLOW3D

The main disadvantages of these simulations include the long time needed for calculation, according to the huge volume of concrete and large dimensions of the formworks. On the other hand, the accuracy of the results of these simulations are highly depended to the accuracy of experimental measurement of the rheological parameters of the investigated mixtures, which have been used as the inputs of the numerical simulations. Accordingly, when the rheological parameters were not selected properly, or not accurately measured, the results of the simulations are only qualitatively reliable, but not quantitatively.

2. Simulation of flow of fresh concrete using particle based methods:

Using particle based methods, the concrete mixture is discretized by the distinct particles, without consideration of fluid parts. Indeed, the motion of model particles are derived by the Navier-Stokes equations, as well as solving the equations of motion, conservation of mass and momentum, considering the rheological behavior of the fluid part as the interactions between the model particles. These studies are divided in three different main groups of Discrete Element

Method (DEM), Particle Finite Element Method (FEM), and Smoothed Particles Hydrodynamics (SPH), as follows:

1. Discrete Element Method:

Generally, in DEM method, the flow problem is discretized by circular or spherical particles for 2D and 3D analyses, respectively. The interaction between the modelled particles and rheology of the mixture is controlled by appropriate constitutive relations. Accordingly, elastic, viscous, and frictional components of particle interactions are represented by the rheological elements consisting of spring, dashpots, and sliders, respectively. The spring constant of G (shear elasticity modulus) correspond to the elastic state. Once the forces exerted on the particle excess the threshold value of τ_0 (yield stress) of the model slider, the plastic state of the flow is started with a μ_p (plastic viscosity) constant displacement rate of the modelled dashpots. (Fig. 2.21). The properties of the material model should be then calibrated using experimental or theoretical algorithms [164, 165].

The force-displacement law is then used to update the contact force arising from relative motion at each contact. Then, the law of motion is again applied to each particle to re-determine its velocity and position. This is based on the resultant force and momentum arising from the contact forces and gravity acting on the body.

Various studies were carried out on simulation of fresh concrete flow using DEM. These researches include simulation of flow of concrete in workability tests and also filling of the formworks (i.e., casting process), and are summarized in Table 2.10. Employing DEM can lead to develop valuable information of the flow properties of the suspension, such as tracking of particle positions and segregations. For example, Gram and Silfwerbrand [168] simulated the final spread of SCC in slump flow and J-Ring tests using DEM approach. They used flow code PFC3D, to select a user-defined contact model and governing inter-particle forces, using a mechanical tool metaphor. The interaction forces between the particles were also defined mathematically using equivalent dashpots, springs, as well as slip functions to consider frictional stresses. The investigated SCC was also simulated using Bingham model. The simulated solid particles correspond to the actual aggregate greater than 2 mm. On the other

hand, the soft matrix coat, surrounding the solid particles corresponds to cement paste and aggregates smaller than 2 mm. The simulated results were shown to be in very good agreements with experimental values of final spread of SCC in slump flow test. Since aggregates are not supposed to collide in SCC unless segregation or blocking occurs, the soft coated particle technique was shown as an excellent way to reduce the number of spheres to be modeled. Application of DEM technique showed more accurate predictions of final spread compared to CFD models, assuming concrete as a single homogeneous fluid [168].

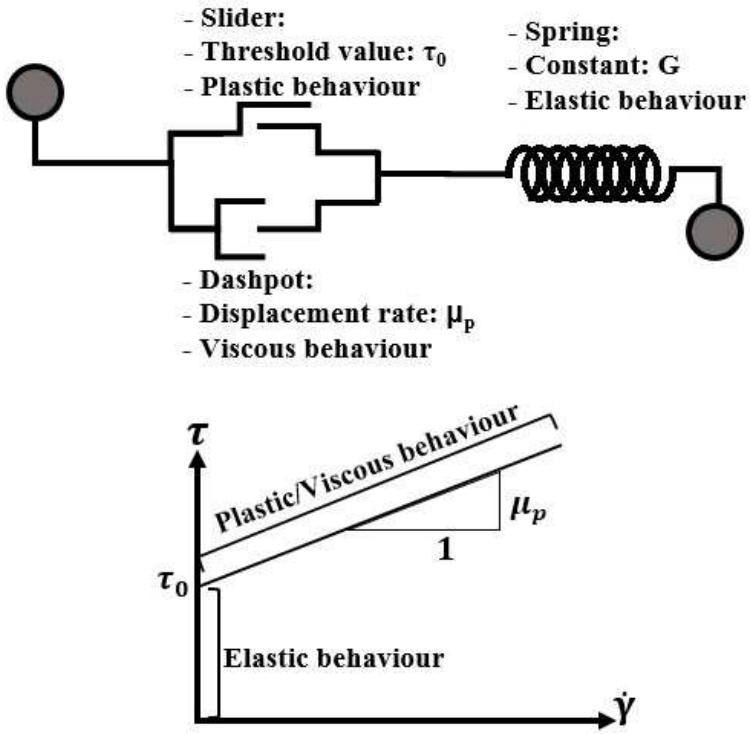

Figure 2. 21 Description of a Bingham fluid by DEM

However, regarding physical point of view, it is difficult to define the direct contact between the solid modelled particles that are assumed to represent the flowing mortar and the solid particles (i.e., coarse aggregates). Moreover, measuring the parameters of the contact law are impossible. On the other hand, in the case of full size casting of large formworks, such as wall and beam elements, simulation of motion of the huge number of particles using DEM is impossible, according to too long calculation times.

Table 2. 10 Numerical simulations of SCC flow using DEM

Researcher	The modelled flow problem	Description
Shyshko and Mechtcherine [165]	Slump flow test	• Two size of particles: 2.5 and 5 mm • Using EDEM software
Mechtcherine and Shyshko [166]	Slump flow test	• Consisted of coarse, fine, and combination of coarse and fine particles • Presence of still fibers
Mechtcherine and Shyshko [167]	J-Ring test	• Poly sizes particles • Well predictions of the final spread
Gram and Silfwerbrand [168]	L-Box test	• Verification at 20 and 40 cm located after the gate, and final state • Satisfactory agreement with experimental results
Mechtcherine and Shyshko [167]	V-funnel test	• Evaluation of plastic viscosity effect • Using PCF3D software
Noor and Uomoto [169]	Slump flow, L-Box, and V-funnel	• Particles larger than 7.5 mm • Using PCD3D software
Petersson and Hakami [170]	L-Box and Slump flow tests	• 3D simulation
Petersson [171]	J-Ring and L-Box tests	• 2D simulation
Mechtcherine and Shyshko [166]	Beam casting	• Simulation of flow of fiber reinforce concrete • Beam dimensions: 500 mm × 100 mm × 100 mm • Employing PFC3D software

2. Particle Finite Element Method:

Cremonesi et al. [172] employed a Lagrangian approach, which is called Particle Finite Element Method, to simulate the evolution of the free surface of SCC by tracking the motion of the material particles. In this method, the meshes remain attached to the material nodes, and a remeshing process (continuous re-triangulation) is needed to remedy the resulting severe mesh distortion. Accordingly, the flow of materials in the L-Box, slump flow, mini slump, and Marsh cone set-ups were simulated using this method. The simulations used Bingham rheological model and showed very good accuracy comparing to experimental results.

3. Smoothed Particles Hydrodynamics (SPH) method:

SPH is an interpolation method to approximate values and derivatives of continuous field quantities by using discrete sample points. The sample points are identified as smoothed particles that carry concrete entities, e.g. mass, position, velocity, etc., but particles can also carry estimated physical field quantities dependent of the problem, e.g. mass-density, temperature, pressure, etc. Compared to other well-known methods for numerical approximation of derivatives, e.g. the finite difference method, which requires the particles to be aligned on a regular grid, SPH can approximate the derivatives of continuous fields using analytical differentiation on particles located completely arbitrary. Each particle is thought of as occupying a fraction of the problem space, and to get more accurate weighted quantity averages, the sample particles must be dense. [173]

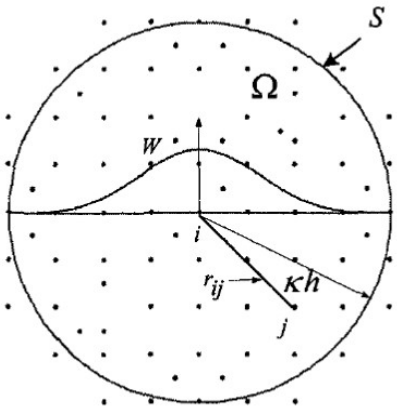

Figure 2. 22 Schematics of a typical SPH particle and its adjacent particles [173]

As can be observed in Fig. 2.22, the SPH quantities are macroscopic and obtained as weighted averages from the adjacent particles. The integral interpolant of any quantity function, $f_i(x)$, is defined over all the space, Ω, by:

$$f_s(x) = \sum_j f_j \frac{m_j}{\rho_j} W(x - x_j, h) \tag{2.49}$$

Where W is the weighting kernel function, and h is the smoothing distance or kernel range, which determines the degree which a particle interacts with neighboring particles. Considering the equation for the conservation of momentum, conservation of energy, and the particulate

attention to calculate density, the integration/differential formats are changed to summation interpolant SPH discretized equations, as follows:

$$f_i(x) = \int_\Omega f(x')W(x - x', h)dx' \tag{2.50}$$

For example, continuity equation (conservation of mass) can be changed to Eq. (2.51), where, V and ρ denote velocity and density, respectively.

$$\frac{D\rho}{Dt} = -\rho\nabla.V \quad \Rightarrow \quad \frac{\partial\rho_i}{\partial t} = -\rho_i \sum_j \frac{m_j}{\rho_j}\left(V_i^\alpha - V_j^\alpha\right)\nabla_i^\alpha W_{ij} \tag{2.51}$$

Recently, there are several studies carried out on simulation of flow of cement based materials using SPH method. Indeed, assuming SCC as a homogeneous fluid that consists of particles of different sizes and shapes, SPH (as a mesh-free particle method) is an ideal computational method to predict concrete flow performance accurately. This method can also assist in proportioning SCC mixtures, thus improving on the traditional trial and error SCC mix design process. SPH method was used to simulate (two and three dimensional) the rheological behavior and free surface flow profile evolution of SCC in different workability tests, such as vane viscometers [174], slump flow [175 and 176], L-Box [180], J-Ring [178], and V-funnel [183] set-ups. These simulations considered the presence of different size of coarse particles, as well as fibers and their orientations [177, 179, 181, and 182] during the flow. These studies are summarized in Table 2.11. For example, Deeb et al. [175] presented 3D simulation of flow of SCC in slump flow set-up using SPH method, with and without presence of fibers. In that study, the flow of fluid was simulated using Bingham constitutive model, as well as considering distribution of coarse spherical particles larger than 8 mm. The particles smaller than 8 mm represented the viscous paste portion of the suspension. Accordingly, a maximum total number of modelled particles of 23581 were simulated. A bell-shaped cubic spline function was also used as the kernel function because of its stability and accuracy. The results show the ability of SPH method to simulate particle-particle interactions, particle tracking, and prediction of flow performance of SCC as a heterogeneous material. On the other hand, Deeb et al. [175] showed that orientation and motion of fibers suspended in a SCC matrix can be predicted well using SPH method.

Table 2. 11 Numerical simulations of SCC flow using SPH method

Researcher	Flow problem simulated by SPH
Zhu et al. [174]	2D simulation of vane and cylinder rheometers
Deeb et al. [175]	3D modelling of Slump flow, with or without steel fibers
Badry et al. [176]	3D simulation of slump flow, for four different size of particles
Deeb et al. [177]	3D modeling fiber orientation in slump flow test
Abo Dhaheer [178]	3D modeling of J-ring flow, considering four different size of particles
Deeb et al. [179]	3D modelling of L-Box set-up, as well as fiber orientation
Lashkarbolouk et al. [180]	2D simulation of L-Box test
Kulasegaram et al. [181]	2D simulations of slump flow and L-box, with and without presence of fibers
Deeb [182]	3D simulations of slump flow and L-box, with and without presence of fibers
Lashkarbolouk et al. [183]	2D simulation of V-funnel test

3. Heterogeneous simulation of flow of fresh concrete as a suspension:

Recently, there is a great interest to study shear-induced migration and gravitational settlement of solid particles suspended in non-Newtonian suspending fluids [18-21]. Numerical simulation using computational fluid dynamics (CFD) was employed as a powerful tool to study these heterogeneous behaviors of the suspensions [184-187]. SCC is a highly flowable suspension of different sized solid particles in a non-Newtonian medium. The fluidity of cement/mortar portion of concrete suspension makes it more sensible in terms of segregation and blocking through the narrow gaps between the obstacles (i.e., reinforcing bars and formwork walls). Accordingly, dynamic stability and passing ability are two key parameters which should be satisfied as the quality requirements for successful SCC casting process. Developing numerical techniques to predict flow characteristics of SCC during casting can improve the selection of mixture composition and ensure better planning of concrete placement to achieve successful filling of the formwork. The numerical modeling of fresh SCC flow should take into account the interaction between the aggregates, the suspending fluid cement paste/mortar, configuration of reinforcing bars, and formwork wall characteristics [29, 42-44]. In the recent years, numerical simulations have been employed as a theoretical tool to predict dynamic stability and passing ability of SCC [29, 42-47].

In the previous sections, the numerical simulations of concrete flow, as a homogeneous single fluid, and particle discretized materials were presented. However, in few number of studies the

flow of concrete mixtures is modelled as a suspension of coarse particles in a non-Newtonian suspending fluid. These simulations considered the interaction of the fluid part of the suspension (mortar matrix as the homogeneous and stable portion) and coarse aggregates (solid particles). Spangenberg et al. [46] studied flow induced particle migration in SCC. According to the competition between gradients in particle collision frequency and gradients in viscosity of the suspension, and on the other hand, the competition between the difference in density of the mixture components that force them to separate, and the viscous drag of the flowing suspending fluid that slows down the phenomenon, some characteristic flow times to indicate flowability (T_c^f), shear-induced (T_c^{shear}), and gravity induced particle migrations ($T_c^{gravity}$) were presented in [46], as follows:

$$T_c^f = \frac{L}{V} \quad and \quad \dot{\gamma} = \frac{V}{H} \tag{2.52}$$

$$T_c^{shear} = \frac{H^2}{10\, a^2 \phi^2\, \dot{\gamma}} \tag{2.53}$$

$$T_c^{gravity} = \frac{18 n K \dot{\gamma}^{n-1} H}{g\, \Delta\rho\, a^2} \tag{2.54}$$

Where, V is the average velocity, L is the flow characteristic length (i.e. the propagation length in transient flows or the largest flow dimension in steady state flows), H is the flow characteristic thickness (or the smallest dimension of the element to be cast), $\dot{\gamma}$ is the shear rate, ϕ and a are the volume fraction and size of the particles, respectively, n and K are respectively the shear thinning degree and consistency of Herschel-Bulkley model, and Δρ is the density gradient between the particles and the suspending fluid. It is concluded in [46] that although shear induced particle migration and wall effect dominate during pumping processes, gravity induced particle migration dominates during typical industrial concrete casting processes. Moreover, migration of three sizes of particles (2, 5, and 7 mm) were studied experimentally and numerically for free surface filling process of a 20 × 20 × 60 cm container. The numerical simulations have been carried out using FLOW3D® software. The suspending fluid followed Bingham law, considering its plastic viscosity and yield stress. The evolution of the particle volume fraction was computed by an advection and a settling calculation. The advection made

the volume fraction follow the streamlines of the global flow, while the settling calculation captured the actual settling of the particle. The settling calculation is derived from a mass conservation of the particles, as follows:

$$\frac{\partial \phi}{\partial t} + div(\phi \vec{V}) = 0 \tag{2.55}$$

Where ϕ is the local particle volume fraction and V is the local particle velocity which is vertical downward settling velocity (V_s) and can be derived from Stokes law:

$$V_s = -\frac{g\, a^2\, \Delta\rho}{18\mu_0} \tag{2.56}$$

Where *a* is the particle size, and μ_0 is the tangential viscosity of the suspending fluid in a given shear rate. The results of numerical simulations showed very good agreements with the experimental flow induced migration of different sizes of the particles. It was also concluded that coarser particles are more prone to shear induced migrations.

Spangenberg et al. [47] employed same theory to simulate the patterns of gravity induced particle migration in a beam with 4m length × 0.2 width × 0.3 m height dimension. Accordingly, particle positions and contents in 9 sampling sections through the horizontal channel were experimentally measured and also numerically simulated. Moreover, distribution of particles in vertical direction of each sampling section is measured to evaluate the flow performance of the investigated mixture in vertical directions. The results of simulation showed that there is a plug flow in the top vertical layer which resulted to no segregation in this layer. On the other hand, the middle layer corresponded to the sheared zone where particles migrate to the bottom layer. Therefore, the bottom layer is found as the settlement layer with higher local viscosity, as a result of the accumulation of the settled particles from the above layers. On the other hand, the experimental and numerical simulation results showed that the particle migrations mostly happened in the last 1/3 of the horizontal channel. Moreover, increasing the casting rate resulted in lower flow induced dynamic segregations.

CHAPTER 3 ORIGINALITY AND OBJECTIVES

In the previous sections a summary of state of the art of carried out on flow analysis of cement based materials is presented. These studies were divided in two main groups of homogeneous and heterogeneous analysis of flow. Homogeneous analysis part consisted of the analytical and numerical models proposed for flow of concrete in workability tests, as well as numerical simulations of casting of SCC in full-scale formworks. In these simulations, concrete mixture was assumed as a single homogeneous fluid, without taking into consideration of presence of solid particles. On the other hand, heterogeneous analysis part included the researches carried out on modelling of flow of concrete mixture as a suspension of solid particles and a flowable fluid portion, or even a composite of distinct particle elements, which show virtual rheological behavior of the flowing concrete.

A high efficient workability design can result in proper selection of mixture proportions and optimization/modification of construction conditions. Theoretical (analytical and numerical) analysis of flow of concrete is one of the main steps of the workability design of concrete mixture. According to the summarized literature review presented in the chapter 2, some gaps are observed. This gaps should be filled in order to improve the capability and efficiency of the workability design of SCC. These observed gaps and the proposed solutions are presented in this section. Accordingly, they can be divided in two main groups of homogeneous and heterogeneous analysis.

3.1 Homogeneous analysis of flow of SCC as a single fluid

- In the case of modeling the workability test set-ups, the analytical predictions were developed mostly based on the dimensional analysis for slump flow, L-Box, and marsh cone set-ups. The majority of the analytical predictions have been done using Bingham rheological model, neglecting the friction and inertia effects. On the other hand, in the most cases, only the final profile of the mixture in the stoppage state was studied. Therefore, the effect of viscosity on evolution of the shape of free surface profile was

neglected, while only the stoppage profiles were related to the yield stress values. This can also be observed for the simulation of full size casting of SCC as a single homogeneous fluid. Therefore, for the simulation of empirical set-ups, it is required to employ new analytical methods, which are able to consider different rheological models, such as Herschel-Bulkley model, and evaluate the effect of other rheological parameters rather than yield stress, such as plastic viscosity and shear elasticity modulus, on evolution of shapes of the free surface profiles during the flow period. Considering the effects of rheological parameters in elastic and plastic states, fluid density, and different levels of gravitational forces can lead to take into account the inertia and gravitational stress effects on flow performance of SCC.

- Consideration of presence of reinforcing bars, and consequently prediction of passing ability, is not possible by analytical models. However, this is not neither studied widely for formwork filling predictions, as well as the effect of different rheological parameters of the concrete mixture on passing ability and flowability of SCC.

- Any relationship between the results of the homogeneous analyses of concrete flow and heterogeneous behaviour of concrete mixture cannot be found in the literature. While, derivation of flow velocity and shear rate values from the numerical simulation of concrete flow as a homogeneous material can give some important insights to predict and find the possible critical zones in the formwork corresponding to higher risks of blocking, dynamic segregation, poor formwork filling, and dead zones.

- Calculation of flow velocity, shear rate, and kinetic energy in different directions (i.e., horizontal and vertical directions) can result in prediction of flow performance of SCC in terms of flowability and passing ability in these directions. This can lead to classify the investigated mixtures by self-leveling and self-consolidating properties, as a function of rheological parameters of the mixture, using single homogeneous fluid approach. These classifications cannot also be found in the single fluid simulations presented in the literature review.

3.2 Heterogeneous analysis of flow of SCC as a suspension of coarse aggregates and suspending fluids

- The major challenge of the simulations of heterogeneous behavior of concrete mixtures, as a suspension of solid particles and suspending fluid, is the very long running times needed for the calculation process. Therefore, this is necessary to apply some simplifications to reduce the calculation time, and at the same time keep the accuracy and performance of the predicting models.

- One of the suggested solutions consists in using the output results of the single fluid simulations to find the critical zones of blocking, poor flowability, and dynamic segregation in the formwork during casting period. Indeed, these casting quality failures only happen in the critical zones where very high or very low values of flow velocity, shear rate, displacement, deformations, and kinetic energy exist. Single fluid simulations can accurately predict these critical zones, and then, the heterogeneous analyses can only carry out in these zones. This can help to reduce the size of the materials and geometry which are supposed to be simulated, and consequently decrease the required calculation times.

3.3 Workability design

- As main steps of the workability design process, workability tests are used to evaluate the flow performance properties of the investigated concrete mixtures in order to confirm the quality construction demands. Each of the empirical tests can evaluate one (or more) of the quality requirements, such as flowability, passing ability, and stability, in a smaller dimensions. Therefore, given the construction conditions and required performance levels, the selection of a proper workability test, which can represent comprehensively flow performance behavior of concrete suspensions in presence of reinforcing bars and obstacles, can accelerate significantly the workability design process. On the other hand, this can lead to having more clear insights of the fresh concrete behavior in the

formwork, which are not visible and neither measurable during casting. Accordingly, another solution to reduce the volume of the calculations consists in establishing relationships between the single fluid casting simulations and experimental/theoretical results obtained from a selected workability test.

- The current status of the workability confirmation step in workability design procedure is presented in Fig. 3.1. As can be observed, any relationship between the results of the theoretical flow analysis and experimental workability tests steps cannot be found in the literature. In addition of the longer calculation time required for simulating the whole casting process, lack of physical meaning of the results of the numerical simulations can be observed. Indeed, the outputs of theoretical analyses consist of a group of numbers, magnitudes, matrixes, colors, and animations which need to be translated to the understandable physical items, such as qualitative and quantitative levels of flowability, passing ability, and stability. These flow performance properties can be obtained by the empirical tests to confirm the workability of the designed mixture and satisfy the construction quality demands.

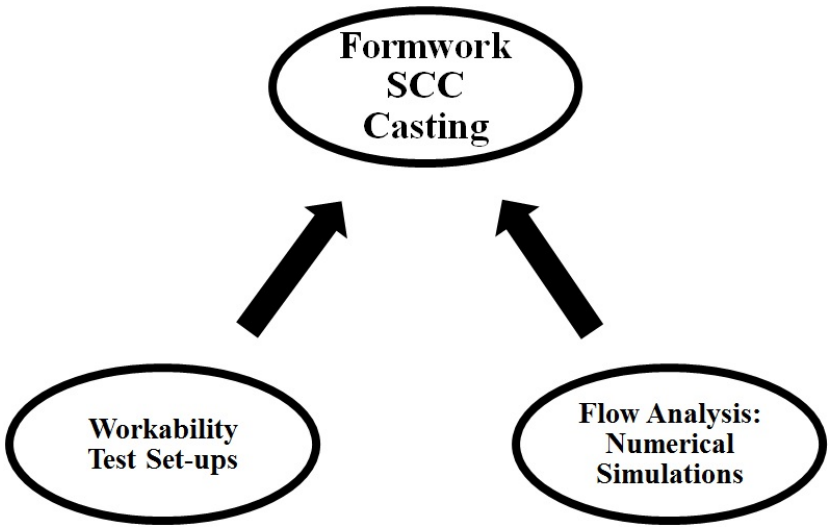

Figure 3. 1 Current status of the workability confirmation step in workability design procedure

- As presented in Fig. 3.2, establishing relationships between the numerical outputs of the theoretical flow analyses and experimental/theoretical results of the workability tests can

lead to decrease significantly in the running times of the numerical simulations. Indeed, comparing the volume and dimension of a workability test with the full size casting problem confirms the amount of this reduction. For example, in order to simulate the filling process of a 2 m × 3 m × 30 cm wall formwork, it is necessary to simulate a huge amount of 1.8 m^3 of concrete, 14.1 m^2 formwork wall boundary surface area, in presence of numerous reinforcing bars. It also consists of at least 700 L of coarse aggregate which means more than 170,000 number of 20 mm diameter coarse aggregate particles. Obviously, it needs a huge time to simulate the casting process of this wall, as a normal size structural section in concrete construction. These amounts of calculations are impossible for the capacity of the current computers. On the other hand, the workability quality failures (i.e., poor filling, dynamic segregation, and blocking) are not expected to happen in all zones of the formwork. Indeed, the concrete can keep its homogeneity and proper flowability in majority spaces of the formwork. It means that simulation of the whole casting process would waste time or can even lead to less convergences in the calculations, according to accumulation of the calculation errors corresponded to all the simplifying assumptions.

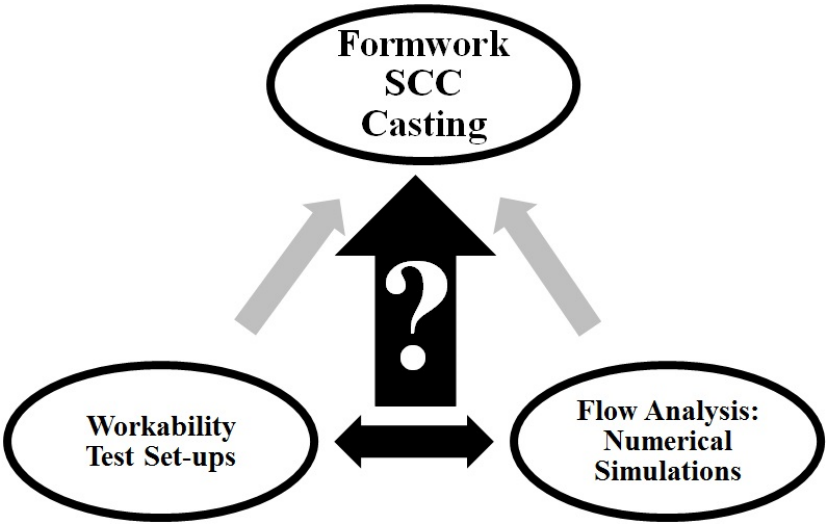

Figure 3. 2 Making relation between the numerical outputs of the theoretical flow analyses and experimental/theoretical results of the workability tests

- As an example, the L-box test can evaluate well the flow performance of concrete in presence of bars and at the same time can assess the flowability of the mixture in

horizontal and vertical directions. Moreover, simulation of dynamic segregation of same concrete mixtures in the L-Box test set-up needs to consider only 12 L of concrete volume (i.e. 1/150 smaller than the full size casting), 0.71 m^2 wall boundaries surface area (i.e. 1/20 smaller area than the wall formwork), and enormously less number of reinforcing bars and solid particles, while having the same clear spacing as in the formwork. Therefore, having almost the same congestion and restriction flow conditions in the L-Box test and the wall, the calculation time to predict dynamic stability of the investigated mixture can significantly decrease. Consequently, the results of the heterogeneous simulation of L-Box test can be used to predict the heterogeneity behavior of concrete in the critical zone, which were determined previously using the single fluid simulation of the wall casting process. In this way, better physical agreements between the quantitative and numerical results of the theoretical predicting models and the qualitative responses of the workability tests can be found.

- Therefore, it is necessary primarily to select proper workability tests depending on given construction application, casting conditions, and casting quality demands to represent flow behavior of the concrete mixture. These can be classified based on vertical and horizontal applications, self-leveling and self-consolidating properties, and demanded levels of flowability, passing ability, and stability through restricted or non-restricted spaces in the formwork. Regarding the empirical tests corresponding to workability of SCC, L-Box and T-Box set-ups can be selected as the most comprehensive tests which can evaluate almost all of the flow characteristics of SCC during casting process, such as flowability, passing ability, and dynamic stability in different directions (vertical and horizontal). L-Box and T-Box tests can evaluate filling ability of SCC in reinforced and non-reinforced zones of the formwork, respectively, which can be important for structural, rehabilitation, and repair applications. On the other hand, unlike the slump flow and J-ring set-ups, the minimum thickness of the flow profile in both L-Box and T-Box tests are more than 3 times larger than the maximum size of the aggregates. Therefore, these set-ups can represent the behavior of the reference concrete mixture. Moreover, compared to other empirical tests, L-Box and T-Box set-ups are more adjustable to become able to evaluate the effect of higher gravitational forces, longer

distance traveled by the flow, narrower gaps between the obstacles. This can be done by increasing the height of the vertical part and length of the horizontal channel in L-Box set-up, increasing the number of cycles in T-Box set-up, and modification of the distribution of reinforcing bar obstacles in the L-Box channel. This can lead to providing more similar conditions which exist in the predetermined critical zones of the casting process.

- Another advantage of numerical simulations of concrete flow consists in evaluating the effect of a wide range of the rheological parameters, including plastic viscosity, yield stress, and shear elasticity modulus of the flowable portion of the concrete matrix (i.e., cement paste and mortar) on flow characteristics of SCC as a heterogeneous material. This can be much more expensive and time consuming by experimental measurements. However, this evaluation is missed in the literature. Actually, the effect of yield stress was only considered on the final flow spread. On the other hand, the effect of different values of plastic viscosity on evolution of the flowability, passing ability, and dynamic stability of SCC during flow period were not evaluated. Considering the effect of rheological parameters of the fluid components of the concrete suspension using numerical analyses can lead to classify the SCC mixtures based on the flow performance properties and construction quality demands in order to find the optimum mixture proportioning to reach the desired rheology.

- Apart from the rheological behavior of suspending fluid, the solid parts of the flow, including aggregates and reinforcing obstacles play the second important role on flow characteristics of SCC in a casting problem. Accordingly, the effect of particle-particle and particle-bars interactions, as well as the different coarse aggregate content, aggregate collisions, and various bar spacings on flow performance properties of SCC are necessary to be taken into consideration in the numerical simulation and flow analysis process. This can lead to develop some technical tools to optimize the proportioning of aggregates, and also to modify the design of the formwork in terms of geometry, density and spacing of the reinforcing bars, in order to satisfy the construction quality demands.

3.4 Summary

In summary, regarding the gaps observed in the published literature in the field of numerical simulation of fresh SCC flow, this thesis aims to study the following items:

3.4.1 Homogeneous analysis

In order to confirm the feasibility of using single fluid analysis method, new analytical method will be employed to predict flow performance of SCC in workability tests, specifically the L-Box set-up. On the other hand, numerical simulation of L-Box test and full scale casting of SCC are carried out by assuming the investigated SCC mixtures as single homogeneous materials. This can lead to evaluate the flowability and passing ability of the investigated mixtures in horizontal and vertical directions using different formwork geometries. The numerical predictions can also be verified by comparing the experimental results of the flow of SCC in the L-Box set-up and full size casting. On the other hand, the outputs of the numerical simulations can lead to provide some insights on the heterogeneous behavior of the mixtures and to determine of critical zones of dynamic segregation and blocking.

3.4.2 Heterogeneous analysis

Flow characteristics of SCC in the workability test set-ups is simulated numerically as a heterogeneous suspension material. The empirical set-ups of L-Box and T-Box are simulated. These set-ups can evaluate comprehensively the main three quality demands of flowability, passing ability, and dynamic stability in both horizontal and vertical direction and in presence and absence of reinforcing bar obstacles. In these simulations, the effect of the rheological parameters of fluid part of the concrete suspension on flow characteristics of SCC during casting process is evaluated. Consequently, the SCC mixtures is classified based on the effect of the rheological parameters on flow characteristics of SCC, using the results of the numerical simulations of heterogeneous analysis of L-Box and T-Box tests. Moreover, the coupled effect of reinforcing bars and coarse aggregate content on the heterogeneous flow behavior of SCC mixtures during casting is also analyzed.

3.5 Objectives

The main objectives of this project can be expressed as establishing theoretical models to predict of flow performance (including flowability, passing ability, and shear-induced and gravitational dynamic segregation) of SCC during casting process, as a homogeneous and heterogeneous material. Accordingly, the specific objectives of this study can be summarized in two main groups of homogeneous and heterogeneous analysis. It must be noted that the results of each objectives were submitted as the technical research papers to different scientific journals.

3.5.1 Analytical modelling of flow of fresh SCC in the L-Box test set-up (Homogeneous analysis)

- Developing new analytical models to simulate flow performance of SCC, as a single homogeneous fluid, in L-Box test set-up.

- Study the effect of application of different rheological models, including Bingham and Herschel-Bulkley models, on accuracy of analytical predictions.

- Comparison between the accuracy of the analytical models and CFD numerical simulation in order to predict flow performance of SCC, as a single homogeneous fluid

- Verification of theoretical predictions with experimental results

3.5.2 Numerical simulation of SCC casting of a reinforced L-Shaped beam using CFD (Homogeneous analysis)

- Developing numerical simulation to predict flow performance of SCC in a full scale reinforced beam

- Verification of evolution of free surface profile shapes of the investigated mixtures during casting period with experimental results

- Evaluation of effect of plastic viscosity of SCC on flow characteristics in horizontal direction (along the beam) in terms of flowability and passing ability.

- Evaluation of effect of plastic viscosity on flowability of SCC in vertical direction through different shaped sections

- Prediction of critical zones of higher risk of dynamic segregation and blocking using results of the single fluid simulation of SCC flow

3.5.3 Numerical simulation of flow of SCC in L-Box test set-up as a heterogeneous suspension of coarse aggregate and a non-Newtonian suspending fluid – Effect of rheological parameters on flow performance

- Evaluation of effect of rheological parameters, including plastic viscosity, yield stress, and shear elasticity modulus of suspending fluid on flowability, passing ability, and dynamic stability of SCC, flowing in the horizontal and vertical directions

- Evaluation of the effect of density difference between suspending fluid and coarse aggregates on flow characteristics of SCC, in the horizontal and vertical directions

- Classification of SCC mixtures based on filling ability, as a contribution of flowability and passing ability properties, and rheological parameters

3.5.4 Numerical simulation of coupled effect of reinforcing bars and coarse aggregate content on flow characteristics of SCC in horizontal and vertical directions (Heterogeneous analysis)

- Evaluation of effect of different coarse aggregate contents on flowability, passing ability, and dynamic segregation of SCC suspension

- Evaluation of effect of reinforcing bar distributions and spacings on flowability, passing ability, and dynamic segregation of SCC

- Evaluation of bar-particle coupled effect on flow characteristics of SCC in the horizontal and vertical directions

3.5.5 Numerical simulation of flow performance of SCC in T-Box test set-up using CFD (Heterogeneous analysis)

- Evaluation of effect of plastic viscosity of suspending fluid on flowability and dynamic stability of SCC in non-restricted flow conditions (T-Box test), in the horizontal and vertical directions

- Evaluation of effect of yield stress of suspending fluid on flowability and dynamic stability of SCC in non-restricted flow conditions (T-Box test set-up), in the horizontal and vertical directions

- Classification of SCC mixtures based on non-restricted performability of SCC, as a contribution of flowability and dynamic stability properties, and rheological parameters

CHAPTER 4 THESIS METHODOLOGY

4.1 Analytical approach

As presented earlier, the analytical models predicting flow of SCC in workability tests were mostly developed using dimensional analysis. On the other hand, these models only considered the final shape of the flow profile in the stoppage state of the concrete. In this study, the effect of rheological parameters, and different levels of gravitational forces on the evolution of the free surface profile of SCC in a modified L-Box set-up is modeled using Dam Break Theory. The flow of SCC in the L-Box set-up is very similar to the dam break flow and can be described as a free surface transient flow of a non-Newtonian viscoplastic material. Dam break flow occurs when a volume of fluid is instantaneously released and flow, driven by gravitational forces, through a domain. This type of fluid motion has wide applications in hydraulic engineering [188-190] and has been also applied for viscoplastic materials [95, 191-196].

The proposed model in this study is developed based on the Matson and Hogg [193], which predicted 2D dam break flows of viscoplastic fluids using a Herschel-Bulkley constitutive law and a lubrication model of motion. Accordingly, the velocity is predominantly horizontal, and the pressure is approximately hydrostatic. The concrete is considered as an incompressible fluid with yield stress flowing under gravitational forces, using both Bingham and Herschel-Bulkley models. Neglecting the inertia effect, for flows over horizontal surface, the motion can be arrested when the gravitational and viscous forces driving the flow are unable to overcome the fluid's yield stress. The evolution of flows is derived by numerically integrating the equations of motions. Using an analytical solution, perturbation [100, 197] to the final state is calculated resulting in the determination of flow profile from initiation to a stationary state.

The modelled modified L-Box set-ups consisted of two different initial casting heads of 0.5 and 1.1 m in the vertical compartment of the apparatus, as well as a 1.5 m long horizontal channel. This design can lead to evaluate the effect of different levels of gravitational forces in longer horizontal domain. On the other hand, the analytical prediction models are proposed for two

different rheological models of Bingham and Herschel-Bulkley. The applicability and accuracy of these models are compared and verified by the experimental data of some SCC mixtures with different levels of static stability. Moreover, the experimental measurements are carried out in different waiting times to evaluate the effect of static stability of the mixtures on accuracy of the analytical predictions.

4.2 Numerical approach

4.2.1 FLOW3D® software

In order to carry out the numerical simulation of flow of SCC, a CFD software which is called FLOW3D® is employed. The free surface flows can be modeled with the Volume of Fluid (VOF) method (more details on VOF can be found in chapter 2). FLOW3D® has all of the ingredients recommended for the successful treatment of free surfaces. Moreover, the software incorporates major improvements beyond the original VOF method to increase the accuracy of boundary conditions and tracking of interfaces. The program increases its capability by using free gridding, fractional area volume obstacle representation (FAVOR), improved volume of fluid technique (truVOF), and multi block meshing system. FAVOR gridding approach combines the advantages of simple rectangular grids with the flexibility of deformed and body-fitted grids. Fixed grids of rectangular control elements are simple to generate and possess many desirable properties (e.g., improved accuracy, smaller demands on memory, and simpler numerical approximations). The approach is referred to as “free-gridding” because grids or geometry can be freely changed, each independent of the other. This feature eliminates the tedious task of generating body-fitted or finite element grids. Advanced features such as conforming meshes make it possible to have highly-refined grids only in relevant regions of the computational domain. Using this feature it is possible to generate meshes that conform to very thin components or void regions while retaining a coarser grid in the surrounding region [198].

FLOW3D® offers a multitude of meshing capabilities, such as; linked, nested, conforming, and/or partially overlapping mesh blocks, and body-fitted finite element meshes, that are designed to be simple yet efficient and robust in modeling complex flows. The use of multiple

mesh blocks allows local refinement in areas of interest and significantly reduces computational times required for a given simulation (Fig. 4.1).

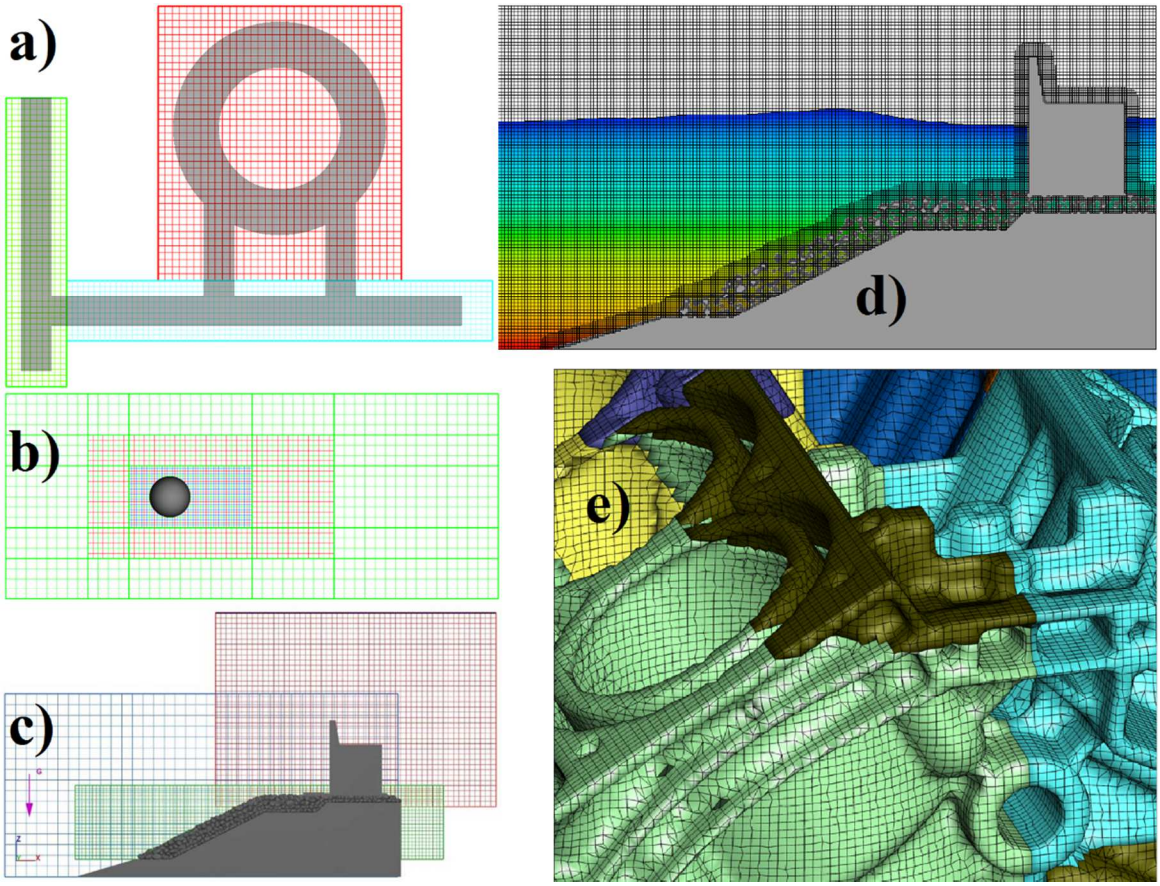

Figure 4. 1 Meshing capabilities provided by FLOW3D: a) linked meshes, b) conforming meshes, c) nested mesh block, d) partially overlapping mesh, e) finite element mesh [198]

There is recently big interests to employ FLOW3D® software to simulate various flow problems in many industrial and research applications, such as aerospace, automotive, biotechnology, coastal and maritime, coating processes, metal casting, energy, inkjets, manufacturing, micro fluids, and hydraulics and hydrology, and environmental applications [198].

As in many other commercial codes, the steps of a problem solution using FLOW3D® can be listed as follows:

1. The flow domain is defined using predefined geometrical tools of the software or importing files from a drawing software (e.g., AutoCAD).

2. The initial and interface boundary conditions are defined in the software. These boundary conditions include wall or symmetry, continuative or periodic, and specified pressure, velocity, or volume flow rate, or outflow in or towards different directions.

3. Volume is discretized by constructing a computational grid system. Each mesh block include six mesh planes in x, y, and z directions. A proper boundary condition is allocated to each plane of the mesh blocks.

4. Physical parameters are defined, such as compressibility, elasto-visco-plasticity, rheological models, gravity and non-inertial reference frame, moving and/or deforming objects, presence of friction, collision models, and turbulence of flow. For each of the physical aspects, the proper physical parameters should be assigned as the inputs of the model, such as the rheological parameters and density of the fluid, properties of particles, and other solid objects, gravitational acceleration, friction coefficient, surface tension constants, coefficient of restitution, degree of freedom, and initial conditions of the moving objects.

5. Choosing numerical items which include determination of the initial and minimum calculation time steps, selecting implicit or explicit solving options, and order of momentum advection. On the other hand, depending the type of the flow problem, a finishing condition should be assigned for the model. For example, for a simulation of whole process of casting a formwork, the fill fraction of the formwork volume should be set as unity. Therefore, once the formwork gets its maximum filling degree, the numerical simulation terminates. An optional finish time can also be chosen to simulate a limited period of the flow.

6. A postprocessor is used to evaluate the results, in forms of the data sheets and also visualizing the results as the figures or animations.

4.2.2 General Moving Objects (GMO) technique

In order to simulate the motion of the moving boundaries, such as the gate in L-Box test, or the cone of the slump flow, or the suspended particles in the heterogeneous simulation by FLOW3D® software, a General Moving Object (GMO) technique is employed. A general moving object (GMO) is a rigid body under any type of physical motion which is either dynamically coupled with fluid flow or prescribed. It can move with six degrees of freedom or rotate about a fixed point or a fixed axis. The GMO model allows to have multiple moving objects in one problem, and each moving object can have any independently defined type of motion. GMO components can be of a mixed motion type, namely have translational and/or rotational velocities that are coupled in some coordinate directions and prescribed in the other directions.

A body-fixed reference system (body system), defined for each moving object, and the space reference system (space system) are employed. At each time step, the hydraulic force and torque due to pressure, gravitational, and shear stresses are calculated, and equations of motion are solved for the moving objects under coupled motion with consideration of hydraulic, gravitational, shear forces, and torques. Area and volume fractions are recalculated at each time step based on updated object locations and orientations. Source terms are added in the continuity equation and the VOF transport equation to account for the effect of moving objects to displace fluid. The tangential velocity of the moving object boundaries is introduced into shear stress terms in the momentum equation. Implicit numerical method is recommended to calculate iteratively coupling of fluid flow and GMO motion in each time step, using the force and velocity data from the previous time step.

The GMO model also includes the capability to simulate rigid body collisions. Collisions are assumed to be instantaneous. They are allowed to occur between moving rigid bodies, and between rigid bodies and wall/symmetry boundaries of the computational domain. At each time step, once a collision is detected, a set of impact equations are integrated. Depending on the value of coefficient of restitution, a collision can be perfectly elastic, partially elastic or completely plastic. Friction at the point of contact is also allowed to exist during collision. There

can be relative sliding between two colliding bodies at their contact point and the speed and direction of sliding can vary throughout the collision process.

4.2.3 Inputs of the numerical models

According to the governing equations which should be solved in the numerical simulations (i.e., Navier-Stokes/Cauchy equations, equations of motion, mass, and energy), the input variables of the numerical simulations, corresponding to the characteristics of the materials consist of:

1. **Rheological parameters of the fluid material:** These correspond to the plastic viscosity, yield stress, shear elasticity modulus, and density of the concrete as a single fluid, or the suspending fluid portion of the concrete suspension. The suspending fluid corresponds to mortar matrix or the stable and homogeneous portion of the concrete which keeps its homogeneity during the flow period. In order to take into consideration of slippage, friction coefficient of interface of the fluid and solid objects are also considered. Accordingly a wide range of rheological parameters are used in this study, as follows: plastic viscosity between 10 to 50 Pa.s, yield stress between 14 to 75 Pa, shear elasticity modulus of 100 and 1000 Pa, and density of 2000 and 2500 kg/m^3.

2. **Characteristics of the solid materials:** These variable include density of the solid particles and the friction coefficient between solid particles, between solid particles and reinforcing bars, and between solid particles and formwork walls. In order to take into consideration of collision model, the coefficient of restitution of particle-particle, particle-bars, and particle-walls interactions are necessary to be entered to the simulations as the input. Accordingly two different initial volumetric contents of 4.6% and 8.7% of spherical particles with diameter of 20 mm and density of 2500 kg/m3 were considered in this study. In order to evaluate the effect of obstacles, different distributions of 12 mm diameter reinforcing bars were considered. Coefficients of friction and restitution of 0.4 (according to Coulomb's law of friction) and 0.8, respectively, are applied in the numerical simulations to consider the effect of frictional stresses and particle-particle, particle-bars, and particle-wall boundaries interactions.

4.3 Feasibility study of application of single fluid assumption in numerical simulation of flow of SCC as a homogeneous material

In this section, the ability of the CFD software to simulate the flow of SCC as a homogeneous single fluid and to establish relationship between SCC flow model in full casting simulations and those in workability tests are examined. In order to do that, the FLOW3D® software is employed to simulate flow of a SCC mixture in a reinforced wall, and three typical workability tests of slump flow, V-funnel, and L-Box set-ups. The results of the simulations of the workability tests are compared to the wall casting analyses in four different zones of the formwork.

4.3.1 Wall casting simulation

Numerical simulation of casting of a reinforced wall with 3.16 m length, 2.12 m height, and 0.46 m width is presented in this section. As can be observed in Fig. 4.2, the simulation consisted of the reinforcing bars with 20 mm diameter in x, y, and z directions. The concrete is cast by a 12 cm diameter pump located in top left corner of the formwork and middle of the width in y direction, with 20 L/s flow rate. The modelled concrete is assumed as a single homogeneous fluid with yield stress of 15 Pa, plastic viscosity of 25 Pa.s, shear elasticity modulus of 100 Pa, and density of 2500 kg/m^3.

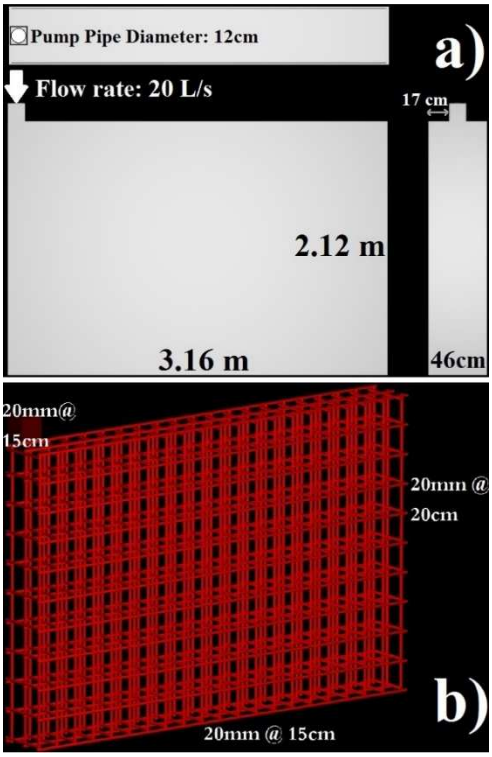

Figure 4. 2 a) Schematics of the wall to be cast by 20 L/s pumping, and b) reinforcing bars spacing and distributions

The evolution of free surface flow profile of the concrete, simulated by the FLOW3D® software, is presented in Fig. 4.3 for different flow times of t = 10, 30, 100, and 149 s.

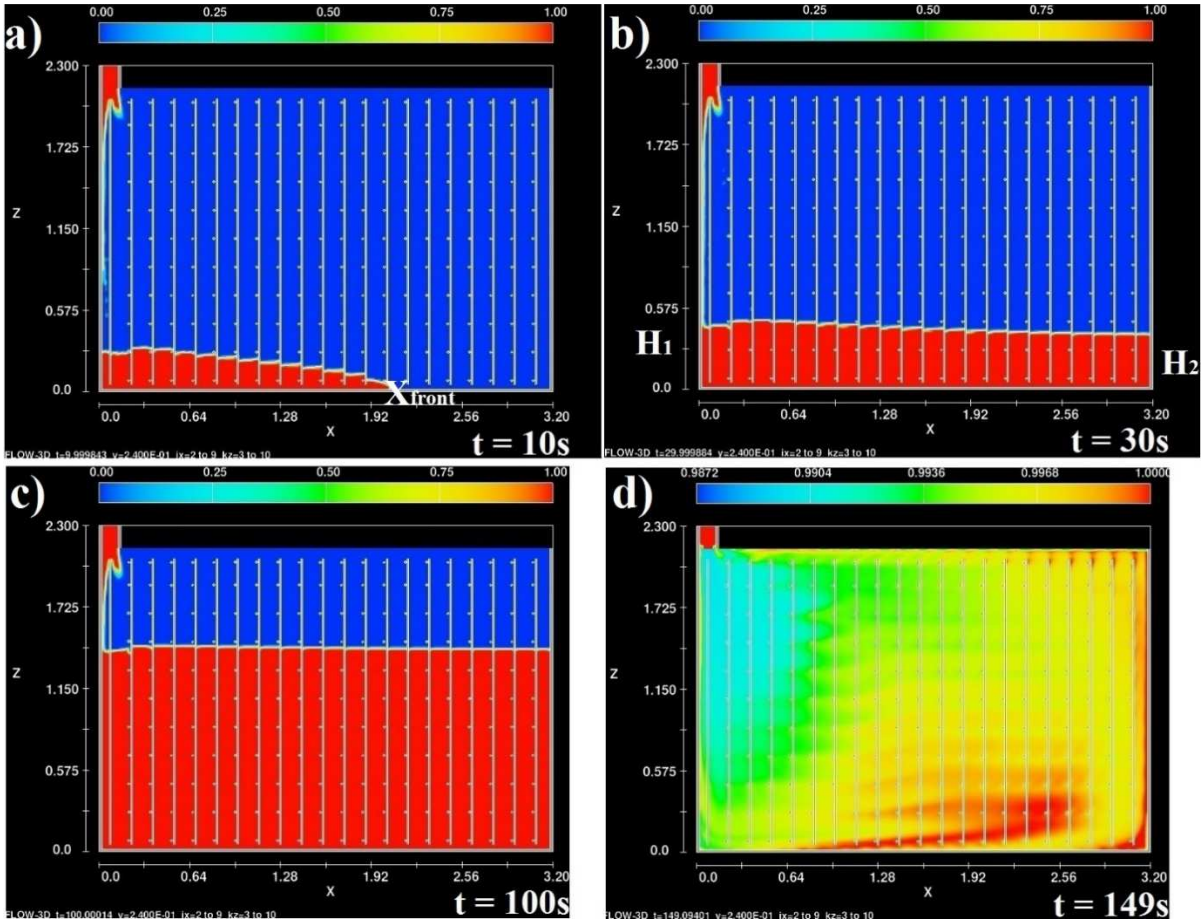

Figure 4. 3 Screen shots of numerical simulation of the evolution of free surface flow profile of the concrete in the wall formwork in flow times t = a) 10 s, b) 30 s, c) 100 s, and d) 149 s

The predicted values of the flow front position and H_2/H_1 values for the casting period are presented in Fig. 4.4, where X_{front} is the front position of the flow, H_1 is the height of the concrete beneath the casting point, and H_2 is the height of the concrete at the opposite side of the casting point, located in the end side wall of the formwork. As can be observed in Fig. 4.4, X_{front} and H_2/H_1 values increase with time till gradually tend to the maximum values of 3.16 m and 1.00, respectively. These curves can indicate the filling ability of the investigated SCC mixture.

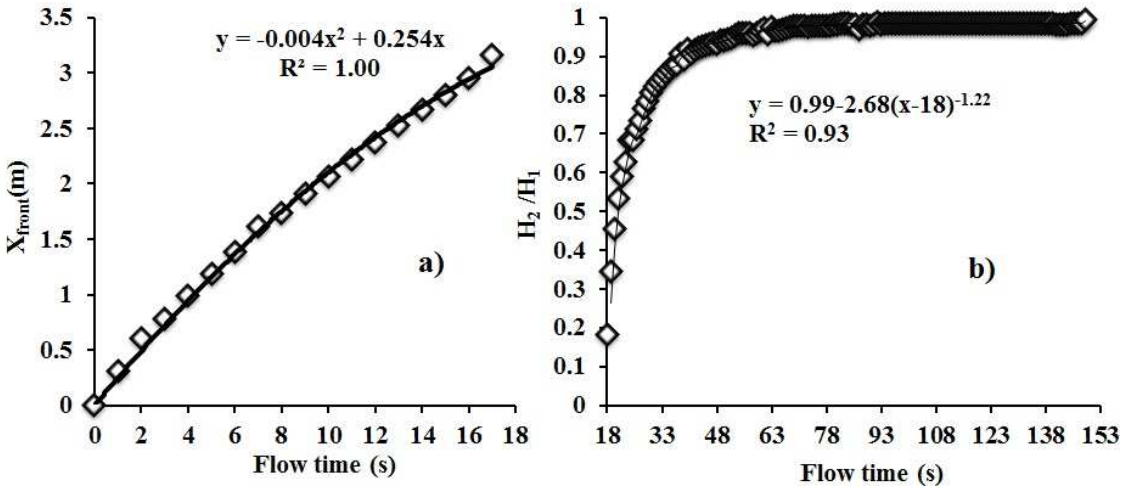

Figure 4. 4 a) Position of flow front (X_{front}) and b) H_2/H_1 values, versus flow time

The pressure exerted on the wall can also be predicted during the flow period. As presented in Fig. 4.5, the maximum pressure values, obtained at the bottom of the formwork, increases with increasing in the H_1 values with a very good correlation ($R^2 = 1$).

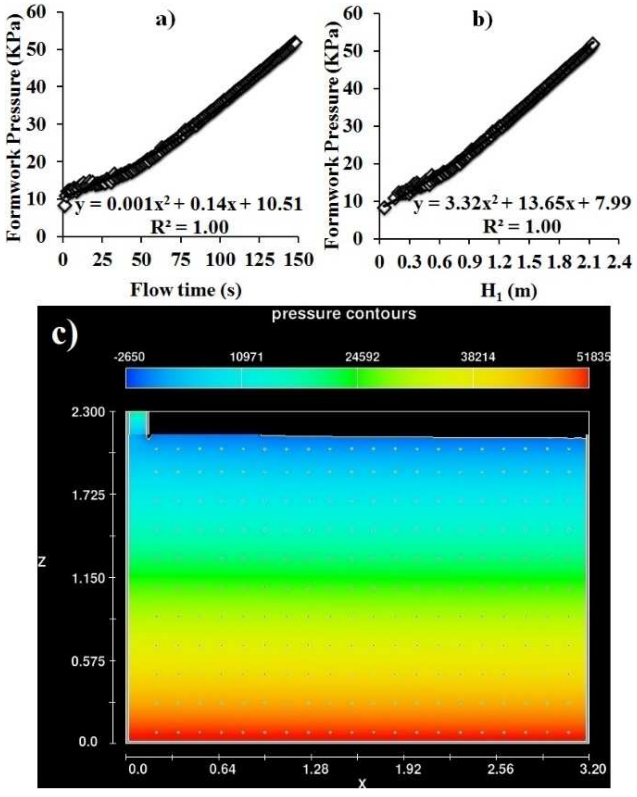

Figure 4. 5 Maximum formwork pressure versus a) flow time, b) H_1, and c) final pressure distribution

4.3.2 Numerical simulation of workability tests

The flow of the same mixture cast in the wall, is simulated in three workability tests of SCC, including slump flow, V-Funnel, and L-Box set-ups. The evolution of flow profiles during the flow period in these simulated tests are presented in Fig. 4.6.

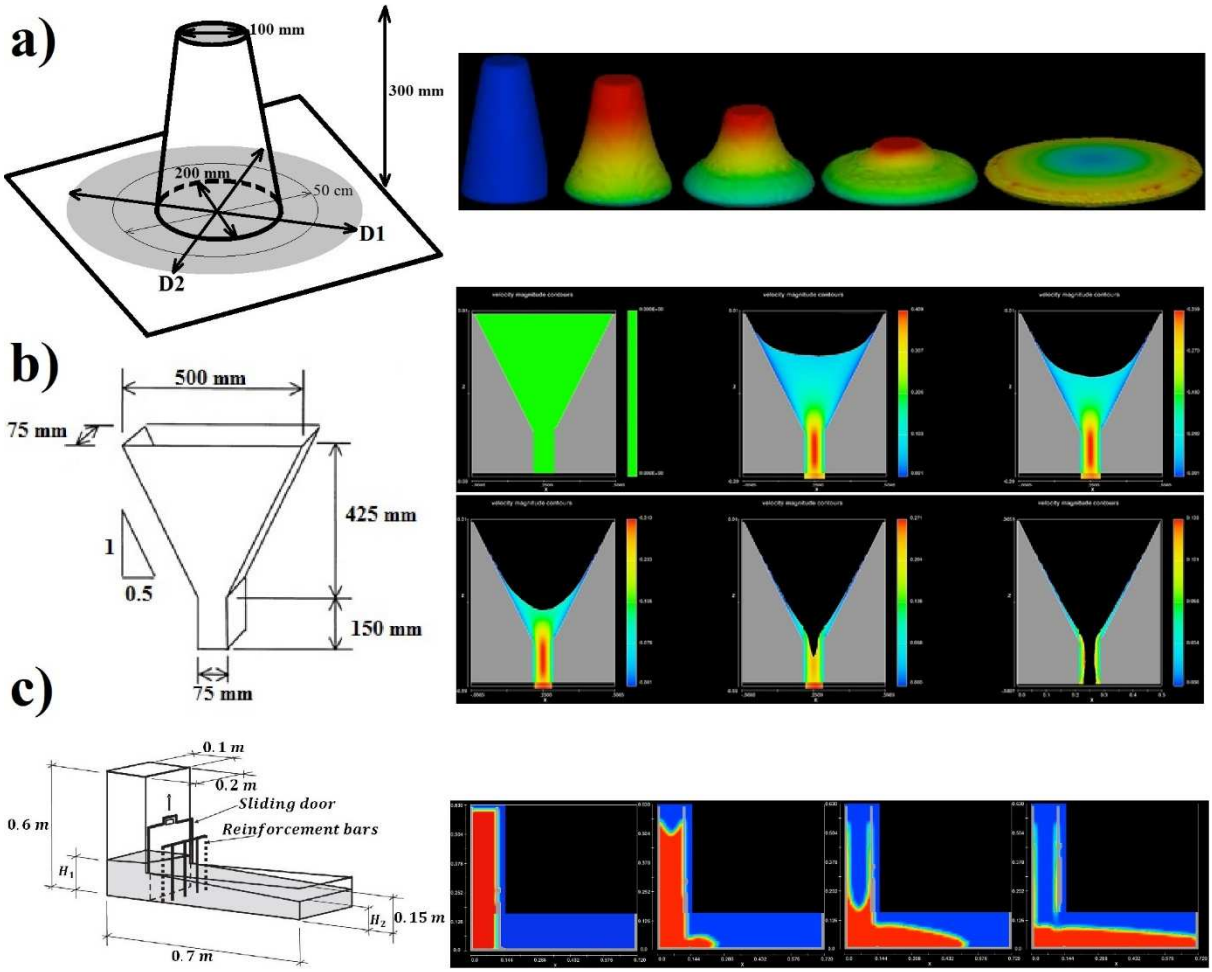

Figure 4. 6 Numerical simulation of workability tests: a) slump flow, b) V-funnel, and c) L-Box set-ups

The results of numerical simulation showed that FLOW3D software can successfully simulate flow of SCC in different flow conditions, providing by different workability tests, to evaluate flow performance of SCC as a homogeneous single fluid.

4.3.3 Relationship between results of numerical simulations of wall casting and workability tests

As presented in Figs. 4.7 and 4.8, the simulated ranges of flow velocity and strain rates in the workability tests are compared to those which were obtained in four different zones of the wall, located in 1) left bottom, 2) right bottom, 3) right top, and 4) left top corners of the formwork.

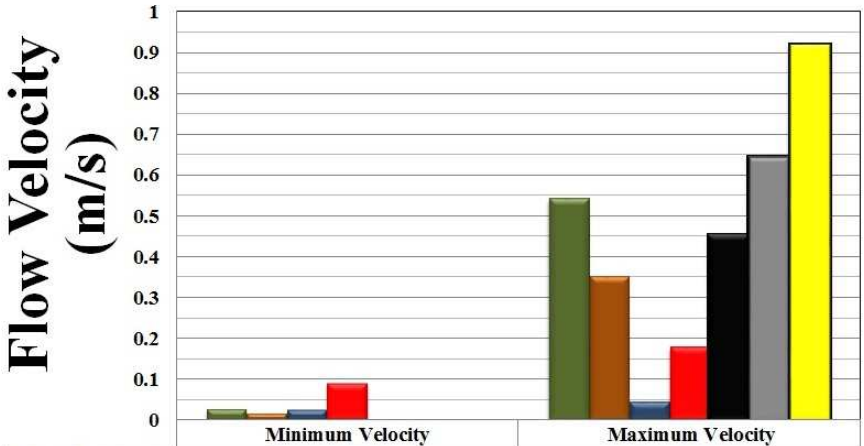

	Minimum Velocity	Maximum Velocity
1 (Left Bottom)	0.0269	0.541
2 (Right Bottom)	0.015	0.351
3 (Right Top)	0.0231	0.0424
4 (Left Top)	0.0873	0.177
Slump Flow	0	0.453
L-Box	0	0.646
V-Funnel	0	0.92

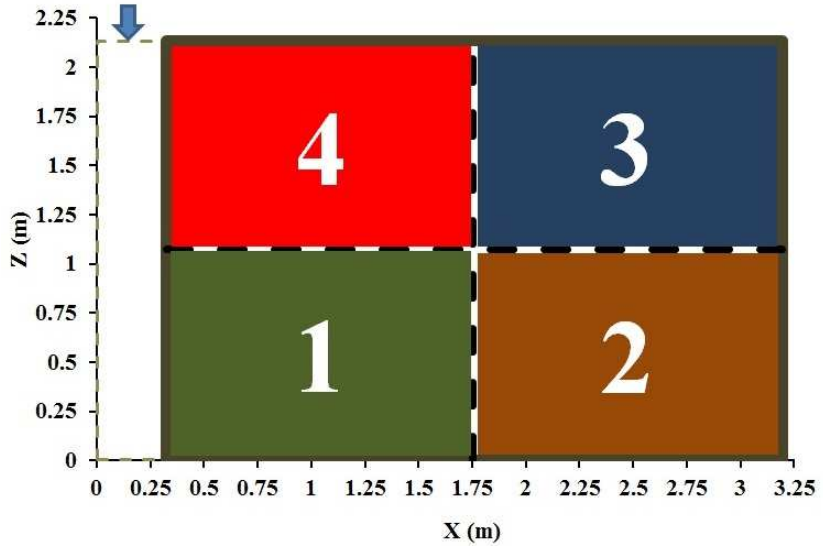

Figure 4. 7 Comparison between the range of flow velocity in workability tests and 4 different zones of the cast wall

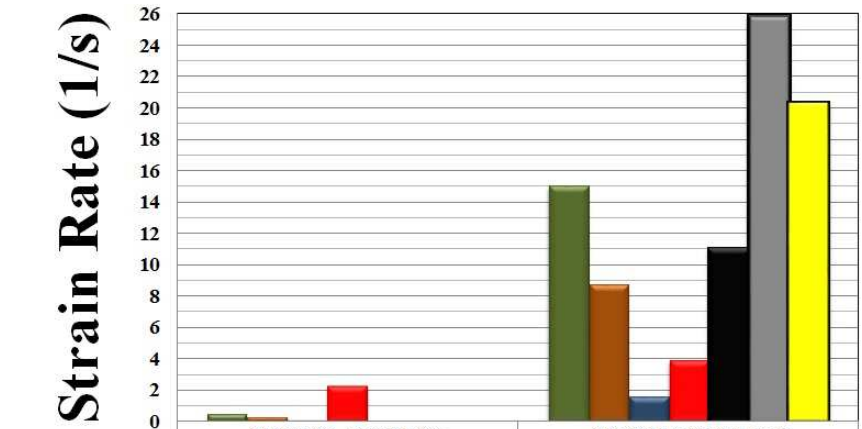

	Minimum Strain Rate	Maximum Strain Rate
1 (Left Bottom)	0.478	15
2 (Right Bottom)	0.297	8.66
3 (Right Top)	0.0603	1.56
4 (Left Top)	2.21	3.85
Slump Flow	0	11
L-Box	0	25.9
V-Funnel	0	20.3

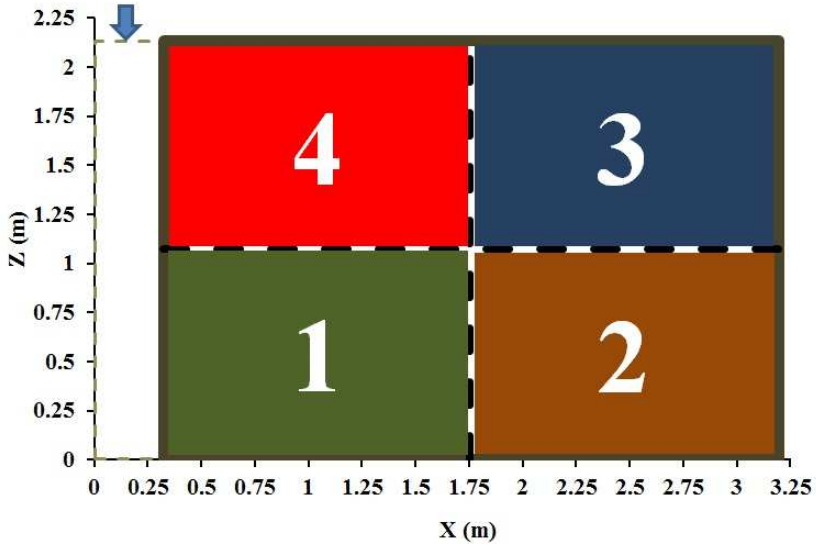

Figure 4. 8 Comparison between the range of flow strain rate in workability tests and 4 different zones in the cast wall

The results presented in Figs. 4.7 and 4.8 confirm that the use of FLOW3D® software and VOF method can successfully simulate the flow of SCC in workability tests and full-scale casting. These results are in qualitative agreement with the well-known ranges of the values of flow behavior of SCC, such as, final spread, flow velocity, and strain rate, in different casting applications and workability tests [29]. Moreover, it can be concluded that flow of SCC in the common workability tests can reach comparable velocity and strain rate magnitudes than those

obtained in a full-scale casting in different locations of the formwork, especially for L-Box set-up. For example, the maximum values of flow velocity and strain rate in the cast wall were obtained in the zone no.1, located at left bottom corner of the wall formwork, are 0.541 m/s and 15 s^{-1}, respectively. On the other hand, the flow of the investigated SCC in the L-Box set-up exhibited the maximum flow velocity and strain rate magnitudes of 0.646 m/s and 25.9 s^{-1}, which are 19% and 75% higher than those obtained in the wall casting simulation, respectively.

Therefore, in order to achieve the objectives presented in the chapter 3, Dam Break Theory and VOF methods can be employed to simulate analytically and numerically the flow performance of SCC. The procedure and results of these simulations are presented in the next chapters. These results are submitted for publication in scientific journals.

It should also be noted that in order to consider effect of size of the mesh cells on accuracy of the simulations and on the other hand calculation time, different grid resolutions from very fine to large cells (i.e., 0.001 m to 0.05 m) are examined in this study. According the preliminary results, the optimum size of 0.005 m for discretization of reinforced sections (around reinforcing bars) and spherical particles, and 0.02 m for non-restricted sections and single fluid simulations were obtained.

CHAPTER 5 ANALYTICAL AND NUMERICAL MODELING OF FLOW PERFORMANCE OF SELF-CONSOLIDATING CONCRETE USING THE DAM BREAK THEORY AND CFD

Authors and Affiliations:

Masoud Hosseinpoor: Ph.D. Candidate, Department of Civil Engineering, Université de Sherbrooke, Sherbrooke, Quebec, Canada, J1K2R1
Email: masoud.hosseinpoor@usherbrooke.ca

Ammar Yahia: Associate Professor, Department of Civil Engineering, Université de Sherbrooke, Sherbrooke, Quebec, Canada, J1K2R1
Email: ammar.yahia@usherbrooke.ca

Kamal H. Khayat: Professor, Department of Civil, Architectural and Environmental Engineering, Missouri University of Science and Technology, 224 Engineering Research Laboratory, 500 W. 16th St., Rolla, MO 65409-0710, USA.
Email: khayatk@mst.edu

Paper submitted to Computers and Concrete, An International Journal, on 7th July 2016

Abstract

Self-consolidating concrete (SCC) is designed to exhibit low yield stress to ensure high deformability and moderate viscosity to maintain homogenous suspension of coarse particles.

These properties are key parameters to ensure successful casting of SCC and adequate structural performance. The L-box test can reproduce a 3D free-surface flow of concrete that may occur in the presence of obstacles. The flow performance of SCC depends on its rheology and reinforcement density.

The main objective of this study is to evaluate the applicability of the Dam Break Theory to simulate analytically the flow profile of SCC in a modified L-box set-up given rheological properties estimated using the Bingham and Herschel-Bulkley models. SCC mixtures with low, moderate, and high stability are prepared, and their flow performance is assessed. The concrete is cast in the vertical compartment of a 1.5 m long L-box at heights of 50 and 110 cm in order to evaluate the effect of gravitational force on flow profile. A computational fluid dynamics software was also employed to simulate numerically the free surface flow properties of the investigated SCC mixtures. Unlike the Dam Break Theory models, numerical simulations take into consideration the effects of inertia and friction stresses, as well as presence of obstacles.
The analytical and numerical models results showed very good accuracy of the predicted flow profiles to describe the flow performance of SCC. The numerical simulations are found to ensure better accuracy than the analytical models. It is worthy to mention that the Herschel-Bulkley model can provide better predictions than the Bingham model.

Keywords: Bingham model; Computational Fluid Dynamics; Dam Break Theory; flow profile; Herschel Bulkley model; L-box test; rheology; self-consolidating concrete

5.1 Introduction

Self-consolidating concrete (SCC) is a deformable concrete that can spread and flow under its own weight without any mechanical consolidation to achieve uniform formwork filling, even in the presence of obstacles without blockage during the flow [24, 31, and 199]. SCC behaves as a viscoplastic material with yield stress [27, 54, and 96-98]. The existence of yield stress introduces a certain discontinuity between the flowing and stationary SCC. The evolution of the flow and the shape of free-surface profile are therefore dependent of the rheological behavior of SCC mixtures.

Viscoplastic models are used typically to describe the flow behavior of liquid materials in manufacturing industrial processes, such as food [95] and fresh concrete [27, 54, and 96-98] as well as environmental phenomena (e.g. mud flow [99-101], volcanic lava [102 and103], snow avalanche [104 and 105], and granular and debris flow [106-108 and 200].

A viscoplastic material behaves as solid for shear stress lower than the yield stress and flows when the shear stress overcomes the yield stress. The motion of a viscoplastic material is eventually arrested when the gravitational forces are in equilibrium with the viscous forces [109-114]. Consequently, the shape of the free-surface profile is directly linked to the material yield stress and density. Accordingly, some laboratory tests are developed to feature viscoplastic flows with this kind of behavior, such as Bostwick consistometer for food industry [95]. Recently, there is also a great interest to develop analytical models [115-124] and numerical simulations [125-128] to link the free surface profile of viscoplastic materials and the rheological parameters.

The design and optimization of SCC is based largely on experience and empirical testing to tailor a given passing ability and filling capacity and achieve good material performance. A possible approach to understanding SCC flow and filling performance is to develop fundamental theoretical analyses [39-41] and numerical modeling [42, 48, 93, and 94]. An extensive comprehensive review regarding numerical simulation of fresh concrete flow can be found in [44]. However, it should be recognized that modeling the flow of concrete presents a great challenge because of the necessity of taking into account the complex interaction between the various solid particles in the system, while simultaneously solving the Navier-Stokes equations for the liquid phase in which they are immersed [40]. Navier-Stokes equations governing the flow of incompressible fluids are based on Newton's 2nd law and describe the conservation of momentum.

Various empirical workability tests are developed and used to study the flow performance of SCC. For example, relationship between the final height of the concrete in the slump cone and the yield stress were proposed [39, 41, 93, 118, and 119]. The L-box test is also often used to simulate the flow conditions of SCC in the presence of obstacles. It consists of vertical and

horizontal compartments that are separated by a sliding door. The concrete is cast in a vertical compartment, and once the sliding door is opened, the concrete is gravitationally driven in the horizontal channel. Nguyen and Roussel [40] studied L-box flow behavior of limestone powder grouts with yield stress values of 15 to 150 Pa. They reported that inertia effect is not important when its value is equal or less than that of the yield stress. The authors found that if no segregation (paste level) of the material occurs during the experiment, the flow characteristics should depend only on the yield stress and plastic viscosity of the material. Accordingly, by calculating inertia stress value, in the case of SCC with the lowest yield stresses (15 Pa), the lifting rate of the gate should be around 10 s [40].

Since the L-box test and Bostwick consistometer [95] are very alike, the flow of SCC in the L-flow set-up is likewise very similar to the dam break flow and can be described as a free surface transient flow of a non-Newtonian viscoplastic material. Dam break flow occurs when a volume of fluid is instantaneously released and flow, driven by gravitational forces, through a domain. This type of fluid motion has wide applications in hydraulic engineering [188-190] and has been also applied for viscoplastic materials [95, 191-196].

The main objective of this study is to evaluate the applicability of the Dam Break Theory to simulate analytically flow profiles of SCC in the L-box test set-up using the Bingham and Herschel-Bulkley rheological models. A computational fluid dynamics software was also employed to simulate numerically the free surface flow properties of the SCC mixtures in the L-box set-ups as a homogeneous Bingham material. Unlike the Dam Break Theory models, numerical simulations take into account the effects of inertia and friction stresses as well as presence of obstacles.

The experimental program includes three SCC mixtures proportioned with slump flow of 670 ± 20 mm and different stability levels. The rheological properties of the mixtures are determined according to the Bingham and Herschel-Bulkley models.

The concrete is cast in the L-box at different initial heights to simulate the effect of gravitational forces on flow profiles of SCC. On the other hand, the effect of static stability of concrete on

the passing ability and flow profile properties is evaluated by allowing various waiting times of concrete resting in the vertical compartment. The flow profiles in the L-box set-up of the investigated mixtures are evaluated at different locations from the sliding gate. The Dam Break Theory and CFD analysis are then used to evaluate the applicability of the Bingham and Herschel-Bulkley models to simulate the flow profiles of SCC in the modified L-box test set-up. The experimental results are then compared to the estimated values obtained by the analytical and numerical models.

5.2 Mathematical formulation

Matson and Hogg [193] theoretically studied dam break flows of viscoplastic fluids using a Herschel-Bulkley constitutive law and a lubrication model of motion. In the dam break flows, the velocity is predominantly horizontal, and the pressure is approximately hydrostatic. The material is considered as incompressible with yield stress flowing under gravitational forces. Neglecting the inertia effect, for flows over horizontal surfaces or down slopes, the motion can be arrested when the gravitational and viscous forces driving the flow are unable to overcome the fluid's yield stress. The evolution of flows is derived by numerically integrating the equations of motions. Using an analytical solution, perturbation [100 and 197] to the final state is calculated resulting in the determination of flow profile from initiation to a stationary state. Matson and Hogg [193] assumed that the fluid layer is shallow and solely moving so that lubrication style asymptotic reduction of the governing equations can be applied. In the lubrication regime, the length scale of the streamwise motion far exceeds the depth of the flow [95, 103, 115, 122, 193, and 201].

Matson and Hogg [193] considered the two-dimensional slow flow of a sheet of incompressible viscoplastic fluid down an inclined plane. Although they derived a single equation for the fluid depth in a differential form in the case of inclined plane, only the case of a horizontal plane was comprehensively solved and discussed.

For the current study, the coordinate system was chosen such that the x'-axis is aligned along the channel bed, and the z'-axis is perpendicular to the channel bed. The depth of the flowing

layer is denoted by h′ (x′, t′), while the fluid density and the gravitational acceleration are noted by ρ and g, respectively. The rheology of the viscoplastic fluid is represented by the Herschel-Bulkley constitutive law which relates the components of the shear stress to the shear rate as follow:

$$\tau_{ij} = \left(K_n \dot{\gamma}^{n-1} + \frac{\tau_0}{\dot{\gamma}} \right) \dot{\gamma}_{ij} \; when \, \tau \geq \tau_0 \; and \; \dot{\gamma}_{ij} = 0 \; for \, \tau < \tau_0 \tag{5.1}$$

where K is the consistency, n is the power index (when n > 1, the material is shear thickening, and when n < 1, the material is shear thinning), τ_0 is the yield stress, and $\dot{\gamma}$ is the shear rate. The motion was studied in the 'lubrication regime', for which the characteristic length scale along the bed (L) was much greater than the characteristic fluid depth, (H). The following dimensionless variables are defined:

$$\{x', z', h', t'\} = \left\{ Lx.Hz, Hh, \frac{L}{U} t \right\} \tag{5.2}$$

where $U = \rho g H^3/\mu L$ denotes a velocity scale toward the positive x' direction and the unadorned variables are dimensionless, $\mu = K_n(U/H)^{n-1}$ is the effect of viscosity for a Herschel-Bulkley fluid where K_n is the consistency, and n is a power law index that denotes the degree of shear thinning or thickening.

The governing equations of the motion of the flowing layer with low Reynolds number (≈ 1) were formulated by combining the mass and momentum equations. The governing equation for the fluid depth is given by:

$$\frac{\partial h}{\partial t} = \frac{n}{1+2n} \frac{\partial}{\partial x} \left[\left(\frac{\partial h}{\partial x} \right)^{-2} \left(-h \frac{\partial h}{\partial x} - B \right)^{\left(1+\frac{1}{n}\right)} \left(h \frac{\partial h}{\partial x} - \frac{n}{1+n} B \right) \right] \tag{5.3}$$

The condition under which the fluid flows is given by:

$$-h\frac{\partial h}{\partial x} > B \tag{5.4}$$

where B is the Bingham number that demonstrates how the viscous forces and gravitational forces are interacting and is given by:

$$B=\frac{\tau_0 L}{\rho g H^2} \tag{5.5}$$

Consider a fluid enclosed between an impenetrable back-wall located at x = 0 and a sliding gate located at x = 1. Before opening the slide gate, the depth of the fluid behind the gate is assumed to be unity (dimensionless depth). Once the sliding gate is removed, the front position and the depth of the material are given by: $x = x_f(t)$ and $h(x_f, t) = 0$, respectively, for all times. Matson and Hogg [193] assumed that the fluid flows when the yield criterion given by Eq. (5.4) is exceeded. After a certain period of time, the fluid reaches a static profile $h_\infty(x)$, corresponding to the state at which the yield criterion is not exceeded. They also assumed that for B values less than 1/3, all the fluid behind the gate flow. Integrating Eq. (5.4) and assuming that the height at the front must be forced to be zero,

$$h_\infty(x) = \sqrt{2B(x_{f\infty} - x)} \tag{5.6}$$

where $x_{f\infty}$ is the maximum flow distance of the fluid in the channel bed. Conservation of volume gives:

$$\int_0^{x_{f\infty}} h_\infty(x)dx = 1 \tag{5.7}$$

By enforcing volume conservation, Eq. (5.7), and substitute into Eq. (5.6), the following relationships can be derived:

$$x_{f\infty} = \left(\frac{9}{8B}\right)^{1/3} \tag{5.8}$$

$$h_{\infty}(x) = \sqrt{2B\left[\left(\frac{9}{8B}\right)^{1/3} - x\right]} \tag{5.9}$$

The integration of Eq. (5.3) using an explicit finite difference scheme, the following equation is derived [193]:

$$\frac{\partial h}{\partial t} - \frac{1}{x_a}\left(\xi \dot{x}_a + \dot{x}_y\right)\frac{\partial h}{\partial \xi} = \frac{n}{1+2n} x_a \frac{\partial}{\partial \xi}\left[\left(\frac{\partial h}{\partial \xi}\right)^{-2}\left(-\frac{h}{x_a}\frac{\partial h}{\partial \xi} - B\right)^{1+1/n}\left(\frac{h}{x_a}\frac{\partial h}{\partial \xi} - \frac{n}{1+n}B\right)\right] \tag{5.10}$$

where: $\xi = (x - x_y)/(x_f - x_y)$, $x_f(t)$ and $x_y(t)$ are the instantaneous positions of the front of the flow and yield point, respectively. This equation is only applicable in the region $0 < \xi < 1$. Note that $x_y(t)$ is a point behind which the fluid does not take part in motion located between $0 < x < 1$. At $x = x_f$, $h = 0$; so boundary conditions are given by:

$h(\xi = 1, t) = 0$ for all t, and $h(x) = 1$ for $0 \leq x \leq x_y$ ($h(\xi = 0, t) = 1$)

For notational convenience, the active length is introduced as $x_a(t) = x_f(t) - x_y(t)$.

Because of the relatively low yield stress of SCC, the range of B is less than 1/3. When B is less than 1/3, the yield point reaches the back wall before the motion is arrested. For long period of time, Matson and Hogg [193] assumed that $x_y = 0$ and therefore $x_a = x_f$.

Considering the height profile as a function of ξ, it is obvious that $h(\xi, t)$ is always greater than the final profile $h_{\infty}(\xi)$, and that the front position $x_f(t)$ must always be less than $x_{f\infty}$. Hence, the positive perturbation variables $\tilde{h}(\xi, t)$ and $\tilde{x}_f(t)$ are defined to these arrested states as follows:

$$h(\xi,t) = h_{\infty}(\xi) + \tilde{h}(\xi,t) \tag{5.11}$$

$$x_f(t) = x_{f\infty} - \tilde{x}_f(t) \tag{5.12}$$

It is assumed that $\tilde{h}/h_\infty \ll 1$, $\tilde{x}_f/x_{f\infty} \ll 1$, $x_{f\infty}$ and $h_\infty(\xi)$ are given by Eq. (5.9). By substituting Eqs. (5.11)-(5.12) into Eq. (5.10) and enforcing the conservation of mass, the following relationships can be derived [193]:

$$\tilde{x}_f(t) = \left[\frac{(1+n)k}{2}\right]^n \left(\frac{3}{B^2}\right)^{(2+n)/3} \frac{1}{t^n} \tag{5.13}$$

$$\tilde{h}(\xi,t) = \left[\frac{(1+n)k}{2}\right]^n \left(\frac{3}{B^2}\right)^{(1+n)/3} \frac{E(\xi)}{t^n} \tag{5.14}$$

where k is a constant depending on the value of n and E(ξ) is the perturbation function produced during the mathematical procedure. The values of E(ξ) can be displayed for different values of n [193]. The values of k for various n are summarized in Table 5.1.

Table 5. 1 Values of the constant k for different power law indices

n	1/5	1/3	1/2	1	2	3	5
k	0.3758	0.2936	0.2159	0.08663	0.01419	0.002345	0.0000646

Some applications of the aforementioned theory are presented in both industry and geophysics; i.e., measuring the consistency of common industrial slurries and food purees [95]. In this paper, this method is used to predict the flow of SCC in a modified L-box test set-up and to compare experimental results with those predicted using the proposed model below.

5.3 Proposed model

Eqs (5.13)-(5.14) are mainly defined with three variables: n, μ, and τ_0. By assuming that SCC behaves as a Bingham material, the value of n is equal to unity. On the other hand, the values of the coefficient k are summarized in Table 5.1. Eq. (5.9) can then be transformed as a function of ξ as follows:

$$h_\infty(\xi) = (3B)^{1/3}\sqrt{1-\xi\frac{x_f}{x_{f\infty}}} \tag{5.15}$$

According to Mason and Hogg (2007), Eq. (5.15) can be approximated by $h_\infty(\xi) = (3B)^{1/3}\sqrt{1-\xi}$, assuming that $\tilde{x}_f/x_{f\infty} \ll 1$, which means that $x_f \cong x_{f\infty}$. However in the L-box test, when τ_0 is relatively small (SCC is more deformable), this assumption becomes somehow inappropriate. In the proposed model, Eq. (5.15) is used without any approximation. Substituting Eqs. (5.8), (5.14), and (5.15) into Eq. (5.11) yields to:

$$h(\xi,t) = (3B)^{1/3}\sqrt{1-x_f\xi\left(\frac{8B}{9}\right)^{1/3}} + \left[\frac{(1+n)k}{2}\right]^n\left(\frac{3}{B^2}\right)^{(1+n)/3}\frac{E(\xi)}{t^n} \tag{5.16}$$

Substituting Eqs. (5.8) and (5.13) into Eq. (5.12) provides:

$$x_f(t) = \left(\frac{9}{8B}\right)^{1/3} - \left[\frac{(1+n)k}{2}\right]^n\left(\frac{3}{B^2}\right)^{(2+n)/3}\frac{1}{t^n} \tag{5.17}$$

The variables n and k are replaced by their values, according to the chosen rheological model, as shown in Table 5.1. The t^n is written as a function of x_f and other parameters (Eq. (5.17)) and then injected in Eq. (5.16) to develop Eq. (5.18):

$$h(\xi) = (3B)^{1/3}\sqrt{1-x_f\xi\left(\frac{8B}{9}\right)^{1/3}} + E(\xi)\left[\left(\frac{3B}{8}\right)^{1/3} - x_f\left(\frac{B^2}{3}\right)^{1/3}\right] \tag{5.18}$$

For a fixed value of B, Eq. (5.18) gives the height profile for any x_f. This equation will be used to estimate flow profiles of SCC in the L-box test set-up. The values of $E(\xi)$ can be simply interpolated from the given curve (Fig. 5.1) obtained for the Bingham rheological model (n = 1) as described in [193].

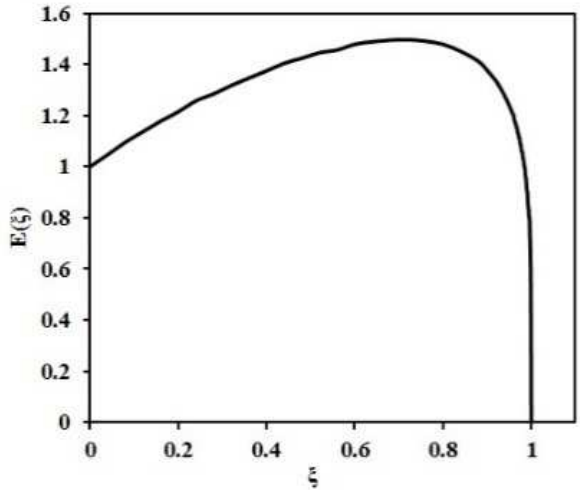

Figure 5. 1 The perturbation E(ξ) as a function of re-scaled distance ξ, when B < 1/3 for n = 1 (the Bingham model) [193]

For the Herschel-Bulkley model, the values of perturbation function E(ξ) need to be estimated as a function of power law index (n). Solving the spatial ordinary differential equation (ODE) given by Matson and Hogg [193], E(ξ) can be defined by following equation:

$$E(\xi) = \frac{1 - P(z)}{z} - z \tag{5.19}$$

where $z = \sqrt{1 - \xi}$ and values of function of P(z) can be estimated as follow:

$$P(z) \approx 1 - \frac{n+1}{n+2}\left(\frac{2}{k}\right)^{\frac{n}{n+1}} z^{\frac{n+2}{n+1}} \quad for\, z << 1 \tag{5.20}$$

The values of k from Table 5.1 can be also estimated exponentially as a correlated function of n, with a R square value of 1.00:

$$k = 0.5323e^{-1.806n} \tag{5.21}$$

The derived theoretical solutions will be compared to experimental results obtained for various SCC mixtures tested using the modified L-box with a horizontal channel measuring 150 cm in length and two different initial heads of SCC corresponding to 50 and 110 cm.

5.4 Experimental program

SCC mixtures were optimized to achieve a fixed slump flow of 670 ± 20 mm and different surface settlement values. The mixtures were proportioned with ternary blast-furnace slag cement (25% blast furnace slag, 5% silica fume, and 70% Type GU cement), a fixed binder content of 475 kg/m^3, and two water-cementitious materials ratios (w/cm) of 0.35 and 0.40. The coarse aggregate volume and sand-to-total aggregate ratio (by volume) were fixed at 30% and 0.50, respectively. Coarse aggregate with nominated maximum size aggregate of 14 mm, specific gravity of 2.70, and water absorption of 0.5% was used. River-bed siliceous sand with a specific gravity of 2.65, finesse modulus of 2.80, and water absorption of 1.2% was used. Polycarboxylate-based high-range water-reducer (HRWR) and cellulose-based viscosity enhancing admixture (VEA) were used. The HRWR had a specific gravity of 1.09 and a solid content of 27%. A set-retarder was used to enhance fluidity retention. As summarized in Table 5.2, SCC1 was proportioned with a w/cm of 0.40 and 2.25 L/m^3 of HRWR to achieve a surface settlement of 0.50%. SCC2 mixture was proportioned with similar w/cm of 0.40 and 4.7 L/m^3 of VEA to secure a surface settlement of 0.35%. SCC3 mixture had a w/cm of 0.35 and no VEA and exhibited similar stability as that of SCC2.

Table 5. 2 SCC mixtures proportioning

Mixture	SCC1	SCC2	SCC3
Binder (kg/m^3)	475	475	475
Mixing water (kg/m^3)	190	190	166
w/cm	0.40	0.40	0.35
Sand (kg/m^3)	840	840	860
Coarse aggregate [5-14 mm] (kg/m^3)	840	840	860
Sand-to-total aggregate ratio, by volume (%)	50	50	50
Polycarboxylate HRWR (kg/m^3)	2.25	10	4.0
VEA (L/m^3)	0	4.7	0
Set-retarder (L/m^3)	0.75	0.75	0.75

5.4.1 Test procedure

The concrete was mixed in batches of 90 L using an open-pan mixer with a capacity of 120 L. The mixing sequence consisted of homogenizing the sand and coarse aggregate for 1 minute before introducing 1/3 of the mixing water. The binder was then introduced along with the HRWR diluted in the second 1/3 of the water. After 3 minutes of mixing, the VEA was introduced along with the set retarder diluted in the remaining water, and the concrete was mixed for 2 minutes. Ambient temperature during mixing and testing was maintained at 22 ± 2°C. The mixtures had a constant temperature of 20 ± 1°C at the end of mixing.

The HRWR dosage was adjusted to secure an initial slump flow of 670 ± 20 mm. Following slump flow adjustment, workability and rheological properties of the investigated mixtures were evaluated. The rheological parameters of the SCC were determined using a modified IBB concrete rheometer in which the H-shaped impeller rotating in a planetary motion was replaced by a four-blade vane impeller rotating in a coaxial manner [202]. The test procedure consisted of increasing the rotational speed from 0.1 to 0.9 rps to ensure the breakdown of structure (ascendant curve) then decreasing the rotational speed gradually to determine the descending curve. The rheological parameters were determined from the descending curve using the Bingham and Herschel-Bulkley models. The rheological parameters were determined at various waiting times of 1, 5 and 15 minutes. For a given time, the concrete was poured in the bowl and covered to avoid evaporation till the measurement time.

Workability properties were also determined by the unit weight, temperature, fresh air content, J-Ring test [82], caisson filling capacity (a workability test which assesses filling ability of SCC in restricted areas [26 and 203], and flow profile in modified L-box with a clear spacing between reinforcing bars of 41 mm (Fig. 5.2). The L-box test consists of filling the vertical compartment at two different heights (50 and 110 cm) and a constant casting rate of 20 L/min. After a waiting period of 1, 5, and 15 min, the sliding door separating the vertical and horizontal compartments is smoothly removed during 5 s allowing the concrete to spread among the obstacles in the horizontal channel. The flowability and performance of SCC are evaluated after the flow

stoppage in terms of flow profile thickness at the centerline of the flow at various locations from the gate (at 0, 30, 60, 90, and 120 cm).

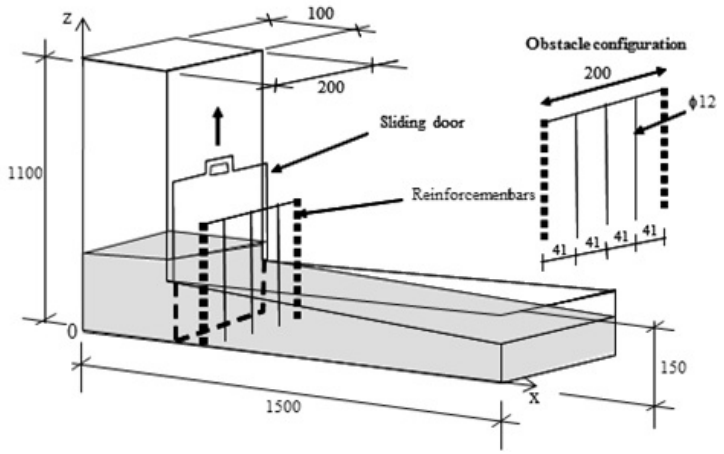

Figure 5. 2 Schematics of the modified L-box set-up used to evaluate restricted flow profile of SCC (all dimensions are in mm) [204]

5.5 Test results and discussion

Workability and rheological properties of the investigated SCC mixtures are summarized in Tables 5.3 and 5.4. The measurements for flow depth of concrete at the entrance of the horizontal channel ($H_{10\,cm}$ at x = 10 cm), the maximum flow distance in the horizontal leg of the L-box (L_{max}), and the flow time needed to the front of profile reaches 30 cm after the opening gate ($T_{30\,cm}$) are also presented in Table 5.4.

Table 5. 3 Workability results of investigated SCC mixtures

Mixture	SCC mixture cast in different initial height in vertical part of L-box	Slump flow (mm)	J-Ring (mm)	Filling capacity (%)
SCC1	SCC1-A ($h_{initial}$ = 50 cm)	660	620	89
	SCC1-B ($h_{initial}$ = 110 cm)	680	640	91
SCC2	SCC2-A ($h_{initial}$ = 50 cm)	660	640	83
	SCC2-B ($h_{initial}$ = 110 cm)	660	620	84
SCC3	SCC3-A ($h_{initial}$ = 50 cm)	690	620	88
	SCC3-B ($h_{initial}$ = 110 cm)	660	620	88

Table 5. 4 Experimental results of L-box tests and rheological parameters of the investigated SCC mixtures, approximated by the Bingham and Herschel-Bulkley models

Mix No.	Initial head (cm)	Waiting time (min)	Density (kg/m^3)	$H_{10\ cm}$ (cm)	L_{max} (cm)	$T_{30\ cm}$ (s)	Bingham model		Herschel-Bulkley model		
							τ_0^* (Pa)	μ_p^* (Pa.s)	τ_0^* (Pa)	n^*	K^* (Pa.s^n)
SCC 1	50	1	2305	6.0	103.5	0.96	94	19	8	0.59	72.95
		5	2305	5.5	142.5	1.19	88	20	46	0.75	44.21
		15	2305	5.8	102.0	1.46	101	19	46	0.69	50.78
	110	1	2340	8.5	150.0	0.55	97	14	102	1.06	11.27
		5	2340	8.5	150.0	0.64	93	16	69	0.82	29.35
		15	2340	9.0	150.0	0.97	80	19	69	0.91	23.97
SCC 2	50	1	2360	5.2	130.0	3.04	64	45	14	0.76	86.41
		5	2360	5.0	121.9	3.86	60	46	21	0.90	66.08
		15	2360	5.7	109.2	5.47	61	50	7	0.85	80.92
	110	1	2345	8.2	150.0	2.81	63	53	19	0.75	113.46
		5	2345	8.2	150.0	2.97	63	55	48	0.77	116.26
		15	2345	8.3	150.0	4.11	67	52	65	0.78	101.34
SCC 3	50	1	2385	6.0	143.9	4.43	41	56	20	0.92	68.90
		5	2385	5.2	150.0	4.61	45	69	26	0.96	65.62
		15	2385	5.0	114.5	5.48	49	56	7	0.88	80.14
	110	1	2360	9.0	150.0	2.85	42	58	20	0.92	68.90
		5	2360	9.0	150.0	3.51	46	56	26	0.96	65.62
		15	2360	9.0	135.4	4.49	49	57	28	0.92	70.52

*τ_0: Yield stress, μ_p: Plastic viscosity, n: Power index; K: Consistency.

5.5.1 Effect of rheological properties, initial casting head, and waiting time on experimental flow profiles

As can be observed in Table 5.4, using the Bingham model, the investigated mixtures exhibited yield stress and plastic viscosity values ranging from 41 to 101 Pa and 14 to 69 Pa.s, respectively. SCC1 exhibited the highest yield stress. However, SCC2 and SCC3 exhibited higher plastic viscosity.

In the case of a height of 50 cm, SCC1 having the highest yield stress values resulted in higher flow depth of concrete at the entrance of the horizontal channel ($H_{10\ cm}$) than SCC2 and SCC3. However, the yield stress did not have a significant effect on $H_{10\ cm}$ values for SCC2 and SCC 3. This can be due to the fact that the yield stress values of these two mixtures were comparable (between 41 and 64 Pa). For example, in the case of SCC1, the average value of $H_{10\ cm}$ was approximately 5.8 cm, where relatively higher depths were observed with higher yield stress, regardless of the waiting time and the plastic viscosity. Correspondingly, SCC2 and SCC3 exhibited comparable average $H_{10\ cm}$ values of 5.3 and 5.4 cm, respectively. As expected the yield stress affected the maximum flow distance L_{max} in the horizontal leg of the L-box. Indeed, concrete with higher yield stress resulted in lower the L_{max} value. For example, for the waiting time of 1 min, L_{max} value of 130.5 cm was obtained for SCC1 with yield stress of 94 Pa. In the case of SCC2 and SCC3 with yield stress values of 64 and 41, L_{max} value increased to 130.0 and 149.0 cm, respectively.

For a higher casting head of 110 cm, as expected all the mixtures achieved higher $H_{10\ cm}$ and L_{max}, and less $T_{30\ cm}$ values. However, it seems that due to more existing inertia effects, plastic viscosity has more dominant effect on $H_{10\ cm}$ values than yield stress. For example, despite that the SCC3 mixtures exhibit less yield stress values than SCC1 and SCC2 (average yield stress of 46 Pa, compared to 90 and 64 Pa), it achieved higher $H_{10\ cm}$ values (9.0 cm). This is due to higher plastic viscosity (average plastic viscosity of 57 Pa.s, compared to 16 and 53 Pa.s). Nevertheless, in this case SCC1 presented higher $H_{10\ cm}$ values (averagely 8.7 cm) than SCC2 (averagely 8.2 cm), due to higher yield stress and surface settlement values which resulted in less stability and passing ability.

By comparing the $T_{30\ cm}$ flow times, it can be observed that increasing waiting times played the dominant role on flowability of the mixtures by increasing $T_{30\ cm}$ values, regardless of the initial head of the concrete (50 vs. 110 cm). For example, in the case of 50 cm initial head, increasing waiting time from 1 to 15 min for SCC1, SCC2, and SCC3 mixtures resulted in increasing $T_{30\ cm}$ values from 0.96 to 1.46 s, 3.04 to 5.47 s, and 4.43 to 5.48s, respectively. In the case of 110 cm initial head, increasing waiting time from 1 to 15 min increases $T_{30\ cm}$ values from 0.55 to 0.97 s, 2.81 to 4.11 s, and 2.85 to 4.49 s for SCC1, SCC2, and SCC3 mixtures, respectively.

It is worthy to note that the use of waiting time of 15 minutes did not have any effect on the $H_{10\ cm}$ depth flow profile in the case of 50 cm initial head. This may due to the fact that the investigated mixtures showed a good surface settlement resistance (less than 0.50%). For example, in the case of SCC1 (less stable mixture with surface settlement of 0.45%) cast at height of 50 cm, the $H_{10\ cm}$ values obtained after 1, 5, and 15 min of waiting time were 60, 55, and 5.8 cm, respectively. In the case of SCC3 (more stable mixture with surface settlement of 0.30%), $H_{10\ cm}$ values after 1, 5, and 15 minutes were 6.0, 5.2, and 5.5 cm, respectively. When the concrete was filled to a height of 110 cm, increasing waiting time from 1 to 15 min exhibited however more effect on less stable mixture (SCC1) by increasing $H_{10\ cm}$ values from 8.5 cm to 9.0 cm. In the case of SCC (higher stability) the $H_{10\ cm}$ values are comparable (9.0 cm).

5.5.2 Analytical Dam Break Theory analysis using the Bingham rheological model

Replacing the experimental values of density and the Bingham rheological parameters from Table 6.4 in Eqs. (5.5)-(5.18), flow depth of the final profiles at different locations from the gate are predicted using the proposed model according to Dam Break Theory. The derived theoretical solutions using the Bingham model are compared to experimental results. The mean value of estimation ratio (E.R.) calculated as the ratio of predicted to measured flow profile depths, the correlation coefficient (R^2), and root-mean-square error (RMSE) values for every single analysis were used to evaluate the accuracy of the model to predict the flow behavior of SCC. RSME values were calculated as follow:

$$RMSE = \sqrt{\frac{\sum_{i=1}^{N}\left[(flow\,depth_{Experimenal_i} - flow\,depth_{Theoretical_i})^2\right]}{N}} \tag{5.22}$$

where N is the number of measurements at different locations from the opening gate (0, 30, 60, 90, and 120 cm) to be compared with theoretical results.

The overall comparison between the experimental results and theoretical predictions by Dam Break Theory, using the Bingham model are presented in Fig. 5.3 as well as comparisons for different initial casting heads of 50 and 110 cm.

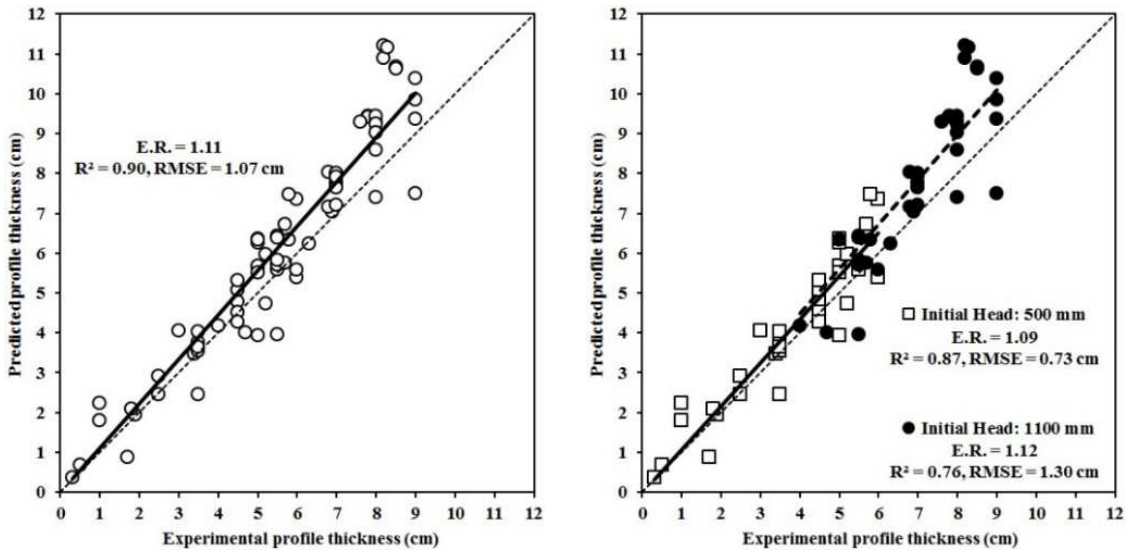

a) Overall comparison

b) Comparison for different initial casting heads of 50 and 110 cm

Figure 5. 3 Comparison between experimental (thicknesses at different locations along the horizontal channel) and theoretical results predicted by Dam Break Theory analysis using the Bingham model

As can be observed in Fig. 5.3a, the theoretical profile depths calculated for the Bingham model are in very good agreement with experimental measurements (E.R. = 1.11, R^2 = 0.90, and RMSE = 1.07 cm). On the other hand, as can be observed in Fig. 5.3b, the proposed model exhibits more accuracy in the case of 50 cm than 110 cm initial casting head. This is confirmed by estimation ratio closer to 1 (E.R. = 1.09) and less RMSE of 0.73 cm. Higher errors are occurred mostly for higher profile thicknesses corresponding to 5-6 cm and 8-9 cm for 50 and 110-cm initial casting heads, respectively. Indeed, these data are related to the initial part of the flow profile which is located in the first 30 cm from the opening gate. This discrepancy can therefore be explained by inertia effects on flow performance of SCC mixtures in initial periods of the flow.

Using experimental values of $T_{30\,cm}$ from Table 5.4, average flow velocity of the mixtures in the first 30 cm of the flow can be estimated by $V_{30\,cm} = \frac{0.3\ m}{T_{30\,cm}}$. The results provide average initial velocity values ranging from 0.05 to 0.31 m/s and 0.07 to 0.55 m/s for 50 and 110-cm initial heads, respectively. Consequently, the initial average inertia stress values can be estimated by $I_{30\,cm} = \rho V_{30\,cm}^2$. This results in average initial inertia stresses ranging from 7 to 225 Pa (i.e. 12% to 239% of the yield stress) and 11 to 686 Pa (i.e. 19% to 707% of the yield stress) for 50 and 110-cm initial heads, respectively. It means the inertia effect can have almost three times higher value when the SCC was filled to a height of 110 cm compared to 50 cm.

5.5.3 Analytical Dam Break Theory analysis using the Herschel-Bulkley rheological model

The experimental values of density and the Herschel-Bulkley parameters from Table 5.4 are replaced in Eqs. (5.5)-(5.21) to predict the flow profile thicknesses of the investigated mixtures by Dam Break Theory using the Herschel-Bulkley model. The theoretical results are compared to experimental profiles obtained for the SCC mixtures at different locations after the sliding gate for two different initial casting heads of 50 and 110 cm (Fig. 5.4).

The use of the Herschel-Bulkley model in the proposed Dam Break Theory analysis can result in very accurate prediction of the flow performance of the SCC mixtures in different L-box set-ups. This is indicated in Fig. 5.4a by the overall estimation coefficient values of E.R. of 1.05, R^2 of 0.90, and RMSE of 0.84 cm.

As discussed in the previous section, increasing initial casting head from 50 to 110 cm can lead to less accurate predictions due to inertia effects in first period of flow. Accordingly, the proposed model provides more accurate predictions in the case of 50-cm initial casting head (E.R. = 0.96 and RMSE = 0.74 cm) compared to 110 cm (E.R. = 1.08 and RMSE = 0.93 cm), as can be observed in Fig. 5.4b.

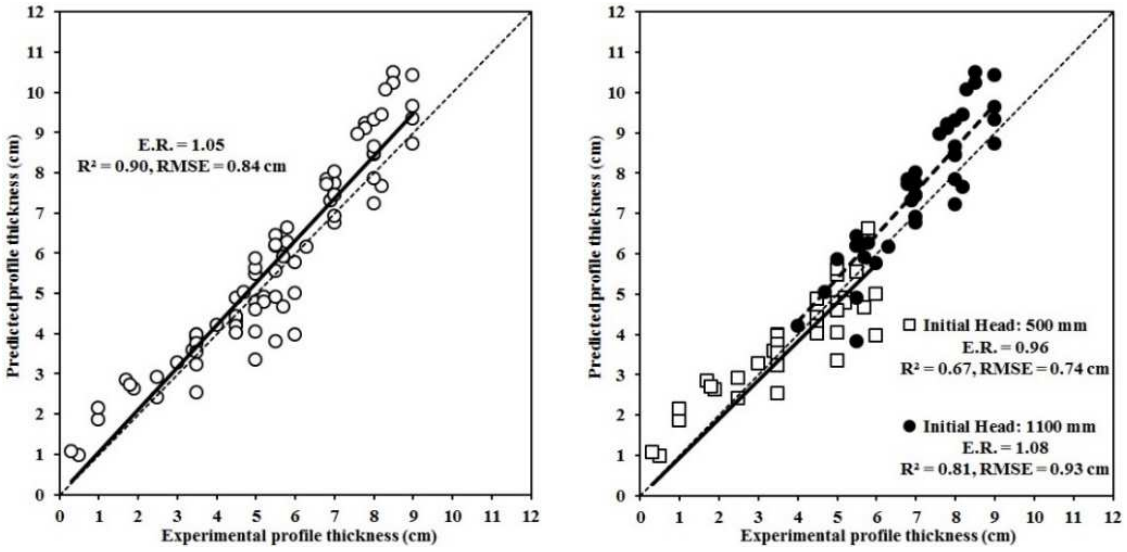

a) Overall comparison

b) Comparison for different initial casting heads of 50 and 110 cm

Figure 5. 4 Comparison between experimental and theoretical results predicted by Dam Break Theory analysis using the Herschel-Bulkley model

As can be observed in Figs. 5.3a and 5.4a, an overall comparison revealed that the Herschel-Bulkley model provided better estimation coefficients (E.R. = 1.05, and RMSE = 0.84 cm) than the Bingham model (E.R. = 1.11, and RMSE = 1.07 cm). This conclusion is valid even if the results were compared for initial heads of 50 and 110 cm (see Figs. 5.3b and 5.4b). For example, in the case of 50-cm initial head, the estimation ratio provided by the Herschel-Bulkley model (E.R. = 0.96) is more close to unity than that one provided by the Bingham model (E.R. = 1.09). The corresponding RMSE values are comparable for two models (0.73 and 0.74 cm). Similarly, for 110-cm initial head, applying the Herschel-Bulkley model resulted in less RMSE value (0.93 cm) than the Bingham model (1.30 cm), as well as better estimation ratio ($E.R._{Herschel\text{-}Bulkley}$ = 1.08, and $E.R._{Bingham}$ = 1.12). This suggests that under higher shear rate magnitudes, the Herschel-Bulkley model can describe the behavior of the SCC mixtures better than the Bingham model.

Since the overall estimation ratios of the proposed models applied for both the Bingham and Herschel-Bulkley models are more than unity ($E.R._{Herschel\text{-}Bulkley}$ = 1.05, and $E.R._{Bingham}$ = 1.11), it can be concluded that the proposed models slightly overestimated the flow profile depths of

the investigated SCC mixtures. This can be due to the fact that the proposed Dam Break Theory solutions neglected the effect of presence of the obstacles (three reinforcing bars). Therefore, the analytical models are not able to take into account the decreasing effect of the bars on the final flow profile depths which is called passing-ability of SCC.

5.5.4 Numerical simulation of SCC flow in the modified L-box set-up using computational fluid dynamics (CFD)

In order to simplify the mathematical formulations, the effects of inertia and friction stresses, as well as presence of the obstacles were assumed to be neglected in the Dam Break Theory analysis. Numerical simulations can be used as a powerful tool to quantify the passing ability of SCC in the presence of obstacles and taking into consideration the inertia and friction effects using computational fluid dynamics (CFD). Therefore, a CFD software (FLOW3D®) was employed to simulate 3D free surface flow of the investigated SCC mixtures in the modified L-box test set-up, using 1st order momentum advection.

The basic equations of the conservation of mass for incompressible materials and the Navier–Stokes equations are discretized with the Finite Volume Method (FVM) in order to obtain the velocity field. In addition, the Volume of Fluid (VOF) method [150] is used to track the fluid motion with time. In order to discretize the geometry, solid elements, and the fluid, two mesh blocks of the numerous cubic cells with 5-mm size in the x, y, and z directions were created. The mesh configurations include consisted of 523,072 and 681,472 cells for 50 and 110-cm initial casting heads, respectively.

The Dirichlet-Neumann boundary conditions were imposed to the flow domain based on the geometry of the modified L-box. The velocity of the walls and the gate rising rate were set to zero and 0.03 m/s, respectively, as indicated in Fig. 5.5. The friction boundary conditions were assumed between the fluid, solid obstacles (three reinforcing bars), and the walls of the apparatus with a friction coefficient value of 0.4 (according to Coulomb's law of friction) [205]. The modelled fluids are considered as homogeneous Bingham fluids using an elasto-viscoplastic model with implicit numerical approximation. Therefore, the experimental values of the

Bingham rheological parameters of the SCC mixtures (see Table 5.4) are used in these simulations. Furthermore, a shear elasticity modulus of 100 Pa is also assumed for all the modelled fluids in order to calculate the elastic models. Gravity stresses are calculated using gravitational acceleration of 9.81 m/s^2 and the modelled flow is assumed to be laminar.

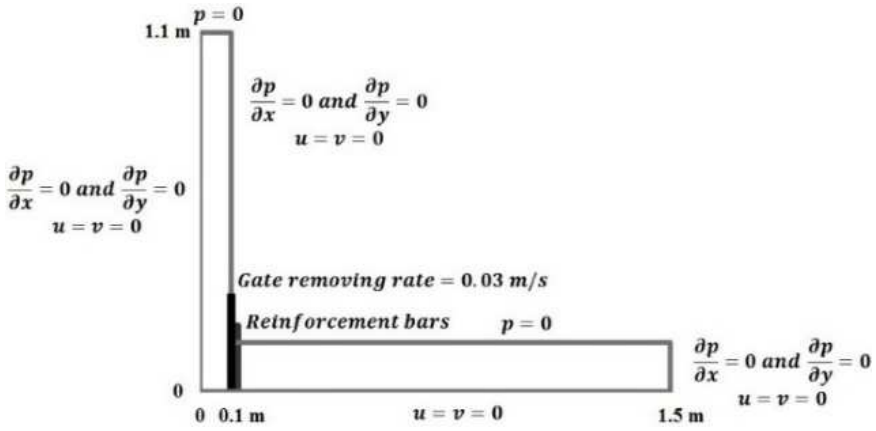

Figure 5. 5 Schematics of the applied boundary conditions in the numerical simulations

As can be observed in Fig. 5.6, the simulated profiles were compared to experimental results obtained with the investigated SCC mixtures, in different waiting times, and various locations after the opening gate for the two initial heads of 50 and 110 cm. As can be observed in Fig. 5.6a, the numerical simulations are in very good agreements with experimental results. This is highlighted by E.R. value of 1.01, R^2 of 0.91, and RMSE of 0.58 cm. These results confirm that the assumptions for boundary conditions, friction coefficient, and mesh settings were appropriate. Moreover, by comparing the results of Figs. 5.3a and 5.6a, it can be concluded that for the given range of the Bingham rheological parameters of the investigated SCC mixtures, the developed numerical simulations can predict the final flow profiles depths with higher accuracy than the analytical Dam Break Theory model ($E.R._{\text{Dam Break Theory}}$ = 1.11, $RMSE_{\text{Dam Break Theory}}$ =1.07 cm, and R^2 values are approximately equal 0.90).

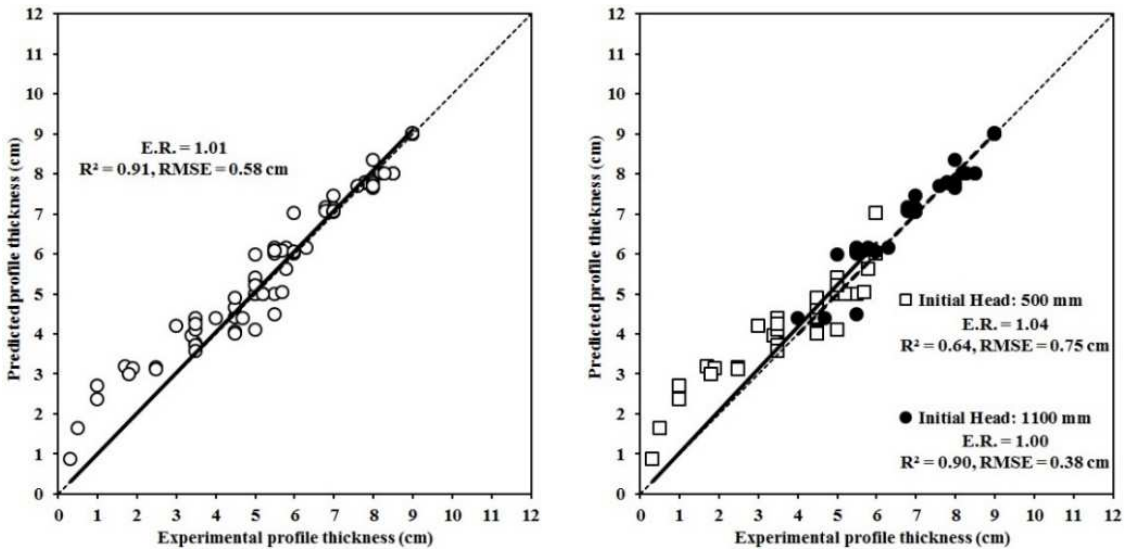

a) Overall comparison

b) Comparison for different initial casting heads of 50 and 110 cm

Figure 5. 6 Comparison between experimental and theoretical results predicted by numerical simulations (CFD) using the Bingham rheological parameters

The same conclusions can be obtained by comparing different initial heads (see Figs. 5.3b and 5.6b). For example, in the case of 50-cm initial head, the CFD model provides better estimation ratio E.R. of 1.04 than the analytical one ($E.R._{\text{Dam Break Theory}}$ of 1.09), and comparable RMSE values of 0.73 and 0.75 cm. In a similar way, for the initial concrete height of 110 cm, despite that higher inertia effects exist, numerical simulations can predict the flow profile thicknesses with a perfect E.R. value of 1.00, and a RMSE of 0.38 cm, which is smaller (almost 1/3) than the RMSE of the analytical model ($RMSE_{\text{Dam Break Theory}}$ =1.30 cm) and the minimum size of the coarse aggregate (5 mm).

As can be observed in Fig. 5.6, there are some overestimations by the CFD model obtained at small profile depths (0-3 cm). This range of profile thickness is related to the last measurement recording data, which are located at 90 or 120 cm from the sliding gate. Since flow profile depth values at these points are more related to the arrested state, these values are more depended to the yield stress of the mixture. Therefore, the aforesaid overestimation can be explained by the accuracy issues in experimental measuring the yield stress values and fitting errors due to approximation by the Bingham model.

Estimation of critical flow thickness of segregation ($h_{critical}$) using numerical simulations

Using the developed numerical simulations, the maximum flow velocity and strain rate magnitudes can be obtained for every single analysis. In order to determine in which flow depth there is more deformation that may indicate a risk of dynamic segregation, the ratio of the maximum flow velocity to maximum strain rate is examined for all the investigated mixtures and different waiting times. The critical flow thickness of segregation ($h_{critical}$) may be approximated as $h_{critical} \cong \frac{V_{max}}{\dot{\gamma}_{max}}$, where V_{max} is the maximum velocity and $\dot{\gamma}_{max}$ is the corresponding maximum shear strain rate magnitude for each test. As presented in Fig. 5.7, the critical flow thicknesses are compared for different initial casting heights.

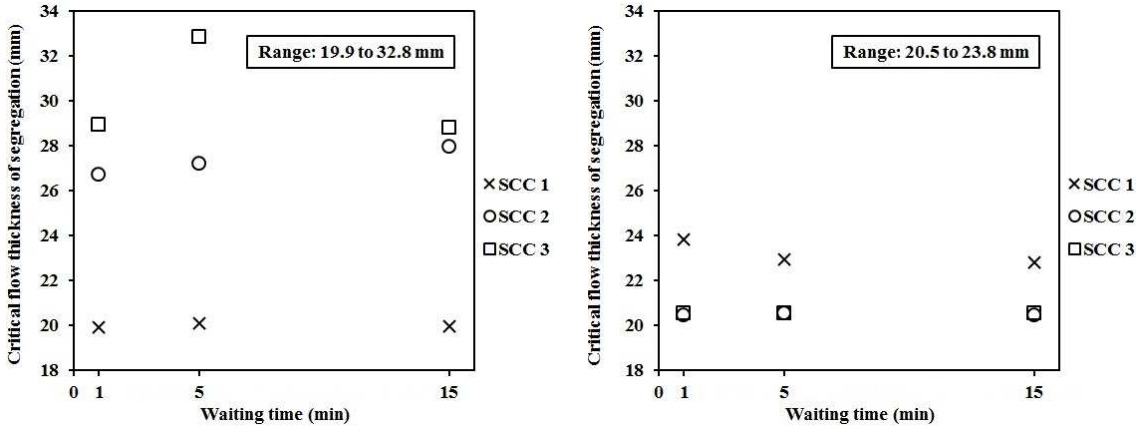

a) Initial casting head of 50 cm b) Initial casting head of 110 cm

Figure 5. 7 Critical flow thickness of segregation of the investigated mixtures for different initial head

As can be observed in Fig. 5.7, increasing the initial head from 50 to 110 cm can minimize the estimated range of critical flow thickness of segregation from 19.9-32.8 mm to 20.5-23.8 mm (i.e. 12.9 to 3.3-mm wide range). This can be due to higher gravitational forces (higher initial casting height). Hence, increasing initial height increases the flow energy to transport the coarse aggregates. By considering the minimum size of coarse aggregates (5 mm), the values of $h_{critical}$ corresponding to 110-cm height can be assumed as the same order (3.3 mm < 5 mm).

It can be also concluded that under low gravitational forces (i.e. initial casting head of 50 cm), the value of $h_{critical}$ is more depended on the plastic viscosity of the mixtures rather than the yield

stress (Fig. 5.7a). For example, SCC1 with the minimum plastic viscosity of approximately 20 Pa.s exhibited the minimum $h_{critical}$ values of 19.9-20.1 mm, while SCC3 having the maximum plastic viscosity values ranging between 56-69 Pa.s resulted in the maximum $h_{critical}$ values of 28.8-32.8 mm. On the other hand, as can be observed in Fig. 5.7b, in case of higher initial height of 110 cm, $h_{critical}$ is more dominated by gravitational forces, regardless of the rheological parameters of the mixture. For example, the investigated mixtures exhibited plastic viscosity values between 14 and 58 Pa.s, but their $h_{critical}$ values are comparable (20.5-23.8 mm).

5.5.5 Effect of waiting time on the accuracy of predicting models

Typical examples of the experimental and theoretical flow profiles obtained for SCC1 after 1-min waiting time, SCC2 after 5-min waiting time, and SCC3 after 15-min waiting time and different initial heads are summarized in Figs. 5.8a, 5.8b, and 5.8c, respectively. As can be observed, the estimation coefficients (E.R., R^2, and RMSE) are also indicated in terms of values. In these figures, the flow profiles on the left correspond to an initial height of 50 cm, while those on the right correspond to an initial height of 110 cm.

As can be observed in Figs. 5.8(a-c), the experimental flow-depth profiles are well predicted using the theoretical models. Furthermore, the obtained E.R. and RMSE values confirm the good accuracy of the proposed model to predict the flow profile of SCC in L-box set-up. Poor accuracy, however, was observed for flow profile depths determined at the entrance of the channel in the case of Dam Break Theory models. As explained earlier, this is may be due to the inertia forces that may rise due to the removal of sliding door and also to frictional stresses of back-wall (i.e. at x = 0). It is worthy to mention that Dam break Theory models neglect the friction effect. Since the sliding door was lifted during approximately 5 s, this value may not be adequate for mixtures with high yield stress values to overcome friction stresses. The difference between predicted and measured depth flow profiles at the entrance of the channel can be also explained by the fact that for mixtures with relatively low plastic viscosity, the material can flow until the extreme end of the horizontal channel. Therefore, the kinetic energy may not be quickly dissipated and the inertia effect can be observed.

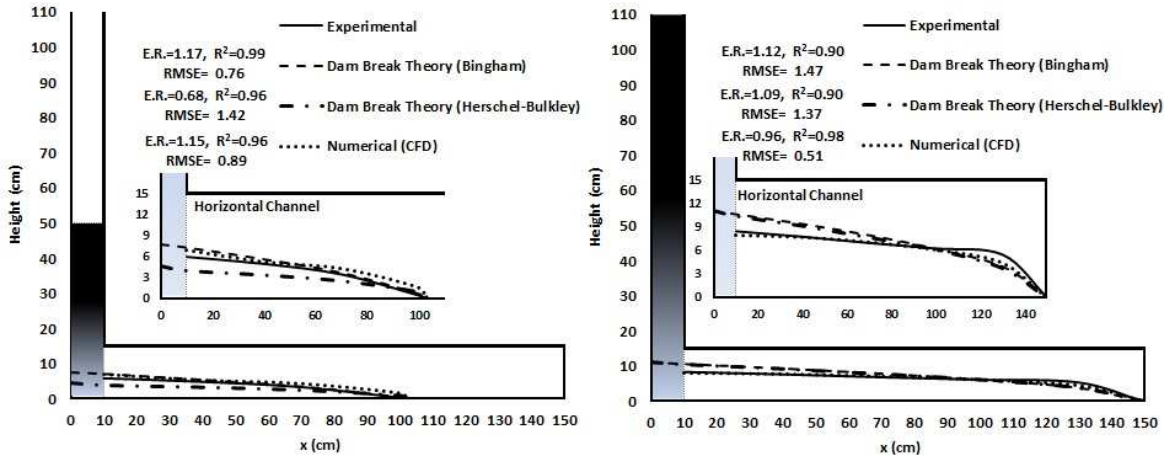

a) SCC1 after 1-min waiting time

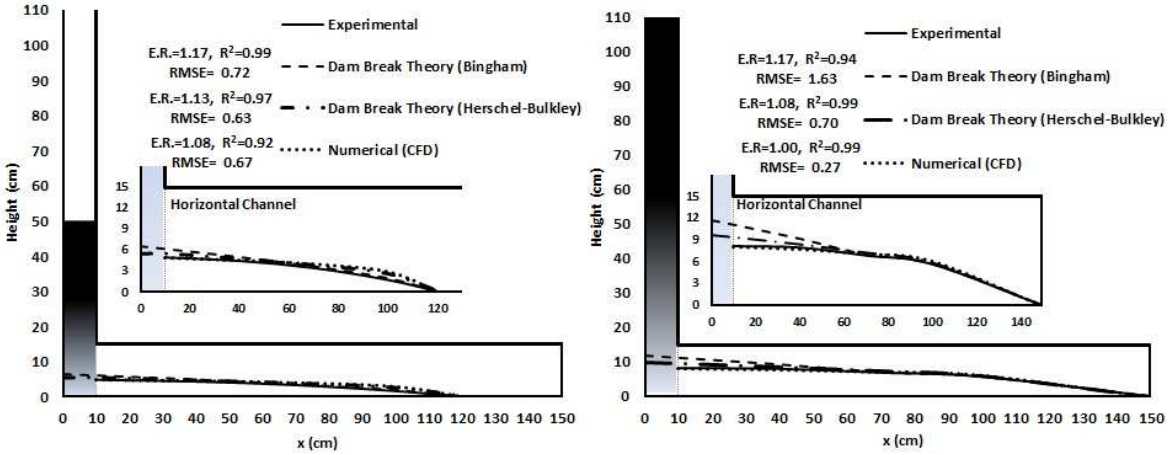

b) SCC2 after 5-min waiting time

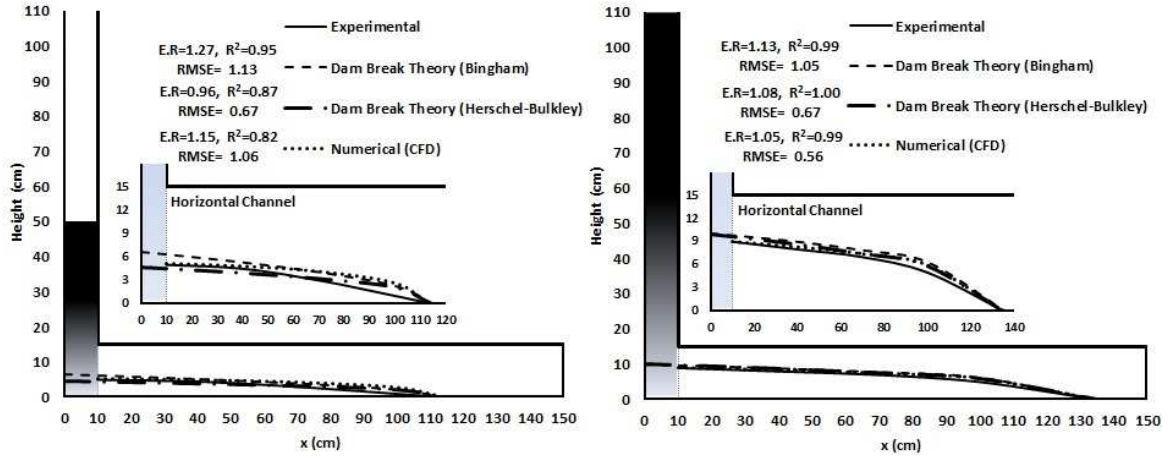

c) SCC3 after 15-min waiting time

Figure 5. 8 Experimental and theoretical flow profiles obtained for SCC1, SCC2, and SCC3 after 1, 5, and 15-min waiting times, respectively (all RMSE values are in cm)

Regarding the stability aspects, the results of numerical simulations are classified in Table 5.5, based on the effect of waiting time on the accuracy of the theoretical models.

Table 5. 5 Ranges of estimation coefficients of the theoretical models for different waiting time values

Estimation coefficients	Waiting time (min)	Theoretical models		
		Dam Break Theory (Bingham model)	Dam Break Theory (Herschel-Bulkley model)	Numerical simulation (CFD)
E.R.	1	0.92 - 1.19	0.68 – 1.09	0.96 – 1.15
	5	0.86 – 1.17	0.94 – 1.15	0.95 – 1.08
	15	1.13 – 1.27	0.85 – 1.17	1.00 – 1.15
R^2	1	0.90 – 0.99	0.90 – 1.00	0.89 – 1.00
	5	0.93 – 0.99	0.92 – 1.00	0.79 – 0.99
	15	0.95 – 1.00	0.87 – 1.00	0.82 – 0.99
RMSE (cm)	1	0.31 – 1.57	0.20 – 1.42	0.18 – 0.89
	5	0.34 – 1.63	0.26 – 1.11	0.27 – 0.91
	15	0.74 – 1.68	0.66 – 1.25	0.35 – 1.06

These results revealed that when the Bingham model was used, both the Dam Break Theory analysis and numerical simulations are less accurate in predicting flow profiles for a waiting time of 15 min compared to 1 and 5 min (E.R. values more far than unity and higher RMSEs). This can be explained by the effect of increasing waiting time on static stability of the mixtures. Changing the homogeneity of the mixtures can indeed induce some errors during rheological measurements, which results in less precise approximation of the rheological parameters, especially the yield stress values. This results in negative effects on the calculation accuracy of the predicting models.

Some scatterings can be observed in the case of the theoretical prediction using the Herschel-Bulkley model. Additional analyses are, therefore, necessary to evaluate the negative effects of

increasing waiting time on the accuracy of the predictions. The predicted profiles of the Dam Break Theory analysis using the Herschel-Bulkley model were compared to the experimental results for three waiting times of 1, 5, and 15 min (Fig. 5.9).

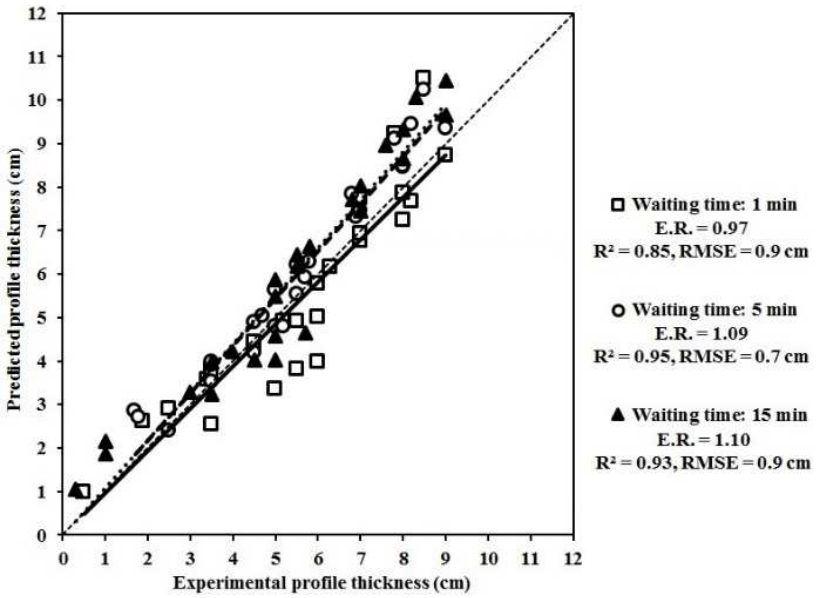

Figure 5. 9 Comparison between experimental results and theoretical predictions by Dam Break Theory analysis, using the Herschel-Bulkley model, for different waiting times of 1, 5, and 15 min

As can be observed in Fig. 5.9, the accuracy of the predictions decreases by increasing waiting times ($E.R._{1\ min}$ = 0.97, $E.R._{5\ min}$ = 1.09, and $E.R._{15\ min}$ = 1.10). This observation confirms the former conclusion regarding the negative effect of waiting time on the accuracy of predictions.

5.6 Conclusions

In this paper, the flow conditions of various SCC mixtures in a modified L-box with obstacles were evaluated. Based on the experimental results, the maximum flow distance is related to the yield stress of the concrete. Greater heights of concrete in the vertical compartment of the modified L-box resulted in higher flow depths at the entrance of the horizontal channel and longer spread, regardless of the yield stress. Test results revealed also that when the concrete was filled to a height of 50 cm, the waiting time of up to 15 minutes did not have any significant

effect on the flow profile of investigated stable SCC (i.e. surface settlement lower than 0.45%). However, for higher initial height (i.e. 110 cm), the mixture with less static stability (SCC1) exhibited higher flow depth at the entrance of the horizontal channel after 15 min waiting time. An analytical model is proposed to predict the flow performance of the SCC in the modified L-box set-up using Dam Break Theory. This model is successfully used to simulate flow profile of SCC. The flow depths at the center line of the horizontal channel were properly reproduced given the rheological parameters of the SCC obtained using the Bingham and Herschel-Bulkley models, the density of the mixture, the geometry of the L-box, and the initial height of the concrete in the vertical compartment of the L-box. The predicted profiles were shown to be in very good agreement with experimental ones. However, poor accuracy was observed at the entrance of the channel because of the inertia forces that may rise due to the removal of sliding door and the frictional stresses of the back-wall of the vertical compartment of the L-box set-up. Accordingly, the increase in initial height (50 vs 110 cm) resulted in less accurate predictions due to more flow velocity and kinetic energy during the first periods of the flow.

The knowledge of free surface flow of SCC can be useful to adjust the rheological parameters of the SCC mixture to optimize the form filling process of the concrete. It is worthy to mention that the Herschel-Bulkley model provided better estimation coefficients than the Bingham model.

Contrary to analytical models in which the effects of inertia and friction stresses, as well as the presence of obstacles were neglected, CFD numerical simulations were successfully carried out to adequately predict flow profile of SCC by taking into account these effects. These results showed better agreement with experimental ones than those obtained with Dam Break Theory, especially when higher initial height is used. Furthermore, the numerically simulated maximum flow velocity and shear strain rate values, are exploited to calculate the critical flow depth ($h_{critical}$) corresponding to the highest potential of dynamic segregation of SCC. It is found that increasing initial casting head can lead to minimize the estimated range of critical thickness of segregation by providing higher flow energy to transport the coarse aggregates.

The results revealed that the waiting time of up to 15 minutes can negatively affect the accuracy of the predicting models because of the disturbed homogeneity of the mixtures, which results in less precise approximation of the rheological parameters, especially the yield stress values.

Excellent correlation between predicted and experimental arrested profiles showed that both Dam Break Theory and CFD are useful in predicting flow profiles of SCC through a restricted flow condition. This can be a powerful tool to adjust rheological parameters of the mixture, as well as the obstacles to ensure proper filling of the formwork.

CHAPTER 6 HOMOGENEOUS ANALYSIS OF SELF-CONSOLIDATING CONCRETE (SCC) CASTING IN REINFORCED BEAM USING COMPUTATIONAL FLUID DYNAMICS (CFD)

Authors and Affiliations:

Masoud Hosseinpoor: Ph.D. Candidate, Department of Civil Engineering, Université de Sherbrooke, Sherbrooke, Quebec, Canada, J1K2R1
Email: masoud.hosseinpoor@usherbrooke.ca

Kamal H. Khayat: Professor, Department of Civil, Architectural and Environmental Engineering, Missouri University of Science and Technology, 224 Engineering Research Laboratory, 500 W. 16th St., Rolla, MO 65409-0710, USA.
Email: khayatk@mst.edu

Ammar Yahia: Associate Professor, Department of Civil Engineering, Université de Sherbrooke, Sherbrooke, Quebec, Canada, J1K2R1
Email: ammar.yahia@usherbrooke.ca

Habib A. Mesbah: Associate Professor, Department of Civil Engineering, Laboratoire de Génie Civil et Génie Mécanique (LGCGM), Institut National des Sciences Appliquées, 20 Avenue des Buttes de Coësmes, 35043 Rennes Cedex, France
Email : habib-abdelhak.mesbah@univ-rennes1.fr

Paper submitted to Construction and Building Materials, on 19th September 2016

Abstract

In this study, the casting process of 162 L of self-consolidating concrete (SCC) in 4.05×0.2×0.2 m reinforced beam was simulated using a computational fluid dynamics (CFD) software. The simulated SCC was cast under gravity using a 1.69-m high vertical funnel. The horizontal part of the L-shaped formwork is reinforced using four 10-mm diameter longitudinal bars and 10-mm diameter stirrups, placed at every 15 cm along the beam. The effect of bar distribution and confinement on flow and passing ability of the SCC is evaluated in 0.1-s time steps during the casting process. The various predicted responses are compared to experimental values determined using three different SCC mixtures. The numerical simulations are shown to successfully predict the flow performance of the SCC in the horizontal direction along the cast beams. Furthermore, the flow behavior of SCC in different shaped sections of the vertical compartments of the beam is evaluated. A critical thickness of segregation of 38 mm is also calculated which indicates the flow depth with the most deformation and the highest risk of dynamic segregation.

Keywords: Casting Simulation; Flowability; Homogeneous Flow Analysis; Passing Ability; Rheology; Self-Consolidating Concrete.

6.1 Introduction

Whether on site or in a prefabrication plant, problems related to ensuring complete filling of the formwork are encountered regularly, especially in the case of densely reinforced structural elements and highly restricted sections. SCC is used in the precast and cast-in-place industries to facilitate and speed up casting operations and secure high surface finish. The main functional requirements of SCC are the filling ability, the passing ability, and stability. Passing ability refers to the ability of SCC to flow through tight openings, such as space between reinforcing bars. The filling capacity refers to the ability of the concrete to complete filling of the formwork under its own weight. Achieving proper passing and filling abilities depends on the mixture composition and rheological properties of the concrete, the element characteristics, including the reinforcement detailing and density, as well as the casting conditions [23, 25, and 26].

SCC behaves as an elasto-viscoplastic material with yield stress [27, 54, and 98]. The material behaves as solid for shear stress values lower than the yield stress, and flows when the shear stress overcomes the yield stress [116]. The motion of concrete is eventually arrested when the gravitational forces are in equilibrium with the viscous forces. The evolution of flow and the shape of free-surface profile are therefore dependent on the rheological behavior of the concrete [29, 96, and 97]. It is essential to develop some numerical techniques for predicting casting operation given a set of properties of concrete, geometry of the element to be cast, and the selected casting process (gravitational, pumping, etc.). Recently, there is a great interest to employ numerical methods to simulate the flow behavior of fresh concrete [29, 42, 46, 47, 180, and 183]. These studies include numerical simulation of concrete flow in empirical test set-ups [29, 42, 180, and 183] and full scale castings [29, 46, and 47]. An extensive comprehensive review regarding numerical simulation of fresh concrete flow can be found in Roussel et al. [44].

In this study, a computational fluid dynamics (CFD) software (FLOW3D®) was employed to simulate casting process of 162 liters of SCC in 4.05 m length reinforced beam. Using rheological properties of SCC as the input parameters for the software, the effect of viscosity on flow properties of SCC was evaluated for a given constant yield stress. The simulations are found to be in very good agreements with the experimental results in terms of free surface profiles, velocity, strain rate, kinetic energy, and volume flowrate magnitudes for each time step.

6.2 Materials and experimental program

As summarized in Table 6.1, three SCC mixtures were optimized to achieve an initial slump flow of 700 mm but different V-funnel times. The mixtures were proportioned with a binder content of 450 kg/m^3 (350 kg/m^3 of GU cement and 100 kg/m^3 of Class F fly ash), and three sand-to-total aggregate ratios of 0.47, 0.50 and 0.56 by mass. The mixtures were proportioned with a water-cementitious material (w/cm) of 0.47 and three high-range water reducer (HRWR) dosages of 3.6, 3.9, and 5.8 L/m^3.

Table 6. 1 SCC mixtures proportioning and rheological properties

Mixture	SCC1	SCC2	SCC3
Cement (kg/m^3)	350	350	350
Fly Ash (kg/m^3)	100	100	100
w/cm	0.47	0.47	0.47
Sand (kg/m^3)	907	823	748
Coarse Aggregate (4-8 mm) (kg/m^3)	144	162	179
Coarse Aggregate (8-12.5 mm) (kg/m^3)	576	650	671
HRWRA (L/m^3)	3.6	3.9	5.8
Slump Flow (mm)	700	700	700
J-Ring (mm)	-	680	680
Filling Capacity (%)	-	95	95
V-Funnel Time (s)	-	2.88	3.99
L-Box Ratio (H_2/H_1)	-	0.58	0.74
Yield Stress (Pa)	60	60	60
Viscosity (Pa.s)	40	30	20
Density (kg/m^3)	2300	2304	2340

The L-shaped beam that was cast and modeled is shown in Fig. 6.1. It consisted of a vertical section measuring 1.69 m in height and a horizontal section measuring 4.05 m in length with a cross section of 0.2×0.2 m. The sections are separated by a sliding door. The top surface of the first 3 m of the horizontal part is closed by a plexiglass plate to avoid splashing out the concrete during casting. The vertical part is composed of three sections, including the upper rectangular section (1 m width × 0.19 m height), the middle 0.8 m height trapezoid V-funnel part (with 1 m and 0.2 m width at top and bottom, respectively), and the lower rectangular section having 0.7 m height and 0.2 m width. Each of the three sections is 0.2 m in depth. The horizontal part of the formwork is reinforced by four longitudinal 10 mm diameter bars and 26 vertical stirrups of 10 mm diameter equally spaced (0.15 m). This was done to evaluate the effect of bars on the flowability and passing ability of SCC. The schematics of the beam and the reinforcement bars are shown in Fig. 6.1.

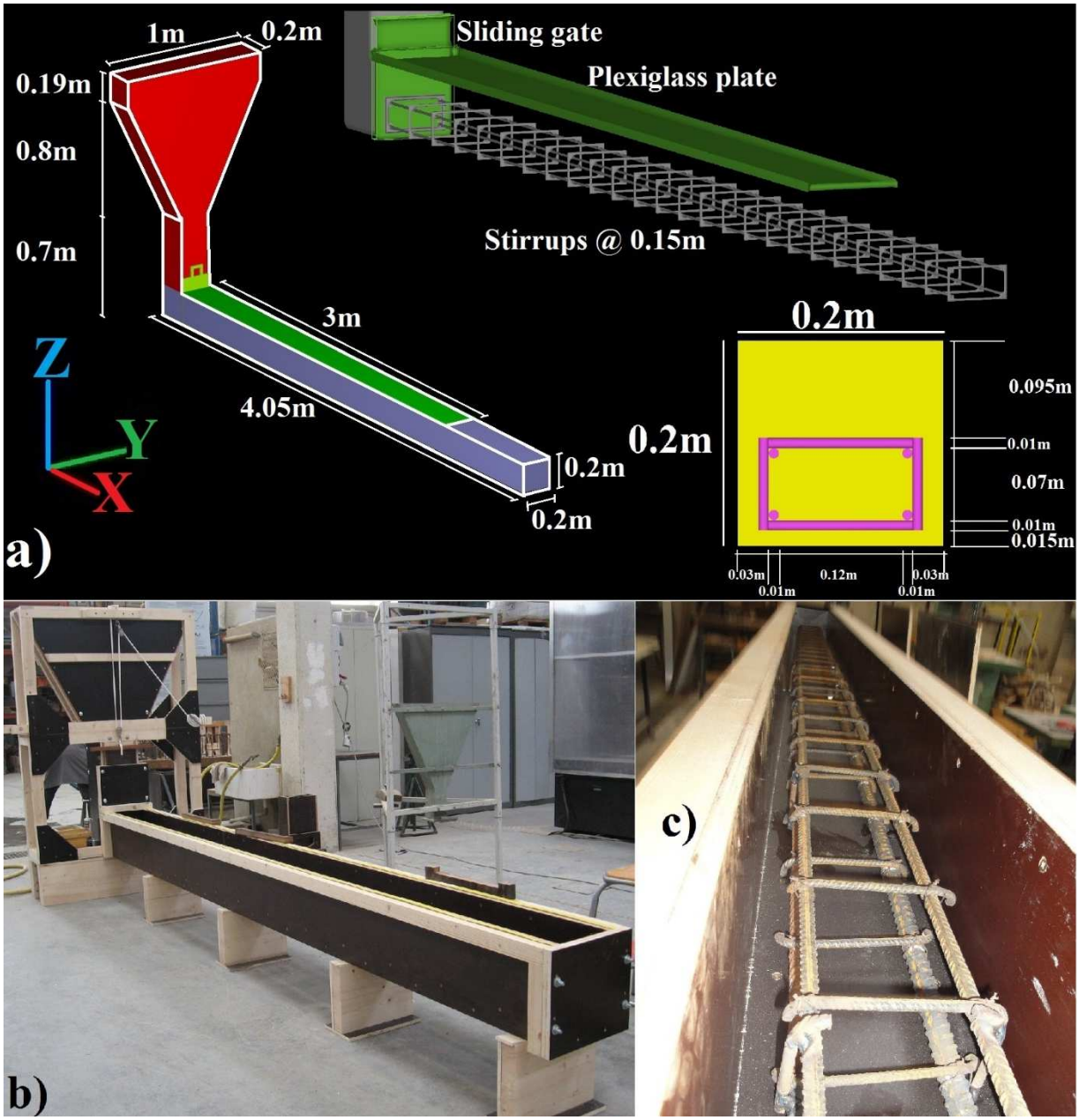

Figure 6. 1 a) Schematics of the L-shaped beam and reinforcement bars arrangement, b) formwork of the beam, and c) cage of the reinforcement bars

The concrete with a total volume of 162 L is cast in the vertical compartment. The sliding door is then opened, and the concrete is gravitationally driven in the horizontal part. In order to evaluate the flowability and passing ability characteristics, the positions of the front of flow surface along the horizontal compartment and the corresponding flow times to reach these positions are recorded till the concrete reaches the end of the beam. In order to do that, several

observation gates were fixed throughout the horizontal part of the formwork, and the complete flow process of casting was recorded using a high-speed video camera. As presented in Fig. 6.2, for a given flow time, SCC with lower viscosity is shown to achieve further horizontal motion of the flow front. For example, after 15 s flow time, the flow front of SCC1 (μ_p = 40 Pa.s), SCC2 (μ_p = 30 Pa.s), and SCC3 (μ_p = 20 Pa.s) mixtures exhibited displacement values of 2.405, 2.856, and 3.687 m along the horizontal channel of the beam, respectively. The experimental results showed also that SCC with higher viscosity would take a longer time to reach the end of beam. For example, the flow front took 40, 30, and 19 s time for SCC1 (μ_p = 40 Pa.s), SCC2 (μ_p = 30 Pa.s), and SCC3 (μ_p = 20 Pa.s), respectively, to reach to the end wall of the horizontal channel.

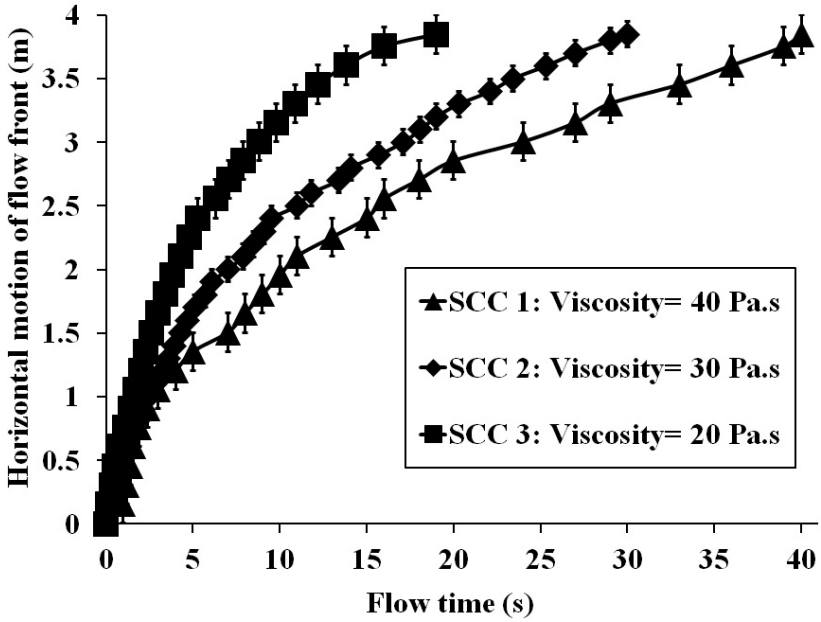

Figure 6. 2 Experimental results of horizontal displacement of flow front versus flow time

6.3 Numerical simulation and boundary conditions

In this paper, a computational fluid dynamics (CFD) software (FLOW3D®) was employed to simulate the free surface flow of SCC as a homogeneous Bingham fluid in the reinforced L-shaped beam. The 3D Navier–Stokes equations for incompressible materials are solved by the Volume of Fluid (VOF) [150] method in order to predict free surface profiles and flow properties in terms of velocity, strain rate, and energy magnitudes in each time step, using 1st

order momentum advection.. In order to discretize the geometry, solid elements, and the fluid, a total of 36 mesh blocks, resulting in 334,240 cells with 0.005- to 0.02-m mesh size in the x, y, and z directions were created. The velocity of the fixed reinforcing bars, wall boundary, and the rate of raising the dividing gate were set to zero, zero, and 0.05 m/s, respectively. The friction coefficient between fluid and walls of apparatus is fixed at 0.4 (according to Coulomb's law of friction) [205]. The modelled fluids are implicitly approximated using an elasto-viscoplastic model. Gravitational acceleration and shear elasticity modulus are set to 9.81 m/s^2 and 100 Pa, respectively. The modelled flows are assumed as laminar flow type [48]. It is worthy to mention that numerical simulations carried out on an i7-2600 CPU 3.40 GHz processor required a total running time between 151 and 566 hours. The running times depend mostly on the plastic viscosity of the suspending fluid. Indeed, the simulation of the flow of higher viscous suspensions took more calculation time than less viscous ones.

6.4 Results and discussions

6.4.1 Effect of the plastic viscosity of the investigated mixtures on flow performance of SCC in the horizontal direction

The horizontal displacements of the flow front for the three mixtures are simulated and compared with the experimental observations, extracted from the recorded videos, as summarized in Fig. 6.3. As can be observed, the numerical simulations are in very good agreements with experimental results with a coefficient of correlation (R^2) greater than 0.96. The predicted-to-experimental profile ratio ranged between 0.92 and 1.09. It shows that the assumptions for boundary conditions, friction coefficient, and mesh settings were adequate. Moreover, it can be seen that the numerical simulations can predict very well the final time needed for flow front to reach the end of the beam for the three mixtures. As can be seen, the minimum R^2 of 0.96 was obtained for the mixture with the minimum plastic viscosity (20 Pa.s corresponding to SCC3). On the other hand, some underestimations by the numerical simulations can be observed in the initial flow times (first 5-7 s) for the three mixtures. These two phenomena could be explained by the inertia effect on flow properties and precision of the numerical models.

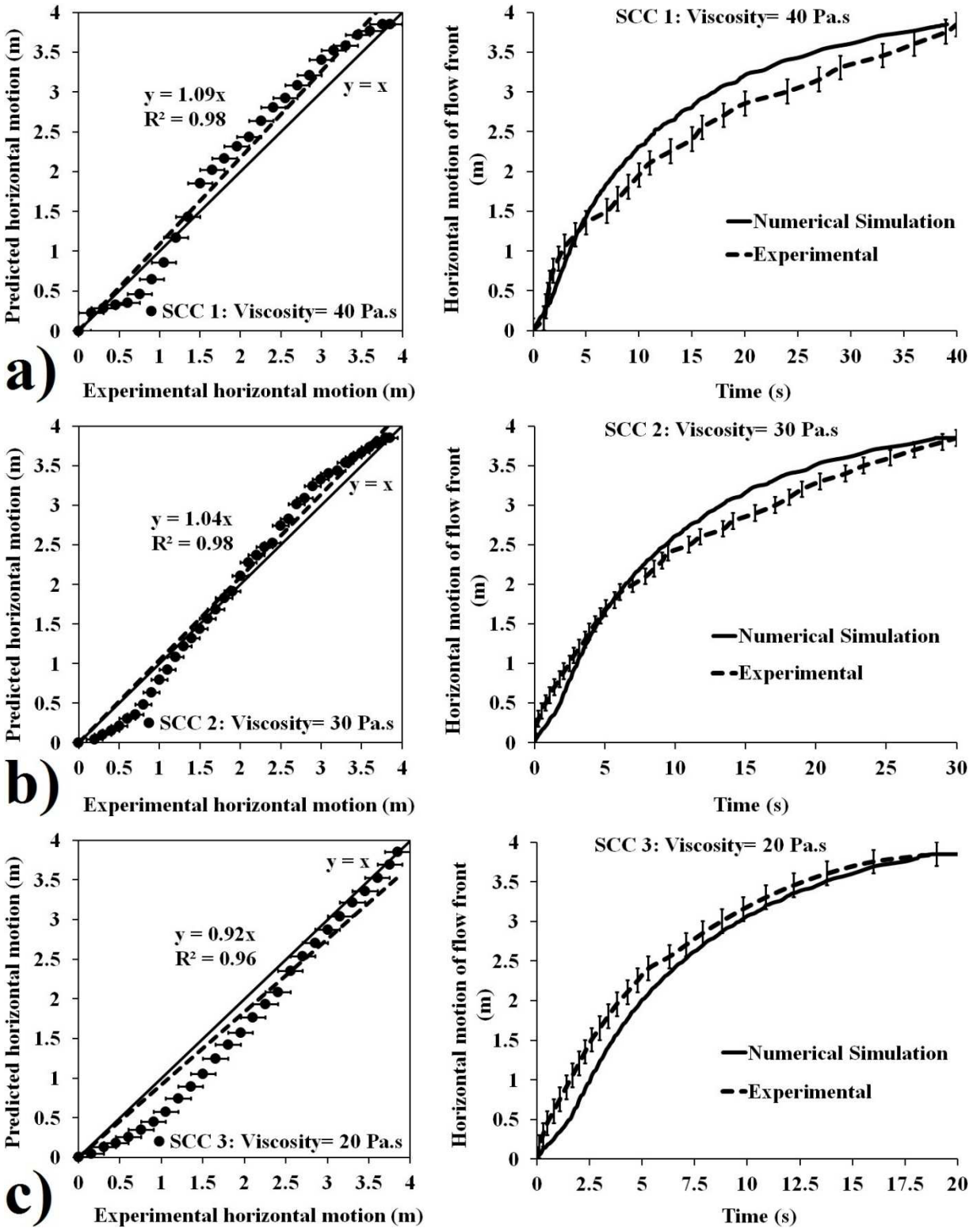

Figure 6. 3 Flow front displacement, a comparison between numerical simulation and experimental results: a) SCC 1, b) SCC 2, and c) SCC 3

In order to evaluate the effect of viscosity on flowability and passing ability of the investigate SCC mixtures, the flow profiles of two additional fluids having a yield stress of 60 Pa, different viscosity values of 15 and 50 Pa.s, and density (ρ) of 2300 kg/m^3 are simulated for a maximum 40 s flow period. This flow time of 40 s was obtained for the SCC1 as the maximum experimental flow time required for the flow front to reach the end of the beam. The simulation results for flow front displacements in the horizontal beam are presented in Fig. 6.4.

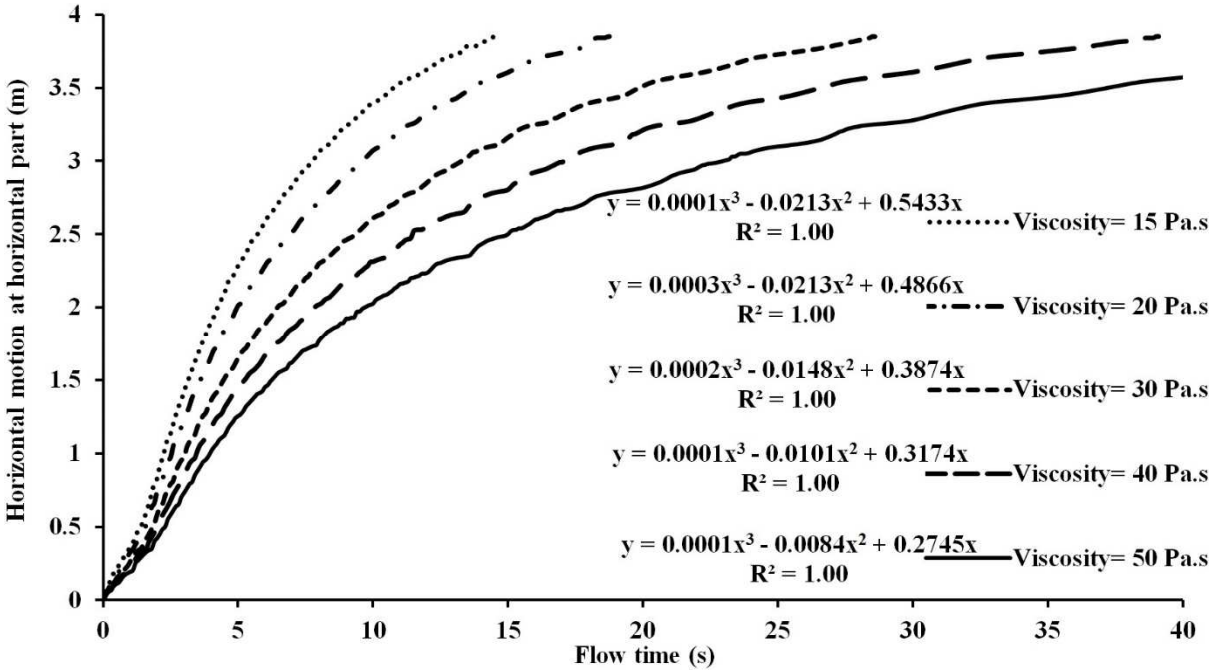

Figure 6. 4 Predicted flow front displacements in horizontal beam versus flow time

As can be observed in Fig. 6.4, in a given flow time, the SCC with higher viscosity travels less displacement in the horizontal part of the formwork. Therefore, for a given yield stress, SCC with higher viscosity can exhibit less flowability and lower passing ability. For example, after 14 s flow time, the investigated fluids having plastic viscosity values of 15, 20, 30, 40 and 50 exhibited 3.802, 3.754, 3.081, 2.751, and 2.431 m flow front displacements in the horizontal channel of the beam, respectively. On the other hand, the materials with higher viscosity need longer time to reach a given flow front displacement in the horizontal channel. For example, the flow fronts of the SCC mixtures having plastic viscosity values of 15, 20, 30, 40, and 50 take 10.8, 14.2, 19.9, 26.6, and 37.2 s flow times to travel 3.5 m in the horizontal beam.

Calculating the derivatives of the polynomial correlated functions at time equal 0 s, the initial velocity of flow front can be estimated for all the mixtures. As can be seen, increasing viscosity from 15 to 50 Pa.s can lead to decrease the estimated initial velocity of flow fronts from 0.5433 to 0.2745 m/s (i.e., 49% reduction). These estimations allow us to compare initial typical inertia stresses for the selected range of plastic viscosity, using a constant density of 2300 kg/m^3, as follows:

$$I = \rho(V_{initial})^2 \tag{6.1}$$

where I is the initial typical inertia stress, $V_{initial}$ is the initial velocity and ρ = 2300 kg/m^3 is the density for all the investigated mixtures. Accordingly, increasing plastic viscosity from 15 to 50 Pa.s can lead to decrease the initial inertia stress from 679 to 173 Pa (i.e., 75% reduction) which are much greater than yield stress of the mixtures (60 Pa).

Based on the results of Fig. 6.4, the front flow velocity magnitudes are calculated in 1-s time steps as follows:

$$V_f(t) = \frac{X_f(t) - X_f(t-1)}{\Delta t = 1\ s} \tag{6.2}$$

where $V_f(t)$ is the estimated velocity of the flow front at the end of each Δt = 1-s time step, $X_f(t)$ and $X_f(t\text{-}1)$ are the horizontal positions of the flow front, measured at the center line, in the horizontal channel at the end and beginning of the 1-s time step after passing flow time t, respectively. On the other hand, the strain rate and kinetic energy values were simulated. As can be observed in Figs. 6.5a, 6.6a, and 6.7a the flow front velocity, strain rate, and kinetic energy magnitudes increase during the first 3 s of flow time and reach their maximum values. This can be due the initial inertia stresses in the initial flow periods. Comparing these maximum values, as can be observed in Figs. 6.5b, 6.6b, and 6.7b, the use of SCC with higher viscosity resulted in lower flow front velocity, strain rate, and kinetic energy. Furthermore, these properties are well correlated with the viscosity values with R^2 coefficients more than 0.99. For example, increasing the plastic viscosity of the mixtures from 15 to 50 Pa.s can decrease the maximum magnitudes of the flow front velocity at horizontal channel, strain rate, and mass-averaged

kinetic energy from 0.596 to 0.309 m/s (i.e., 48% reduction), from 86.1 to 40.3 s^{-1} (i.e., 53% reduction), and from 0.1233 to 0.0273 J/kg (i.e., 78% reduction), respectively.

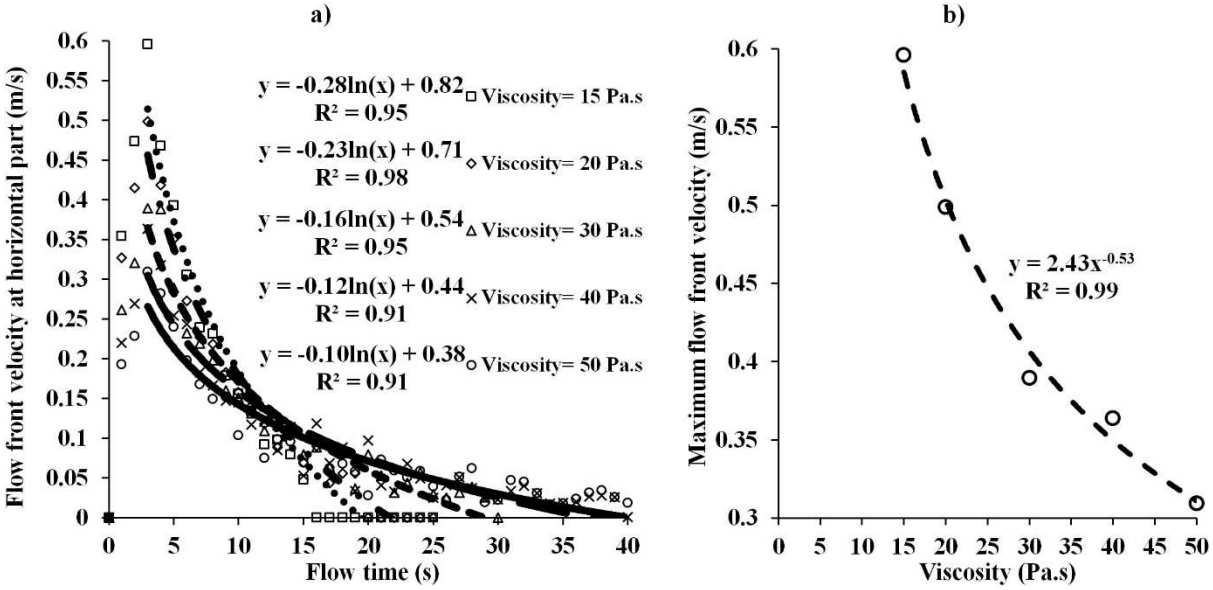

Figure 6. 5 Flow front velocity versus a) flow time, b) viscosity

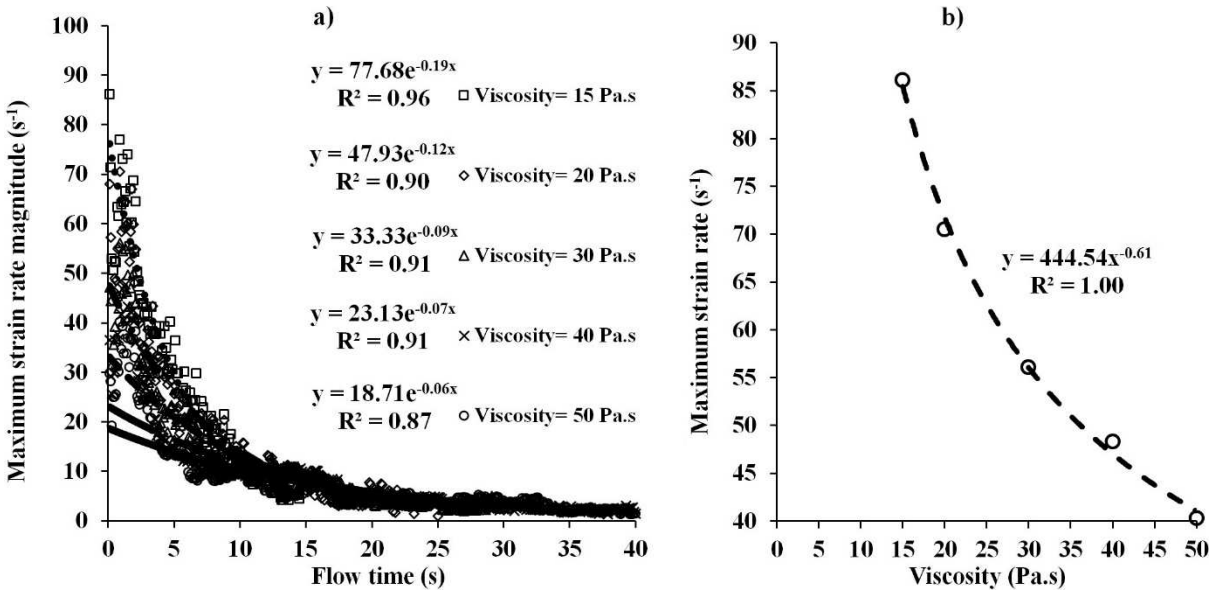

Figure 6. 6 Maximum flow strain rate magnitude versus a) flow time, b) viscosity

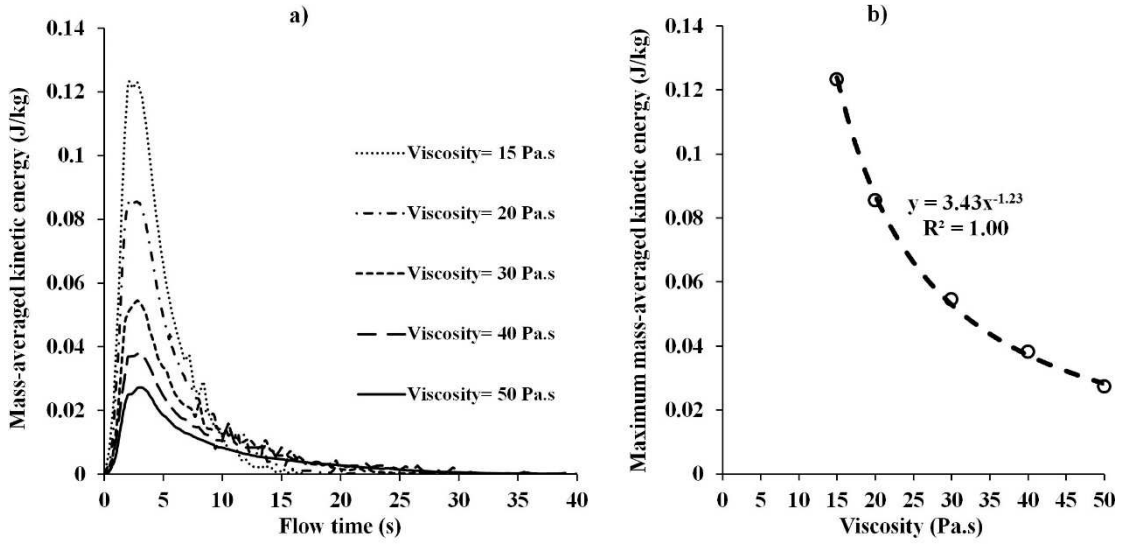

Figure 6. 7 Mass-averaged kinetic energy versus a) flow time, b) viscosity

6.4.2 Effect of the plastic viscosity of the investigated mixtures on flow performance of SCC in the vertical direction

The effect of viscosity on flowability of concrete in the vertical direction is evaluated by comparing the vertical motion observed in the vertical compartment of the beam. As can be observed in Fig. 6.8, in a given flow time, decreasing the plastic viscosity can lead to an increase in the vertical motion of the flow surface in the vertical section. For example, after 14 s flow time, the investigated fluids having plastic viscosity values of 15, 20, 30, 40 and 50 exhibited 1.269, 1.087, 0.793, 0.674, and 0.581 m flow surface displacements in the vertical part of the formwork, respectively. These vertical displacements for the investigated mixtures with plastic viscosity of 15 to 50 Pa.s, obtained at flow time t = 14 s, are 33% to 24% lower compared to their corresponding flow front horizontal displacements, respectively. Therefore, it can be concluded that given the design of the beam, the concrete undergoes more horizontal displacement than the vertical one. This can lead to faster filling of the reinforced beam, as it is desired in the horizontal applications.

It can be also observed that the SCC with higher viscosity takes longer time to reach a certain vertical motion. For example, the investigated mixtures having plastic viscosity values of 15 to

50 Pa.s take 10.1 to 27.1 s flow time to exhibit 1 m flow surface motion in the vertical part of the beam. Therefore, it can be concluded that increasing the viscosity can lead to a decrease in the velocity of the flow surface in the vertical section. Furthermore, it seems there is some changes in the flow pattern at vertical motion value of 1.07 m, which corresponds to the time that flow surface reached the lower rectangular zone of the vertical section of the formwork.

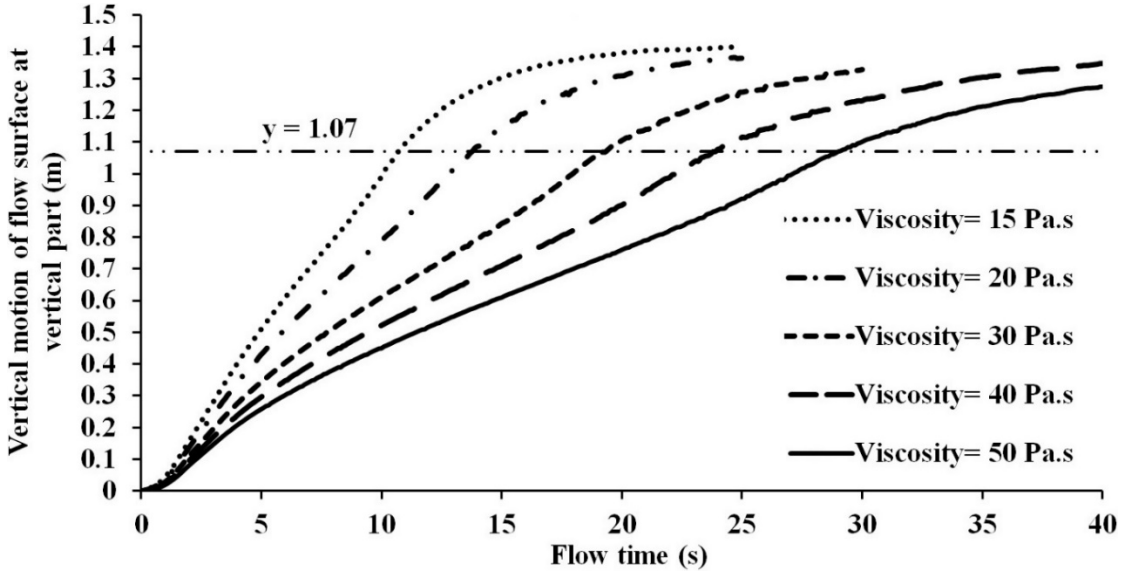

Figure 6. 8 Vertical motion of the flow surface versus flow time for the investigated mixtures with different plastic viscosity values

The flow surface velocity of the investigated suspensions are calculated as follows:

$$V_s(t) = \frac{Z_s(t) - Z_s(t-1)}{\Delta t = 1\ s} \tag{6.3}$$

where $V_s(t)$ is the estimated velocity of the flow surface at the vertical part at the end of each Δt = 1-s time step, $Z_s(t)$ and $Z_s(t-1)$ are the vertical levels of the flow surface in the center line of the vertical part of the beam at the end and beginning of the 1-s time step after passing flow time t, respectively. The maximum values of the flow surface velocity, obtained by Eq. (6.3), are presented for the investigated mixtures with different plastic viscosity values. As can be observed in Fig. 6.9, fluids with higher viscosity showed lower velocity of surface flow in the vertical compartment in different sections of the vertical part of the beam. For example,

increasing the plastic viscosity of the mixture can result in decreasing the maximum values of flow surface velocity from 0.122 to 0.065 m/s (i.e., 47% reduction) with a very good correlation coefficient (R^2 = 1.00). This reduction is almost equal to that one observed in the flow velocity of the flow front in horizontal part of the beam.

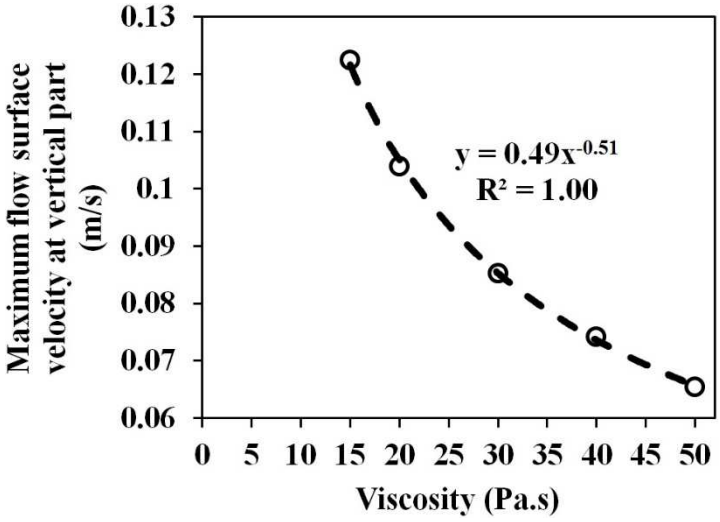

Figure 6. 9 Maximum flow surface velocity at vertical part versus plastic viscosity

In order to study the flow behavior of the investigated mixtures in different shaped sections of the vertical part of the beam, the flow surface velocity of the suspensions, obtained by Eq. (6.3) in each 1-s time step, are correlated to the displacement of the flow surface in the vertical part of the formwork, for whole the flow period. The results of this correlation are presented for all the investigated mixtures, having different plastic viscosity values (Fig. 6.10). As can be observed in the Figs. 6.10 and 6.11, four different patterns can be observed based on surface flow position at different parts of the vertical compartment of the beam.

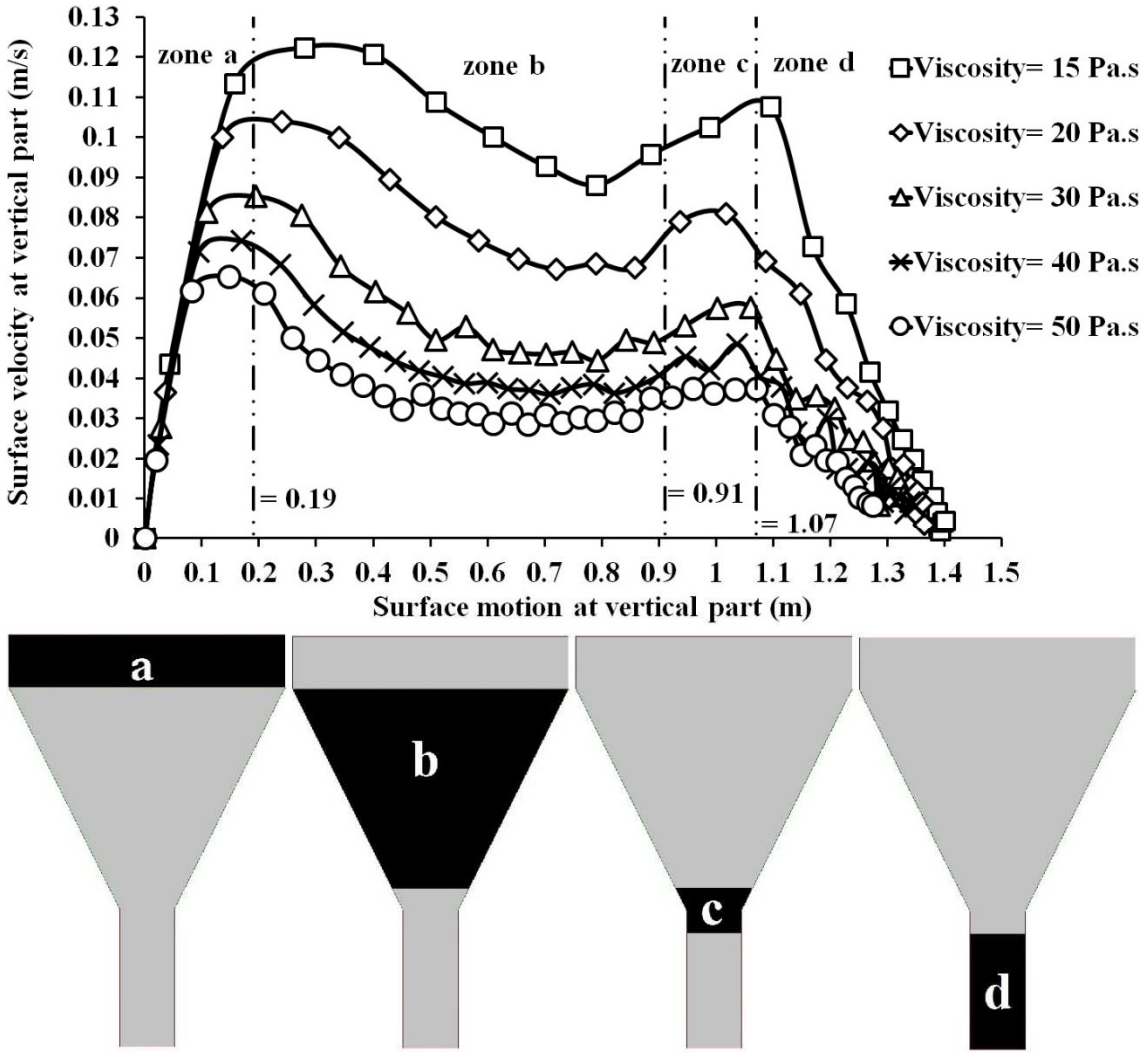

Figure 6. 10 Velocity of flow surface versus vertical motion of flow surface in different sections of the vertical part of the formwork, examined for the investigated mixtures with different plastic viscosities

As can be observed in Fig. 6.11, velocity of flow surface can increase in the upper rectangular part (a), unlike the other parts of the vertical section. This can be explained by the inertia effect on the flow velocity in the first moments of the flow. For example, as long as the flow surface descends in the upper rectangular part (a), the surface velocity increase up to 0.113, 0.100, 0.085, 0.074, and 0.065 m/s for the mixtures having plastic viscosity values of 15, 20, 30, 40, and 50 Pa.s, respectively.

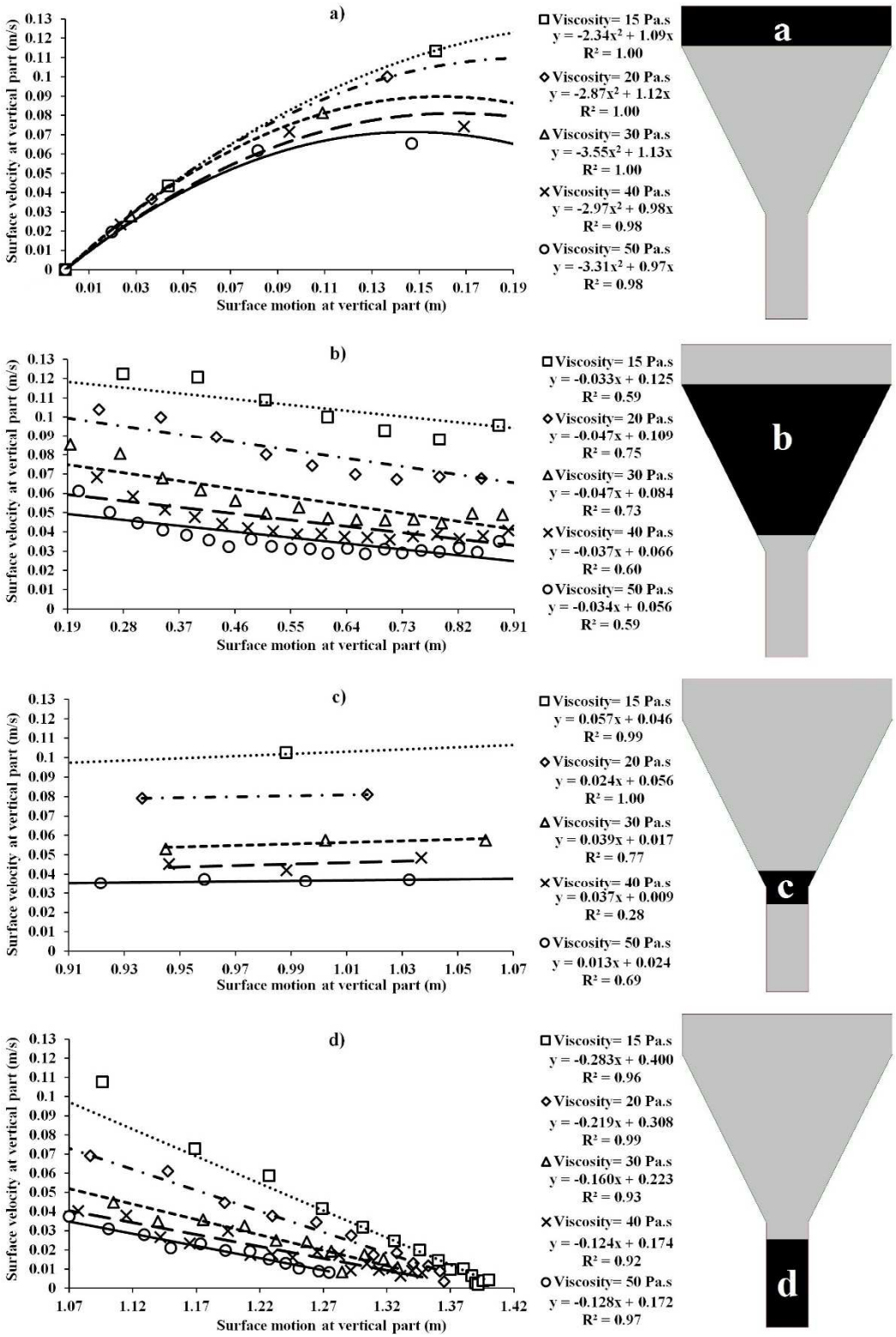

Figure 6. 11 Variation of velocity with surface motion in different parts of the vertical section: a) upper rectangular part, b) V-shaped funnel part, c) transition zone between V-shaped funnel and lower rectangular parts, and d) lower rectangular part

Once the flow surface passes through the V-funnel shaped zone (b), the velocity decreases by 21% to 43% for the mixtures with plastic viscosity values of 15 to 50 Pa.s. This can be due to the lower flow energy corresponding to the lower gravitational forces obtained by lower flow surface level in the vertical part of the beam. This can also be due to the frictional forces between the mixtures and the formwork walls.

In the transition part (c), the flow velocity increased slightly. This can be due to the inertia effect created by the change in flow section which is showed to be more dominant than the decreasing effect of the frictional and gravitational forces. The maximum and minimum increments in flow velocity in this part are 11% and 6% for the mixtures with the minimum and maximum plastic viscosity values of 15 and 50 Pa.s, respectively. Therefore, the inertial effect of the section change is higher for the lower viscosity mixtures.

According to the comparison of the calculated slopes of the correlated curves in Figs. 6.11b and 6.11d, velocity losses in the lower rectangular zone (d) are almost 3.4 to 8.6 times higher than those observed in the V-shaped funnel zone (b). Therefore, it can be concluded that SCC mixtures can show higher flowability with lower velocity loss in the V-shaped sections than in the rectangular part of the vertical section.

6.4.3 Calculation of the flow rate magnitudes of the investigated mixtures, provided by the L-beam set-up

Flow rates of SCC mixtures having different viscosity values are calculated for each 1-s time step as follow:

$$Q(t) = V_s(t).A(t) \tag{6.4}$$

where Q(t) is the flow rate of the mixture in the flow time t, and $V_s(t)$ is the velocity of the flow surface, having a cross-sectional area of A(t), calculated in each 1-s time step. The results of these calculations are presented in Fig. 6.12a for the investigated mixtures with different plastic viscosity and for the whole period of the flow. As can be observed, the values of flow rates increase in the first 3 s of the flow time, due to the inertial stresses and head difference. The

maximum values of the flow rates, obtained from Fig. 6.12a, are correlated to the plastic viscosity values of the investigated mixtures and presented in Fig. 6.12b.

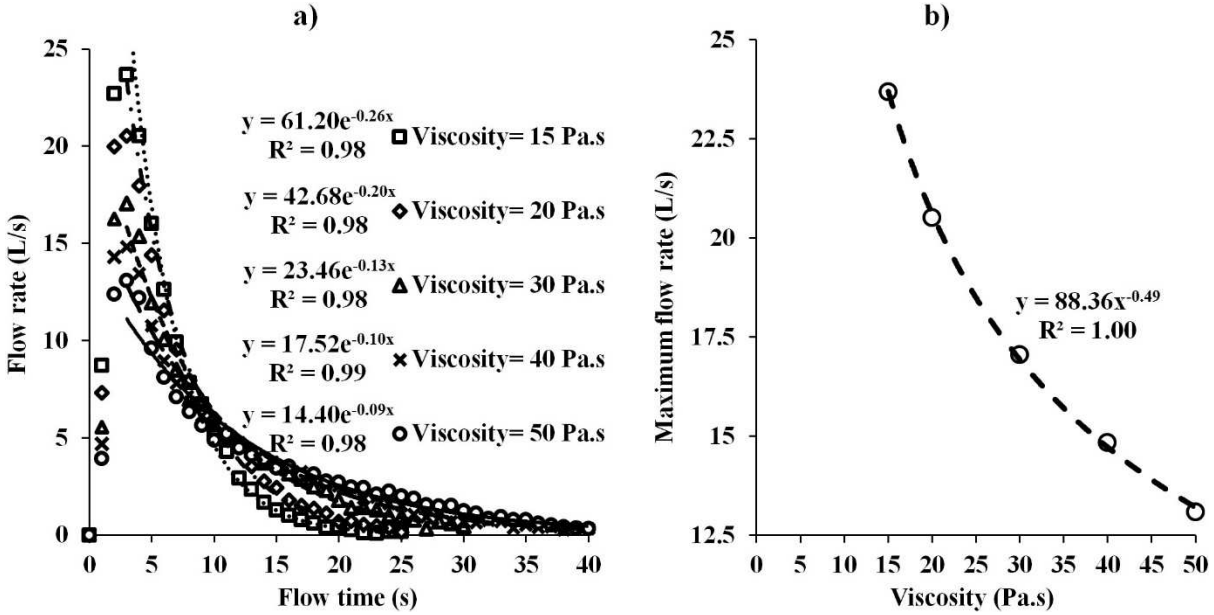

Figure 6. 12 a) Flow rate versus time, and b) maximum flow rate versus viscosity

As can be observed, the increase in viscosity resulted in decreasing the flow rates which is following a perfect correlation (R^2 = 1.00). The design of vertical comportment of the beam (three different shapes) provides maximum flow rate values ranging between 13.1 and 23.7 L/s, obtained for the plastic viscosity values of 50 and 15 Pa.s, respectively. Therefore, increasing plastic viscosity of the mixtures from 15 to 50 Pa.s can decrease the flow rate of the mixture by 45%. On the other hand, these values of flow rate (i.e., 13.1-23.7 L/s) are comparable to those encountered in SCC pumping operations [207 and 208].

6.4.4 Estimation of the critical thickness of segregation

In order to determine in which flow depth there is more deformation that may indicate a risk of dynamic segregation, the correlation of the maximum flow velocity magnitudes with maximum strain rate magnitudes (presented in Figs. 6.5a and 6.6a, respectively) is examined for the total flow period, as presented in Fig. 6.13. From this correlation, critical thickness of segregation

($h_{critical}$) may be approximated as $h_{critical} \cong V/\dot{\gamma}$, where V is the maximum velocity and $\dot{\gamma}$ is the corresponding maximum shear strain rate magnitude.

As can be observed in Fig. 6.13, the $h_{critical}$ value of 0.0376 m can be estimated. This value refers to the region located above the bottom row of horizontal reinforcing bars. Therefore, higher risks of shear-induced segregation are expected around the bottom row of longitudinal reinforcing bars and close to the bottom sides of the stirrups. Also, it must be noted that in this zone, the risk of the gravitational induced migrations of the coarse particles from the top layer towards the bottom one is high. On the other hand, according to the narrower spaces between the reinforcing bars and the formwork walls, compared to the upper levels in the horizontal beam, the risk of blocking of the coarse particles in this zone is higher. Accordingly, the flow performance of the mixtures in this critical zone can be decisive in order to confirm the formwork filling quality demands, such as filling capacity, passing ability, and stability (i.e., static, shear-induced, and gravitational segregation).

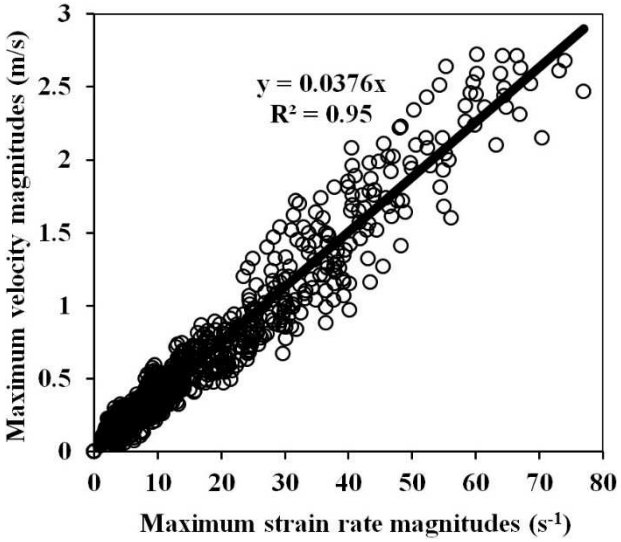

Figure 6. 13 Maximum flow velocity versus maximum strain rate magnitudes

6.5 Conclusions

The flowability and passing ability of three SCC mixtures designed with different plastic viscosity of 20, 30, and 40 Pa.s in a reinforced beam were experimentally evaluated and numerically simulated. Flow simulations were successfully carried out using a CFD software to reproduce the experimental results that were observed in casting these SCC mixtures. Based on the presented results, the main concluding remarks are as follows:

- For a given yield stress value of 60 Pa, the maximum flow time is greatly affected by the viscosity of the mixture. According to the experimental results, increasing the plastic viscosity of the mixtures from 20 to 40 Pa.s resulted in increasing the flow time required for the flow front to reach the end of the beam from 19 to 40 s (i.e., 111% increase).

- The numerical simulations are found to be in very good agreements with the experimental results in terms of free surface profiles, for each time step, having estimation ratios between 0.92 and 1.09 (i.e., the maximum dispersion of -8% to +9%), as well as coefficients of correlation (R^2) higher than 0.96.

- The numerical simulations showed that for a given yield stress of 60 Pa, increasing the viscosity of the SCC from 15 to 50 Pa.s can lead to a decrease in maximum magnitudes of the flow rate, velocity of the flow surface in the vertical compartment of the beam, velocity of the flow front in the horizontal channel, strain rate, and mass-averaged kinetic energy by 45%, 47%, 48%, 53%, and 78%, respectively. These properties are strongly correlated with the viscosity of the mixture with correlation coefficients (R^2) higher than 0.99.

- The calculated velocity and shear strain rate values were exploited to calculate the critical flow depth ($h_{critical}$) corresponding to the highest potential of dynamic segregation. This value is estimated to be 38 mm which is located right above the bottom row of horizontal bars in the reinforced cage inside the horizontal leg of the modeled beam. According to the narrow gaps existing between the bars and the formwork walls, the flow performance

of the mixtures in this critical zone can be decisive in order to confirm the formwork filling quality demands, such as filling capacity, passing ability, and stability (i.e., static, shear-induced, and gravitational segregation).

- The numerical simulations revealed that the design of the beam (i.e., a V-shaped vertical part together with an L-shaped beam) resulted in more horizontal displacement of SCC mixtures compared to the vertical one, having more than 3 times higher values. This can lead to a faster filling of the reinforced beam. Furthermore, the estimated maximum values of flow rate, ranged between 13 and 24 L/s (i.e., 47 to 86 m^3/hr), which are comparable to those encountered in SCC pumping operations.

- The simulations of flow surface displacement and flowability of SCC in the vertical direction showed that the investigated mixtures exhibited four different flow behaviors in the different shaped sections of the vertical compartment of the beam. Unlike the lower located sections, the velocity of the flow surface in the upper rectangular part of the vertical compartment increases by higher surface flow displacements. These plastic viscosity dependent increments vary between 0.065 to 0.113 m/s.

- The numerical results showed that the initial inertia stress values ranged between 173 to 679 Pa which are much greater than yield stress of the mixtures (60 Pa) and, therefore, can have highly effects on the flow performance of the mixtures. The inertia stresses can also prevent the velocity loss in the transition zone between V-shaped funnel and lower rectangular parts due to the suddenly change in the flow sections.

- The numerical simulation showed that the flow velocity loss in the V-shaped funnel is 3.4 to 8.6 times less than those observed in the lower rectangular part. SCC mixtures can therefore show higher vertical flowability with lower velocity loss in the V-shaped sections than rectangular ones. This can lead to higher efficiency in designing structural elements, regarding formwork filling ability and workability aspects of the SCC mixtures.

CHAPTER 7 NUMERICAL SIMULATION OF SELF-CONSOLIDATING CONCRETE FLOW AS A HETEROGENEOUS MATERIAL IN L-BOX SET-UP – EFFECT OF RHEOLOGICAL PARAMETERS ON FLOW PERFORMANCE

Authors and Affiliations:

Masoud Hosseinpoor: Ph.D. Candidate, Department of Civil Engineering, Université de Sherbrooke, Sherbrooke, Quebec, Canada, J1K2R1
Email: masoud.hosseinpoor@usherbrooke.ca

Kamal H. Khayat: Professor, Department of Civil, Architectural and Environmental Engineering, Missouri University of Science and Technology, 224 Engineering Research Laboratory, 500 W. 16th St., Rolla, MO 65409-0710, USA.
Email: khayatk@mst.edu

Ammar Yahia: Associate Professor, Department of Civil Engineering, Université de Sherbrooke, Sherbrooke, Quebec, Canada, J1K2R1
Email: ammar.yahia@usherbrooke.ca

Paper submitted to Cement and Concrete Composites, on 24th August 2016

Abstract

A CFD software (FLOW3D®) was used to simulate the effect of rheological parameters on the flowability, blocking resistance, and dynamic segregation of self-consolidating concrete (SCC)

in the horizontal and vertical directions of the L-Box set-up. Different suspending fluids having five plastic viscosity values (10-50 Pa.s), three yield stress values (14-75 Pa), two fluid densities (2000 and 2500 kg/m^3), and two shear elasticity modulus values (100 and 1000 Pa) were considered. The suspensions consisted of a number of 135 in total spherical particles with 20-mm in diameter and 2500 kg/m^3 density.

The results of 25 simulations in total are found to correlate well with the rheological parameters of the suspending fluid. Plastic viscosity of the suspending fluid was shown to be the most dominant parameter affecting flow performance of SCC in the L-Box test. A new approach was also proposed to classify the investigated SCC mixtures based on the filling ability properties.

Keywords: Dynamic Stability; Flowability; L-Box Test; Numerical Simulation; Passing Ability; Self-Consolidating Concrete

7.1 Introduction

Dispersion of suspended particles has a significant effect on flow behavior of materials in various domains, including debris flow [1], snow avalanche [2], conventional hydrotransport processes [3-5], and industrial applications [6-8]. On the other hand, separation of coarse particles from the suspending fluid has negative influence on the performance of the suspensions and must be prevented in production processes. Therefore, there is a wide concern to study particle migration in granular flow motion and suspension dynamics transport [9-13]. Segregation of solid particles can be due to the gravitational and shear induced particle migration. Gravitational segregation occurs when there is a gradient in gravitational forces between the coarse particles and the suspending fluid due to a difference of density of the materials [14]. On the other hand, shear-induced segregation is defined as the migration of particles from regions of higher shear rates to the regions of lower shear. This results a decrease in the suspensions viscosity after a given shearing period even though the viscosity of the homogeneous suspending fluid remains constant under a given shear history applied on the suspension [9, 15-17]. Recently, there is a great interest to study shear-induced migration and gravitational settlement of solid particles suspended in Non-Newtonian suspending fluids [18-

21]. Numerical simulation using computational fluid dynamics (CFD) was employed as a powerful tool to study these heterogeneous behaviors of the suspensions [184-187].

Self-consolidating concrete (SCC) has pushed back traditional limits concerning the casting of densely reinforced and complex structural elements in concrete construction [23]. SCC is a suspension of fine and coarse aggregates in a viscoelastoplastic cement paste. SCC is characterized by a relatively high fluidity compared to conventional concrete, which makes it more sensitive to segregation during flow (i.e., dynamic segregation) and thereafter at rest (i.e., static segregation) [28-30]. Static segregation occurs when the concrete is at rest, and aggregate particles can settle down given their higher density compared to the paste/mortar suspending fluid [83]. Several experimental tests were developed to evaluate static stability of SCC. This includes the determination of coarse particle contents and different vertical layers [84 and 85], electrical conductivity [86], penetration depth [87 and 88], and image analysis techniques [89].

Dynamic segregation corresponds to the separation of aggregate from cement paste/mortar during flow of concrete [36, 38, 90, and 208]. Dynamic segregation occurs in both horizontal and vertical directions, which results in less aggregate content at flow front and top layers of the flowing concrete, respectively [29]. New experimental tests are developed recently to evaluate dynamic stability of SCC [36, 37, 91, and 92]. For example, SCC is allowed to spread in a channel, and particle contents of samples token at the entrance and end of the channel are compared to determine horizontal dynamic segregation [91]. Esmaeilkhanian et al. [36 and 37] developed the T-box test which simulates the horizontal motion of the concrete by tilting motion of the box in rotating cycles. Vertical and horizontal dynamic segregation of SCC are measured by determining the penetration depths and relative coarse aggregate contents at two sides of the box, respectively.

Dynamic segregation can increase when SCC flows over a long distance or in the presence of obstacles (i.e., passing ability). Passing ability refers to the ability of the concrete to pass through the narrow gaps between the obstacles to hold the aggregates in the suspension and, consequently, maintain its homogeneity [24, 31, and 32]. Several empirical tests were developed to evaluate the passing ability of SCC, such as J-Ring [82], U-Box, Filling box, and L-Box [25]

test set-ups. The properties of the final flow profiles are measured and compared at locations before and after the obstacles to quantify the blocking resistance of the concrete.

The L-Box test is often used to evaluate the restricted flow of SCC in the presence of obstacles and evaluate the passing ability and dynamic segregation [25]. The L-Box consists of vertical and horizontal compartments that are separated by a sliding door. The concrete is cast in the vertical compartment, and once the sliding door is opened, the concrete is gravitationally driven into the horizontal channel. Limited studies have been conducted to investigate the relationship between the rheological parameters of the SCC mixtures and the L-Box response [40 and 180]. Turgut et al. [92] developed a modified L-Box set-up to evaluate dynamic segregation of SCC at different locations in the horizontal channel. Nepomuceno et al. [209] proposed semi-empirical models to optimize the maximum aggregate volume fraction to achieve a proper passing ability of SCC under different flow restrictions and bar spacings. Yahia et al. [204] developed statistical models to evaluate the coupled effect of mix design and rebar spacing on passing ability of SCC.

Dynamic stability and passing ability are two key parameters which should be satisfied as the quality requirements for successful SCC casting process. Developing numerical techniques to predict flow characteristics of SCC during casting can improve the selection of mixture composition and ensure better planning of concrete placement to achieve successful filling of the formwork. The numerical modeling of fresh SCC flow should take into account the interaction between the aggregates, the suspending fluid cement paste/mortar, arrangement of reinforcing bars, and formwork wall characteristics [29, 42-44]. In the recent years, numerical simulations have been employed as a theoretical tool to predict dynamic stability and passing ability of SCC [29, and 52-47]. Spangenberg et al. [46] studied flow induced particle migration in SCC and showed that in the case of industrial casting of SCC, gravity induced particle migration dominates all other potential sources of dynamic segregation induced by flow. Spangenberg et al. [47] investigated different patterns of gravity induced dynamic segregation during casting of SCC using experimental tests and numerical simulations. They showed that gravity induced particle migration has dominant effect on the coarsest particles resulting in a

decrease of coarse aggregate content along the horizontal distance from the casting point and also in the vertical direction at the top layer of the concrete.

In this paper, a computational fluid dynamics (CFD) software was employed to simulate free surface flow of SCC in the L-Box test apparatus. The Navier–Stokes and conservation of mass equations for incompressible materials are solved by the volume of fluid (VOF) method [150]. In total, 25 simulations were developed to study the effect of rheological parameters and density of suspending fluid on flowability, passing ability, blocking resistance, and dynamic stability of SCC in the horizontal and vertical directions along the horizontal leg of the L-Box. Suspending fluids, which corresponds to the stable and homogeneous portion of the mixture, with various yield stress, plastic viscosity, and shear elasticity modulus values were considered to evaluate the effect of rheological parameters on shear-induced segregation at elastic and plastic states of the fluid. It must be noted that shear elasticity modulus is the ratio of shear stress to shear strain in the elastic state. On the other hand, two different suspending fluid densities were investigated to evaluate gravitational induced segregation of the modelled suspensions. The paper discusses the results of the numerical simulation in terms of flow velocity, strain rate, kinetic energy, flow profiles, and particle distribution throughout the L-Box channel (horizontal direction) and fluid depth (vertical direction) for a given period of flow time.

7.2 Properties of modelled materials

The investigated parameters of the CFD modeling included five plastic viscosity values (μ_p = 10, 17, 25, 38, and 50 Pa.s), three yield stress values (τ_0 = 14, 45, and 75 Pa), and two shear elasticity modulus values (G = 100 and 1000 Pa) for the suspending fluid. Furthermore, two different suspending medium densities (ρ = 2000 and 2500 kg/m^3) were used to suspend solid particles with a density of 2500 kg/m^3. Also, the modelled suspensions included 135 spherical particles of 20 mm of diameter with a density of 2500 kg/m^3. The L-Box set-up included the three standard bars of 12 mm in diameter and 200 mm in height located right after the gate separating the vertical and horizontal compartments of the L-Box

7.3 Numerical simulations and boundary conditions

A CFD software (FLOW3D®) was employed to simulate free surface flow of the SCC in the L-Box test apparatus. The basic equations of the conservation of mass for incompressible materials and the 3D Navier–Stokes equations are solved by the Volume of Fluid (VOF) method [150], using 1st order momentum advection. In total, 25 simulations were carried out for a period of flow of 6.4 s, which is the minimum duration to empty the vertical section of the L-Box for the selected range of plastic viscosity values investigated in this study. In order to discretize the geometry, solid elements, and suspension, two mesh blocks of 326,832 cells with 5-mm size in the x, y, and z directions were created.

The Dirichlet-Neumann boundary conditions were imposed to the flow domain based on the geometry of the L-Box; the velocity of the walls and the gate rising rate were set to zero and 0.03 m/s, respectively, as indicated in Fig. 7.1. The friction boundary conditions were assumed between particles, fluid, and the walls of the apparatus with a friction coefficient value of 0.4 (according to Coulomb's law of friction) [205]. The modelled fluids are considered as Non-Newtonian Bingham fluids using an elasto-viscoplastic model with implicit numerical approximation. Gravity stresses are calculated using gravitational acceleration value of 9.81 m/s^2. In order to consider particle-particle, particle-obstacle, and particle-wall interactions, a coefficient of restitution of 0.8 was applied for collision physical model. The modelled flow is assumed as laminar flow type [48]. It is worthy to mention that numerical simulations carried out on an i7-2600 CPU 3.40 GHz processor, required a total running time between 26 and 154 hours. The running times depend mostly on the plastic viscosity of the suspending fluid. Indeed, the simulation of the flow of higher viscous suspensions took more calculation time than less viscous ones.

7.3.1 Sampling methods and anticipated results

In order to evaluate flowability of the modelled suspensions, the results of the simulations are presented in 0.1-s time steps in forms of flow velocity, strain rate magnitudes, and flow profiles. The modelled mixtures could be then classified based on self-leveling and self-consolidating

properties using calculated horizontal and vertical motions of the fluid in two perpendicular parts of the L-Box apparatus. Blocking resistance and dynamic stability properties of the suspensions in the horizontal direction are also calculated by measuring the volumetric particle contents in seven 10-cm long sections through the L-Box horizontal channel that are illustrated in Fig. 7.1b. The number and position of the particles, as well as the volume of the fluid in each section are calculated at each 0.1-s time steps. On the other hand, dynamic stability of the suspensions in the vertical direction is evaluated by comparing the volumetric particle contents in three vertical layers (bottom, middle, and top) at the end of the flow. As presented in Fig. 7.1c, the thickness of both the bottom and middle layers is 3 cm, and the remaining thickness (Z > 6 cm) corresponds to the top layer. The thicknesses were decides based on the maximum typical values 8 to 10 cm (average: 9 cm) for SCC profile thicknesses in L-Box test, in arrested state.

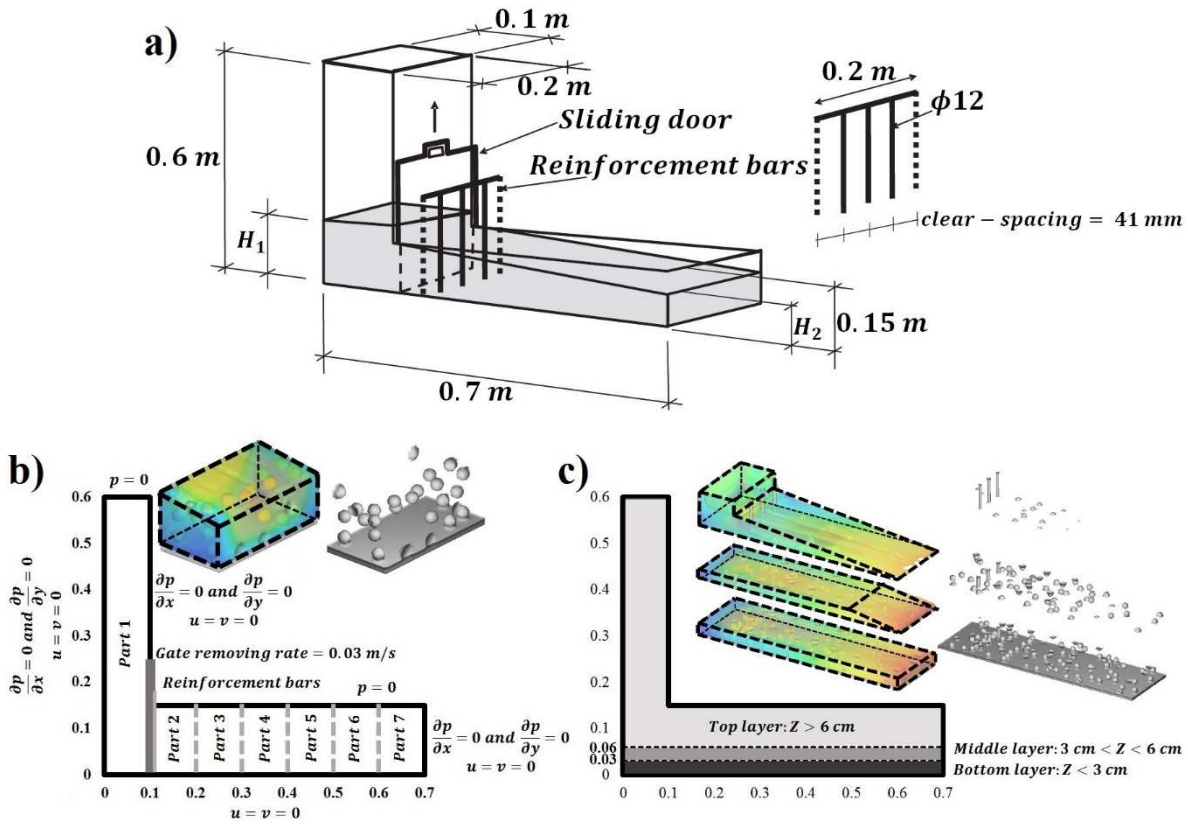

Figure 7. 1 a) Schematics of L-Box set-up and obstacle configuration, b) horizontal sampling sections, and boundary conditions, and c) vertical sampling sections

7.4 Results and discussion

7.4.1 Effect of viscosity and yield Stress of the suspending fluid on flowability of the suspension

The numerical simulations presented in this section were carried out on suspensions with a fluid density of 2500 kg/m^3 and shear elasticity modulus of 100 Pa. As expected, for a given viscosity, the increase in yield stress decreases the L-Box blocking ratio (H_2/H_1), where H_2 and H_1 values are the depths of the final profile at the end of horizontal channel and the back wall of the vertical compartment of the L-Box set-up behind the bars, respectively. As shown in Fig. 7.2, increasing both the viscosity and yield stress of the suspending fluid resulted in lower H_2/H_1. For example, in the case of suspension having suspending fluid plastic viscosity of 25 Pa.s, the increase in yield stress from 14 to 75 Pa can decrease H_2/H_1 from 0.81 to 0.56 (i.e., 31% reduction). On the other hand, for a yield stress of 14 Pa, the increase in plastic viscosity from 10 to 50 Pa.s can decrease the H_2/H_1 from 0.94 to 0.26 (i.e., 72% reduction). The plastic viscosity seems to have a more dominant effect on H_2/H_1 than yield stress.

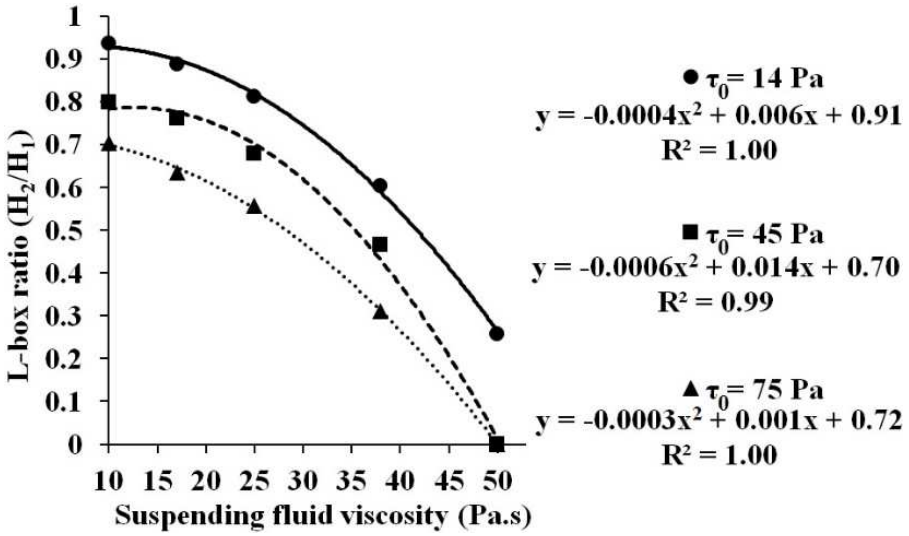

Figure 7. 2 L-Box ratio for different mixtures versus plastic viscosity of the suspending fluid

As shown in Fig. 7.3, higher viscosity and yield stress values resulted in less horizontal displacement of flow front in horizontal part and higher free surface level in the vertical part of

the L-Box. For example, in the case of a suspension having suspending fluid plastic viscosity of 25 Pa.s, in a given flow time of 3 s, the increase in yield stress from 14 to 75 Pa can decrease the flow front position in horizontal leg from 0.605 to 0.566 m (i.e., 6% decrease) and increase the free surface level in the vertical part from 0.145 to 0.160 m (i.e., 10% increase). On the other hand, for a yield stress of 45 Pa in a given flow time of 2 s, the increase in plastic viscosity from 10 to 50 Pa.s can result in decreasing the flow front position in horizontal leg from 0.631 to 0.311 m (i.e., 51 % decrease) and increasing the free surface level in the vertical part from 0.175 to 0.410 m (i.e., 134% increase). Therefore, it can be concluded that plastic viscosity has a higher effect on flow profile positions in the vertical and horizontal parts of the L-Box than the yield stress.

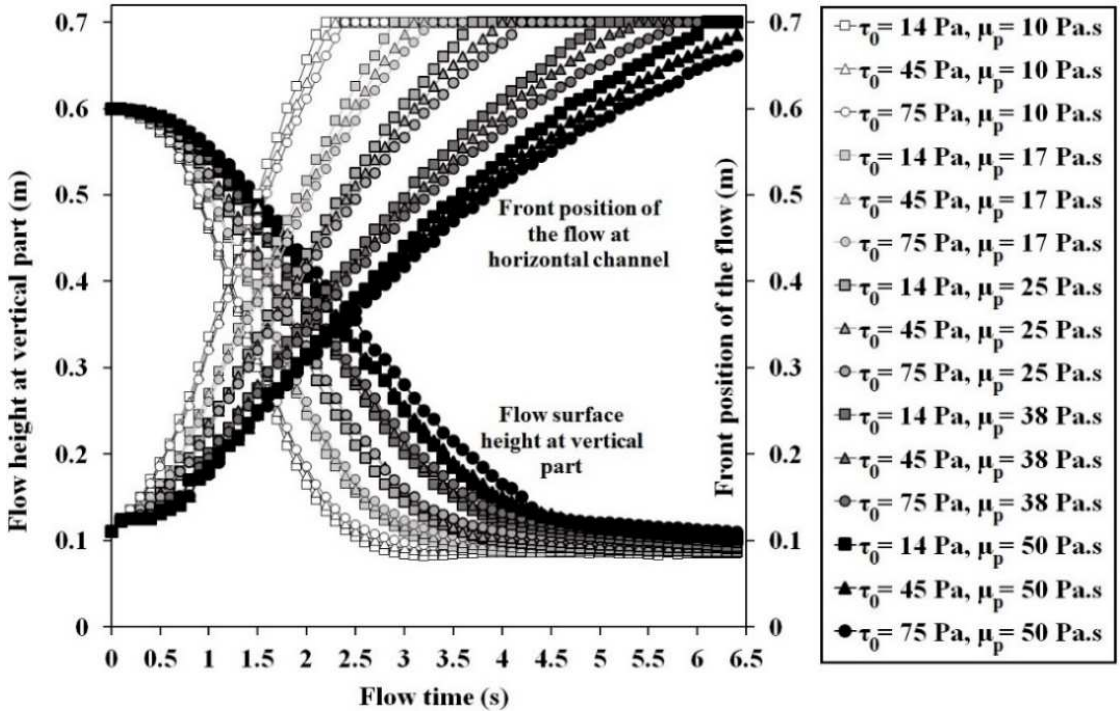

Figure 7. 3 Flow height and front position of the flow at vertical and horizontal parts

The displacement of flow surface and profile front in the vertical and horizontal compartments of the L-Box, respectively, calculated from data in Fig. 7.3 are used to evaluate the effect of rheological parameters on self-consolidating and self-leveling properties of the mixtures (Fig. 7.4). As can be observed, higher viscosity of the suspending fluid can result in higher vertical displacement of flow surface in the vertical part than horizontal motion of flow front along the

horizontal leg of L-Box, regardless of the yield stress. Therefore, higher viscosity SCC can be recommended for vertical applications, such as casting of column or tremie concreting, where higher flowability is needed in the vertical direction (self-consolidating properties). On the other hand, lower viscosity SCC can be more appropriate for horizontal applications like casting of beam and slab elements (self-leveling properties).

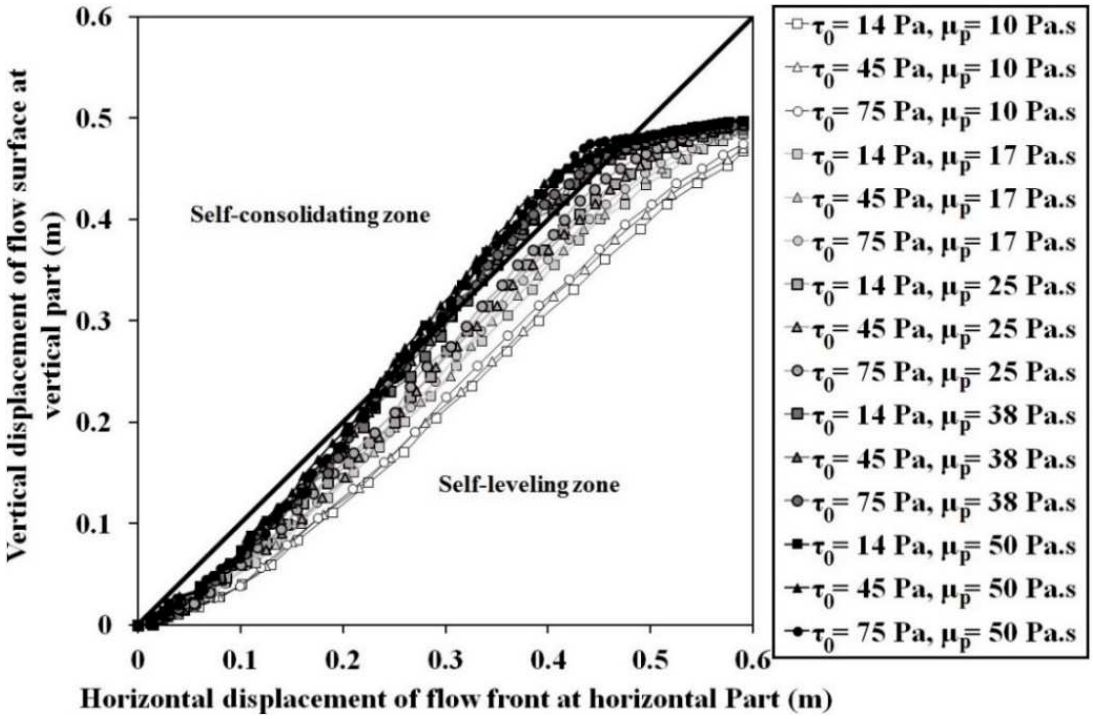

Figure 7. 4 Vertical flow displacement versus horizontal flow motion

Time values taken by the flow front to reach 40 cm after the sliding door ($T_{40\ cm}$) are presented in Fig. 7.5. As expected, the viscosity of suspending fluid shows more dominant effect on flow times than yield stress. Moreover, as can be observed, the values of $T_{40\ cm}$ increase when plastic viscosity of suspending fluid increases. The linear correlation between $T_{40\ cm}$ and viscosity is showed to have a coefficient of correlation (R^2) of 1.00. Accordingly, increasing the plastic viscosity of suspending fluid can decrease flow velocity and deformation of the suspensions for a given coarse particle content.

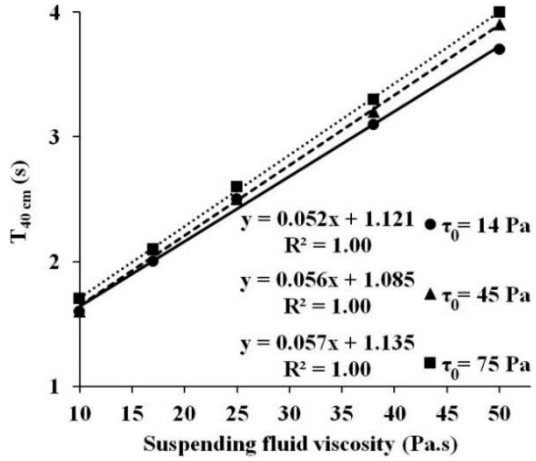

Figure 7. 5 $T_{40\ cm}$ versus plastic viscosity of the suspending fluid

The simulation results presented in Fig. 7.6 showed that maximum velocity and strain rate decrease when the viscosity and yield stress of the suspending fluid increase. It is worthy to mention that excellent correlations were observed (R^2 > 0.99). For example, in a given suspending fluid plastic viscosity value of 10 Pa.s, increasing yield stress from 14 to 75 Pa can decrease the maximum magnitudes of velocity and strain rate from 0.6 to 0.565 m/s (i.e., 6% reduction) and from 128 to 88.1 s^{-1} (i.e., 31% reduction), respectively. On the other hand, in a given suspending fluid yield stress of 14 Pa, increasing plastic viscosity from 10 to 50 Pa can decrease the maximum magnitudes of velocity and strain rate from 0.6 to 0.22 m/s (i.e., 63% reduction) and from 128 to 36.4 s^{-1} (i.e., 72% reduction), respectively.

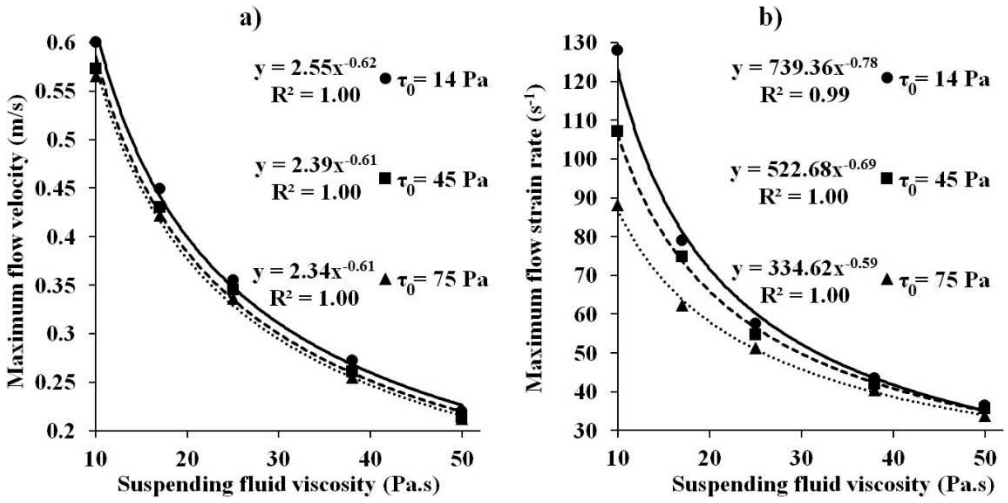

Figure 7. 6 a) Maximum velocity and b) strain rate magnitudes versus plastic viscosity of the suspending fluid

7.4.2 Effect of viscosity and yield stress of the suspending fluid on passing ability of the suspension

Calculating the fluid volume and particle content in two horizontal sampling sections, located behind the bars (Part 1) and at the end of horizontal channel (Part 7), the blocking index (B.I.) can be defined for each 0.1-s time step using Eq. (8.1):

$$\text{B.I.}\,(\%) = \frac{\text{Particle content @ Part1} - \text{Particle content @ Part7}}{\text{Initial mean particle content}} \times 100\% \qquad (7.1)$$

As shown in Fig. 7.7, increasing the viscosity of the suspending fluid has more effect on increasing the blocking index of the suspension than yield stress.

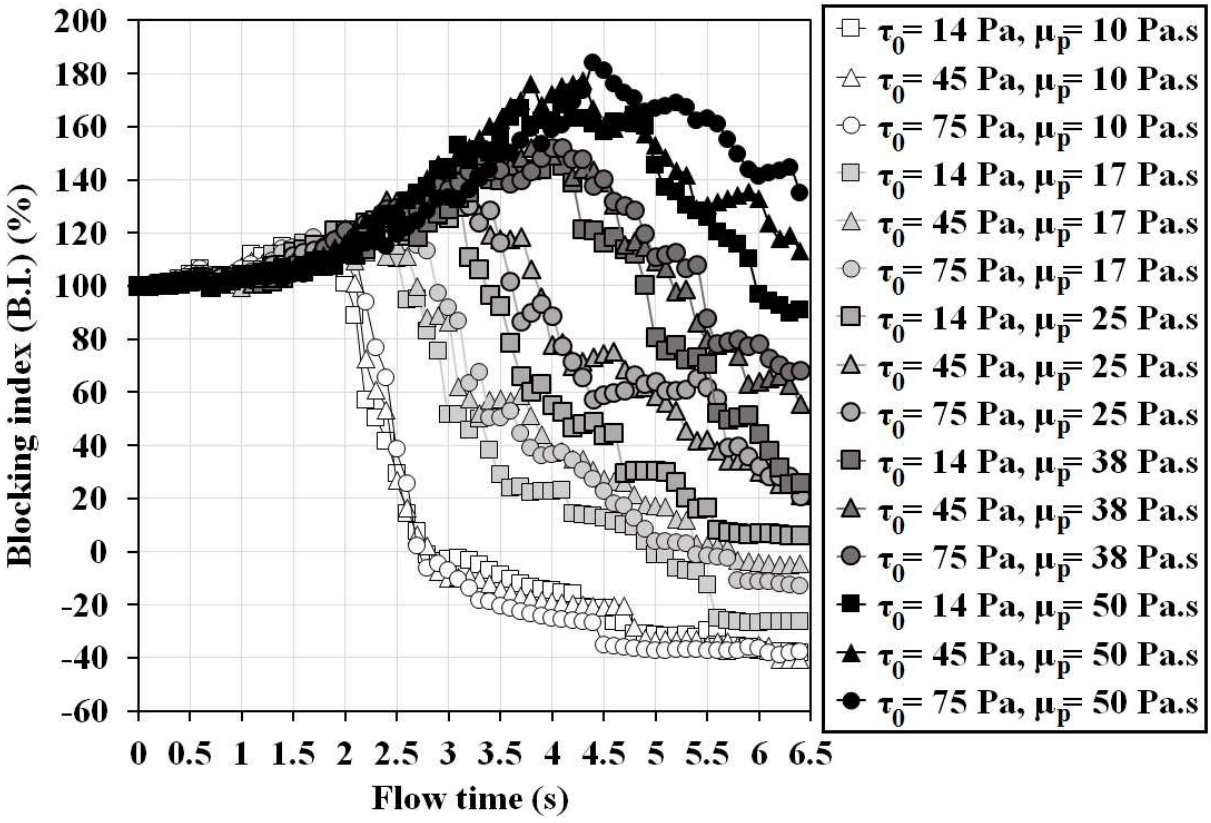

Figure 7. 7 Blocking index versus flow time

As can be observed, for all the investigated suspensions the B.I. value increases with time to a maximum value and then decreases. The ascending part of the curves can be related to the blocking period, which refers to the flow times where the vertical part is not completely empty and the particles are accumulated behind the bars (Part1) with less velocity than the suspending fluid. On the other hand, the behavior of suspensions in the descending part of the curve can be explained by the flowability of the mixtures which can push the blocked particles to move and pass through the bars and reach the end of the horizontal channel (Part7). For example, the most flowable mixtures with the minimum viscosity values (10 Pa.s) showed higher particle content at the end of the channel (Part7) than in Part1 (i.e., negative B.I. values) at the end of the flow period. Accordingly, for each suspension, the maximum B.I. value, which is called $B.I._{max}$, is selected to indicate the risk of blocking (Fig. 7.8). As can be observed, $B.I._{max}$ can increase with viscosity of the suspending fluid with very high correlation. However, the yield stress showed less effect on $B.I._{max}$ than viscosity.

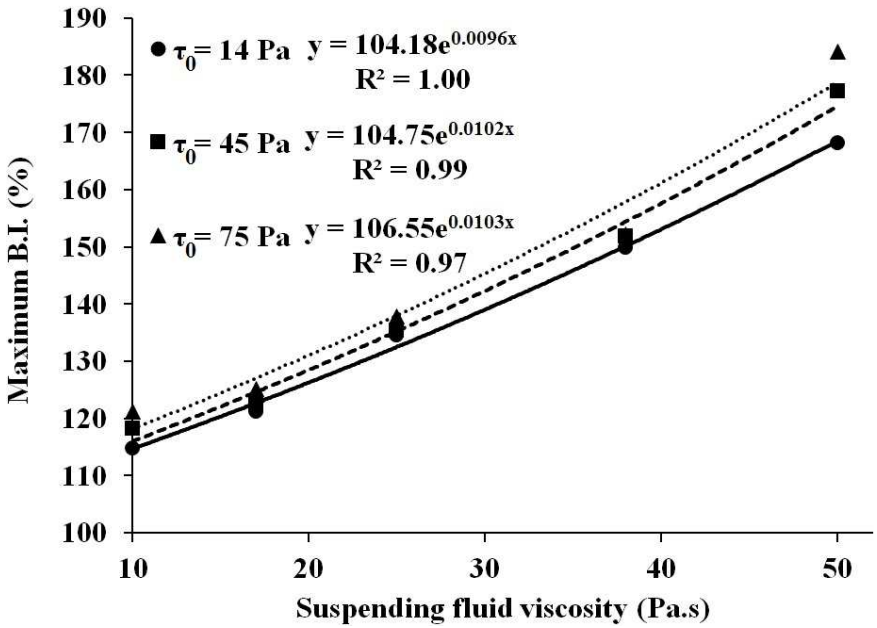

Figure 7. 8 Maximum blocking index versus plastic viscosity of the suspending fluid

7.4.3 Effect of viscosity and yield stress of the suspending fluid on dynamic stability of the suspension

Calculating the fluid volume and particle content in each of the seven horizontal sections along the horizontal leg of the L-Box, shear-induced dynamic segregation of the mixtures in the horizontal direction can be quantified for each 0.1-s time step by coefficient of variation of particle contents in all the seven horizontal parts (Parts 1 to 7), as follows:

$$\mathrm{COV} = \frac{\text{Standard deviation of particle contents (Parts 1,2,3,4,5,6,and 7)}}{\text{Average of particle contents (Parts 1,2,3,4,5,6,and 7)}} \tag{7.2}$$

As can be observed in Fig. 7.9, increasing the plastic viscosity of the suspending fluid can increase dynamic segregation of the suspension, regardless of the yield stress. Also, it can be concluded that according to flowability of the mixtures, the values of COV decrease with flow time. Indeed, it takes less flow time for higher flowable mixtures to reach a comparable value of COV. This flow time is called the "stabilization time", which means the time taken by the flowing suspension to reach its maximum filling capacity. For example, increasing viscosity of the suspending fluid from 10 to 50 Pa.s can lead to increase the stabilization time from 2.2 to 4 s.

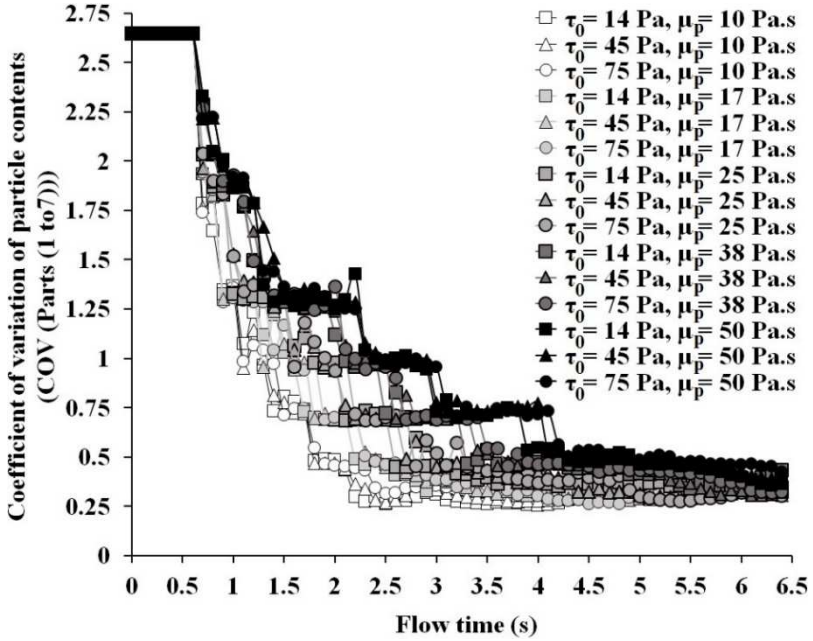

Figure 7. 9 COV values of particle contents in horizontal sections versus flow time

In order to evaluate dynamic stability in the vertical direction, the ratio between particle contents at the end of flow (i.e., after 6.4 s) in three successive layers (top, middle, and bottom) and initial particle content are presented in Fig. 7.10 for different rheological parameters of the suspending fluid (i.e., yield stress from 14 to 75 Pa, and plastic viscosity from 10 to 50 Pa.s). As can be observed, particles migrated from top layers to middle and bottom layers of the L-Box horizontal leg. This results in less particle content in the top layer than the initial particle content. It can be observed that the particle contents in the middle and bottom layers are higher than the initial particle content. Numerical simulations revealed that, regardless of yield stress values of 14 to 75 Pa, the increase of viscosity of the suspending fluid from 10 to 50 Pa.s, can decrease both particle migration from the top layer and accumulation of particles in the bottom layers. This results in particle content ratio closer to 100% and simultaneously increases the particle content in the middle layer.

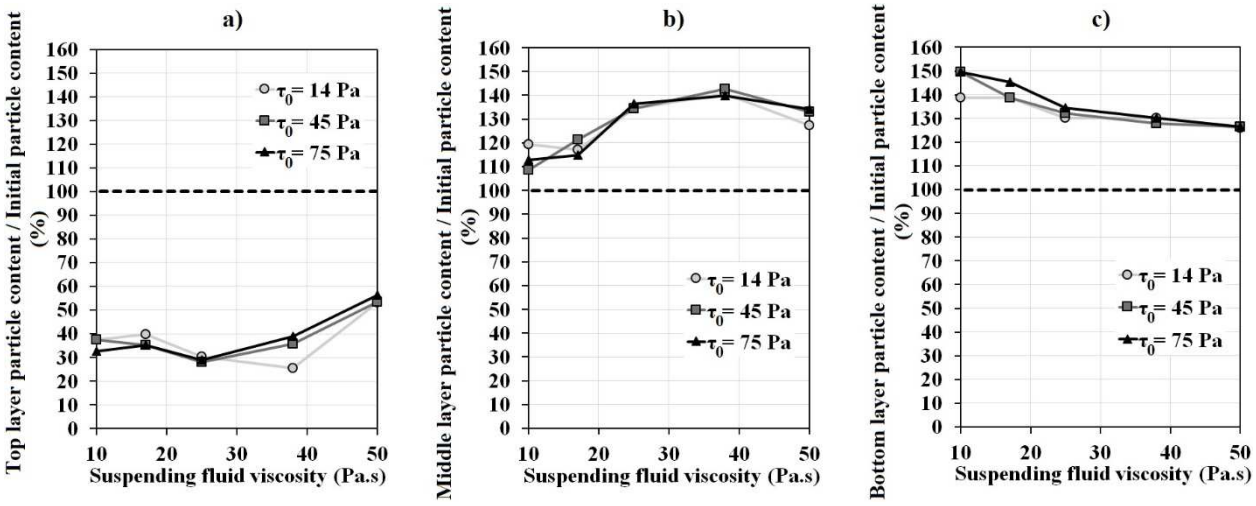

Figure 7. 10 The ratio of particle content in different vertical layers of a) top, b) middle, and c) bottom to initial particle content versus plastic viscosity of the suspending fluid

As a result, vertical dynamic segregation index (V.D.S.I.) can be defined as the ratio of the spread in particle content of the top and bottom layers to the initial particle content, as follows:

$$\text{V. D. S. I. (\%)} = \frac{\text{Particle content @ bottom layer} - \text{Particle content @ top layer}}{\text{Initial mean particle content}} \times 100\% \qquad (7.3)$$

The values of the vertical dynamic segregation index (V.D.S.I.) are compared for different rheological parameters in Fig. 7.11. As can be observed, in a given yield stress value of the suspending fluid, the SCC mixtures can exhibit less dynamic segregation in the vertical direction by increasing plastic viscosity of suspending fluid. For example, for the suspending fluids with yield stress values of 14, 45, and 75 Pa, increasing the plastic viscosity of the suspending fluid from 10 to 50 Pa.s can decrease the V.D.S.I. values from 99% to 73% (i.e., 26% reduction), from 104% to 73% (i.e., 31% reduction), and from 117% to 70% (i.e., 47% reduction), respectively. This can be due to the fact that increasing plastic viscosity of the suspending fluid can increase the drag forces exerted on the particles. This can prevent particles to migrate towards the bottom layer and reduce the vertical dynamic segregation of the suspension.

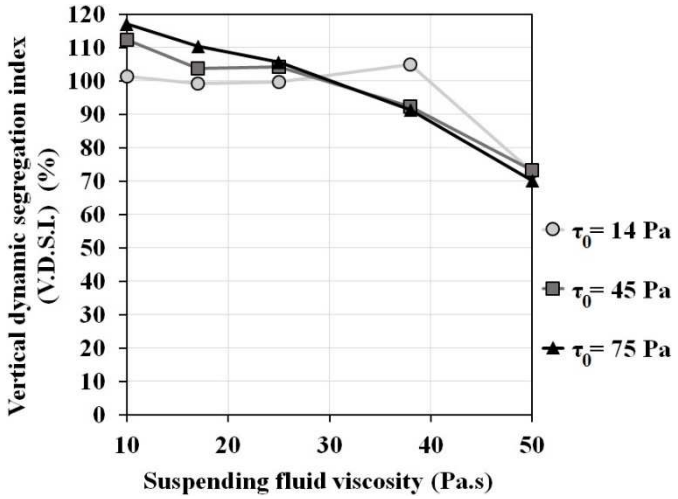

Figure 7. 11 Vertical dynamic segregation index versus plastic viscosity of the suspending fluid

The maximum blocking indices ($B.I._{max}$) and V.D.S.I. values are correlated to the plastic viscosity of the suspending fluid (Fig. 7.12), where $B.I._{max}$ is calculated by the maximum values of B.I. obtained for each mixture, using Eq. (7.1). As can be observed, the plastic viscosity of suspending fluid has opposite effects on passing ability and vertical dynamic stability of suspensions, regardless of the yield stress values.

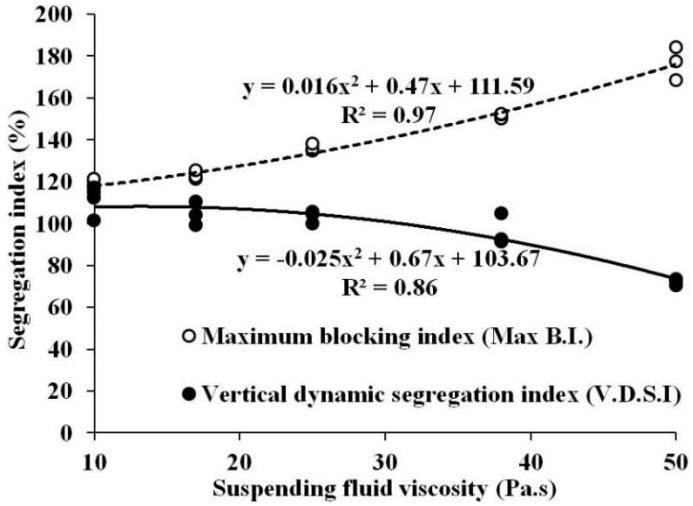

Figure 7. 12 Opposite effect of the plastic viscosity of the suspending fluid on passing ability and vertical dynamic segregation: values of $B.I._{max}$ and V.D.S.I. versus plastic viscosity of the suspending fluid

Based on these results, it can be concluded that higher viscosity SCC mixtures are more appropriate when higher dynamic stability is needed in the vertical direction (tall elements, such as walls and columns) than in the horizontal direction. Lower viscosity SCC mixtures are, however, recommended for horizontal applications to exhibit higher passing abilities in reinforced areas of the formwork.

7.4.4 Effect of density of the suspending fluid on flowability of the suspension

As seen in the previous section, the maximum $B.I._{max}$ values are obtained with the suspending fluids that have a yield stress of 75 Pa. The effect of density is studied for this relatively high yield stress considering two different fluid density of 2000 and 2500 kg/m^3. As can be observed in Fig. 7.13, suspensions with less fluid density exhibited more displacement in the vertical direction than the horizontal direction. This resulted in more self-consolidating behavior than self-levelling properties.

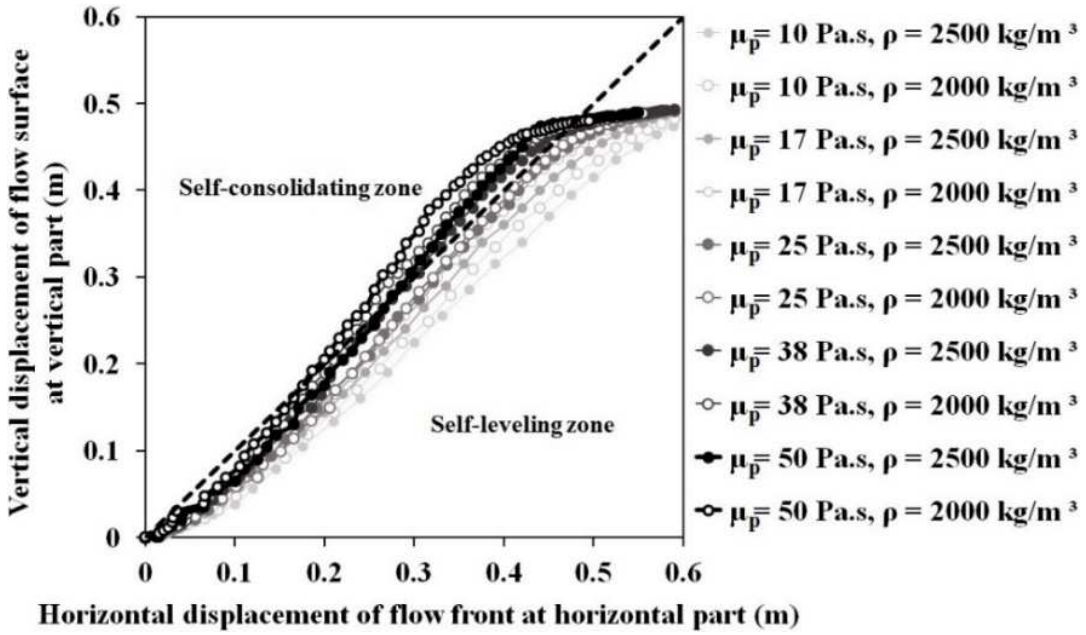

Figure 7. 13 Vertical flow displacement versus horizontal flow motion for modeled SCC mixtures with different rheological properties

The results presented in Fig. 7.14 revealed also that decreasing the density of the suspending fluid resulted in increasing of the final profile angle ($\tan^{-1}((H_1 - H_2)/0.7m)$) and $T_{40\,cm}$ values, regardless of plastic viscosity values. Therefore, the mixtures with less density of suspending fluid exhibit less flowability in horizontal direction. It is worthy to mention that final profile angle and $T_{40\,cm}$ values are well correlated with plastic viscosity of suspending fluid ($R^2 > 0.97$).

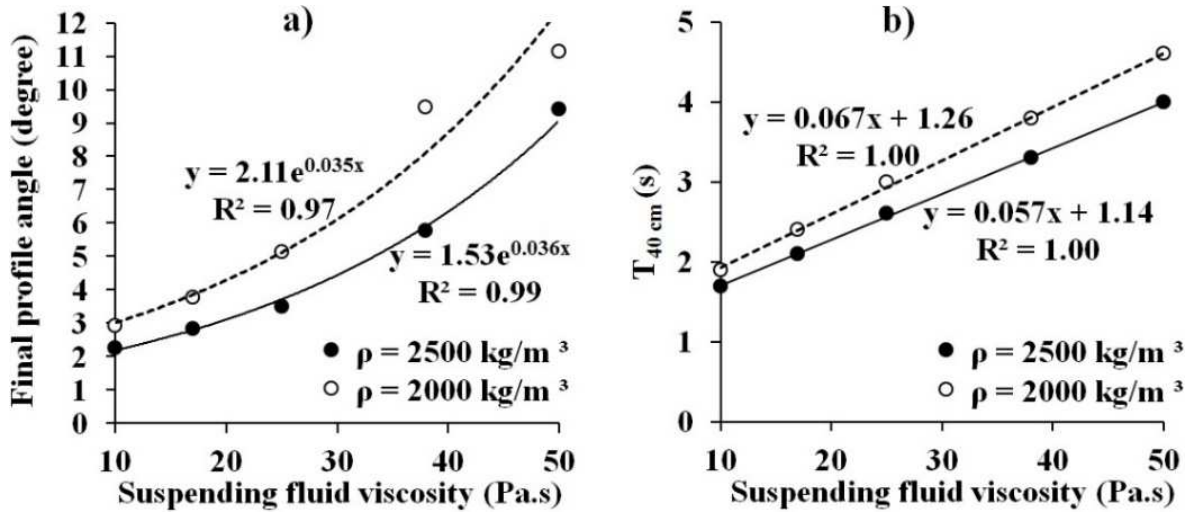

Figure 7. 14 a) Final profile angle and b) $T_{40\,cm}$ values versus plastic viscosity of the suspending fluid

It can also be observed in Fig. 7.15 that the use of a lower density suspending fluid can lead to lower flow velocity, strain rate, and energy For example, for the suspending fluid with plastic viscosity of 10 Pa.s, decreasing density from 2500 to 2000 kg/m^3 can decrease the maximum flow velocity, strain rate, and mass-averaged kinetic energy magnitudes from 0.565 to 0.490 m/s (i.e., 13% reduction), from 88.1 to 82.9 s^{-1} (i.e., 6% reduction), and from 0.0482 to 0.0376 J/kg (i.e., 22% reduction), respectively. This can be explained by the reduction in gravitational forces corresponding to the reduction in density of the suspending fluid.

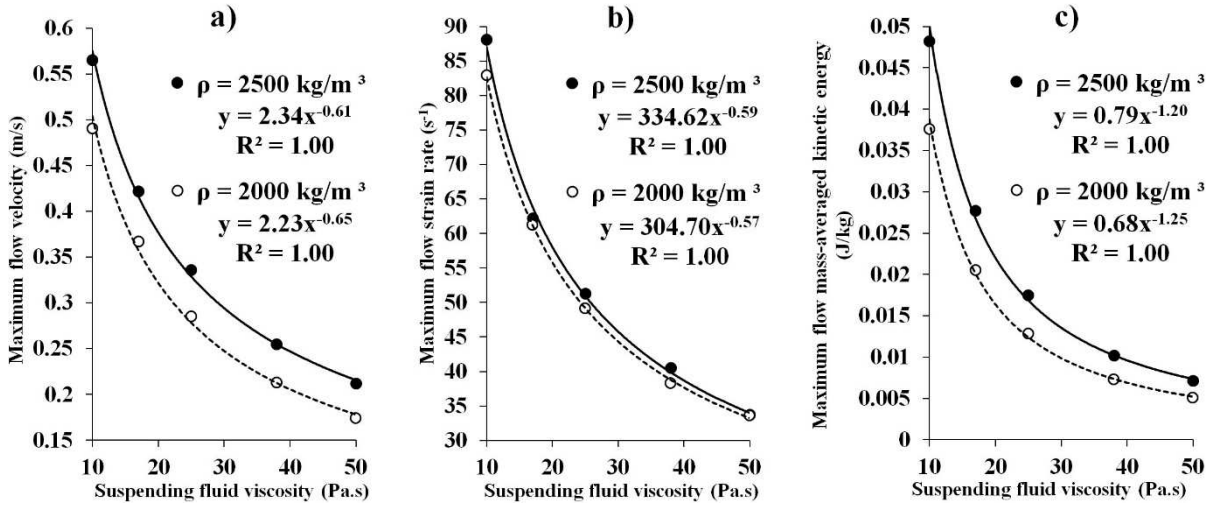

Figure 7. 15 Maximum a) velocity, b) strain rate, and c) mass-averaged kinetic energy magnitudes versus plastic viscosity of the suspending fluid

7.4.5 Effect of density of the suspending fluid on passing ability of the suspension

As a result of decreasing the fluid density, the relative velocity between the fluid and particles decreases. This results in decreasing the blocking index, as shown in Fig. 7.16. For example, for the suspending fluids with the plastic viscosity of 50 Pa.s, decreasing the density from 2500 to 2000 kg/m^3 resulted in decreasing the maximum values of blocking index from 184% to 175% (i.e., 9% reduction).

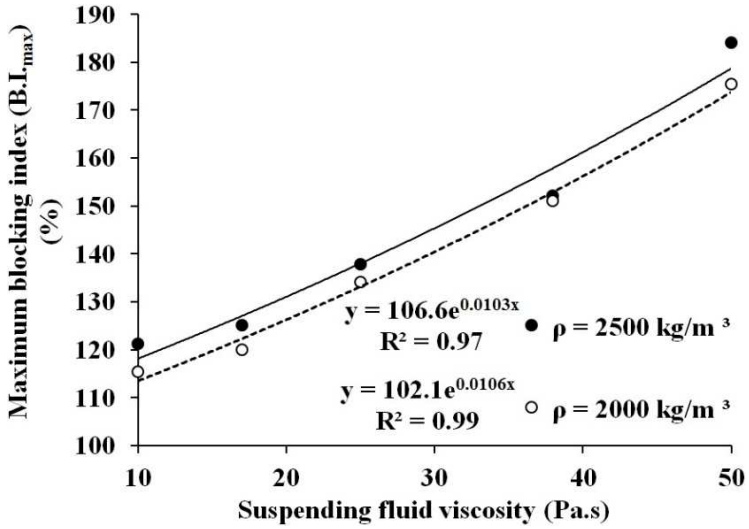

Figure 7. 16 Maximum blocking index versus plastic viscosity of the suspending fluid

7.4.6 Effect of density of the suspending fluid on dynamic stability of the suspension

Comparing the coefficient of variations of particle contents in seven horizontal sections obtained for the suspensions with different suspending fluid density, it can be revealed that a decrease in suspending fluid density can increase dynamic segregation in the horizontal direction. This can also be explained by the fact that decreasing gravitational forces results in lower kinetic flow energy available to bring along the particles to the longer distances (Fig. 7.15c). As can be observed in Fig. 7.17, it can also result in higher stabilization time, which means the flow time needed for each suspension to reach its maximum filling capacity. For example, in the case of suspending fluid viscosity of 50 Pa.s, decreasing fluid density from 2500 to 2000 kg/m^3 resulted in increasing the stabilization time from 4.3 to 5.3 s.

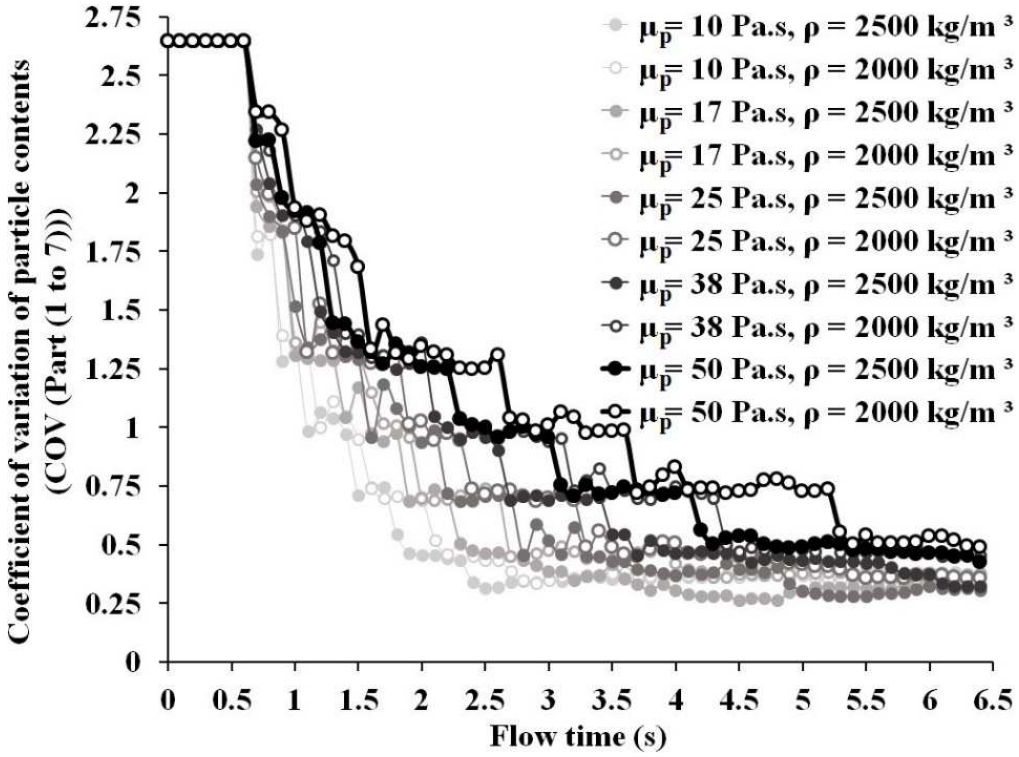

Figure 7. 17 COV values of particle content in horizontal sections versus flow time

In order to evaluate the effect of density of suspending fluid on dynamic segregation in vertical direction, the V.D.S.I. values are calculated using Eq. (7.3) for suspending fluid densities of 2000 and 2500 kg/m^3 and different viscosity values. As can be observed in Fig. 7.18, decreasing the suspending fluid density can highly affect vertical dynamic segregation. This can be explained by the gravitational induced particle migration that can take place due to the increase in the difference between the densities of particles and suspending fluid. Comparing these results with those of the passing ability, presented in Fig. 7.16, it can be concluded that changes in suspending fluid density has more effect on gravitational induced segregation than blocking resistance. However, this effect decreases when the viscosity of suspending fluid increases. For example, for the given suspending fluid plastic viscosity values of 10 and 50 Pa.s, decreasing suspending fluid density from 2500 to 2000 kg/m^3 can increase the values of vertical dynamic segregation index from 117% to 212% (i.e., 95% increase) and from 70% to 78% (i.e., 8% increase), respectively. Moreover, increasing viscosity of the suspending fluid has more effect (almost three times) on vertical dynamic segregation of the particles suspended in a fluid with less density. For example, increasing the suspending fluid viscosity from 10 to 50 Pa.s can

decrease the vertical dynamic segregation index from 212% to 78% (i.e., 134% reduction) and from 117% to 70% (i.e., 47% reduction) for the suspending fluid density values of 2000 and 2500 kg/m^3, respectively.

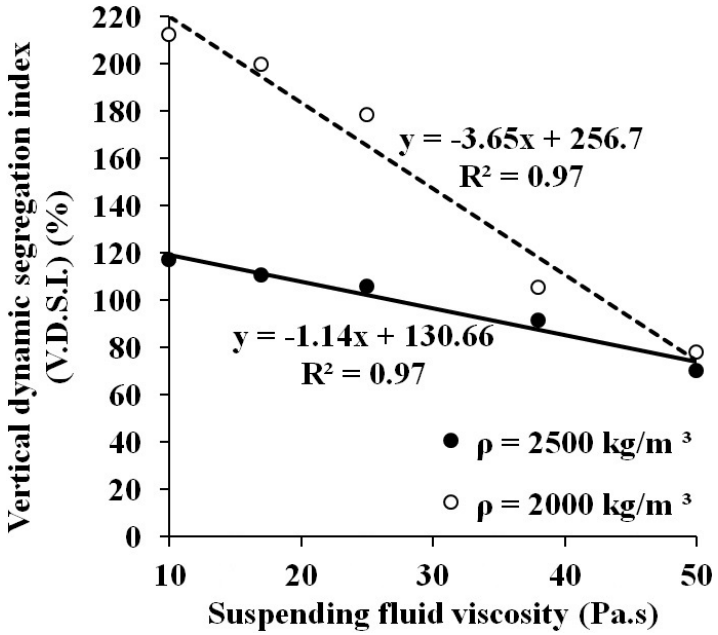

Figure 7. 18 Vertical dynamic segregation index versus plastic viscosity of the suspending fluid

7.4.7 Effect of shear elasticity modulus of the suspending fluid on flowability of the suspension

In order to evaluate the effect of shear elasticity modulus on flowability of the suspensions, the flow behavior of five additional suspensions with shear elasticity modulus value of 1000 Pa and fluid density of 2000 kg/m^3 was modelled for various plastic viscosity values of 10, 17, 25, 38, and 50 Pa.s. Maximum magnitudes of flow velocity and strain rate are compared for the suspensions having two shear elasticity modulus of 100 and 1000 Pa (Fig. 7.19).

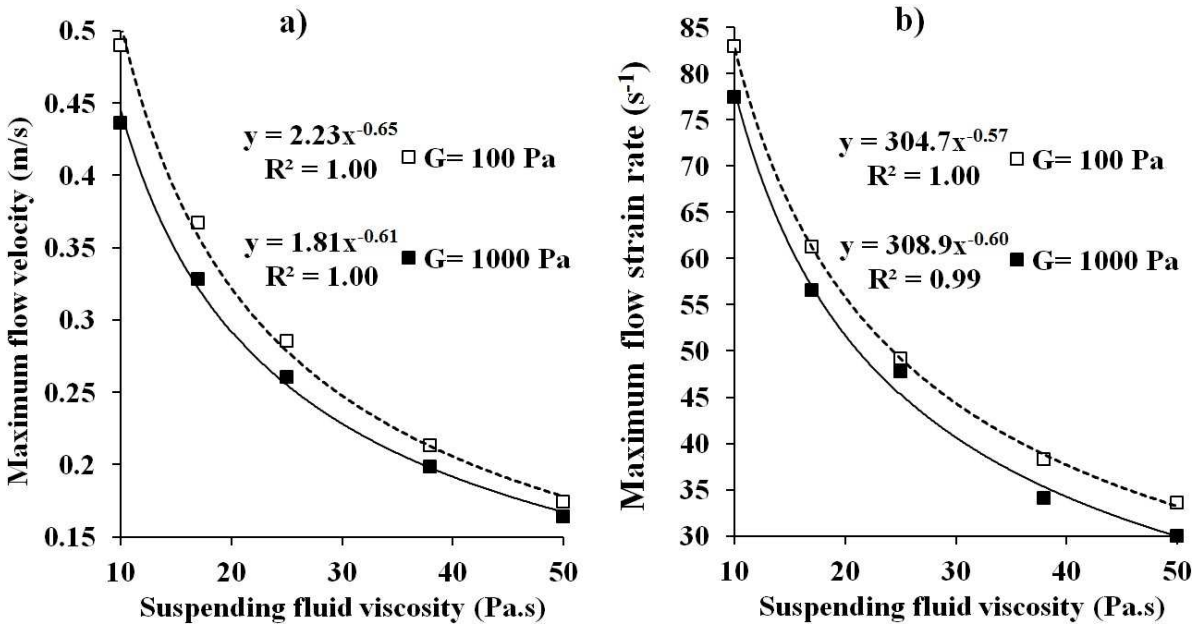

Figure 7. 19 a) Maximum velocity and b) strain rate magnitudes versus plastic viscosity of the suspending fluid

As can be observed, increasing the shear elasticity modulus (G) resulted in reducing the maximum flow velocity and strain rate magnitudes. For example, for the suspending fluid with plastic viscosity value of 10 Pa.s, increasing shear elasticity modulus from 100 to 1000 Pa can decrease the maximum magnitudes of flow velocity and strain rate from 0.49 to 0.436 m/s (i.e., 12% reduction) and from 82.9 to 77.4 s^{-1} (i.e., 7% reduction), respectively. Since G value is only related to the elastic state deformation, in a constant gravitational, viscous, and shear stress state (i.e., the constant density, viscosity, and yield stress), increasing G value results in lower initial flow energy, velocity, and strain rate magnitudes to initiate plastic state based on Hooke's law (Eq. (7.4).

$$F_1 = K_1\Delta x_1, F_2 = K_2\Delta x_2, F_1 = F_2 = F;\ G \propto K \text{ and } K_1 < K_2 \implies \Delta x_2 < \Delta x_1 \implies V_2 < V_1 \quad (7.4)$$

where K_i is the stiffness factor in Hooke's law and V_i is the velocity corresponding to displacement of Δx_i in a constant period of time and under a constant applied force F. Decreasing the flow energy causes less energy applied to transport coarse particles. Therefore, higher blocking indexes are obtained for higher G values, as presented in Fig. 7.20.

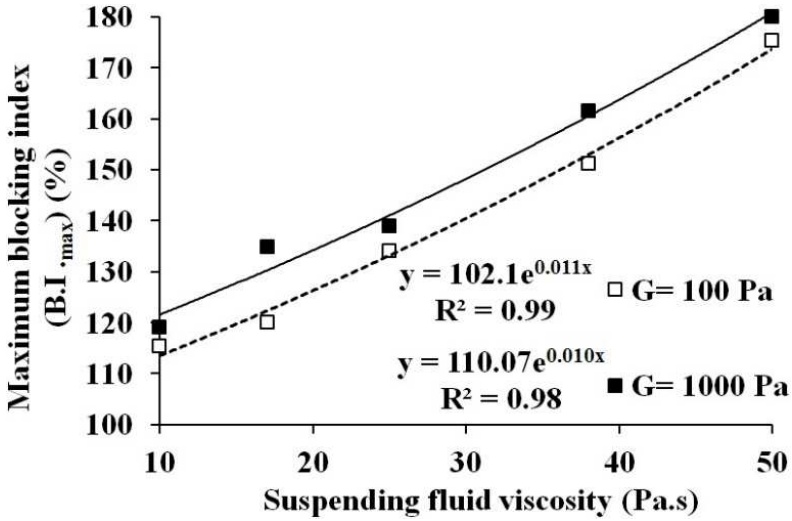

Figure 7. 20 Maximum blocking index versus plastic viscosity of the suspending fluid

For example, for the suspending fluid with plastic viscosity value of 38 Pa.s, increasing shear elasticity modulus from 100 to 1000 Pa can increase the maximum blocking index from 151% to 162% (i.e., 11% increase).

7.4.8 Effect of shear elasticity modulus of the suspending fluid on dynamic stability of the suspension

As presented in Fig. 7.21, comparing the coefficient of variation (COV) of particle contents in seven horizontal sections for shear elasticity modulus values of suspending fluid of 100 and 1000 Pa shows that the shear elasticity modulus has no significant effect on dynamic stability in the horizontal direction. This can be due to the fact that G values are more related to the elastic state. Therefore, since COV values are calculated during flow, no effect of shear elasticity modulus is expected on shear-induced segregation of the suspensions during flow.

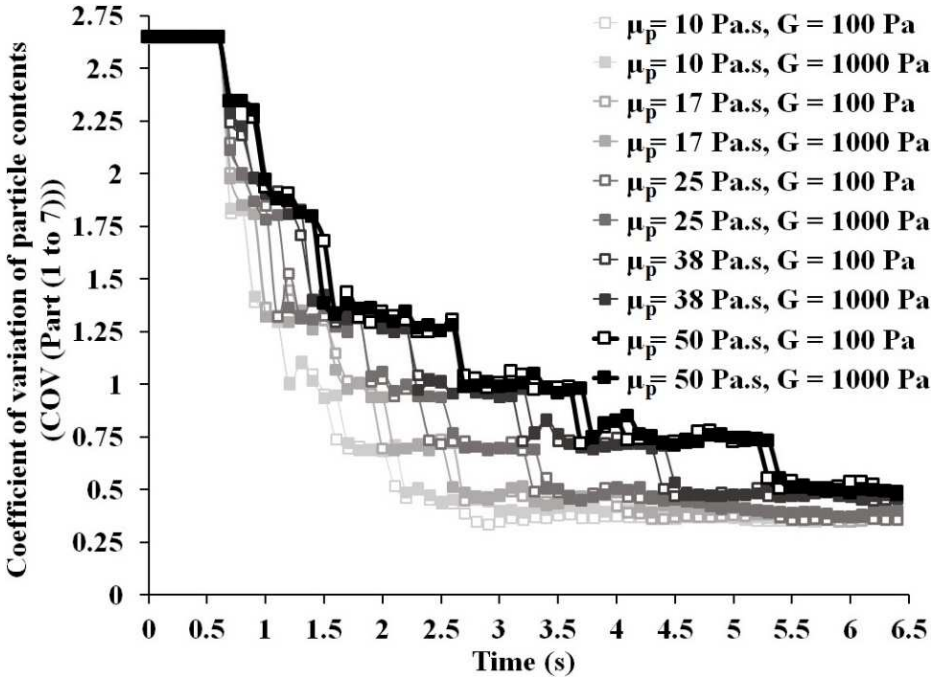

Figure 7. 21 COV values of particle content in horizontal sections versus flow time

Unlike the horizontal dynamic segregation (COV) and blocking indices ($B.I._{max}$) that are calculated during flow, the vertical dynamic segregation index (V.D.S.I) values are calculated at the end of the flow and, therefore, V.D.S.I. value should be related to the elastic state properties rather than dynamic behavior of the suspending fluid. As can be observed in Fig. 7.22, comparing the segregation indices obtained for G values of 100 and 1000 Pa showed that the shear elasticity modulus has more effect on vertical dynamic segregation than the blocking resistance of the simulated mixtures. Furthermore, it can be observed that shear elasticity modulus exhibited an opposite effect on $B.I._{max}$ and V.D.S.I. Indeed, increasing shear elasticity modulus of suspending fluid from 100 to 1000 Pa can lead to 5% increase in the maximum blocking index ($B.I._{max}$) values, while at the same time it resulted in 16% decrease in vertical segregation index.

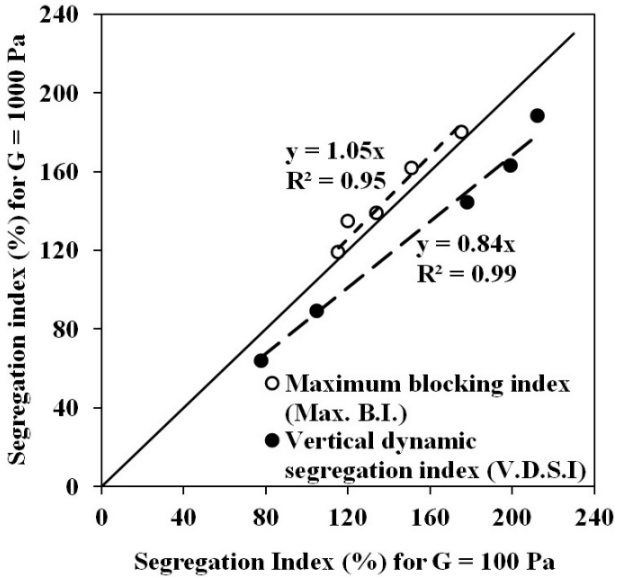

Figure 7. 22 Opposite effect of shear elasticity modulus of suspending fluid on passing ability and vertical dynamic segregation

7.4.9 Proposed approach to evaluate filling ability of suspension

Filling ability is defined as the ability of SCC mixtures to flow through narrow gaps between solid obstacles (reinforcing bars and formwork walls) while maintaining the homogeneity of coarse aggregates suspension in the suspending fluid, which is defined by the stable and homogeneous portion of the concrete mixture having particles with the diameter less than 20 mm. Therefore, filling ability is a contribution of flowability and passing ability properties of the mixture. Accordingly, simulated blocking index values are correlated to the maximum flow velocity, strain rate, and mass-averaged kinetic energy. This can help to evaluate filling ability of the modelled mixtures given the rheological properties of suspending fluid (i.e., plastic viscosity of 10 to 50 Pa.s, yield stress of 14 to 75 Pa, density of 2000 and 2500 kg/m^3, and shear elasticity modulus of 100 and 1000 Pa). The results of these correlations are presented in Figs. 8.23-8.25.

As can be observed in Figs. 7.23-7.25, passing ability indices (i.e., the maximum blocking index values obtained from Eq. (7.1): B.I.$_{max}$) are well correlated to flowability measurements (i.e., maximum flow velocity, strain rate, and kinetic energy) where correlation coefficients (R^2) higher than 0.86 are observed. The numerical simulations revealed that for the investigated

ranges of the plastic viscosity values of 10 to 50 Pa.s, yield stress values of 14 to 75 Pa, shear elasticity modulus of 100 to 1000 Pa, and density of 2000 to 2500 kg/m^3 for the suspending fluid, the suspensions of a 4.6% volumetric content value of 20-mm diameter spherical particles exhibited a wide range of flowability and passing ability properties. As can be observed in Figs. 7.23-7.25, for the investigated suspensions, the maximum magnitudes of flow velocity, strain rate, mass-averaged kinetic energy, and blocking index are ranging from 0.164 to 0.6 m/s, from 30 to 128 s^{-1}, from 0.0049 to 0.0562 J/kg, and from 115% to 184%, respectively. On the other hand, the results show that increasing flowability of the suspensions can increase their blocking resistance. According to the obtained ranges of the flowability properties, increasing the maximum magnitudes of the flow velocity, strain rate, and mass-averaged kinetic energy by 266%, 327%, and 1047%, respectively, can lead to decrease the maximum blocking index values by 69%.

Moreover, according to these results, three different levels of filling ability corresponding to low, medium, and high can be defined. This classification corresponds to the three B.I.$_{max}$ (i.e., maximum blocking index) ranges of 100%-130%, 130%-160%, and 160%-190%, respectively.

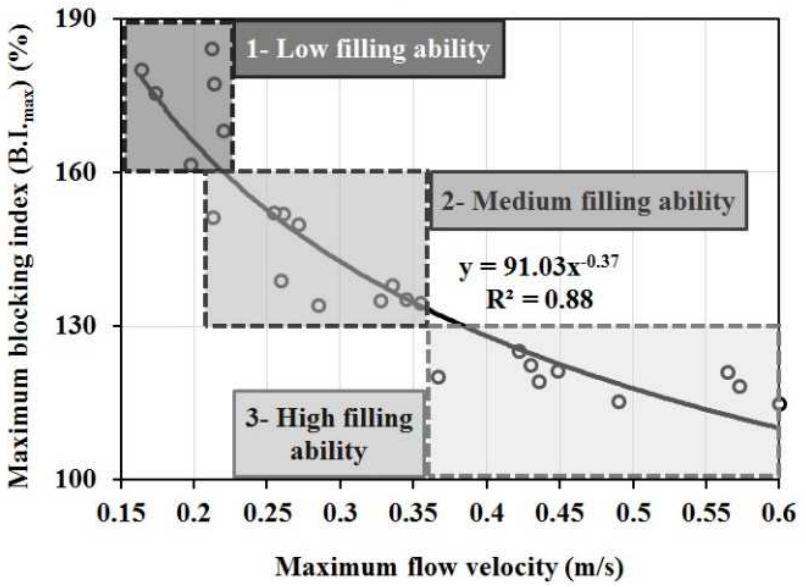

Figure 7. 23 Classification of modelled suspensions based on filling ability properties: B.I.$_{max}$ versus maximum flow velocity

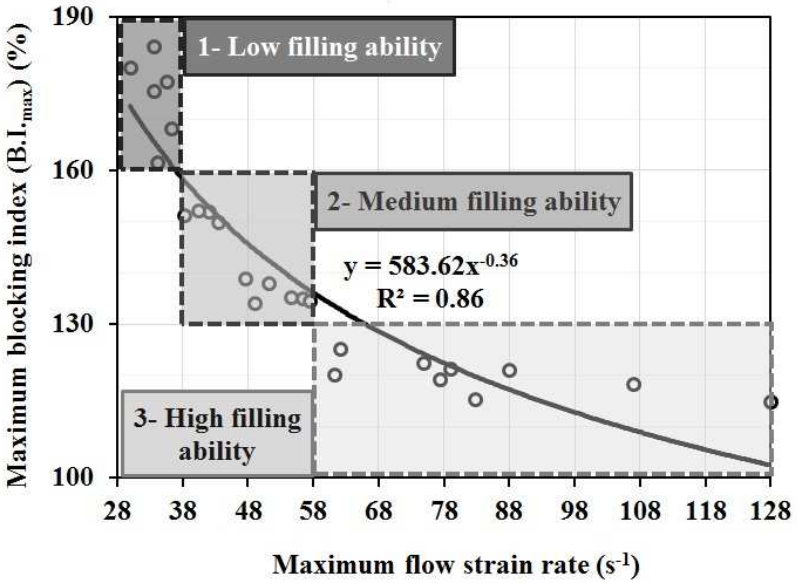

Figure 7. 24 Classification of modelled suspensions based on filling ability properties: $B.I._{max}$ versus maximum flow strain rate

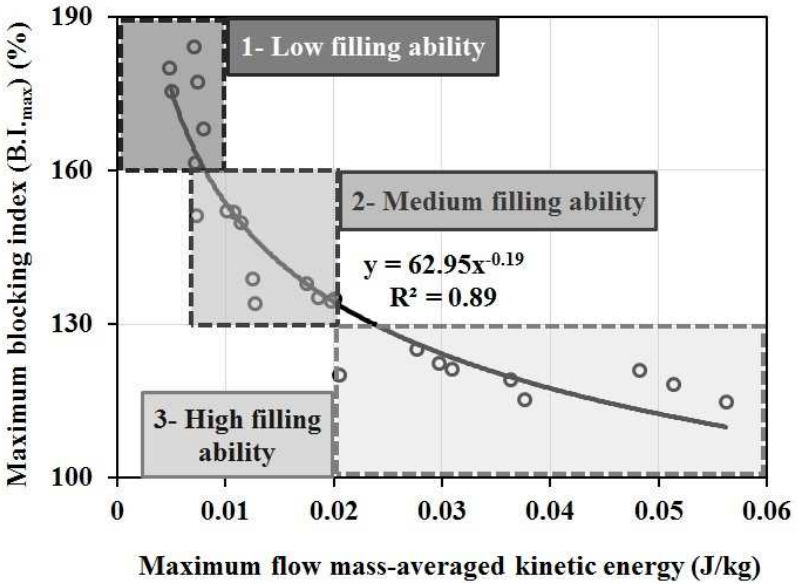

Figure 7. 25 Classification of modelled suspensions based on filling ability properties: $B.I._{max}$ versus maximum flow mass-averaged kinetic energy

The data presented on Figs. 7.23-7.25 are summarized in Table 7.1. As can be observed, combination of different rheological parameters of the modelled suspensions can be classified in three levels of filling ability using numerical simulations of SCC flow in the L-Box test set-

up. This classification can be used as a practical sheet to choose a proper combination of rheological parameters of the suspending fluid (i.e., mortar matrix or the homogeneous portion of the concrete mixture), that can achieve the required formwork filling quality demands, such as flowability and blocking resistance. This can also lead to prevent extra cost of unnecessary higher flowable mixtures proportions, especially for low reinforcement density (i.e., more clear spacing between bars or walls of the formwork).

Table 7. 1 Classification of modelled mixtures according to filling ability aspects

Filling ability level	**Passing ability level**	**Flowability level**			**Rheological parameters of suspending fluid**				
		Velocity	**Strain rate**	**Kinetic energy**	**μ_p (Pa.s)**		**τ_0 (Pa)**	**ρ (kg/m^3)**	**G (Pa)**
High	High	Medium to high	Medium to high	Medium to high	Low	10	14	2500	100
							45	2500	100
							75	2500	100
								2000	100
									1000
						17	14	2500	100
							45	2500	100
							75	2500	100
								2000	100
Medium	Medium	Low to medium	Low to medium	Low	Low	17	75	2000	1000
					Medium	25	14	2500	100
							45	2500	100
							75	2500	100
								2000	100
									1000
						38	14	2500	100
							45	2500	100
							75	2500	100
								2000	100
Low	Low	Low	Low	Very low	Medium	38	75	2000	1000
					High	50	14	2500	100
							45	2500	100
							75	2500	100
								2000	100
									1000

7.5 Conclusions

In this paper, a CFD software was employed to evaluate the flowability, passing ability, and dynamic stability of SCC cast in the L-Box test set-up. The concluding remarks can be expressed by the effect of plastic viscosity, yield stress, shear elasticity modulus, and density of the suspending fluid, on the flow performance and filling ability properties of SCC as a heterogeneous material, as follows:

7.5.1 Effect of the plastic viscosity and yield stress of the suspending fluid on flow performance of the investigated suspensions

The results showed that increasing plastic viscosity and yield stress of the suspending fluid can result in decreasing flowability, dynamic stability in horizontal direction, and blocking resistance of the suspension. Regarding the flowability aspects, for the investigated range of yield stress values of the suspending fluids (14 to 75 Pa) increasing plastic viscosity of the suspending fluid from 10 to 50 Pa.s resulted in decrease the maximum magnitudes of flow velocity and strain rate up to 63% and 72%, respectively. On the other hand, for a given plastic viscosity of suspending fluid ranging from 10 to 50 Pa.s, increasing yield stress from 14 to 75 Pa can lead to decrease the maximum magnitudes of flow velocity and strain rate up to 6% and 31%, respectively. On the other hand, the numerical results showed that increasing plastic viscosity and yield stress values of the suspending fluid from 10 to 50 Pa.s and from 14 to 75 Pa, respectively, can increase the maximum values of blocking index up to 51% and 9%, respectively. Therefore, it can be concluded that the plastic viscosity has more dominant effect on flow performance of the suspensions than the yield stress, with very good correlations. Numerical simulation also revealed that unlike the horizontal dynamic segregation, increasing the plastic viscosity of the suspending fluid can result in decreasing vertical dynamic segregation of the suspensions up to 47%. Moreover, it was also concluded that higher viscosity SCC mixtures are more appropriate when higher flowability and dynamic stability is needed in the vertical direction (tall elements, such as walls and columns) than in the horizontal direction. Lower viscosity SCC mixtures are, however, recommended for horizontal applications (such as

casting of long beam and slab elements) to exhibit higher flowability and passing abilities in reinforced areas of the formwork.

7.5.2 Effect of the density of the suspending fluid on flow performance of the investigated suspensions

According to the numerical results, in a given yield stress and plastic viscosity values of the suspending fluid, the suspensions with less fluid density exhibit more displacement in the vertical direction than the horizontal direction. This results in more self-consolidating behavior than self-levelling properties. It can also be concluded that under given viscous and shear stress conditions, decreasing the suspending fluid density can lead to less flowability and blocking index. The numerical simulations showed that decreasing density of the suspending fluid from 2500 to 2000 kg/m^3 results in decrease the maximum magnitudes of flow velocity, strain rate, and mass-averaged kinetic energy up to 13%, 6%, and 22%, respectively. On the other hand, decreasing the density of the suspending fluid from 2500 to 2000 kg/m^3 results in decreasing the maximum blocking index up to 9%. However, less density of the suspending fluid can increase the vertical dynamic segregation up to 95%. Therefore, suspending fluid density has more dominant effect on gravitational induced dynamic segregation, than plastic viscosity. Moreover, it was concluded that changes in suspending fluid density has more effect on gravitational induced segregation than blocking resistance. However, this effect decreases when the viscosity of suspending fluid increases. For the given suspending fluid plastic viscosity of 10 and 50 Pa.s, decreasing suspending fluid density from 2500 to 2000 kg/m^3 can increase the vertical dynamic segregation index by 95% and 8%, respectively. Moreover, increasing viscosity of the suspending fluid showed more effect (almost three times) on vertical dynamic segregation of the particles suspended in a fluid with less density. For example, increasing the suspending fluid viscosity from 10 to 50 Pa.s can decrease the vertical dynamic segregation index by 134% and 47% for suspending fluid density values of 2000 and 2500 kg/m^3, respectively.

7.5.3 Effect of the shear elasticity modulus of the suspending fluid on flow performance of the investigated suspensions

In a given yield stress and plastic viscosity conditions, increasing the shear elasticity modulus from 100 to 1000 Pa was showed to decrease flow velocity, strain rate, and vertical dynamic segregation up to 12%, 7%, and 16%, respectively. On the other hand, the higher shear elasticity modulus of the suspending fluid (1000 Pa) results in lower kinetic flow energy available to bring along the particles to pass through the closely spaced obstacles. Therefore, unlike the vertical dynamic segregation, this can lead to increase the maximum blocking index values by 5% compared to the suspending fluid with lower shear elasticity modulus of 100 Pa. However, increasing shear elasticity modulus did not show any significant effect on horizontal dynamic segregation.

7.5.4 Proposed approach to evaluate filling ability of suspension

Filling ability is defined as a contribution of flowability and passing ability properties of the mixture. Accordingly, simulated blocking index values were correlated to the maximum flow velocity, strain rate, and mass-averaged kinetic energy. This can help to evaluate filling ability of the modelled mixtures given the rheological properties of suspending fluid. Therefore, a new approach is proposed to classify the suspensions based on filling ability in three levels corresponding to low, medium, and high as a contribution of flowability and passing ability properties. This classification corresponds to the three $B.I._{max}$ (i.e., maximum blocking index) ranges of 100%-130% (high passing ability), 130%-160% (medium passing ability), and 160%-190% (low passing ability), respectively. The results of this classification can be used as a practical tool to choose a proper combination of rheological parameters of the suspending fluid (i.e., mortar matrix or the homogeneous and stable portion of the concrete mixture with the maximum particle diameter less than coarse aggregates) to achieve the required formwork filling quality.

CHAPTER 8 NUMERICAL SIMULATION OF SELF-CONSOLIDATING CONCRETE FLOW AS A HETEROGENEOUS MATERIAL IN L-BOX SET-UP – COUPLED EFFECT OF REINFORCING BARS AND AGGREGATE CONTENT ON FLOW CHARACTERISTICS

Authors and Affiliations:

Masoud Hosseinpoor: Ph.D. Candidate, Department of Civil Engineering, Université de Sherbrooke, Sherbrooke, Quebec, Canada, J1K2R1
Email: masoud.hosseinpoor@usherbrooke.ca

Kamal H. Khayat: Professor, Department of Civil, Architectural and Environmental Engineering, Missouri University of Science and Technology, 224 Engineering Research Laboratory, 500 W. 16th St., Rolla, MO 65409-0710, USA.
Email: khayatk@mst.edu

Ammar Yahia: Associate Professor, Department of Civil Engineering, Université de Sherbrooke, Sherbrooke, Quebec, Canada, J1K2R1
Email: ammar.yahia@usherbrooke.ca

Paper submitted to Materials and Structures, on 24th August 2016

Abstract

A computational fluid dynamics (CFD) software was employed to simulate the coupled effect of reinforcing bar spacing and coarse aggregate content on the blocking resistance and shear-induced segregation of self-consolidating concrete (SCC) along the horizontal channel of the L-Box apparatus. The rheology of the modelled suspending fluid, which corresponds to the stable and homogeneous portion of the mixture, consists of plastic viscosity value of 25 Pa.s, yield stress values of 75 Pa, fluid density of 2500 kg/m^3, and shear elasticity modulus value of 100 Pa. Two different values of 20-mm spherical particles (135 and 255 particles in total), as well as three bar arrangements consisting of 0, 3, and 18 bars distributed along the horizontal channel of the L-Box were considered in the numerical simulations. A new approach is proposed to evaluate the coupled effect of reinforcing bar arrangements and the number of spherical particles on the flow performance of SCC.

Keywords Blocking, Dynamic Segregation, Flow Simulation, Heterogeneous Analysis, L-Box Test, Self-Consolidating Concrete.

8.1 Introduction

Recently, there has been a great interest in using self-consolidating concrete (SCC) in cast-in-place and precast construction as a new class of high performance concrete. The highly flowable nature of SCC facilitates the casting process and reduces the placing energy and workforce requirement compared to conventional vibrated concrete. The high filling capacity of SCC makes it ideal for casting densely reinforced structural members to pass thought the narrow gaps in the formwork. In doing so, the material should maintain homogeneous distribution of the coarse particles in the mortar matrix [23 and 26]. In order to achieve higher flowability and passing ability, the rheological parameters of SCC, such as yield stress and plastic viscosity, should be significantly less than conventional concrete. For example, typical ranges of plastic viscosity and yield stress for conventional concrete are 500-2000 Pa.s and 50-100 Pa, respectively, while those corresponding to SCC are 0-100 Pa.s and 0-80 Pa, respectively [27]. In a given coarse particle content, the lower rheological parameters for SCC are due to its highly

flowable paste and mortar matrix which surround the coarse particles in a stable concrete suspension system. Accordingly, due to the low values of viscosity and yield stress of mortar in SCC and high flow kinetic energy required for casting of such SCC, there is an increased risk of separation of coarse particles from the suspending fluid (mortar), during the flow (i.e., blocking and shear induced segregation) or thereafter when the material is at rest (i.e., static segregation). Greater risk of dynamic segregation can be due to lower drag forces exerted on coarse particles to maintain them homogenously distributed in the suspension system. Therefore, the investigation of the interaction of reinforcement bar spacing and coarse particle concentration in mortar systems of various rheological properties can enable the evaluation of the dynamic performance of the SCC during the casting process [29].

Dynamic segregation can increase when SCC flows over a long distance or in the presence of obstacles (i.e., risk of blockage affecting the passing ability characteristics of the concrete). Passing ability refers to the ability of the concrete to pass through narrow gaps between various obstacles, such as reinforcing steel, to hold the aggregates in the suspension and, consequently, maintain its homogeneity [24, 31, and 32]. Therefore, comparing the properties of the final profiles through the flow path (in horizontal and vertical directions) and also, in the locations around the obstacles (i.e., reinforcement bars) can enable the evaluation of dynamic stability and blocking resistance of SCC, respectively. This can be carried out using empirical and theoretical tools.

As an empirical tool, the L-Box test is often employed to evaluate the restricted flow of SCC in the presence of obstacles and evaluate the passing ability and dynamic segregation of the suspension [25]. The L-Box set-up consists of vertical and horizontal compartments separated by a diving door that slides up enabling the material cast in the vertical compartment to flow gravitationally into the horizontal channel. Limited studies have been conducted to investigate the relationship between the rheological parameters of SCC and the various responses that can be determined using the L-Box test [40 and 180]. Turgut et al. [92] developed a modified L-Box set-up to evaluate dynamic segregation of SCC at different locations in the horizontal channel. Nepomuceno et al. [209] proposed semi-empirical models to optimize the maximum aggregate volume fraction to achieve a proper passing ability of SCC under different flow restrictions and

bar spacings. Yahia et al. [204] developed statistical models to evaluate the coupled effect of mix design and rebar spacing on the passing ability of SCC using a modified L-Box test setup.

Numerical simulations have been employed recently as theoretical tools to predict dynamic stability and passing ability of SCC [29, 42-47]. The numerical modeling of fresh SCC flow should take into account the interaction between the aggregates, the suspending fluid (i.e., cement paste/mortar), the configuration of the reinforcement, and the formwork wall characteristics [29, and 42-44]. Spangenberg et al. [46] studied flow induced particle migration in SCC and showed that in the case of industrial casting of SCC, gravity induced particle migration dominates all other potential sources of dynamic segregation induced by the flow of SCC into place. Spangenberg et al. [47] investigated different patterns of dynamic segregation during casting of SCC using experimental tests and numerical simulations. They showed that gravity induced particle migration has dominant effect on the coarsest particles resulting in a decrease of coarse aggregate content along the horizontal distance from the casting point and also in the vertical direction at the top layer of the concrete.

In this paper, a computational fluid dynamics (CFD) software was employed to simulate free surface flow of SCC in the L-Box test apparatus. The Navier–Stokes and conservation of mass equations for incompressible materials are solved by the volume of fluid (VOF) method [150]. In total, six simulations were carried out to study the effect of reinforcing bar spacing and aggregate particle content on the resistance to blocking and shear-induced dynamic segregation of SCC in the horizontal and vertical directions along the horizontal leg of the L-Box apparatus.

The investigation considered one suspending fluid that corresponds to a stable and homogeneous portion of an SCC mixture. This suspending fluid includes the fraction of the coarse and fine aggregates that can be rather homogeneous during the casting process. The investigated suspending fluid (i.e., the stable fraction of the SCC mixture) has a moderate plastic viscosity, a high yield stress, and a similar density as the suspended particles (large coarse aggregate fraction) in order to minimize gravity induced segregation. Segregation and blocking phenomena are only calculated for two contents of suspended coarse aggregates, which are less than typical contents of coarse aggregates in SCC (i.e., 10% to 30%). Indeed, it was assumed

that the finer coarse aggregate fraction that can remain in homogeneous suspension in the SCC mixture during the flow period are a part of the suspending fluid. Accordingly, the suspending fluid can be assumed as the stable portion of the SCC mixture. It can be explained by the fact that segregation and blocking do not occur for all the aggregates of the concrete suspensions, but only for a portion of them, having larger sizes (20 mm). On the other hand, due to the limits in calculation capacity, tracking of the positions of all the coarse aggregate particles (having typical contents and sizes, ranging from 10% to 30% and 5 mm to 20 mm, respectively) would have been impossible. Accordingly, two different initial suspended mono-size (20 mm) particle contents and three distributions of reinforcing bar obstacles were simulated to evaluate the coupled effect of reinforcing bars and particle loading on the flow performance of SCC. The paper discusses the results of the numerical simulation in terms of flow profiles, and particle distribution throughout the L-Box channel (horizontal direction) and fluid depth (vertical direction) for a given period of flow time.

8.2 Properties of modelled materials

The investigated parameters of the CFD modeling that were considered included a plastic viscosity of 25 Pa.s, a yield stress of 75 Pa, a shear elasticity modulus of 100 Pa, as well as a density of the suspending fluid of 2500 kg/m^3. The shear elasticity modulus is the ratio of shear stress to shear strain in the elastic state of the fluid, which is before the beginning of the plastic state. The modelled suspensions included the introduction of 135 and 255 spherical particles measuring 20 mm of diameter. This corresponds to particle contents of 4.6% and 8.7%, by volume, and was done to study the effect of coarse particle content on shear-induced segregation of the investigated SCC mixtures. The particles have the same density as the suspending fluid (i.e., 2500 kg/m^3) to minimize gravity induced segregation.

The L-Box set-ups included three bar arrangements placed immediately downstream from the sliding gates with different bar spacing and densities. In order to evaluate the pure particle content effect on non-restricted dynamic stability, two simulations were carried out in the absence of obstacles. Two other simulations included the use of three standard bars measuring 12 mm in diameter and 200 mm in height that are located right after the gate separating the

vertical and horizontal compartments of the L-Box. In addition, 18 bars consisting six rows of three bars positioned at 100-mm spacings distributed along the horizontal channel were modelled. These models included two different particle contents. The schematics of the L-Box set-up and configuration of the obstacles are presented in Fig. 8.1.

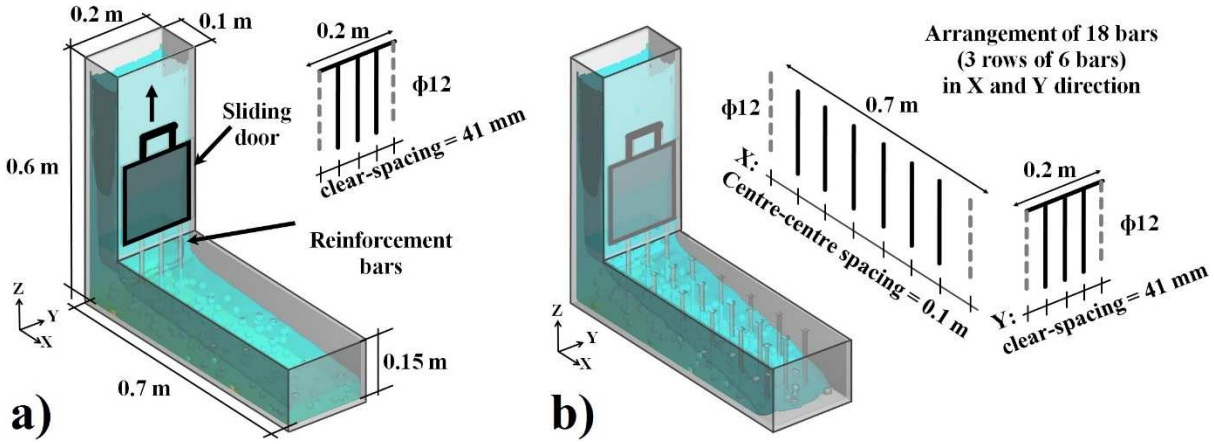

Figure 8. 1 a) Schematics of the L-Box set-up and configuration of standard 3 bars after the sliding door, b) 18 bars

8.3 Numerical simulation and boundary conditions

A CFD software (FLOW3D®) was employed to simulate free surface flow of the SCC in the L-Box test apparatus. The basic equations of the conservation of mass for incompressible materials and the 3D Navier–Stokes equations are solved by the Volume of Fluid (VOF) method [150], using 1st order momentum advection. In total, six simulations were carried out for a period of flow of 6.4 s, which was found to be the minimum duration needed to empty the SCC from the vertical leg of the L-Box for the investigated rheological properties investigated earlier by the authors [Chapter 7]. In order to discretize the geometry, solid elements, and suspension, two mesh blocks of 326,832 cells with 5-mm size in the x, y, and z directions were created.

The Dirichlet-Neumann boundary conditions were imposed to the flow domain based on the geometry of the L-Box; the velocity of the walls and the gate rising rate were set to zero and 0.03 m/s, respectively, as indicated in Fig. 8.2. The friction boundary conditions were assumed between particles, fluid, and the walls of the apparatus with a friction coefficient value of 0.4

(according to Coulomb's law of friction) [205]. The modelled fluids are considered as Non-Newtonian Bingham fluids using an elasto-viscoplastic model with implicit numerical approximation. Gravity stresses are calculated using gravitational acceleration value of 9.81 m/s^2. In order to consider particle-particle, particle-obstacle, and particle-wall interactions, a coefficient of restitution of 0.8 was applied for collision physical model. The modelled flow is assumed to be a laminar flow type [48]. It is worthy to mention that numerical simulations carried out on an i7-2600 CPU 3.40 GHz processor required a total running times between 60 to 135 hours per simulation. The running times depended mostly on the number of the particles and obstacles. In total, six simulations were require to complete the investigation.

8.3.1 Sampling methods and anticipated results

In order to evaluate flow performance of the modelled suspensions, the simulated flow profiles were calculated at 0.1-s time steps. Blocking resistance and dynamic stability properties of the suspensions in the horizontal direction were calculated by measuring the volumetric particle contents across seven 10-cm long sections located along the horizontal channel of the L-Box, as illustrated in Fig. 8.2. The number and position of the particles, as well as the volume of the fluid in each section were calculated at each 0.1-s time steps.

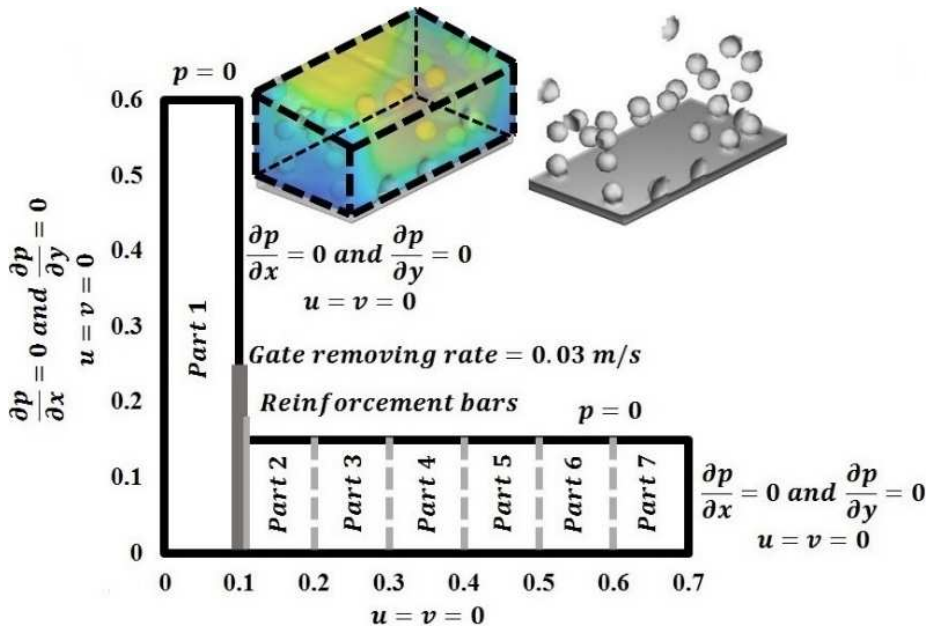

Figure 8. 2 Boundary conditions and horizontal sampling sections

On the other hand, dynamic stability of the suspensions in vertical direction was evaluated by comparing the volumetric particle contents across three vertical layers (bottom, middle, and top) measured at the end of the flow period (i.e., t = 6.4 s). As presented in Fig. 8.3, the thicknesses of the bottom and middle layers are 3 cm, and the remaining thickness (Z > 6 cm) corresponds to the top layer.

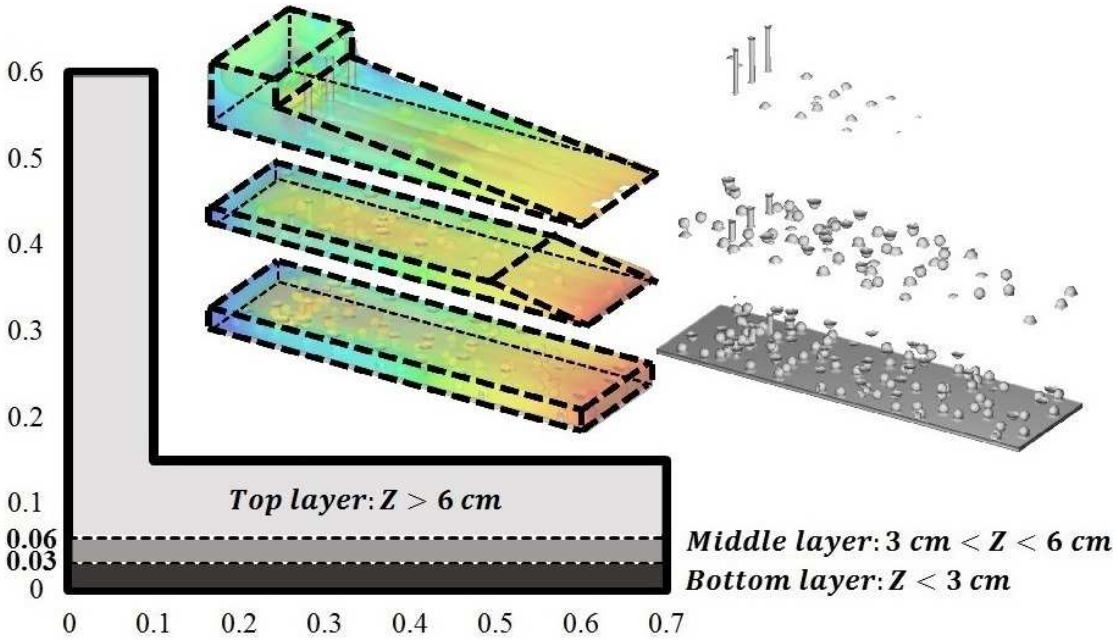

Figure 8. 3 Vertical sampling layers

8.4 Results and discussion

8.4.1 Effect of particle contents on passing ability and dynamic stability of suspensions in horizontal direction

By calculating the fluid volumes and particle contents in two extreme horizontal sampling sections that are located behind the bars (Part 1) and at the end of the horizontal channel of the L-Box (Part 7), the extremity horizontal dynamic segregation index (E.H.D.S.I.) can be defined various durations that can be calculated at frequencies of 0.1 s. The E.H.D.S.I. can be calculated as:

$$\text{E. H. D. S. I. (\%)} = \frac{\text{Particle content @ Part1} - \text{Particle content @ Part7}}{\text{Initial mean particle content}} \times 100\% \qquad (8.1)$$

In order to evaluate the effect of particle contents on the non-restricted dynamic segregation of suspension (i.e., dynamic segregation in the absence of the obstacles), values of E.H.D.S.I. are calculated for two suspension consisted of two different initial particle contents (4.6% and 8.7%, by volume of concrete) and presented in Fig. 8.4. The L-Box set-up for these simulations did not consider the presence of any reinforcement bars in the horizontal channel of the L-Box to evaluate the pure particle effect on the flow performance of SCC.

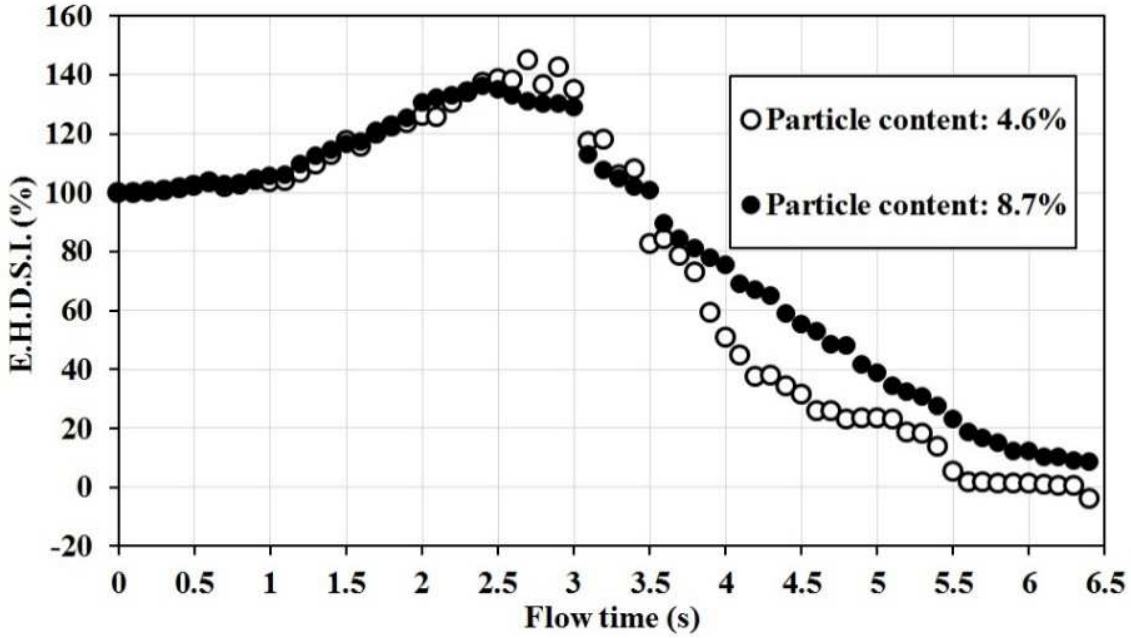

Figure 8. 4 Variations of E.H.D.S.I index values with flow time determined at 0.1 s intervals

As can be observed in Fig. 8.4, for both particle contents, the E.H.D.S.I. values increased with time to maximum values then decreased. The ascending parts of the curves can be related to the period that the vertical compartment of the L-Box is not completely empty (i.e., the flow times from 0 to almost 2.5-3 s) where particles are of greater concentration in Part 1 with less velocity than the suspending fluid. As can be observed in this initial flow period, the values of E.H.D.S.I. obtained for both particle contents are comparable. It can be due to the comparable friction and drag forces exerted on the particles, where friction coefficients, particle sizes, velocity

magnitudes, and plastic viscosity values of the suspending fluids were similar in this period. On the other hand, the behavior of suspensions in the descending part of the curve (i.e., flow times t > 3 s) can be explained by the flowability of the mixtures which can push the accumulated particles to move ahead and reach the end of the horizontal channel (Part 7). However, in this period, the suspension with the higher particle content of 8.7% exhibited greater E.H.D.S.I. values than the simulated SCC with the lower particle content of 4.6%. This can be due to the higher lattice effect [210-212] of the particles, which were already segregated during the first period (i.e., 0 < t < 3 s), on the motion of the particles towards the end of channel (Part 7). The lattice effect corresponds to the internal structure of the segregated particles. This structure can reduce the displacements of the particles, whether inside the lattice network, or the upcoming particles from the vertical compartment of the L-Box.

Shear-induced dynamic segregation of the mixtures throughout the horizontal direction can be evaluated by calculating the maximum horizontal dynamic segregation indices for each horizontal sampling part (i = 1 to 7) individually in the whole period of the flow (i.e., t = 0 to 6.4 s), as follows:

$$I.H.D.S.I.(i)\ (\%) = Max\left(\frac{Particle\ content\ @\ Part(i) - Particle\ content\ @\ Part7}{Initial\ mean\ particle\ content}\right) \times 100\% \quad (8.2)$$

where I.H.D.S.I. (i) is the individual horizontal dynamic segregation index, obtained in the horizontal sampling part i. By comparing the results of the I.H.D.S.I. values for the horizontal samples i = 1 to 6, the variation of segregations of the particles along the horizontal direction can be evaluated. The results of the simulations, corresponded to the L-Box set-up which does not consist any obstacle are presented in Fig. 8.5.

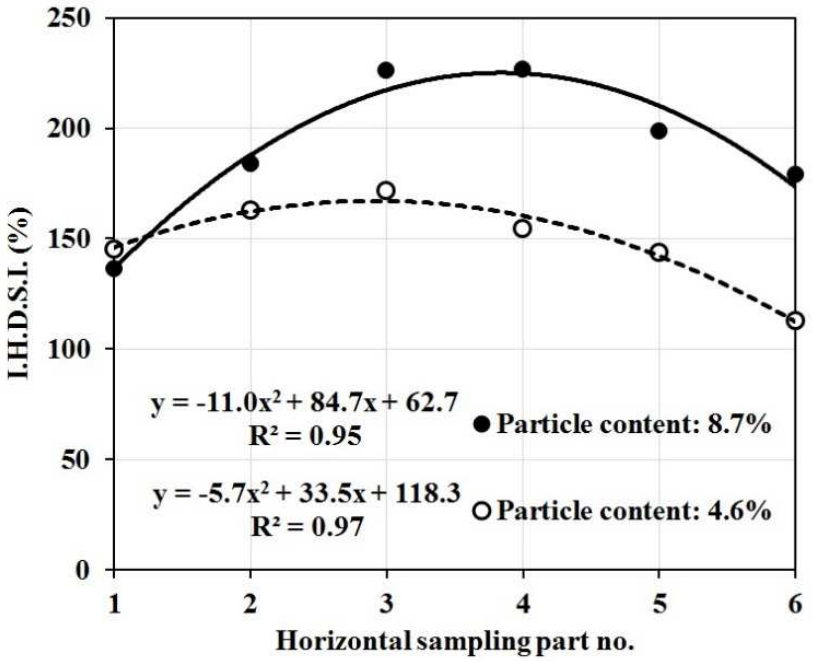

Figure 8. 5 Variations of I.H.D.S.I. index values with horizontal sampling part number (L-Box with no obstacles)

As can be observed in Fig. 8.5, the simulated suspensions made with both particle contents of 4.6% and 8.7% exhibited maximum I.H.D.S.I. values in the third horizontal sampling part. Therefore, the particles segregate mostly in a distance of 0.2 m after the sliding door in the horizontal channel, which means the first 1/3 of the 0.6 m horizontal leg. On the other hand, the suspension with higher particle content of 8.7% exhibited higher I.H.D.S.I. values compared to those obtained by particle content of 4.6%. This can be called as the effect of the "particle-particle interactions" on horizontal dynamic stability of the suspensions. By increasing the particle content, the probability of formation and also strength of the internal structure of segregated particles (i.e., the lattice effect) in horizontal direction increase. This can reduce the relative horizontal displacements of the particles to the suspending fluid, in the case of the higher particle content suspension. For example, an increase in particle content from 4.6% to 8.7% can increase the I.H.D.S.I. values from 163% to 184% (21%), 171% to 226% (55%), 155% to 226% (71%), 144% to 198% (54%), and 113% to 179% (66%) in horizontal sampling parts of 2, 3, 4, 5, and 6, respectively. Therefore, the maximum increase was observed in part 4, which corresponds to the horizontal sampling portion placed at a distance of 0.2 m from the sliding door.

However, in part 1 (located in vertical compartment of the L-Box), the suspension with higher particle content of 8.7% showed slightly (9%) lower I.H.D.S.I. value than the SCC with the lower particle content (4.6%). This can be explained by the fact that unlike the horizontal channel, the major direction of the flow in part 1 is vertical and towards gravity (Z direction). This is due to the geometry of the apparatus, as well as the confinement of the flow by the side walls, in both X and Y directions. On the other hand, as observed earlier in Fig. 8.4, the suspensions reach their maximum E.H.D.S.I. values (which is equal to the I.H.D.S.I. value in part 1) in the period of flow time that the vertical part of the L-Box is not completely empty and suspension still flows down. Therefore, the lattice forces of the particles, which are located in the vertical compartment of the L-Box, are in the same direction of the flow, as well as the gravitational forces. Indeed the particles in the upper vertical levels push the particles of the lower levels to travel from the vertical part of the L-Box towards the horizontal channel. This effect can increase in the case of presence of higher numbers of particles in the vertical parts. Therefore, it can be concluded that in the vertical compartment of the L-Box (i.e., part 1), the lattice structure of the particles has an auxiliary effect on displacement of the particles, which can decrease the I.H.D.S.I. values for the suspensions having greater particle content.

The results of the calculated values of I.H.D.S.I for the L-Box set-ups consisting of 3 and 18 reinforcing bars along the horizontal leg are presented in Figs. 8.6a and 8.6b, respectively. Similar to the non-restricted flow of the suspension presented in Fig. 8.5, increasing the particle content can increase the I.H.D.S.I. values for the L-Box set-ups consisting of 3 and 18 obstacles along the horizontal leg. For example, increasing the particle content from 4.6% to 8.7% can increase the I.H.D.S.I. values for the L-Box set-up with 3 bars, from 239% to 258% (19%) and 121% to 188% (67%) in the 3rd and 6th parts, respectively. In the case of presence of 18 bars through the horizontal channel, the maximum increase of 247% in I.H.D.S.I values (from 270% to 517%) obtained in the part 5. As stated earlier, this can be due to the negative effect of the lattice structure of segregated particles in the horizontal leg of the L-Box on the displacement of upcoming particles towards part 7.

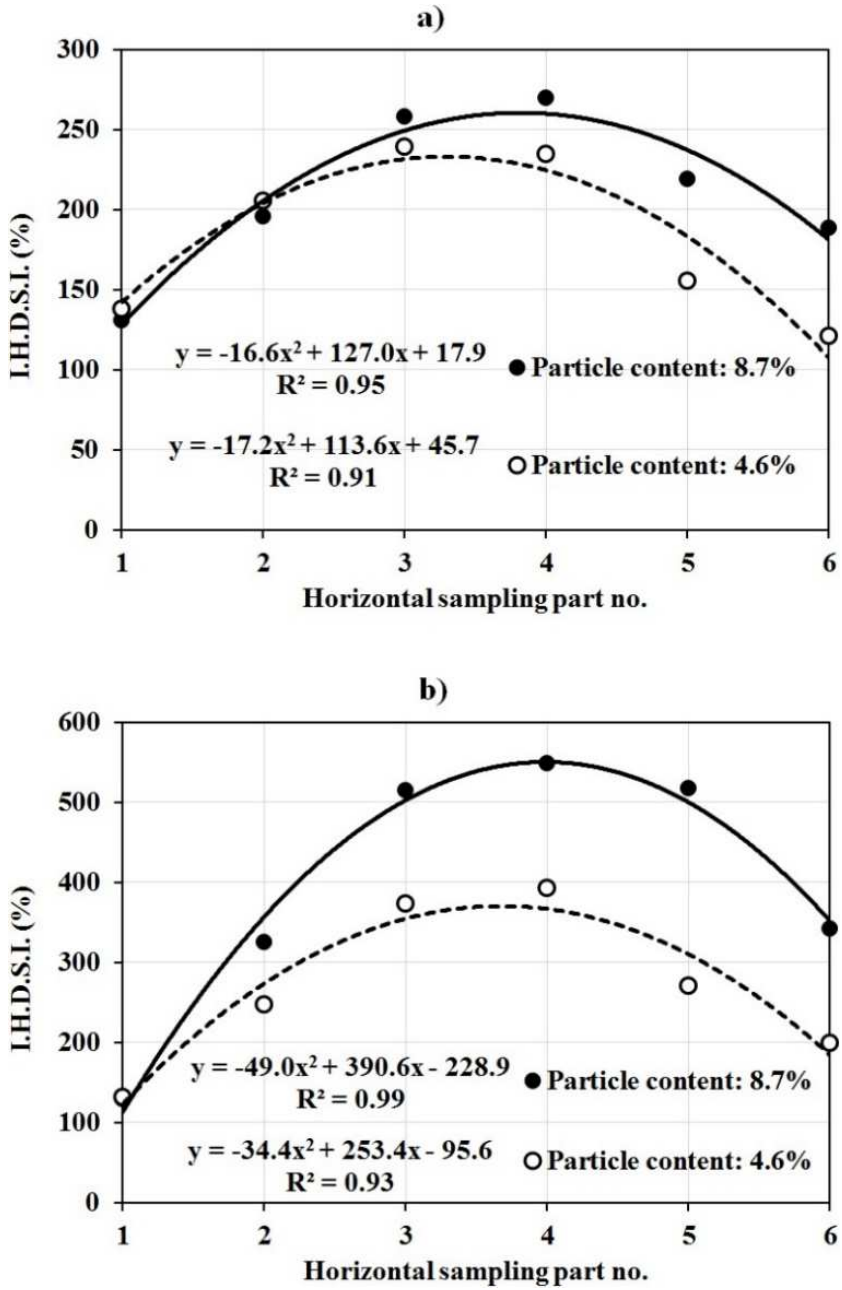

Figure 8. 6 Particles effect: values of I.H.D.S.I. for suspensions with different particle contents versus horizontal sampling location along the L-Box with a) 3 and b) 18 reinforcing bars in the horizontal channel

On the other hand, as can be observed in Fig. 8.6, increasing the particle content can decrease slightly the I.H.D.S.I. values in part 1. As explained earlier, this can be due to the auxiliary effect of the lattice performance of particles in the vertical compartment of the L-Box on the displacement of the particles in lower levels. For example, increasing the particle content from

4.6% to 8.7% can decrease the I.H.D.S.I. values from 138% to 131% (7% decrease) and from 131% to 128% (3% decrease) for the L-Box set-ups consisting of 3 and 18 bars along the horizontal channel, respectively.

It is worthy to mention that the values of I.H.D.S.I.(i) for the L-Box set-up (Eq. (8.2)) with 18 bars, can also be used to evaluate the passing ability of the suspension for each row (i.e., i = 1 to 6) of obstacles. Indeed, by calculating the I.H.D.S.I (i) values, the passing ability of the suspension through each row of reinforcement bars (i between 1 and 6) can be evaluated. This can be calculated by the ratio of difference of particle contents at the part located behind that row (Part (i)) and the last part (i.e., Part 7) to initial particle content. Therefore, the I.H.D.S.I. values for 18 bars L-Box set-up can be used as the maximum blocking index values (i.e., $B.I._{max}$). As can be observed in Fig. 8.6b, for both initial particle contents of 4.6% and 8.7%, the maximum I.H.D.S.I. = $B.I._{max}$ value is obtained for the row number i = 4, which is located at the distance of 0.3 m from the sliding gate of the L-Box. It means that suspensions segregate mostly in the first half of the horizontal channel (i.e., 0.6 m long leg) with an accumulation peak at Part 4 located right behind the reinforcing bars placed at row 4. For example, the maximum blocking index values ($B.I._{max}$) of 393% and 548% were obtained right behind the 4^{th} row of reinforcement bars for 4.6% and 8.7% particle contents, respectively.

8.4.2 Effect of reinforcement bars on passing ability and dynamic stability of suspensions in the horizontal direction

In order to evaluate the effect of reinforcement bars (obstacles) on dynamic stability and blocking resistance of the investigated SCC, the results of simulated values of I.H.D.S.I. are compared for different number of obstacles (i.e., 0, 3, and 18) along the horizontal channel of L-Box. These comparisons are presented for the suspensions with two different particle contents of 4.6% and 8.7% and presented in Figs. 8.7a and 8.7b, respectively.

As can be observed in Figs. 8.7a, and 8.7b, for both particle contents of 4.6% and 8.7%, the simulations showed the maximum values of I.H.D.S.I. for the L-Box set-up consisted of 18 bars along the horizontal channel. On the other hand, in the case of non-restricted flow (i.e., in the

absence of the obstacles), the minimum ranges of values of I.H.D.S.I. were obtained. For example, in the case of presence of 18 bars, the maximum values of 393% and 548% of I.H.D.S.I. were obtained for 4.6% and 8.7% particle contents, respectively. On the other hand, for the no-obstacle L-Box set-up, the I.H.D.S.I. values up to 171% and 226% were obtained for particle content values of 4.6% and 8.7%, respectively. Indeed, for a given set of rheological parameters of suspending fluid and particle content of the suspensions, increasing the number of obstacles in the horizontal channel can lead to increased dynamic segregation of the suspension in horizontal direction. This is called the bar effect on flow performance of the investigated suspensions. This can be explained by the fact that increasing the number of obstacles can restrict the flow space needed for the particles to move freely and, consequently, it can increase the collisions and frictional stresses between the particles and obstacles. Therefore, increasing the number of obstacles in the horizontal direction can restrict the horizontal displacement of the particles. However, as can be observed in Fig. 8.7, increasing the number of obstacles does not show any significant effect on I.H.D.S.I. in part 1, compared to other parts. For example, in the case of the suspension with 8.7% particle content, the simulations revealed comparable I.H.D.S.I. values of 136%, 131%, and 128% for 0, 3, and 18 number of obstacles along the horizontal channel. This is due to the fact that unlike the horizontal leg, the flow in vertical part of the L-Box (part 1) is non-restricted. Therefore, lattice effect of particles, which are placed in the vertical part, on displacement of the particles is more dominant than the effect of configuration of obstacles in the horizontal channel. For a given particle content, the lattice effect of the particles in the non-restricted part 1 are comparable and, consequently, the suspension shows comparable I.H.D.S.I. values in this part, regardless of number of obstacles in the restricted parts.

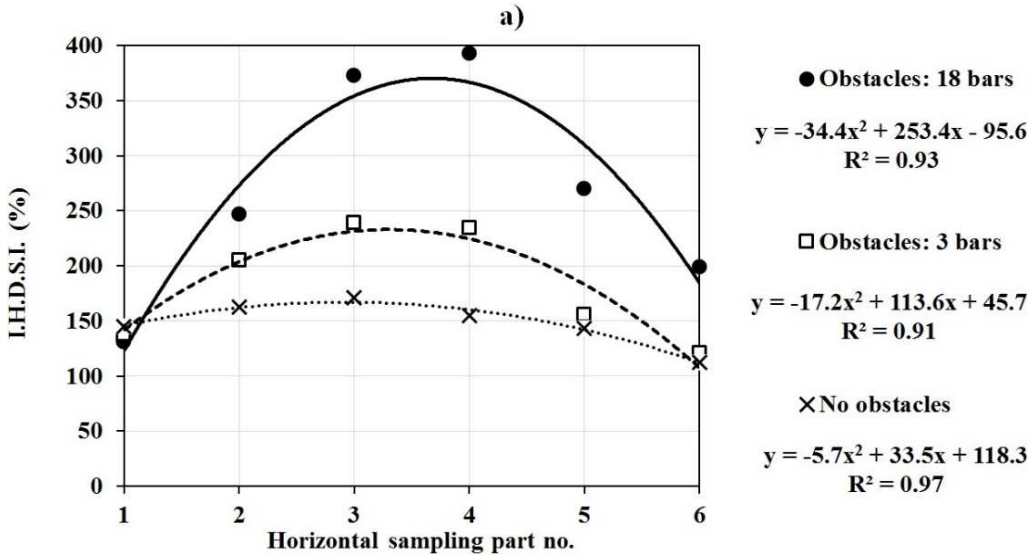

a) Particle content: 4.6%

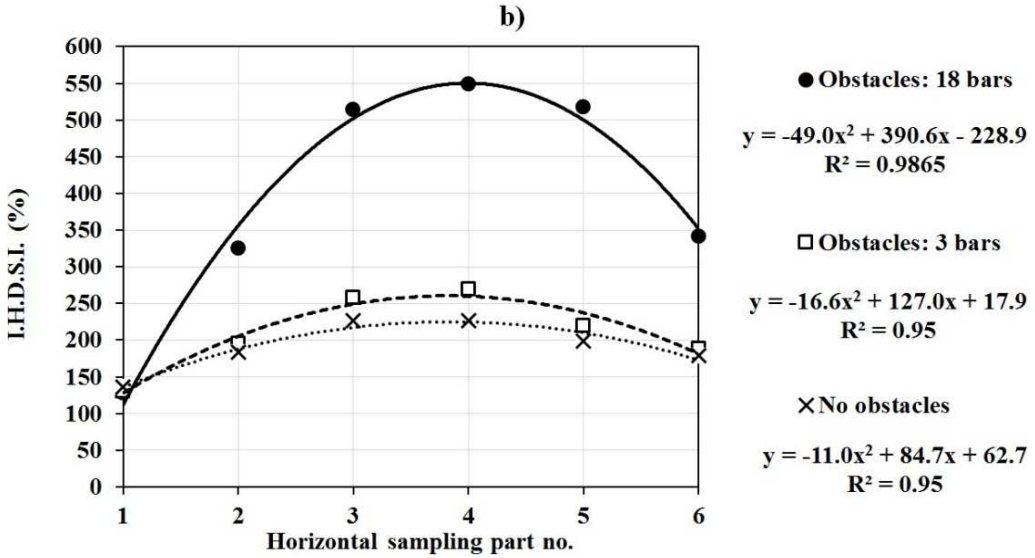

b) Particle content: 8.7%

Figure 8. 7 Bar effect: variation of I.H.D.S.I. values in different horizontal sampling parts for different configurations of obstacles, obtained for values of particle content of a) 4.6% and b) 8.7%

Furthermore, as explained earlier, the results presented for I.H.D.S.I. values of the L-Box set-up consisted of 18 bars along the horizontal leg, can be used to evaluate the passing ability of the suspensions through each row of reinforcing bars. On the other hand, the suspensions

showed their maximum I.H.D.S.I. (or $B.I._{max}$) values in the part 4. As can be observed in Fig. 8.7, for part 6, compared to the middle parts 4 and 5, the bar effect on I.H.D.S.I values decrease. For example, in the case of the suspension with 4.6% particle content, increasing the number of obstacles from 3 to 18 can increase the I.H.D.S.I. values in part 4 from 235% to 393% (158% increase), while this can lead to increase the I.H.D.S.I. values in part 6 from 121% to 199% (78% increase). On the other hand, in the case of the suspension with 8.7% particle content, increasing number of obstacles, can increase the I.H.D.S.I. values in part 4 from 226% for the non-restricted L-Box set up, to 548% value in presence of 18 bars in horizontal leg (322% increase). However, this can lead to increase the I.H.D.S.I. values in part 6 from 179% to 341% (162% increase). Therefore, it can be concluded that the bar effect on dynamic segregation in the middle parts are higher than those which are located in the terminal part 6, right behind the par 7. It is due to the higher particle content observed in the middle sections (according to higher I.H.D.S.I. values) compared to part 6. This can increase the probability of the formation of particle blocking arcs and the friction between the particles and obstacles in these parts. The effect of the interactions, observed between the coarse particles and the reinforcement bars, on dynamic stability and blocking resistance of the suspensions is called "bar-particles coupled effect", and will be discussed in the next section.

8.4.3 Bar-particles coupled effect on flow performance of suspensions in the horizontal direction

In order to evaluate the effect of interactions between the particles and the reinforcing bar obstacles, two new indices are defined. These indices include the particle content effect (P.C.E.) and bar effect (B.E.) in different horizontal sampling parts (i= 1 to 6), as follows:

$$P.C.E._{(i,j,k)}\ (\%) = \frac{I.H.D.S.I._{(i,j)}\ for\ particle\ content\ value\ of\ k=8.7\%}{I.H.D.S.I._{(i,j)}\ for\ particle\ content\ value\ of\ k=4.6\%} \times 100\% \qquad (8.3)$$

$$B.E._{(i,j,k)}\ (\%) = \frac{\text{I.H.D.S.I.}_{(i,k)}\ \text{for j=18 bars along the horizontal channel}}{\text{I.H.D.S.I.}_{(i,k)}\ \text{for j = 3 bars along the horizontal channel}} \times 100\% \qquad (8.4)$$

where $P.C.E._{(i,j,k)}$ and $B.E._{(i,j,k)}$ are the indices of the particle content effect and bar effect on flow performance of the suspensions made with particle content k (k = 4.6% and 8.7%), in the L-Box set-up consisting j number of reinforcing bars (j= 3 and 18). These indices are calculated for the sampling part i (i = 1 to 6). The P.C.E. index in each sampling part (i = 1 to 6) is calculated as the ratio of I.H.D.S.I. values obtained for suspensions with particle content (k) of 8.7% to those values obtained for k of 4.6%. On the other hand, the B.E. index in each horizontal part (i= 1 to 6) is calculated by the ratio of the I.H.D.S.I. values obtained for the L-Box set-up consist of j = 18 bars in the horizontal channel to the values obtained for a j = 3 bars L-Box set-up. Comparing the values of $P.C.E._{(i,j,k)}$ and $B.E._{(i,j,k)}$ in different horizontal parts (i = 1 to 6), in the presence of different number of bars (j = 3 and 18) along the horizontal channel, and different particle content (k = 4.6% and 8.7%), respectively, can enable the evaluation of the coupled effect of reinforcing bar-particle on flow performance of the investigated suspensions in the horizontal direction of the L-Box. The results of these comparisons are presented in Fig. 8.8.

As can be observed in Fig. 8.8, the particle content (P.C.E.) and bar (B.E.) effect indices are found to be more than value of 100% in different horizontal sampling parts (i = 2 to 6). Therefore, it can be concluded that increasing both the particle content and number of obstacles can increase the I.H.D.S.I. values (leading to greater horizontal dynamic segregation). On the other hand, the maximum values of P.C.E. and B.E. were obtained for the highest congested flow (j = 18 bars) and also the suspension with the highest particle content (k = 8.7%). For example, the maximum P.C.E. and B.E. indices were obtained as 191% and 236% for the L-Box set-up consisted of 18 bars, and the suspension with 8.7% particle content, respectively. This can be explained by the fact that increasing the number of reinforcement bars and the number of particles can increase the probability of formation of the blocking arcs, due to higher particle-bars interactions, which means higher friction and collision between the particles and the obstacles.

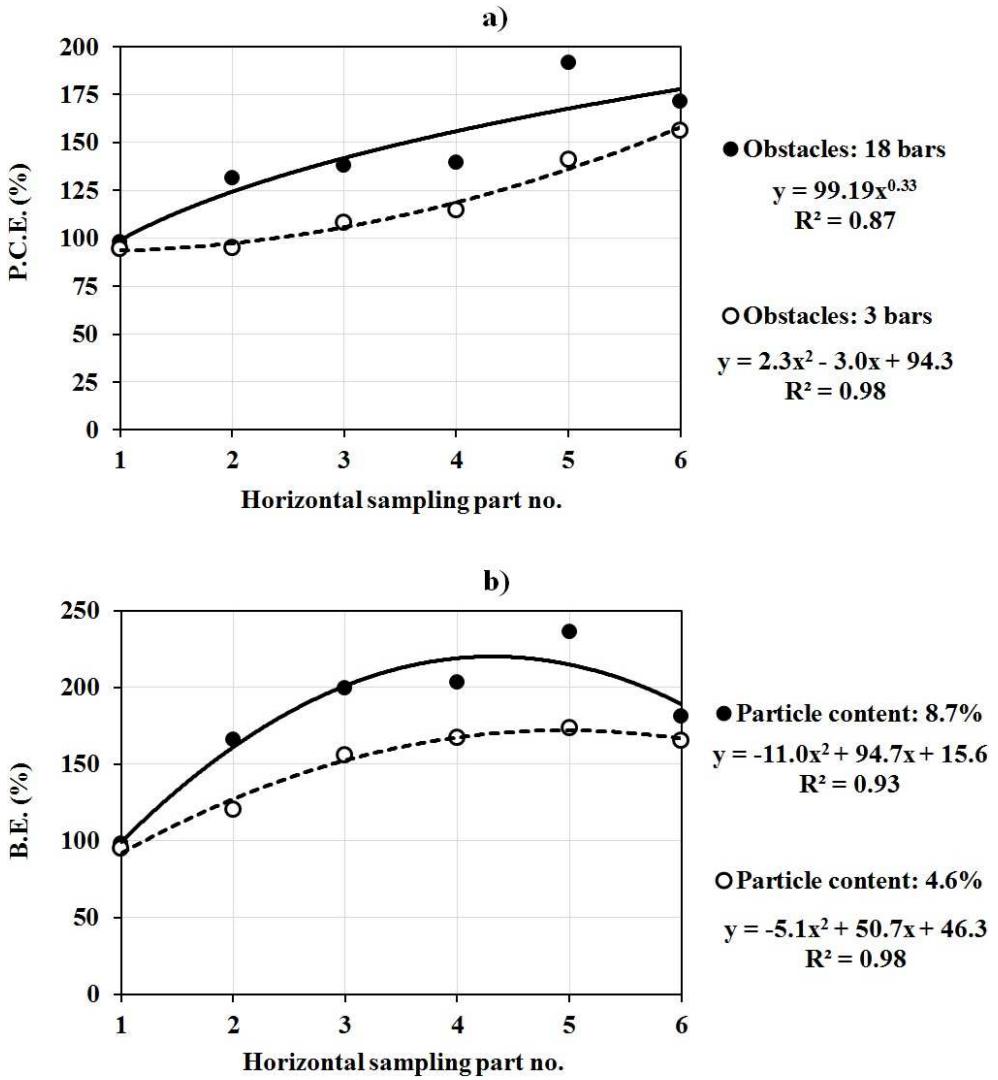

Figure 8. 8 Bar-particles coupled effect on flow performance of the investigated suspensions in different horizontal sampling parts i = 1 to 6: a) variation of particle content effect (P.C.E.) for two different number of obstacles j = 3 and 18, and b) variation of bar effect (B.E.) for two different particle contents k = 4.6% and 8.7%

Furthermore, as can be observed in Fig. 8.8, once the distance from the vertical compartment of L-Box increases (i.e., higher horizontal sampling part no.) the P.C.E. and B.E. values for lower number of obstacles (j = 3 bars) and the suspension made with lower particle content (k = 4.6%), respectively, increase continuously. For example, as can be observed in Fig. 8.8a, in the presence of 3 reinforcing bars, the simulations showed particle effect indices of 95% and 156% in the 1st and 6th horizontal sampling parts, respectively (61% increase). On the other hand, the suspensions with lower particle content of 4.6% exhibited bar effect indices (B.E.) of 95% and

165% in the horizontal sampling parts 1 and 6, respectively (70% increase). Similarly, P.C.E. and B.E. values for higher number of obstacles (j = 18) and the suspension with higher particle content (k = 8.7%), respectively, increase with the distance from the vertical compartment (higher horizontal part number) up to the part 5. For example, in the case of the L-Box set-up consisted of 18 bars, the P.C.E. values of 98% and 191% were obtained in the 1st and 5th parts, respectively (i.e., 93% increase). On the other hand, the suspension with the higher particle content of 8.7% showed the B.E. values of 98% and 236% in the horizontal sampling sections of 1 and 5, respectively (138% increase). This increment in particle and bar effects, obtained by higher horizontal sampling part number can be explained by the fact that in a higher distance from the vertical compartment, the auxiliary lattice effect of the particles located in the vertical part of the L-Box on displacement of the particles in horizontal channel decrease. This is due to dissipation of flow energy, according to the flow surface level descend in the vertical part and consequently, lower gravitational forces. On the other hand, in the horizontal channel, both bar and lattice effect of the segregated particles are in the same direction to resist against the displacement of the particles. This can be more dominant in presence of higher number of bars and the suspensions with higher particle contents, due to higher interactions between the bars and particles. However, once the suspensions segregate mostly in the mid parts of the horizontal channel, accordingly, due to lower particle content in the part 6, the probability of bar-particle interactions (i.e., collision and friction) and, consequently, formation of blocking arcs decrease. Accordingly, as can be observed in Figs. 8.8a, and 8.8b, P.C.E. and B.E. values for higher number of obstacles (j = 18) and the suspension made with higher particle content (k = 8.7%), respectively, decrease in the part 6 compared to the part 5. For example, in presence of 18 obstacle, simulation showed the particle content effect (P.C.E.) index values of 191% and 171 % in the parts 5 and 6, respectively. On the other hand, the suspension with higher particle content 8.7%, exhibited the bar effect (B.E.) index values of 236% and 181%, in the parts 5 and 6, respectively. This means 20% and 55% reduction in P.C.E. and B.E. indices from part 5 to 6, respectively.

Calculating the fluid volume and particle content in each of the seven horizontal sections along the horizontal leg of the L-Box, shear-induced dynamic segregation of the mixtures in the

horizontal direction can be quantified for each 0.1-s time step by coefficient of variation of particle contents in all the seven horizontal parts (parts 1 to 7), as follows

$$\mathrm{COV} = \frac{\text{Standard deviation of particle contents (Parts 1,2,3,4,5,6,and 7)}}{\text{Average of particle contents (Parts 1,2,3,4,5,6,and 7)}} \tag{8.5}$$

The bar-particle coupled effects on dynamic stability of the suspensions are then evaluated by comparing the ratio of COV values corresponding to 18 bars configuration L-Box to those values obtained in presence of 3 bars obstacles, for both 4.6% and 8.7% particle content suspensions, in the whole period of flow (i.e., t = 0 to 6.4 s). These results are presented in Fig. 8.9.

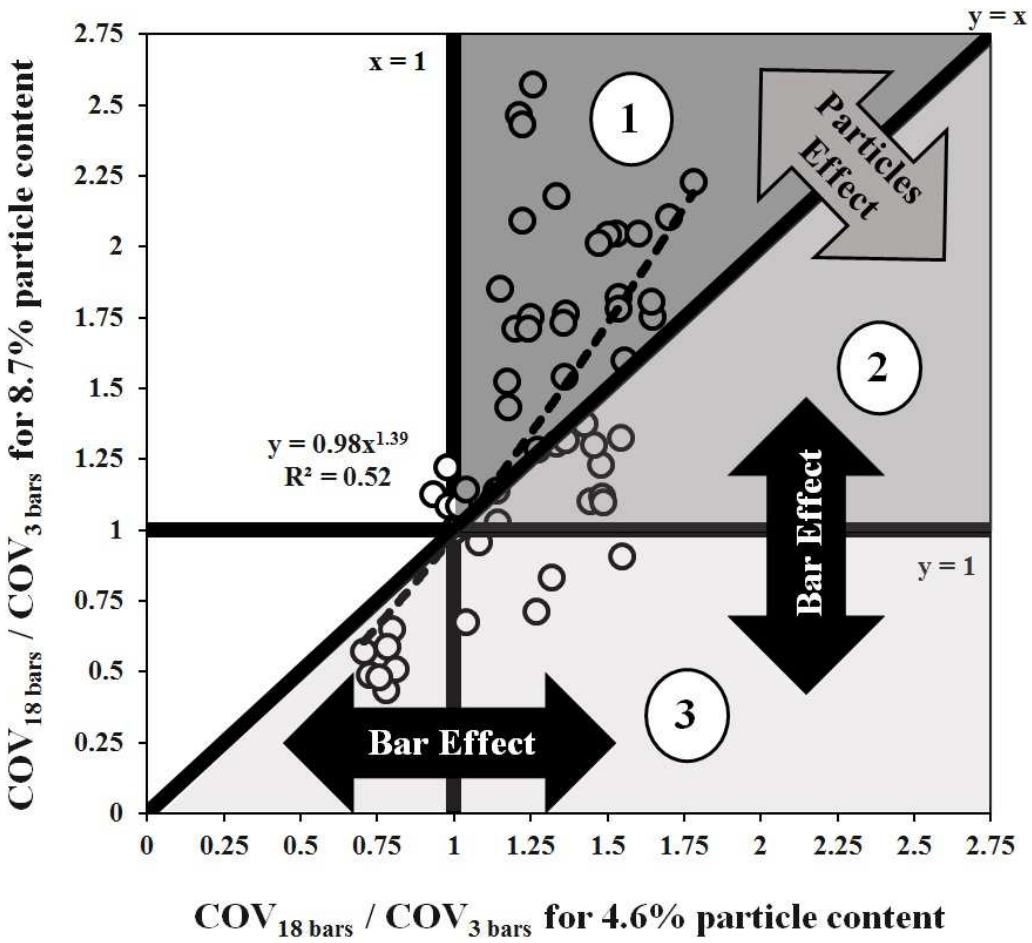

Figure 8. 9 Variation of Bar-Particles coupled effect with dynamic stability of investigated mixtures

According to data presented on Fig. 8.9, the bar-particles coupled effect can be described by three different zones, as follows:

1- Bar-particle parallel effect, zone 1: This zone is limited to the area surrounded by $x > 1$ and $y > x$. In this part, increasing both the number of bars and initial particle contents can result in greater blocking and dynamic segregation. This can be due to the formation of particle blocking arches behind the bars. In this part, both the presence of bars and particle content have dominant effects on this phenomena.

2- Bar-particle opposite effect, zone 2: This zone is limited to the area surrounded by $y > 1$ and $y < x$. In this zone, increasing the number of bars can result in more blocking and dynamic segregation due to greater risk of blocking arch formation. On the other hand, increasing the particle content can improve the dynamic stability and passing ability of the suspension. Such better homogeneous behavior can be explained by particle effects on increasing the overall viscosity and yield stress of the suspension, which leads to a lower fluid deformation and, therefore, less dynamic segregation. In this zone, the presence of bars has more dominant effect.

3- Bar-particle opposite effect, zone 3: This zone is limited to the area surrounded by $y < 1$ and $y < x$. In this part, increasing the particle content can decrease the additive effect of bars on blocking and dynamic segregation by increasing the overall viscosity and yield stress of the suspension. In this zone, the particle content has more dominant effect.

8.4.4 Bar-particles coupled effect on dynamic stability of suspensions in the vertical direction

The vertical dynamic segregation can be defined as the migration of the particles from the top layer towards the bottom layer. As presented in Fig. 8.3, the thickness of both the bottom and middle layers is 3 cm, and the remaining thickness ($Z > 6$ cm) corresponds to the top layer. Accordingly, the vertical dynamic segregation index (V.D.S.I.) can be defined as the ratio of the spread in particle contents of the top and bottom layers to the initial particle content, as follows:

$$\text{V. D. S. I. (\%)} = \frac{\text{Particle content @ bottom layer} - \text{Particle content @ top layer}}{\text{Initial mean particle content}} \times 100\% \qquad (8.6)$$

The results of vertical dynamic segregation index values obtained for the suspensions with 4.6% and 8.7% particle contents in presence of two bar arrangements (3 and 18 bars) are summarized in Table 8.1.

Table 8. 1 Vertical dynamic segregation indexes of 4.6% and 8.7% particle contents and numbers of obstacles (3 and 18 bars)

		Number of obstacles	
		3	18
Particle content (%)	4.6	V.D.S.I. = 106%	V.D.S.I. = 94%
	8.7	V.D.S.I. = 97%	V.D.S.I. = 80%

As can be observed, for a given bar arrangement, increasing the particle content can lead to lower vertical dynamic segregation. This can be explained by the lattice effect resulting in creation of an internal structure of solid particles in a multiphase material [210-212]. Indeed, once the particles settle down to the bottom segment of the L-Box, they create an internal structure which can resist other particles that were supposed to segregate. Increasing the initial particle content can result in strengthening this mentioned internal structure and, therefore, thus leading to decrease in vertical dynamic segregation. On the other hand, as can be observed in Table 8.1, for a given particle content, increasing the number of bars can reduce the vertical dynamic segregation. This can be due the auxiliary effect of obstacles to the lattice performance of the settled particle. Indeed, increasing obstacles prevent the motion of more particles towards bottom layer and works as a sieve. This can be described as the blocking in the vertical direction. Therefore, the minimum V.D.S.I. value of 80% was obtained for the highest particle content of 8.6% and the maximum number of bars (i.e., 18).

8.5 Conclusions

In this paper, a CFD software was employed to evaluate the coupled effect of reinforcing bars and the concentration of relatively large particle (20 mm) on flow performance of SCC cast in an L-Box test set-up. The L-Box had three numbers of 0, 3, and 18 bars distributed along the horizontal channel. Modelling of the L-Box set-up without any obstacles resulted in the evaluation of pure particle effect on non-restricted flow. On the other hand, the presence of 3 and 18 reinforcing bars corresponded to 0.7% and 4% of area of concrete in XY plane of the horizontal channel, that correspond low and highly congested flows, respectively. The CFD modellings was employed successfully to simulate the dynamic segregation and blocking phenomena of the investigated suspension in the L-Box test set-up. The CFD software was shown to be able to enable qualitative simulation the behavior of a non-Newtonian fluid interacting with solid particles, using the VOF method. Solving the Navier-Stokes equation by the CFD software made it possible to track the position and displacements of the solid particles, which their advections were provided by the suspending fluid. Segregation and blocking phenomena are only calculated for a portion of suspended coarse aggregates, which is actually less than typical contents of coarse aggregates in SCC (i.e., 10% to 30%). Indeed, it was assumed that the aggregate fraction that can remains in homogeneous suspension during the flow period can be considered as part of the homogeneous suspending fluid. The modelled materials consisted of a suspending fluid, having moderate plastic viscosity of 25 Pa.s, and high yield stress of 75 Pa.s. The suspensions also consisted of two different contents of the single size solid spherical particles (4.6% and 8.7%, by volume) having a mono size of 20 mm in diameter and a density of 2500 kg/m^3, which is the same as the suspending fluid. It must be noted that these selected coarse particle contents of 20-mm diameter particles correspond to the volume fraction of the aggregate in SCC that have the highest risk to segregate during flow leading to reduction in dynamic stability. Shear-induced dynamic segregation of the investigated suspensions was evaluated by the comparison of the particle content in each section to the last sampling part. The concluding remarks can be expressed by the effects of the initial particle content of the suspension and configuration of reinforcement bars, as well as the interactions between particles and obstacles on passing ability, and dynamic stability of SCC as a heterogeneous material, as follows:

- A new approach is proposed to evaluate the bar-particles coupled effect on the horizontal dynamic stability and risk of blocking in three different interaction zones. These zones indicate parallel and opposite interactions between bars and particles which affect the flow performance of the investigated suspensions, as follows. Increasing both the particle content of the simulated concrete suspension and the number of bars in the L-Box horizontal section can lead to greater possibility of formation of particle arches, which increases the risk of blocking. On the other hand, increasing the particle content can lead to an increase in the overall viscosity and yield stress values of the suspension and decrease of the relative velocity between the surrounding fluid and solid particles. This can improve the dynamic stability of the mixture in the horizontal direction.

- The numerical simulation results showed that in a given rheological properties of the suspending fluid (i.e., stable and homogeneous portion of the concrete), increasing both the particle content and number of reinforcing bars can increase blocking and dynamic segregation of the mixture through the horizontal channel of the L-Box by up to 320% and 250%, respectively. The maximum horizontal dynamic segregation index (I.H.D.S.I) was 550% for the suspension with the higher coarse aggregate content of 8.7% in the presence of 18 bars.

- The highest bar effect was observed in the middle horizontal section, which exhibited the maximum dynamic segregation compared to concrete sampled from sections located at the end of the horizontal channel. On the other hand, in the case of the highest particle content and the maximum number of obstacles, the effects of bars and particle content in the terminal horizontal parts decreased.

- In the case of casting of the SCC mixtures consisting of high concentrations of coarse aggregates in highly reinforced horizontal formworks, the effect of particle content and configurations of bars on passing ability and dynamic segregation of SCC are shown to be dominant in the middle horizontal sections. However, flow performance properties of SCC in the extreme sections located beneath the casting point and at the end of the formwork are found to depend mostly on the casting flow rate and length of formwork, respectively.

- The numerical simulation showed that unlike the horizontal dynamic segregation, increasing both particle content and density of reinforcing bars can decrease the vertical dynamic segregation index (up to 26%).
- An auxiliary lattice effect on the motion of the particles was observed in the vertical compartment of the L-Box with a decrease in dynamic segregation index of up to 9%.

CHAPTER 9 NUMERICAL SIMULATION OF DYNAMIC SEGREGATION OF SELF-CONSOLIDATING CONCRETE IN T-BOX SET-UP

Authors and Affiliations:

Masoud Hosseinpoor: Ph.D. Candidate, Department of Civil Engineering, Université de Sherbrooke, Sherbrooke, Quebec, Canada, J1K2R1
Email: masoud.hosseinpoor@usherbrooke.ca

Kamal H. Khayat: Professor, Department of Civil, Architectural and Environmental Engineering, Missouri University of Science and Technology, 224 Engineering Research Laboratory, 500 W. 16th St., Rolla, MO 65409-0710, USA.
Email: khayatk@mst.edu

Ammar Yahia: Associate Professor, Department of Civil Engineering, Université de Sherbrooke, Sherbrooke, Quebec, Canada, J1K2R1
Email: ammar.yahia@usherbrooke.ca

Paper submitted to Cement and Concrete Research, on 19th September 2016

Abstract

A CFD software was used to simulate free surface flow of self-consolidating concrete (SCC) in the T-Box test apparatus. In total, seven simulations were developed to study the effect of rheological parameters on the non-restricted flowability and dynamic stability of SCC in both

horizontal and vertical directions. Different suspending fluids having five plastic viscosity values between 10 and 50 Pa.s, three yield stress values between 14 and 75 Pa, one density of 2500 kg/m^3, and one shear elasticity modulus of 100 Pa were considered for suspension of 178 spherical particle of 20-mm diameter and 2500 kg/m^3 density. The paper discusses the numerical results in terms of flow characteristics of the suspensions throughout the five horizontal sections and three vertical layers in a T-Box channel for a period of six flow cycles (i.e., t = 0 to 12 s).

The results of the simulations are found to correlate well to changes in rheological parameters of the suspending fluid. Plastic viscosity was shown to be the most dominant parameter affecting flowability and dynamic stability compared to the yield stress. A new approach was proposed to evaluate performability of SCC based on a trade-off between flowability and dynamic stability.

Keywords: Dynamic Stability; Flowability; Heterogeneous Flow Simulation; Performability; Self-Consolidating Concrete; T-Box Test.

9.1 Introduction

Self-consolidating concrete (SCC) is a novel construction material that is gaining market acceptance in various applications. Higher fluidity characteristics of SCC enable it to be used in some special applications, such as densely reinforced sections. However, higher flowability of SCC makes it more sensitive to segregation of coarse particles during flow (i.e., dynamic segregation) and thereafter at rest (i.e., static segregation) [23, 83, and 208].

Dynamic segregation corresponds to the separation of coarse aggregates from the mortar matrix during flow [29]. It can result in less aggregate content in top layers of the cast concrete, which is called vertical dynamic segregation. This type of segregation is more important in the case of vertical applications, such as tremie concreting and casting of tall wall and column elements. This can be accelerated by gravitational induced and static segregation [9, 14-16, 46, and 47]. On the other hand, increasing horizontal flow distance can result in less coarse aggregate content at flow front, regardless of the effect of the obstacles and blocking resistance. This is called

horizontal dynamic segregation which is more concerned in horizontal applications, such as casting of long slabs, beams, and wall elements [26]. Therefore, comparison between the properties of SCC at each horizontal or vertical levels and the casting point, i.e., the point where the concrete is dropped into the formwork, can lead to evaluate the dynamic stability of the mixtures on that level.

Accordingly, new experimental tests are developed, including determination of coarse particle contents in different horizontal and vertical sections of a channel [45 and 90] and penetration depth which measures the depth of the thickness of the cement mortar/paste accumulated above the settled aggregates [87 and 88]. For example, SCC is allowed to flow in a channel and then the particle content at the entrance and the end of the channel are compared to determine the horizontal dynamic segregation [91]. Turgut et al. [92] developed a modified L-box set-up to evaluate the dynamic segregation of SCC in different locations in the horizontal channel.

The T-Box test which resembles the non-restricted flow of the SCC by tilting motion of the box in different rotating cycles was developed [36 and 37]. Displacement of the mass-center of the concrete during rotation process can simulate the motion of concrete in the formwork in vertical and horizontal directions. Vertical and horizontal dynamic segregation of SCC are then measured by determining the penetration depths and coarse aggregate contents at two sides of the box, respectively. Esmaeilkhanian et al. [38] evaluated experimentally the effect of mix design parameters and rheological properties of SCC on the results obtained by T-Box test. It was revealed that increasing yield stress and plastic viscosity can result in higher dynamic stability of SCC due to higher drag force exerted by the mortar matrix on coarse aggregates. Consequently, workability parameters of SCC have a significant effect on its dynamic stability. For example, decreasing slump flow from 700 to 640 mm and increasing V-funnel flow time from 5 to 25 s could result in increasing the dynamic stability of SCC up to 38% to 50%. This is due to higher plastic viscosity and yield stress of the mixture [36-38]. It was also concluded that ensuring proper dynamic segregation resistance is more stringent than static segregation [38].

Disturbing the homogeneity of fresh SCC mixtures results in negative effects on its structural performance and durability in the hardened state. Therefore, there is a great need to develop some theoretical tools to evaluate stability of SCC during the casting process. Using these tools can lead to assess the required conditions to ensure proper dynamic stability and flowability. It must be noted that there is always a trade-off between dynamic stability and flowability of SCC that should be established given the casting conditions [24]. Numerical simulations of flow of SCC can be considered as powerful tool to predict flow performance of the mixture while taking into account flow induced segregation [42-44]. Recently, there is a great interest to employ computational flow modeling to evaluate the dynamic stability of SCC [29, 36, 37, and 44]. Spangenberg et al. [36 and 37] studied different patterns of dynamic segregation of SCC. The results showed that gravitational particle segregation plays the dominant role in dynamic segregation of the coarsest aggregates in both horizontal and vertical directions during the casting process.

In this paper, a computational fluid dynamics (CFD) software was employed to simulate free surface flow of SCC in the T-Box test apparatus as a heterogeneous suspension of coarse particles in a Bingham surrounding fluid. The 3D Navier–Stokes and conservation of mass equations for incompressible materials are solved by the volume of fluid (VOF) method [150], using 1st order momentum advection. In total, 7 simulations were developed to study the effect of rheological parameters of the suspending fluid on flowability and non-restricted dynamic stability of SCC in both horizontal and vertical directions. Modelled suspensions consisted of the suspending fluid that corresponds to the stable homogeneous portions of the SCC mixture, which includes the fraction of the coarse and fine aggregates that can flow in a homogeneous manner during the casting process. Several suspending fluids with various yield stress and plastic viscosity values were investigated. The paper discusses the results of the numerical simulations in terms of flow velocity, strain rate, kinetic energy, flow profiles, and particle distribution throughout the T-Box channel (horizontal direction) and fluid depth (vertical direction) following six tilting cycles of the T-Box test.

9.2 T-Box test set-up

The T-Box test set-up was developed to evaluate dynamic stability of SCC [36-38]. As can be observed in Fig. 9.1, the proposed apparatus consists of a rectangular channel measuring 1 m in long, 0.2 m in width, and 0.4 m in height, hinged in the middle to a 140-mm height support. The rotating motion of the box is limited by another support beneath one end of the channel. An amount of 16 L of SCC is cast in the channel which provides an initial concrete thickness of 80 mm [36].

This test simulates the flow distance traveled by the concrete (typically SCC) in the formwork using a tilting motion of the box in given rotating cycles. Each single 2-s flow cycle is reached when the channel rotates from the initial horizontal position in the non-supported side till the box touches the floor in 1-s half cycle (i.e., titling down), and then moves back to the horizontal state in another 1 s (i.e., tilting up) in a continuous motion. Consequently, as the number of cycle increases, the coarse particles accumulate gradually in the tilt down section, and at the same time this results in formation of a layer of mortar in the top surface of the concrete placed in the tilt up section. Comparing the properties of the concrete in the tilt down section to the one placed in the tilt up section in a given number of tilting cycles can enable the evaluation of dynamic stability of the investigated mixture. In this paper, flow performance of various SCC mixtures are evaluated in T-Box set-up using CFD.

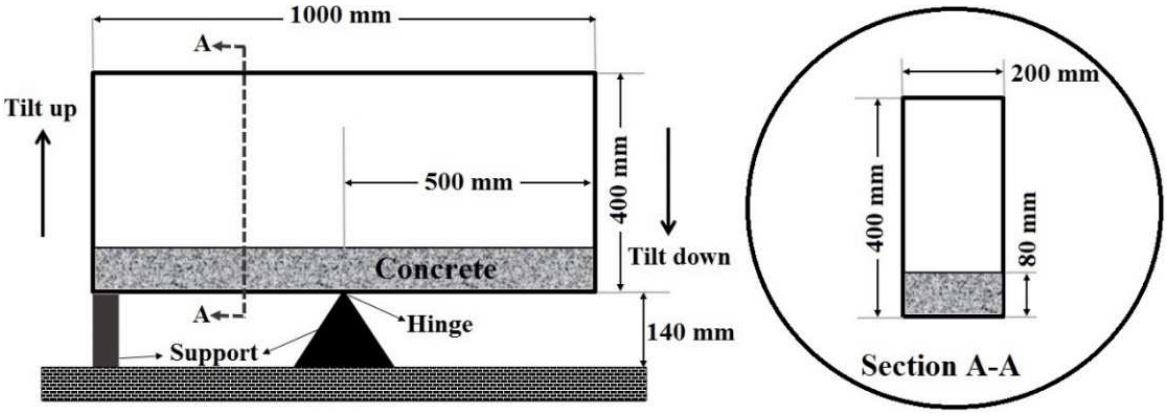

Figure 9. 1 Schematics of T-Box set-up [36-38]

9.3 Properties of modelled materials and T-Box test procedure

The investigated SCC mixtures are considered as suspensions of coarse particles in various suspending fluids. The suspending fluid is assumed actually as the portion of the concrete mixture that shows no segregation and keeps homogeneous during flow. The parameters of the modeling included five plastic viscosity values (10, 17, 25, 38, and 50 Pa.s), three yield stress values (14, 45, and 75 Pa), and a density of 2500 kg/m^3, as well as one shear elasticity modulus value of 100 Pa for the suspending fluids. The shear elasticity modulus is the ratio of the shear stress to shear strain in the elastic state of the suspending fluid. The virtual concrete suspensions included 178 spherical particles of 20 mm of diameter which corresponds to 4.7% volumetric particle content. Indeed, it was assumed that the finer coarse aggregate fraction that can remain in homogeneous suspension in the SCC mixture during the flow period makes up part of the suspending fluid. Accordingly, the suspending fluid can be assumed as the stable portion of the SCC mixture. It can be explained by the fact that segregation and blocking do not occur for all the aggregate particles, and that the finer aggregate potion can remain uniform suspension during the flow in place of stable SCC. It is important to note that, due to the limits in calculation capacity of computers, tracking of the positions of all the coarse aggregate particles (having typical contents and sizes, ranging from 10% to 30% and 5 mm to 20 mm, respectively) would have been impossible. It must also be noted that the effect of five values of suspending fluid plastic viscosity (i.e., 10, 17, 25, 38, and 50 Pa.s) on the flow performance of suspensions is only evaluated for the suspensions having the maximum suspending fluid yield stress value of 75 Pa. On the other hand, the effect of suspending fluid yield stress on flowability and dynamic stability of SCC is only evaluated for the mixtures having the minimum plastic viscosity value of 10 Pa.s.

In total, the first six flow cycles (i.e., t = 12 s) of the tilting motion of the T-Box test was considered in model of the investigated suspensions. As mentioned before, the tilting of the apparatus starts from stationary horizontal state at t = 0 s, and also at the beginning of each flow cycle (i.e., t = 2, 4, 6, 8, and 10 s) by tilting down the channel. Therefore, the initial angular velocity at the beginning of each flow cycle should set to be zero (ω(t = 0, 2, 4, 6, 8, and 10 s) = 0 rad/s). The tilting procedure is ended by a horizontal position at t = 12 s by a tilting up

motion (i.e., ω(t = 12 s) = 0 rad/s). On the other hand, since the box edge touches the floor slightly at the end of each first half of the flowing cycles (i.e., t = 1, 3, 5, 7, 9, and 11 s), the corresponding angular velocity of the tilting procedure is assumed to be zero at these flow times. Considering the fact that tilting pattern should be continuous, it also assumed that angular velocity of the apparatus reaches maximum values at first and third quarter flow cycles (i.e., t = 0.5, 1.5, 2.5, 3.5, 4.5, 5.5, 6.5, 7.5, 8.5, 9.5, 10.5, and 11.5 s). On the other hand, the apparatus should be rotated by a maximum angle of $\alpha = \tan^{-1}(140\ mm/\ 500\ mm) = 0.273$ rad (i.e., 15.642 degree) in every half cycles. Therefore, assuming a sinusoidal function pattern, the angular velocity of modeled T-Box set-ups can be defined as a function of the flow time, according to Eq. (9.1):

$$\omega\ (rad/s) = 0.4288 \sin(\pi t) \tag{9.1}$$

where ω is the angular velocity of the apparatus as function of flow time t, positive and negative values of ω correspond to tilting down and tilting up periods of flow, respectively. A typical example of angular velocity values for a single flow cycle is presented in Fig. 9.2.

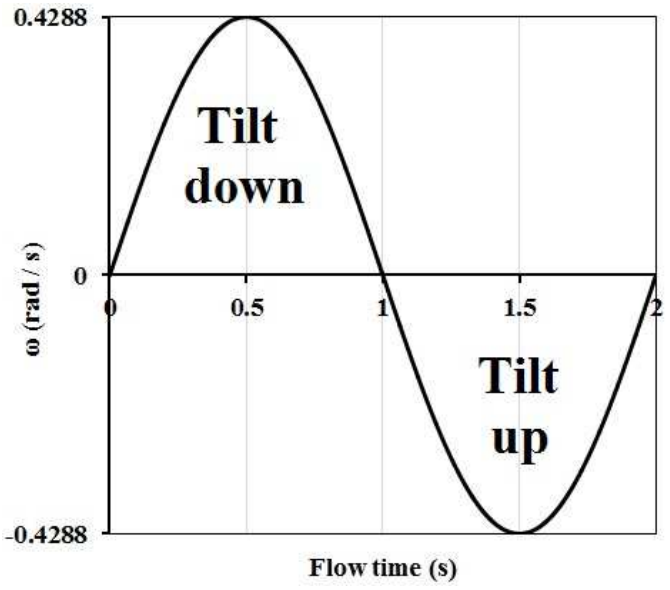

Figure 9. 2 Angular velocity versus time for a single flow cycle

9.4 Numerical simulation and boundary conditions

In order to simulate flow performance of SCC in the T-Box test apparatus, a CFD software (FLOW3D®) was employed. The basic equations of the conservation of mass for incompressible materials and the Navier–Stokes equations are solved by the Volume of Fluid (VOF) method [150]. In total, 7 simulations were carried out for a period of flow of 12 s (i.e., 6 flow cycles). Six mesh blocks of 585,104 cubic cells with 5-mm size in the x, y, and z directions were created to discretize the geometry, solid elements, and suspension.

As presented in Fig. 9.3a-1, the Dirichlet-Neumann boundary conditions were applied based on the geometry of the T-Box set-up; the velocity of the walls of the apparatus was set to zero in y direction. In the x and z directions, the velocity of the walls is governed by Eq. (9.1). The friction boundary conditions between particles, fluid, and the walls of the apparatus were assumed with a friction coefficient value of 0.4 (according to Coulomb's law of friction) [205]. The modelled fluids are considered as non-Newtonian Bingham fluids using an elasto-viscoplastic model with implicit numerical approximation. Gravity stresses are calculated using gravitational acceleration value of 9.81 m/s^2. In order to consider particle-particle and particle-wall interactions, a coefficient of restitution of 0.8 was applied for collision physical model. The modelled flow is assumed to be laminar flow type [48]. It is worthy to mention that numerical simulations carried out on an i7-2600 CPU 3.40 GHz processor required a total running time between 124 and 592 hours. The running time depend mostly on the plastic viscosity of the suspending fluid. Indeed, the simulation of T-Box flow of higher viscous suspensions took more calculation time than less viscous ones.

9.4.1 Sampling methods and anticipated results

In order to evaluate flowability of the modelled suspensions, the results of the simulations are presented in 0.1-s time steps in forms of flow velocity, strain rate, kinetic energy, displacement magnitudes, and flow profiles. Dynamic stability properties of the suspensions in horizontal direction are also calculated by measuring the volumetric particle contents in five 20-cm long sections through the T-Box horizontal channel that are illustrated in Fig. 9.3a. The number and

position of the particles, as well as the volume of the fluid in each section are calculated at each flow cycle (i.e., 2-s periods). On the other hand, dynamic stability of the suspensions in the vertical direction is evaluated by comparing the volumetric particle contents in three vertical layers (bottom, middle, and top) at each flow cycle (i.e., 2-s periods). As presented in Fig. 9.3b, the thickness of both the bottom and middle layers is 3 cm, and the remaining (Z > 6 cm) corresponds to the top layer.

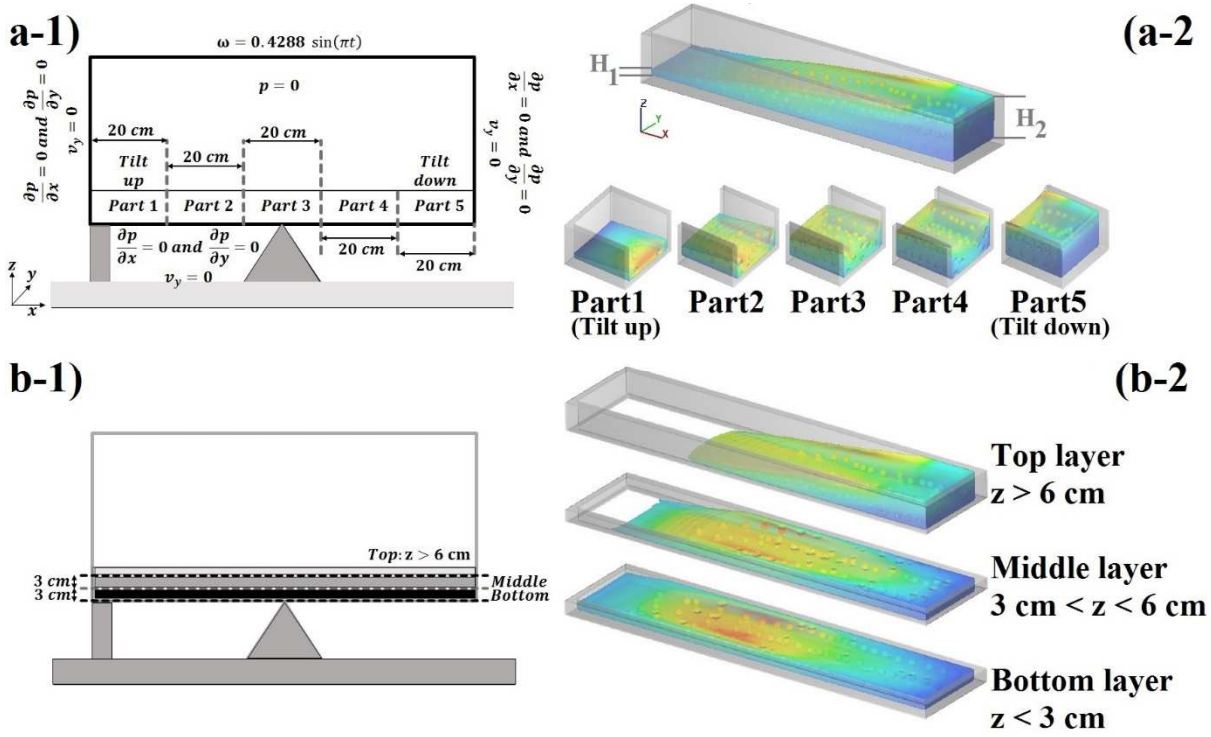

Figure 9. 3 a-1) Boundary conditions and positions of horizontal sampling parts, a-2) horizontal sampling parts, b-1) positions of vertical sampling sections, and b-2) vertical sampling sections

9.5 Results and discussions

9.5.1 Evaluation of flowability of modeled suspensions in T-Box test set-up

In this section, the flowability of the modeled suspensions with five suspending fluid viscosity values corresponding to 10, 17, 25, 38, and 50 Pa.s, and the same yield stress value of 75 Pa, are evaluated using numerical simulation. Flow profile angles can be calculated at the end of each flow cycle using Eq. (9.2).

$$Flow\ profile\ angle\ (degree) = \tan^{-1}\left(\frac{H_2 - H_1}{L = 1\ m}\right) \quad (9.2)$$

where H_2 and H_1 (Fig. 9.3a-2) are the flow profile depths at the tilt down and tilt up sides of the T-Box at the end of each flow cycle, respectively, and L =1 m is the channel length. The results of flow profile angles at the end of each cycle are presented in Fig. 9.4a for different plastic viscosity values of suspending fluid. As can be observed in Fig. 9.4a, for a given viscosity, increasing the number of cycles can result in higher flow profile angle till reach an equilibrium value. Moreover, for a given flow cycle, increasing fluid viscosity results in decreasing the flow profile angle due to the less flowability of higher viscous mixtures. For example, under 2 flow cycles, increasing suspending fluid viscosity from 10 to 50 Pa.s can decrease the flow profile angle from 8.0 to 5.0 degree. Furthermore, it is worthy to mention that increasing the number of flow cycles can lead to decrease the viscosity effect on the angle of flow profile. For example, increasing plastic viscosity of suspending fluid from 10 to 50 Pa.s can decrease the flow profile angle from 5.7 to 2.5 degree (i.e., 56% reduction) and from 8.1 to 6.9 degree (i.e., 15% reduction) under 1 and 6 flow cycles, respectively. This can be explained by the dissipation of initial flow energy in higher flow displacements obtained by more flowing cycles (Fig. 9.4b). Indeed, in a constant gravitational (i.e., constant density) and elastic (i.e., constant yield stress values) force conditions, when the flow energy becomes less, the effect of viscous forces on free surface flow profile shape of the mixtures also decreases. Accordingly, the maximum values of flow mass-averaged kinetic energy in each flow cycle are presented in Fig. 9.4b. As can be observed, flow kinetic energy is mostly dissipated in the second flow cycle due to friction stresses and wall effect. After the second cycle, it reaches equilibrium values for each suspension. These effects are shown to be dominant in the case of lower viscosity values. This shows that flow properties of the mixtures with less suspending fluid viscosity are affected mostly by the initial flow energy provided by the first tilting cycle, while for the higher viscous mixtures the number of flow cycles (Eq. (9.1)) is the most dominant factor. For example, the maximum flow mass-averaged kinetic energy magnitudes in the first flow cycle decrease from 0.0396 to 0.0215 J/kg (i.e., 46% dissipation) and from 0.0095 to 0.0087 J/kg (i.e., 8% dissipation) in the second flow cycle for suspending fluid plastic viscosity values of 10 and 50 Pa.s, respectively.

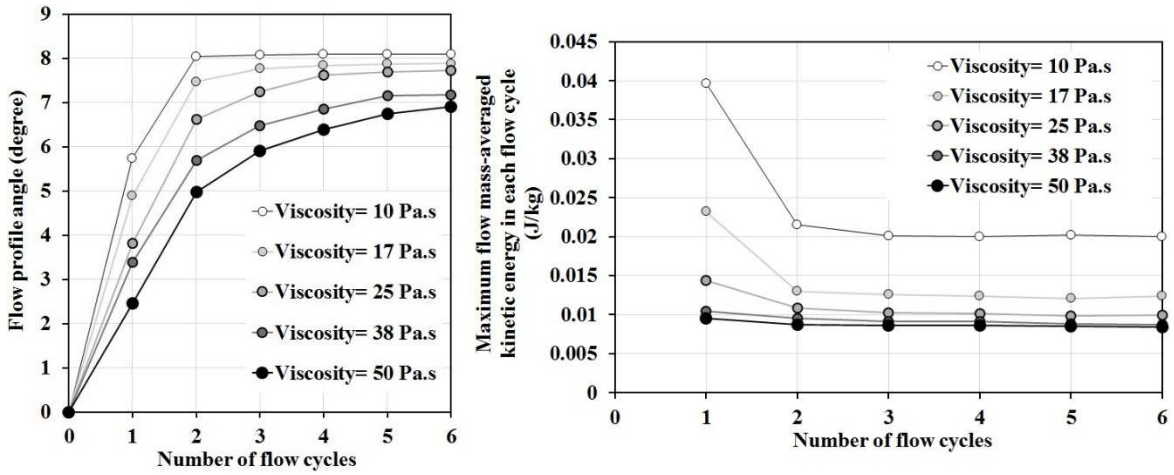

Figure 9. 4 a) Flow profile angle and b) the maximum flow mass-averaged kinetic energy in each flow cycle versus number of flow cycles

The results of the maximum overall values of flow displacement, flow velocity, and mass-averaged kinetic energy obtained for the investigated suspensions during the test duration (i.e., t = 0 to 12 s) are presented in Fig. 9.5a, 9.5b, and 9.5c, respectively. Suspensions with lower plastic viscosity of the suspending fluid can exhibit higher flowability. For example, increasing the plastic viscosity of suspending fluid from 10 to 50 Pa.s resulted in decreasing the maximum overall flow displacement, velocity, and mass-averaged kinetic energy magnitudes from 0.460 to 0.377 m (i.e., 18% decrease), 0.634 to 0.224 m/s (i.e., 65% decrease), and 0.0396 to 0.0095 J/kg (i.e., 76% decrease), respectively.

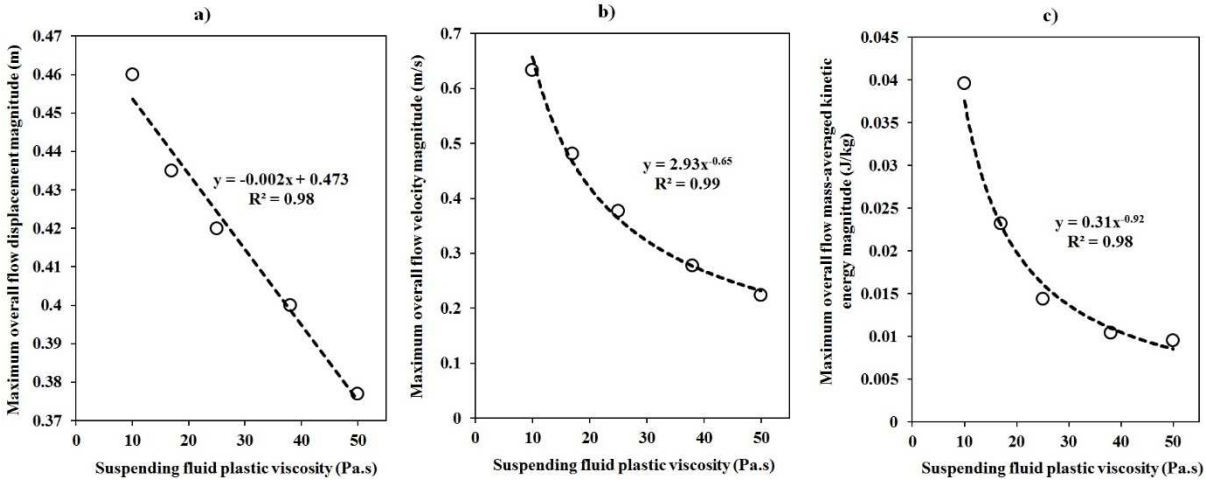

Figure 9. 5 Maximum overall flow a) displacement, b) velocity, and c) mass-averaged kinetic energy versus suspending fluid plastic viscosity

9.5.2 Evaluation of dynamic stability of suspensions in the horizontal direction

In this section, horizontal dynamic stability of the modeled suspensions with suspending fluid viscosity values of 10, 17, 25, 38, and 50 Pa.s and yield stress value of 75 Pa are evaluated using numerical simulations. Fluid volume and particle contents in five horizontal sampling sections (as presented in Fig. 9.3a) are calculated at the end of each flow cycle. Accordingly, shear-induced dynamic segregation of the mixtures in the horizontal direction can be quantified for each flow cycle using the coefficient of variation (COV) of particle contents in all the five horizontal parts (Parts 1 to 5) as follows:

$$COV\ (\%) = \frac{Standard\ deviation\ of\ particle\ contents\ (Parts\ 1,\ 2,\ 3,\ 4,\ and\ 5)}{Average\ of\ particle\ contents\ (Parts\ 1,\ 2,\ 3,\ 4,\ and\ 5)} \times 100\% \qquad (9.3)$$

As can be observed in Fig. 9.6a, for a given suspending fluid viscosity, increasing the number of flow cycles can result in increasing the COV of particle contents in the five horizontal samples, which indicates higher dynamic segregation. This can be due to the increase in flow displacement, which can lead to higher shear-induced heterogeneity in the suspensions. On the other hand, within a given number of flow cycles, the suspensions with higher suspending fluid viscosity show less COV value than those with less suspending fluid viscosity. It is also worthy to mention that increasing the viscosity shows higher effect in the case of less flow cycle numbers due to its effect on the initial flow energy and inertial forces which are provided in the first flow cycle. For example, as can be observed in Fig. 9.6b, increasing the plastic viscosity of the suspending fluid from 10 to 50 Pa.s resulted in decreasing the COV from 41% to 4% (i.e., 37% reduction) and from 52% to 33% (i.e., 19% reduction) under 1 and 6 flow cycles, respectively, with very good coefficient of correlation ($R^2 > 0.96$).

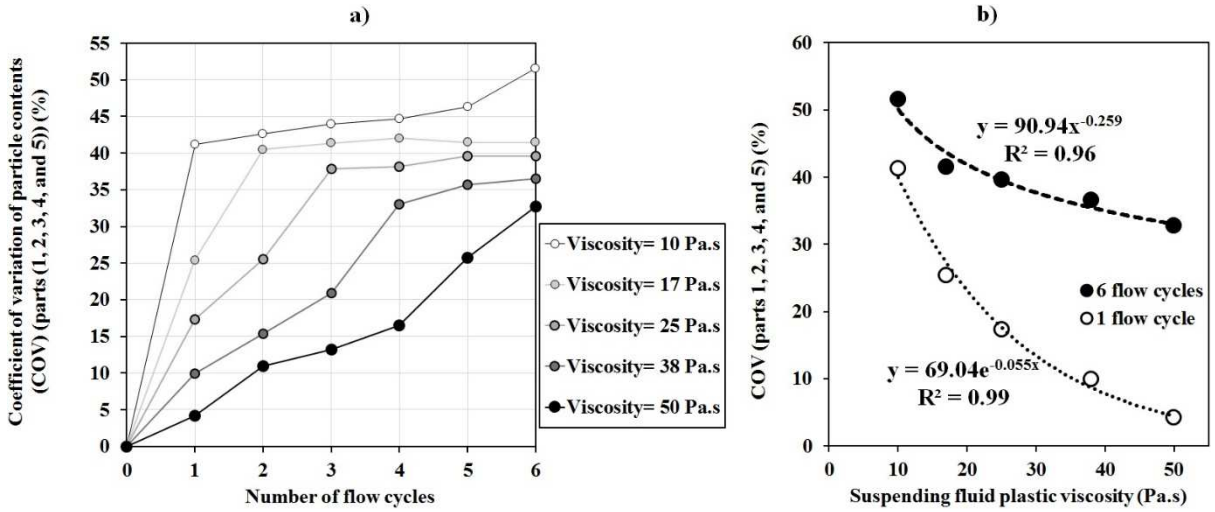

Figure 9. 6 The variation of COV of particle contents in five horizontal sections versus a) number of flow cycles for different suspending fluid plastic viscosity, and b) suspending fluid plastic viscosity for 1 and 6 flow cycles

It can also be concluded from Fig. 9.6b that increasing the number of flow cycles resulted in less effect on the dynamic segregation of the mixtures with less plastic viscosity value of suspending fluid. For example, increasing the number of flow cycles from 1 to 6 resulted in increasing COV from 41% to 52% (i.e., 11% increase) and from 4% to 33% (i.e., 29% increase) for suspending fluid viscosity values of 10 and 50 Pa.s, respectively. This can be due to the less drag forces exerted on particles in the case of less viscosity of suspending fluid. Consequently, less viscous mixtures can mostly segregates dynamically in the initial flow cycles (i.e., less flow distance traveled by the suspension) which flow energy and inertia stresses are significantly higher than those values in subsequent flow cycles, and then reaches to an equilibrium value. The results presented in Fig. 9.4b showed that the flow energy is more dissipated after initial flow cycle in the case of less viscous mixtures. Typical maximum values of inertial stress ($I_{max}(i)$) in the flow cycle (i) can also be estimated using Eq. (9.4).

$$I_{max}(i) = \rho[V_{max}(i)]^2 \tag{9.4}$$

where $\rho = 2500$ kg/m^3 is the density of the suspension and $V_{max}(i)$ is the maximum flow velocity magnitude in the flow cycle i. It is worthy to mention that within a given flow cycle i, suspensions exhibited their maximum flow velocity ($V_{max}(i)$) in the second quarter of the cycle

(i) which refers to the second half of the tilting down steps. Moreover, as the plastic viscosity of suspending fluid increases, the maximum flow velocity for a given number of flow cycle (greater than 1) tends to be obtained mostly at the beginning of the second quarter of that cycle where the angular velocity is at its maximum value. For the less viscous suspensions, this value was obtained mostly at the end of the second quarter of the cycle which corresponds to the end of the tilting down step.

As can be observed in Fig. 9.7, for the suspending fluid with lower plastic viscosity, inertia stress values decrease significantly after the first flow cycle compared to those with higher viscosity where the inertia stresses remain comparable, regardless of the number of flow cycles. For example, the maximum inertia stress in the first flow cycle decreases from 1005 to 625 Pa (i.e., 38% decrease), and from 125 to 121 Pa (i.e., 3% decrease) in the second flow cycle for suspending fluid plastic viscosity values of 10 and 50 Pa.s, respectively.

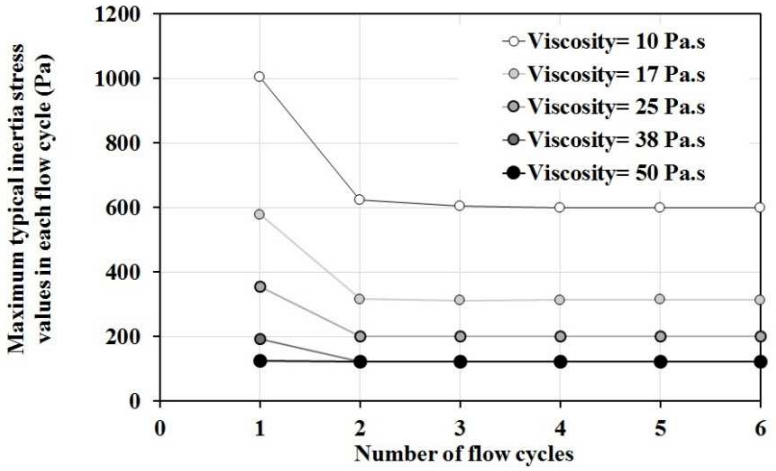

Figure 9. 7 Maximum typical inertia stress values in each flow cycles for different values of suspending fluid viscosity

Accordingly, higher viscous suspensions reach their maximum dynamic segregation capacity after longer flow cycles (i.e., longer flow distances). For example, as can be observed in Fig. 9.6a, 2, 3, and 4 flow cycles are required for the mixtures with suspending fluid viscosity values of 17, 25, and 38 Pa.s, respectively to reach at least 90% of their maximum dynamic segregation capacity which is obtained after 6 flow cycles.

According to Esmaeilkhanian et al. [36-38], comparison between the properties of two horizontal samples located in tilt up and tilt down sides of the T-Box can also be used as an evaluation index for horizontal dynamic segregation of SCC. Therefore, calculating fluid volume and particle content in two horizontal sampling sections located at the tilt down (Part 5) and tilt up (Part 1) sides of the T-Box channel, the horizontal dynamic segregation index (H.D.S.I.) can be defined for each flow cycle using Eq. (9.5):

$$H.D.S.I.(\%) = \frac{Particle\ content\ @\ tilt\ down\ side\ (Part\ 5) - Particle\ content\ @tilt\ up\ side\ (Part\ 1)}{Initial\ mean\ particle\ content} \times 100\% \quad (9.5)$$

Similar to the COV, as can be observed in Fig. 9.8a, for a given suspending fluid's plastic viscosity, increasing the number of flow cycles can result in increasing the H.D.S.I. values. This can be explained by the fact that under higher flow cycles, the mixture travels more distance in the horizontal direction, which affect the homogeneity of the suspensions. On the other hand, under a given number of flow cycles, higher H.D.S.I. values were obtained for lower suspending fluid plastic viscosity mixtures. This can be due to the higher drag forces exerted on the particles in the case of higher viscosity of suspending fluid which results in maintaining more particles in the suspending fluid and prevent them to segregate. Furthermore, increasing the viscosity results in higher effect in the case of less number of flow cycles due to the effect of viscosity on the initial flow energy and inertial forces, which are provided in the first flow cycle to drive the displacements of the particles. For example, as can be observed in Fig. 9.8b, increasing the plastic viscosity of the suspending fluid from 10 to 50 Pa.s can decrease the H.D.S.I. from 91% to 3% (i.e., 88% reduction) and from 101% to 68% (i.e., 33% reduction) after 1 and 6 flow cycles, respectively, with very good coefficient of correlation ($R^2 = 0.98$).

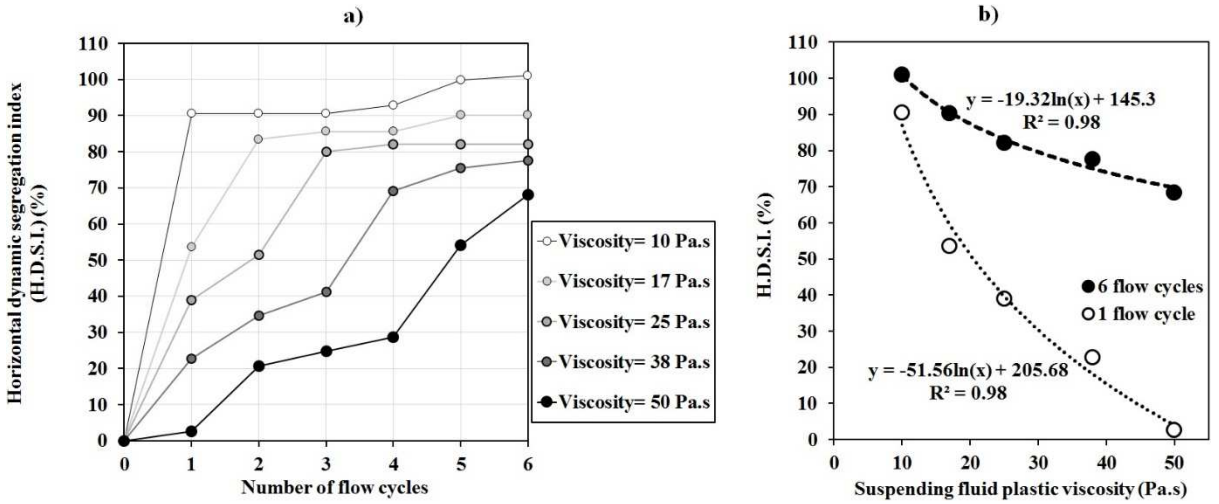

Figure 9. 8 Variation of the horizontal dynamic segregation index (H.D.S.I.) with, a) number of flow cycles and different suspending fluid plastic viscosity, and b) suspending fluid plastic viscosity for 1 and 6 flow cycles

As can be observed in Fig. 9.8b, increasing the number of flow cycles can have a higher effect on the horizontal dynamic stability of the mixtures with higher suspending fluid plastic viscosity. For example, increasing the number of flow cycles from 1 to 6 increased the H.D.S.I. values from 91% to 101% (i.e., 10% increase in horizontal dynamic segregation) and from 3% to 68% (i.e., almost 65% more horizontal dynamic segregation) for suspending fluid viscosity values of 10 and 50 Pa.s, respectively. Indeed, lower viscous mixtures exhibit more dynamic segregation during the first flow cycle (i.e., less flow distance traveled by the suspension), and then they reach an equilibrium value. This can be due to higher initial flow energy (Fig. 9.4b) and inertial stresses (Fig. 9.7), as well as less drag forces exerted on particles in the initial flow cycles. However, in the case of higher viscous suspensions, more flow cycles (which means higher flow distance) is required to reach the maximum dynamic segregation capacity. As can be observed in Fig. 9.8a, the number of flow cycles of 1, 2, 3, and 4 are required for the mixtures with suspending fluid viscosity values of 10, 17, 25, and 38 Pa.s, respectively, to reach almost 90% of their maximum capacity of horizontal dynamic segregation, which is obtained after 6 flow cycles.

9.5.3 Tracking of particles

In order to validate the results of sections 9.5.1 and 9.5.2 the maximum displacements of nine typical particles are calculated for each mixture in a flow time when the mixture reached its maximum flow displacement (i.e., $t_{maximum\ flow\ displacement}$). As presented in Fig. 9.9, these typical particles are located in three different vertical layers (i.e., top, middle, and bottom) and three different horizontal sections (i.e., tilt down, middle, and tilt up). According to the results presented in Fig. 9.5a, for the flow times corresponding to the maximum overall flow displacement (i.e., $t_{maximum\ flow\ displacement}$ which were obtained as 3.4, 5.4, 9.4, 11.4 and 11.5 s for suspending fluid viscosity of 10, 17, 25, 38, and 50 Pa.s, respectively), displacements of each of nine particles in the X, Y, and Z directions are calculated. The maximum total displacement for each particle can be calculated as follows:

$$Displ_{max}(i) = \sqrt{(Displ_X(i)^2 + Displ_Y(i)^2 + Displ_Z(i)^2)} \tag{9.6}$$

where $Displ_{max}(i)$ is the maximum total displacement of the particle i, and $Displ_X(i)$, $Displ_Y(i)$, and $Displ_Z(i)$ are the displacements of particle i in x, y, and z directions, respectively, for a period of time from 0 to $t_{maximum\ flow\ displacement}$.

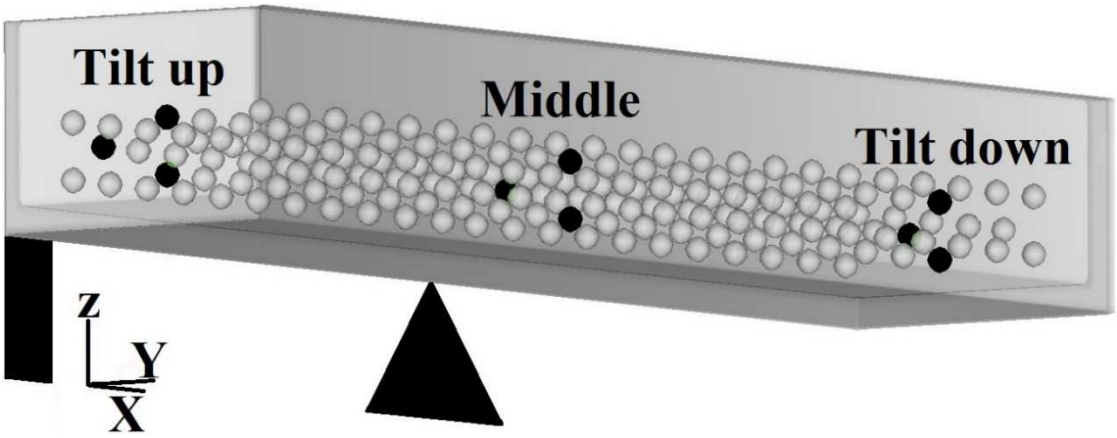

Figure 9. 9 Initial positions of nine representative 20-mm diameter particles, colored in black

The maximum displacement ($Displ_{max}$) values of the particles placed at different initial horizontal and vertical positions are compared to the maximum displacement of the suspending

fluid having different plastic viscosities in Figs. 9.10a, 9.10b, and 9.10c. According to the results presented in Fig. 9.10, for suspending fluid viscosity ranging between 10 and 50 Pa.s, all the typical particles placed in different locations exhibited lower displacements than the suspending fluid, which means that the dynamic segregation occurred definitely in all locations of the suspension medium. For example, in the case of suspending fluid (viscosity between 10 to 50 Pa.s), the maximum displacement vary between 0.377 and 0.460 m. However, in the case of the typical particles, lower maximum displacement (from 0.055 to 0.348 m) is observed. This can be due to the frictional and drag forces exerted on particles, and also to particle-particle and particle-walls interactions which can lead to reducing the capacity of suspending fluid to transport the particles.

However, in the case of particles located in the middle horizontal section, more displacement is observed compared to those located in tilt up and tilt down sections. This can be due to lower interactions with side walls of the T-Box. For example, particles located in the middle, tilt up, and tilt down horizontal sections exhibit displacements from 0.187 to 0.348 m, 0.101 to 0.270 m, and 0.055 to 0.086 m, respectively, regardless of their vertical locations. Therefore, it can also be concluded that the particles placed initially in the tilt down section exhibit the minimum displacement values. This can be explained by the accumulation of particles and formation of an internal structure in the tilt down section, which is called lattice effect [210-212]. This can resists against more particle displacement in the tilt down section.

As can be observed in Fig. 9.10, the viscosity of suspending fluid did not show a significant effect on displacement of the particles in the tilt down section. For example, increasing the viscosity from 10 to 50 Pa.s resulted in decreasing in the displacement of particles located in the tilt down side from 0.072 to 0.055 m (i.e., 0.017 m decrease), 0.086 to 0.061 m (i.e., 0.025 m decrease), and 0.083 to 0.064 m (i.e., 0.019 m decrease) for top, middle, and bottom initial vertical positions, respectively. These decrements are negligible comparing to particle diameters (i.e., 0.02 m). This is due to the lattice effect and interaction between particles and side walls of the T-Box which are more dominant than the effect of viscosity of suspending fluid.

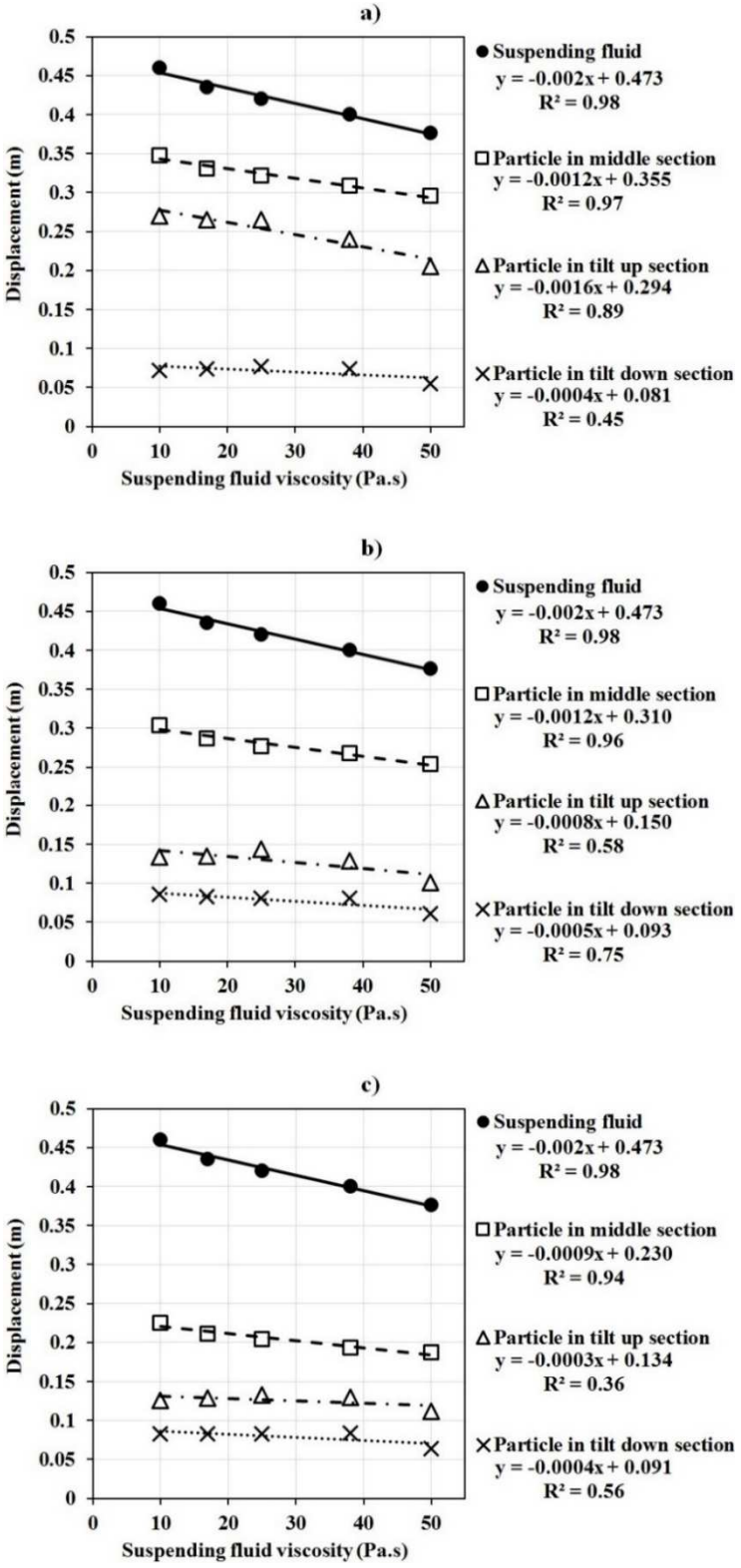

Figure 9. 10 The variation of the maximum displacement of suspending fluid and typical particles located in three horizontal sections (tilt up, middle, and tilt down) and three vertical layers a) top, b) middle, and c) bottom with the plastic viscosity of suspending fluid

On the other hand, particles located in the top layer show larger ranges of displacement than those placed in the middle and bottom layers due to lower distance from the flow surface, and accordingly, less friction and interaction with surrounding fluid and solid walls. For example, regardless of the initial horizontal positions, typical particles located initially in the top, middle, and bottom layers show displacements from 0.055 to 0.348 m, 0.061 to 0.304 m, and 0.064 to 0.226 m, respectively.

As can be observed in Fig. 9.10 a, increasing the viscosity of suspending fluid resulted in decreasing displacement of particles that are mostly located in the middle and tilt up horizontal sections of the top layer. For example, increasing the viscosity from 10 to 50 Pa.s decreases displacement of particles located in the tilt up and middle sections of the top layer from 0.270 to 0.205 m (i.e., 0.065 m decrease) and 0.348 to 0.296 m (i.e., 0.052 m decrease), respectively. However, as can be observed in Fig 9.10, the viscosity of suspending fluid has no significant effect on displacement of particles located initially in bottom layer, which showed the minimum displacements compared to other vertical layers, especially for those placed in tilt up and tilt down horizontal sections. For example, increasing viscosity of the suspending fluid from 10 to 50 Pa.s decreases displacement of particles which are located initially in the tilt up and tilt down sections of the bottom layer from 0.125 to 0.112 m (i.e., 0.013 m decrease), and 0.083 to 0.064 m (i.e., 0.019 m), respectively. These decrements are lower than diameters of the particles (i.e., 0.02 m) and, therefore, can be considered negligible. This can be due to the dominant effect of friction, particle-particle, and particle-walls interactions on flow performance of the suspension at two bottom corners of the horizontal channel, due to lower distance to the base-plate and side walls of the apparatus. It can also be due to the lattice effect of the internal structure of the particles settled down in the bottom layer. Migration of particles towards the bottom layer is called vertical dynamic segregation and will be discussed in the next section.

9.5.4 Evaluation of dynamic stability of the suspensions in the vertical direction

As observed in the previous section, the migration of particles towards the bottom layer (i.e., vertical dynamic segregation) has significant effect on displacement of particles through the suspending fluid. In order to determine in which flow depth there is more deformation that may

indicate a risk of dynamic segregation in the vertical direction, the ratio of the maximum flow velocity to the maximum strain rate is examined for all the investigated mixtures and for the whole flow period (i.e., t = 0 to 12 s) (Fig. 9.11). The critical flow thickness of segregation ($h_{critical}$) may be approximated as follows (Eq. (9.7))

$$h_{critical} \cong \frac{V_{max}}{\dot{\gamma}_{max}} \tag{9.7}$$

where V_{max} is the maximum velocity and $\dot{\gamma}_{max}$ is the corresponding maximum shear strain rate magnitude for each time step.

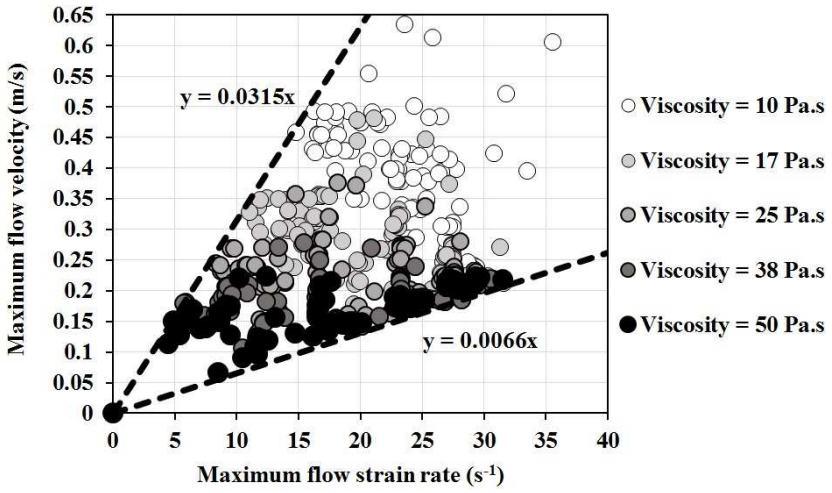

Figure 9. 11 Maximum flow velocity versus maximum flow strain rate

As can be observed in Fig. 9.11, the critical flow thickness of segregation values ($h_{critical}$) are ranging between 0.0066 and 0.0315 m. This means that particles settle down mostly in a vertical layer located in approximately 0.03-m thickness from the bottom of the channel. It proves that the dimensions for the vertical sampling layers, presented in Fig. 9.2b, were properly selected. Therefore, vertical dynamic segregation of the investigated mixtures are evaluated in three vertical layers of top, middle, and bottom, where the thickness of both bottom and middle layers is 3 cm and the remaining (Z > 6 cm) corresponds to the top layer. Moreover, as can be observed in Fig. 9.11, the darker data points corresponding to the higher suspending fluid viscosity are more collected close the minimum estimated boundary (i.e., $h_{critical}$ = 0.0066 m). On the other

hand, data points representing the lower viscosity (brighter data points) tend to the maximum boundary of $h_{critical}$ = 0.0315 m. Therefore, higher vertical dynamic segregation is expected for suspensions with lower suspending fluid viscosity values.

The vertical dynamic segregation index in flow cycle i (i.e., V.D.S.I. (i)) can be defined as the ratio of the difference between the particle content at the top and bottom layers obtained in flow cycle i to the initial particle content as follows:

$$V.D.S.I.(i)\ (\%) = \frac{Particle\ content\ @\ bottom\ layer(i) - Particle\ content\ @\ top\ layer(i)}{Initial\ mean\ particle\ content} \times 100\% \quad (9.8)$$

The V.D.S.I. values obtained for different flow cycles are presented in Fig. 9.12 for the investigated mixtures. As can be observed, in the first flow cycle, the mixtures with lower suspending fluid viscosity of 10, 17, and 25 Pa.s exhibited negative V.D.S.I. values of -23%, -18%, and -6%, respectively, which means having more particle content in the top layer than the bottom one (i.e., inverse vertical dynamic segregation). This can be due to the fact that in the case of lower viscosity, the effect of inertia and initial flow energy on flow displacements of the particles are more dominant than drag capacity of the suspending fluid. On the other hand, as was observed earlier in Fig. 9.4a, considering the higher flow profile angles of less viscous suspensions in the first flow cycle, particles tend to move more toward the top layer rather than the bottom one. However, after dissipation of the initial flow energy (Figs. 9.4b and 9.7), increasing the number of flow cycles resulted in increasing vertical dynamic segregation indices for lower viscosity values. For example, increasing the number of flow cycles from 2 to 6 increases the V.D.S.I values by 22%, 27%, and 16% for viscosity values of 10, 17, and 25 Pa.s, respectively.

However, in the case of suspending fluid having higher relatively viscosity values (i.e., 38 and 50 Pa.s), the mixtures did not show a significant vertical dynamic segregation after several flow cycles. For example, the V.D.S.I. values between -5% to +5% and -2% to +2% were obtained for suspending fluid viscosity values of 38 and 50 Pa.s, respectively and, therefore, these mixtures can be considered as dynamically stable mixtures in vertical direction.

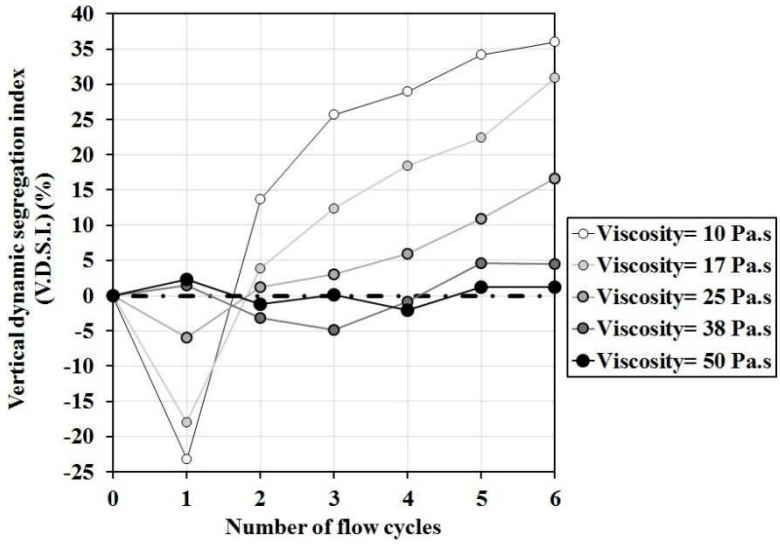

Figure 9. 12 Vertical dynamic segregation index (V.D.S.I.) versus the number of flow cycles

As presented in Fig. 9.13, the final values of vertical dynamic segregation index after 6 flow cycles (i.e., $V.D.S.I._{final}$) are correlated to the plastic viscosity of the suspending fluids. As can be observed, increasing the plastic viscosity of the suspending fluid from 10 to 50 Pa.s can result in decreasing the vertical dynamic segregation indices after 6 flow cycles (i.e., $V.D.S.I._{final}$) by 35%, with a high R^2 of 0.96. This can be due to increasing effect of suspending fluid viscosity on drag forces exerted on the particles, which can lead to decrease the particle settlements towards the bottom layer.

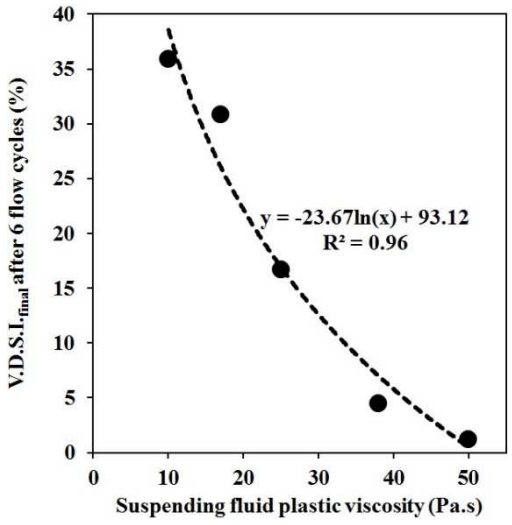

Figure 9. 13 Vertical dynamic segregation index after 6 flow cycles ($V.D.S.I._{final}$) versus plastic viscosity of suspending fluid

9.5.5 Comparison between horizontal and dynamic segregation indices (H.D.SI. vs V.D.S.I)

In order to assess the ability of T-Box test to evaluate dynamic stability of SCC in different directions, the horizontal and vertical dynamic segregation indices after 6 flow cycles are compared for all the investigated suspensions. As can be observed in Fig. 9.14, under 6 flow cycles of T-Box test, the investigated mixtures showed higher dynamic segregation in the horizontal direction (68% < H.D.S.I.$_{final}$ < 101%) than the vertical one (1% < V.D.S.I.$_{final}$ < 36%). Therefore, this set-up can be recommended for horizontal applications, such as these of casting long wall, beam, and slab elements, where the horizontal displacement is higher than the vertical one.

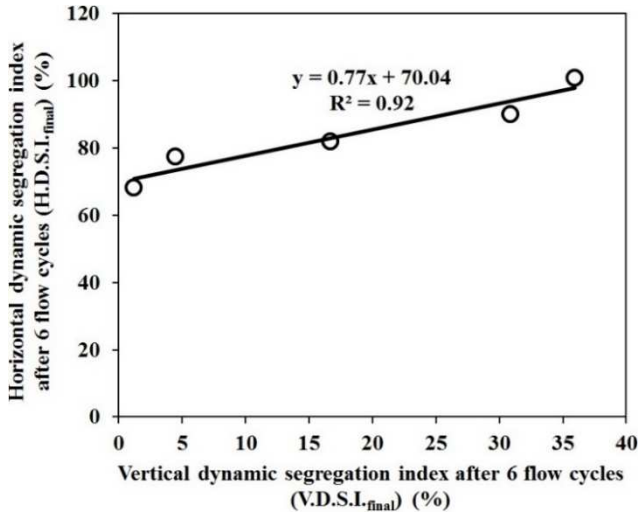

Figure 9. 14 H.D.S.I.$_{final}$ versus V.D.S.I.$_{final}$

9.5.6 Effect of yield stress of suspending fluid on flow performance of suspensions in T-Box set-up

According to the results of the previous sections, the maximum flowability and dynamic segregation in both horizontal and vertical directions were obtained for the suspending fluid with the lowest viscosity (10 Pa.s) investigated in this study. In this section, the effect of three different yield stress values of suspending fluid (i.e., 14, 45, and 75 Pa) on flow performance of

suspensions under 6 flow cycles (i.e., 12-s flow time) is studied only for the mixtures with suspending fluid having a plastic viscosity of 10 Pa.s. The results of these simulations are summarized in Table 9.1.

Table 9. 1 Flowability properties and dynamic segregation for different yield stress values of the suspending fluid with constant viscosity of 10 Pa.s (μ_p is the plastic viscosity and τ_0 is the yield stress of the suspending fluid)

Rheological properties of suspending fluid		Flowability properties				Dynamic segregation		
		Maximum flow displacement (m)	Maximum flow velocity (m/s)	Maximum flow mass averaged kinetic energy (J/kg)	Maximum flow strain rate (s^{-1})	Horizontal direction		Vertical direction
μ_p (Pa.s)	τ_0 (Pa)					Maximum COV (%) (Eq. (10.3))	Maximum H.D.S.I. (%) (Eq. (10.5))	Maximum V.D.S.I. (%) (Eq. (10.8))
10	14	0.554	0.794	0.0546	55.6	67	113	46
	45	0.482	0.708	0.0462	42.6	59	108	45
	75	0.460	0.634	0.0396	35.6	52	101	36

As can be observed in Table 9.1, for a given viscosity of the suspending fluid (10 Pa.s), increasing the yield stress of the suspending fluid can decrease both flowability and dynamic segregation of suspensions in both horizontal and vertical directions. For example, in the case of flowability properties, increasing the yield stress of the suspending fluid from 14 to 75 Pa can lead to 17%, 20%, 27%, and 36% decrease in the maximum magnitudes of flow displacement, velocity, mass-averaged kinetic energy, and strain rate of the suspensions, respectively. However, by comparing to those flowability results presented in section 9.5.1, it can be concluded that the yield stress of suspending fluid showed less effect on flowability of suspension in T-Box test set-up than plastic viscosity. Increasing the suspending fluid plastic viscosity can decrease flow velocity and mass-averaged kinetic energy magnitudes by 65% and 76%, respectively which are almost three times higher than those obtained due to the increase the yield stress (i.e., 20% and 27%).

On the other hand, according to the results of the numerical simulations presented in Table 9.1, increasing the yield stress of suspending fluid from 14 to 75 Pa is showed to reduce the maximum COV, H.D.S.I., and V.D.S.I. values after 6 flow cycles by 15%, 12%, and 10% respectively. However, comparing to the results presented in the sections 9.5.2 and 9.5.4, it can

be concluded that the plastic viscosity of suspending fluid has more significant effect on dynamic segregation of the investigated suspensions in T-Box test than the yield stress. Indeed, increasing the suspending fluid plastic viscosity resulted in higher reduction in the maximum values of COV, H.D.S.I., and V.D.S.I. by 19%, 33%, and 35% values, respectively, compared to those obtained by the increase in yield stress (i.e., 15%, 12%, and 10% reduction, respectively). This can be due to the fact that flow characteristics of suspensions were recorded when the flowing mixture is under shear stress, which has already overcame the yield stress. Therefore, these properties are more influenced by the plastic viscosity than yield stress.

9.5.7 Proposed approach to evaluate "Performability" of suspensions

"Non-restricted dynamic performability" can be defined as the ability of SCC to flow under its own weight through every corner of the formwork while maintaining homogeneity (i.e., uniform suspension of coarse particles), regardless of the presence of reinforcement bars. Therefore, performability is a trade-off between flowability and dynamic stability of SCC [24]. Accordingly, the maximum values of simulated dynamic segregation index in both horizontal and vertical directions after 6 flow cycles in T-Box test are correlated to the maximum flow velocity and mass-averaged kinetic energy magnitudes obtained in the T-Box test (Fig. 9.15).

As can be observed in Fig. 9.15, the investigated suspensions exhibited the maximum values of flow velocity, mass-averaged kinetic energy, and H.D.S.I. and V.D.S.I. indices ranging from 0.224 to 0.794 m/s, 0.0095 to 0.0546 J/kg, 68% to 113%, and 1% to 46%, respectively. It is worthy to mention that the maximum dynamic segregation indices (H.D.S.I. and V.D.S.I. after 6 flow cycles) are well correlated to flowability measurements (i.e., maximum flow velocity and kinetic energy) having correlation coefficients (R^2) higher than 0.96. As can also be observed, increasing flowability of the suspension can reduce its dynamic stability. For example, increasing the maximum flow velocity and mass-averaged kinetic energy obtained for the investigated mixtures by 254% and 475%, respectively, resulted in increasing the maximum values of horizontal and vertical dynamic segregation indices (obtained after 6 flow cycles), by almost 45% (i.e., increasing H.D.S.I and V.D.S.I. indices from 68% and 1% to 113% and 46%, respectively).

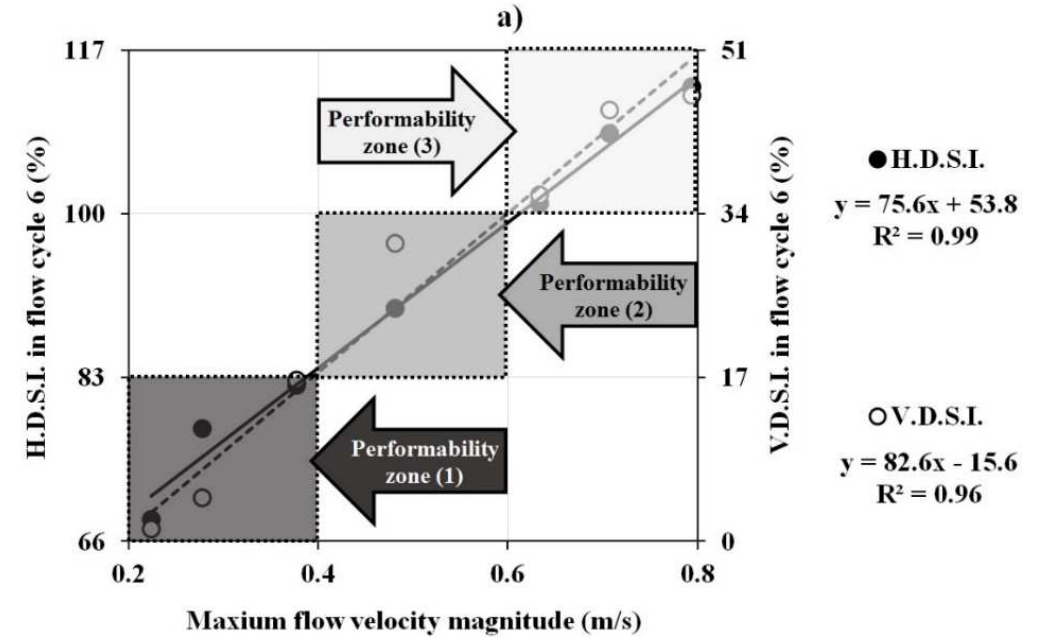

a) H.D.S.I. and V.D.S.I. values after 6 flow cycles versus maximum flow velocity.

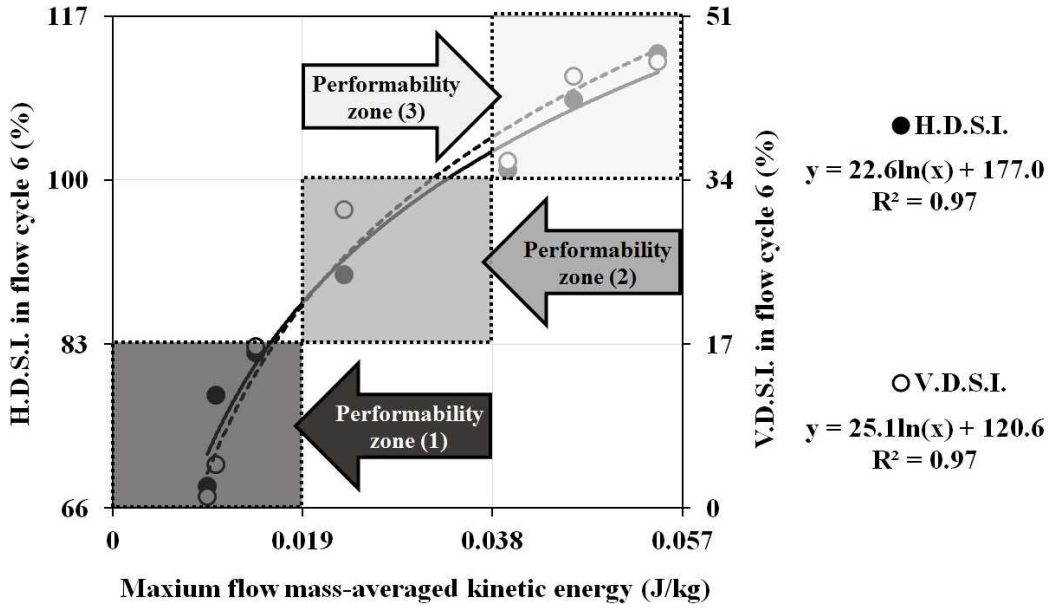

b) H.D.S.I. and V.D.S.I. values after 6 flow cycles versus maximum flow mass-averaged kinetic energy.

Figure 9. 15 Classification of modelled suspensions based on "performability" properties: the maximum dynamic stability indices in both horizontal and vertical directions versus the maximum magnitudes of a) flow velocity and b) mass-averaged kinetic energy

According to the results presented in Fig. 9.15, three different zones of performability can be defined. This classification corresponds to the three H.D.S.I. ranges of 66%-83%, 83%-100%, and 100%-117% and V.D.S.I ranges of 0%-17%, 17%-34%, and 34%-51%. These values are obtained after 6 flow cycles. The trade-off between flowability and dynamic stability properties can be observed in these three performability zones, as follows:

Performability zone 1: This zone corresponds to the suspensions which showed a low level of flowability (i.e., the ranges of maximum velocity and mass-averaged kinetic energy of 0.2 to 0.4 m/s, and 0 to 0.019 J/kg, respectively), but a high level of dynamic stability (maximum H.D.S.I. and V.D.S.I indices in the ranges of 66% to 83% and 0% to 17%, respectively). The suspensions of this zone included the mixtures with suspending fluid with a yield stress of 75 Pa, and plastic viscosity values of 25 to 50 Pa.s. This value of yield stress can be corresponded to a slump flow of 600 mm.

Performability zone 2: This zone consists of the suspensions which showed a medium level of flowability (i.e., maximum velocity and mass-averaged kinetic energy of 0.4 to 0.6 m/s, and 0.019 to 0.038 J/kg, respectively). In this zone, the mixtures also exhibited a medium level of dynamic stability (maximum H.D.S.I. and V.D.S.I indices in the ranges of 83% to 100% and 17% to 34%, respectively). The only suspension appeared in this zone included the mixture with suspending fluid having a yield stress and plastic viscosity values of 75 Pa and 17 Pa.s, respectively.

Performability zone 3: This zone includes the suspensions which showed a high level of flowability (i.e., maximum velocity and mass-averaged kinetic energy of 0.6 to 0.8 m/s, and 0.038 to 0.057 J/kg, respectively), but a low level of dynamic stability having the maximum H.D.S.I. and V.D.S.I indices in the ranges of 100% to 117% and 34% to 51%, respectively. The suspensions which are included in this zone correspond to the suspending fluids with a plastic viscosity of 10 Pa.s and yield stress values of 14 to 75 Pa.

Using the performability classification, the proper combination of rheological properties can be chosen. This depends on the required levels of flowability and dynamic stability given the

applications on hand, considering the fact that there is always a trade-off between these two key flow performance properties of SCC [24].

9.6 Conclusions

In this paper, a CFD software was used to evaluate the effect of rheological properties on non-restricted flowability and dynamic stability of SCC using a T-Box test set-up. The numerical results are in qualitative agreement with those obtained experimentally by Esmaeilkhanian et al. [36-38]. Various suspending fluids, representing the stable and homogeneous portion of concrete, with plastic viscosity, yield stress, and density values of 10 to 50 Pa.s, 14 to 75 Pa, and 2500 kg/m^3, respectively, were investigated. The modelled suspensions consisted of 178 spherical particles in total, with 20-mm diameter (i.e., 4.7% volumetric content) and the same density as the suspending fluid has. Dynamic stability of the suspensions in the T-Box test were evaluated using calculated particle contents of five different horizontal sections and three different vertical sampling layers for different flow cycles. The main concluding remarks are as follows:

- Increasing plastic viscosity of the suspending fluid from 10 to 50 Pa.s can lead to a decrease of the maximum flow displacement, velocity, mass-averaged kinetic energy, and horizontal and vertical dynamic segregation indices by 18%, 65%, 76%, 33%, and 35%, respectively. These reductions are higher than those obtained by increasing the yield stress of the suspending fluid from 14 to 75 Pa (i.e., 17%, 20%, 27%, 12%, and 10%, respectively).

- Increasing the number of flow cycles has more dominant effect on flowability and horizontal dynamic segregation of SCC in the T-Box test set-up for more viscous suspending fluids, while, flow properties of the mixtures with less suspending fluid viscosity are mostly affected by the initial flow energy provided by the first tilting cycle. Indeed, the mixtures with lower viscosity of suspending fluid mostly segregate dynamically in the initial flow cycles (i.e., less flow distance traveled by the suspension),

while for higher viscous suspensions, more flow cycles are required to reach the maximum dynamic segregation capacity.

- Simulations revealed that the particles located in the middle horizontal section and top vertical layer exhibited the maximum displacements. On the other hand, the minimum ranges of displacements were obtained for the particles located in the tilt down horizontal section and bottom vertical layer. No significant effect of the plastic viscosity on the displacements of these particles can be observed. This can be due to the more dominant effect of frictional stresses and lattice effect of segregated particles in these sections compared to the plastic viscosity of suspending fluid.

- Higher dynamic segregation in horizontal direction (H.D.S.I. values ranging from 68% to 101%) was obtained compared to vertical direction (V.D.S.I. values ranging between 1% and 36%) in the T-Box test set-up.

- A new definition and approach were proposed to classify the suspensions based on "non-restricted dynamic performability". This is based on a trade-off between flowability and dynamic stability in both the vertical and horizontal directions. Accordingly, the investigated mixtures were classified in three zones of performability: Zone 1 corresponds to low flowable, but high dynamically stable mixtures. Zone 2 corresponds to medium flowable and medium dynamically stable mixtures. On the other hand, zone 3 consists of high flowable, but low dynamically stable mixtures. This classification can be used as a practical tool to choose a proper combination of rheological parameters of the suspending fluid (mortar or stable and homogeneous portion of concrete mixture) to achieve the required flowability and dynamic stability demands in casting process. The rheology of suspending fluid can be modified by decreasing the water to powder material ratio and/or adding higher content of viscosity modifying agent.

CHAPTER 10 COMPARISON BETWEEN FLOW PERFORMANCE OF SCC IN THE L-BOX AND T-BOX SET-UPS

L-Box and T-Box test set-ups were shown as two main workability tests of SCC which can indicate flowability, and dynamic stability of the investigated mixtures in both horizontal and vertical directions. Moreover, the effect of rheological parameters on flow performance of SCC in these set-ups were evaluated in the Chapters 7-9. These effects are compared in this section to have better understanding of heterogeneous behavior of SCC in restricted and non-restricted areas, as a function of rheological parameters.

It must be noted that effect of five values of plastic viscosity of suspending fluid (ranging from 10 to 50 Pa.s) are presented for a suspending fluid having a high yield stress value of 75 Pa. On the other hand, the effect of three values of yield stress of suspending fluid (ranging from 14 to 75 Pa) are presented for a low suspending fluid viscosity of 10 Pa.s.

10.1 Comparison between flowability of SCC in the L-Box and T-Box set-ups

As can be observed in Figs. 10.1-10.3, increasing both plastic viscosity and yield stress can decrease the flowability of the SCC suspensions in both L-Box and T-box set-ups, as follow:

10.1.1 Flow velocity

As can be observed in Fig. 10.1, increasing both plastic viscosity and yield stress of the suspending fluid can decrease the maximum flow velocity of SCC in both L-Box and T-Box set-ups. However, the T-Box set-up exhibited higher magnitudes of flow velocity than the L-Box test. On the other hand, increasing these rheological parameters, showed higher effect on

flow velocity of SCC in the T-Box set-up. For example, for a given suspending fluid yield stress of 75 Pa, increasing plastic viscosity of the suspending fluid from 10 to 50 Pa.s, can decrease the flow velocity from 0.565 to 0.212 m/s (i.e. 62% reduction) and from 0.634 to 0.224 m/s (i.e., 65% reduction) in the L-Box and T-Box set-ups, respectively. Therefore, the flow velocity magnitudes in the T-Box test are 5% to 11% higher than those obtained in L-Box set-up and more influenced (i.e., 65% vs 62% reduction) by increasing in plastic viscosity of the suspending fluid.

On the other hand, for a given suspending fluid plastic viscosity of 10 Pa.s, increasing yield stress of the suspending fluid from 14 to 75 Pa.s, can decrease the flow velocity from 0.6 to 0.565 m/s (i.e. 6% reduction) and from 0.794 to 0.634 m/s (i.e., 20% reduction) in the L-Box and T-Box set-ups, respectively. Therefore, the flow velocity magnitudes in the T-Box test are 11% to 24% higher than those obtained in L-Box set-up and more influenced (i.e., 20% vs 6% reduction) by increasing in yield stress of the suspending fluid.

Moreover, in both of the L-Box and T-Box set-ups, effect of plastic viscosity of suspending fluid on flow velocity of SCC mixture is more dominant than yield stress (i.e., 62% vs 6%, and 65% vs 20% reductions for L-Box and T-Box tests, respectively).

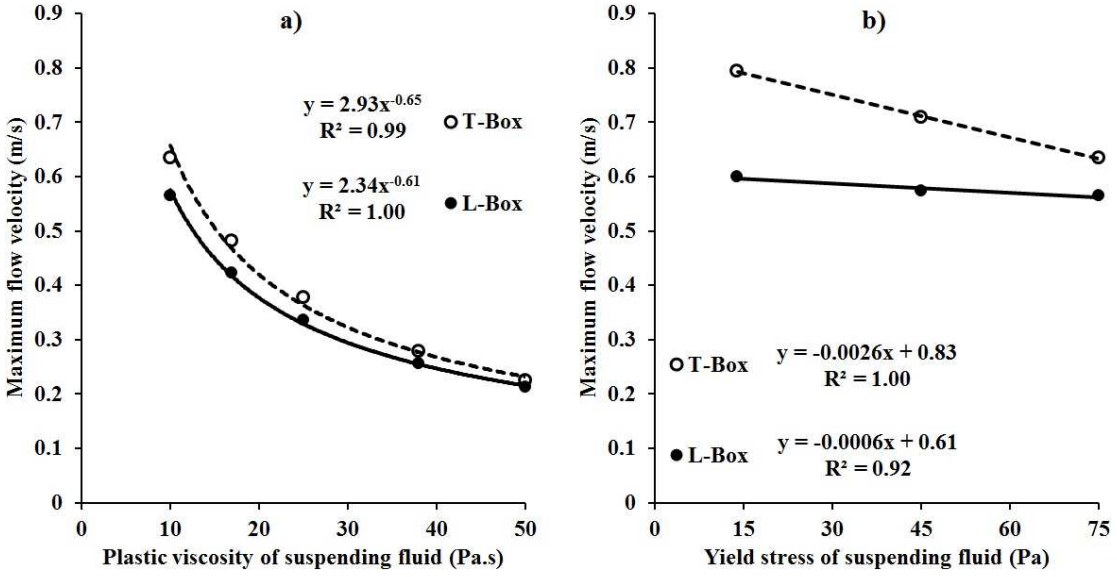

Figure 10. 1 Maximum flow velocity versus a) plastic viscosity (where τ_0 = 75 Pa), and b) yield stress (where μ_p = 10 Pa.s) of suspending fluid in L-Box and T-Box test set-ups

10.1.2 Flow strain rate

As can be observed in Fig. 10.2, increasing both plastic viscosity and yield stress of the suspending fluid resulted in decrease in the maximum flow strain rate of SCC in both L-Box and T-Box set-ups. However, the L-Box test showed higher strain rate magnitudes and more influenced by rheological parameters of suspending fluid, compared to the T-Box set-up. For example, for a given suspending fluid yield stress of 75 Pa, increasing plastic viscosity of the suspending fluid from 10 to 50 Pa.s, can decrease the maximum flow strain rate from 88.1 to 33.7 s^{-1} (i.e. 62% reduction) and from 35.6 to 31.5 s^{-1} (i.e., 12% reduction) in the L-Box and T-Box set-ups, respectively. Therefore, the flow strain rate magnitudes in the L-Box test are 7% to 60% higher than those obtained in T-Box set-up and more influenced (i.e., 62% vs 12% reduction) by increasing in plastic viscosity of the suspending fluid compared to the T-Box test.

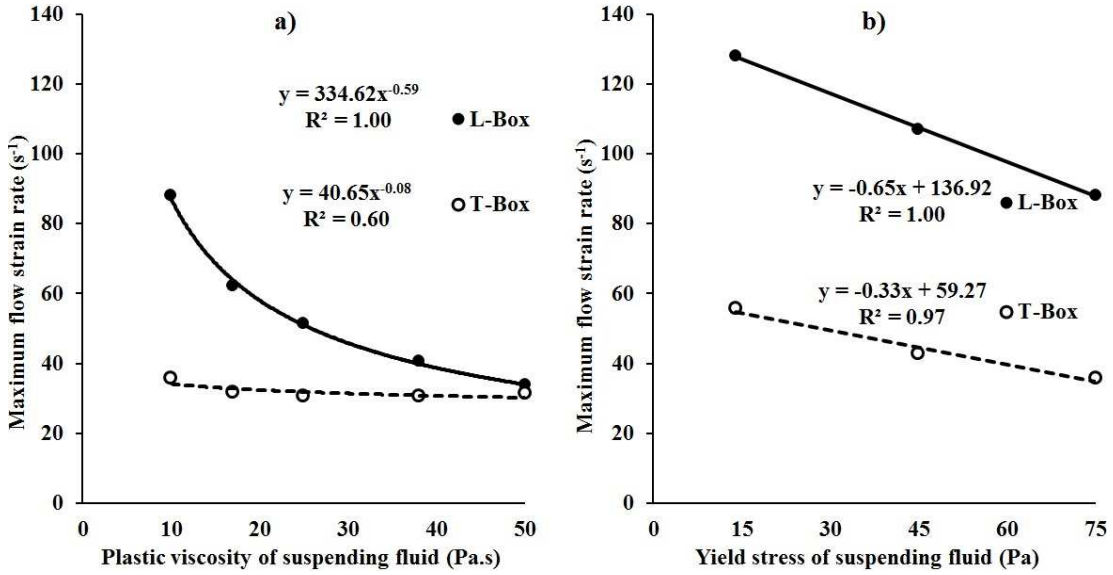

Figure 10. 2 Maximum flow strain rate versus a) plastic viscosity (where τ_0 = 75 Pa), and b) yield stress (where μ_p = 10 Pa.s) of suspending fluid in L-Box and T-Box test set-ups

On the other hand, for a given suspending fluid plastic viscosity of 10 Pa.s, increasing yield stress of the suspending fluid from 14 to 75 Pa.s, can decrease the flow strain rate from 128 to 88.1 s^{-1} (i.e. 31% reduction) and from 55.6 to 35.6 s^{-1} (i.e., 36% reduction) in the L-Box and T-Box set-ups, respectively. Therefore, L-Box test showed 57% to 60% higher flow velocity magnitudes than those obtained in T-Box set-ups. It is worthy to mention that the yield stress

showed slightly higher effect on flow strain rate in T-Box test, compared to the L-Box set-up (i.e., 36% vs 31%). On the other hand, plastic viscosity showed higher effect on strain rate of SCC in the L-box set-up, than the yield stress (62% vs 31% reduction), while yield stress plays dominant role on strain rate of SCC in the T-Box set-up, compared to the plastic viscosity (i.e., 36% vs 12% reduction).

10.1.3 Flow energy

As can be observed in Fig. 10.3, increasing both plastic viscosity and yield stress of the suspending fluid can decrease the maximum flow mass-averaged kinetic energy in both L-Box and T-Box set-ups. However, higher magnitudes were obtained in L-Box test than the T-Box set-up. Also, higher effect of the increment in the rheological parameters of suspending fluid was observed in L-Box test. For example, for a given suspending fluid yield stress of 75 Pa, increasing plastic viscosity of the suspending fluid from 10 to 50 Pa.s, can decrease the flow mass-averaged kinetic energy from 0.0482 to 0.0071 J/kg (i.e. 85% reduction) and from 0.0396 to 0.0095 J/kg (i.e., 76% reduction) in the L-Box and T-Box set-ups, respectively. Therefore, the flow mass-averaged kinetic energy magnitudes in the L-Box test are up to 18% higher than those obtained in T-Box set-up, and slightly more influenced (i.e., 85% vs 76% reduction) by increasing in plastic viscosity of the suspending fluid.

On the other hand, for a given suspending fluid plastic viscosity of 10 Pa.s, increasing yield stress of the suspending fluid from 14 to 75 Pa.s, can decrease the flow mass-averaged kinetic energy from 0.0562 to 0.0482 J/kg (i.e. 14% reduction) and from 0.0546 to 0.0396 m/s (i.e., 27% reduction) in the L-Box and T-Box set-ups, respectively. Therefore, the flow mass-averaged kinetic energy magnitudes in the L-Box test are 3% to 18% higher than those obtained in T-Box set-up. However, mass-averaged kinetic energy in T-Box test were found to be more influenced (i.e., 27% vs 14% reduction) by increasing in yield stress of the suspending fluid than L-Box set-up.

As can be observed in Fig. 10.3, in both of the set-ups, effect of plastic viscosity of suspending fluid on mass-averaged kinetic energy of SCC is more dominant than yield stress (i.e., 85% vs 14%, and 76% vs 27% reductions for L-Box and T-Box tests, respectively).

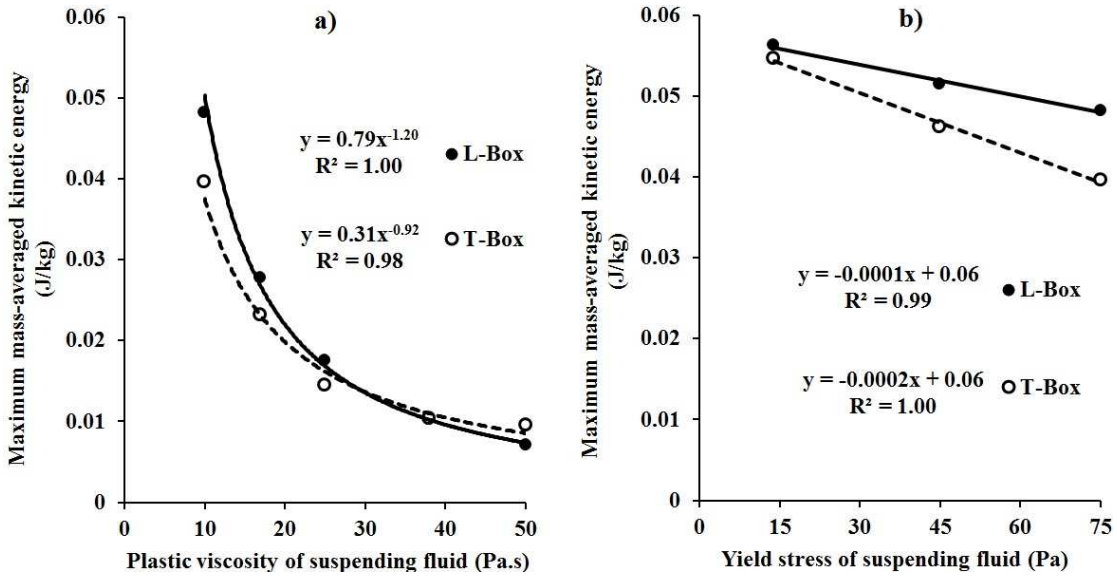

Figure 10. 3 Maximum mass-averaged kinetic energy magnitudes versus a) plastic viscosity (where τ_0 = 75 Pa), and b) yield stress (where μ_p = 10 Pa.s) of suspending fluid in L-Box and T-Box test set-ups

10.2 Comparison between dynamic stability of SCC in L-Box and T-Box set-ups

10.2.1 Horizontal dynamic segregation

In this section, horizontal and vertical dynamic segregation indices obtained in L-Box and T-Box set-ups are compared. As can be observed in Fig. 10.4, increasing both plastic viscosity and yield stress increase horizontal dynamic segregation index (H.D.S.I.) in L-Box test, while this resulted in decrease in H.D.S.I. values in T-Box set-up. Therefore, it can be concluded that rheological parameters of suspending fluid show opposite effects on dynamic segregation pattern in the horizontal direction, in presence and absence of reinforcing bars obstacles (i.e., restricted and non-restricted flows). For example, for a given suspending fluid yield stress of 75 Pa, increasing plastic viscosity from 10 to 50 Pa.s can increase H.D.S.I. values obtained in L-

Box test from 121% to 184% (i.e., 63% increase), while this decreases in T-Box set-up from 101% to 68% (i.e., 33% reduction). On the other hand, in a given suspending fluid viscosity of 10 Pa.s, increasing yield stress from 14 to 75 Pa can lead to decrease H.D.S.I. values in T-Box test from 113% to 101% (i.e., 12% reduction), while it increases slightly in L-Box set-up from 115% to 121% (i.e., 6% increase).

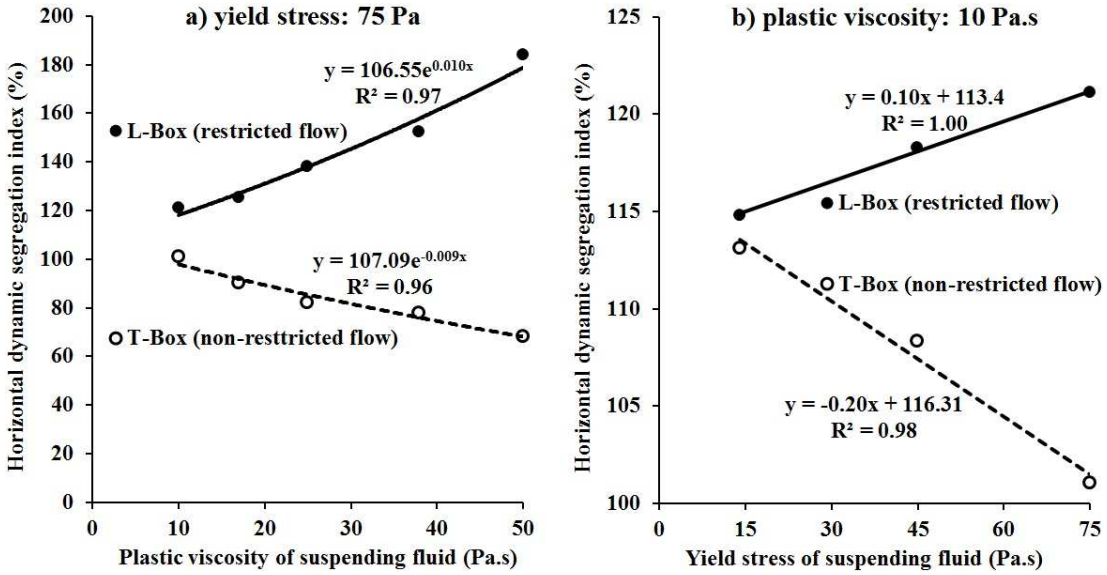

Figure 10. 4 Horizontal dynamic segregation index versus a) plastic viscosity (where τ_0 = 75 Pa), and b) yield stress (where μ_p = 10 Pa.s) of suspending fluid in L-Box and T-Box test set-ups

As can be observed in Fig. 10.4, L-Box set-up exhibited higher values of H.D.S.I. compared to the T-Box test. For example, in a given suspending fluid yield stress of 75 Pa and plastic viscosity values of 10 to 50 Pa.s, H.D.S.I. values in L-Box set-up are 20% (i.e., 121% vs 101%) to 116% (i.e., 184% vs 68%) higher than those obtained in T-Box test. For a given plastic viscosity of 10 Pa.s and yield stress values of 14 to 75 Pa, this difference ranged between 2% (i.e., 115% vs 113%) and 20% (i.e., 121% vs 101%). Therefore, it can also be concluded that plastic viscosity of suspending fluid has more dominant effect on horizontal dynamic segregation in both L-Box and T-Box set-ups, compared to the yield stress.

10.2.2 Ratio of vertical dynamic segregation to horizontal dynamic segregation

In order to compare the ability of these two tests to evaluate dynamic stability of SCC in the vertical and horizontal directions, the ratio of vertical to horizontal dynamic segregation indices are presented for both set-ups in Fig. 10.5.

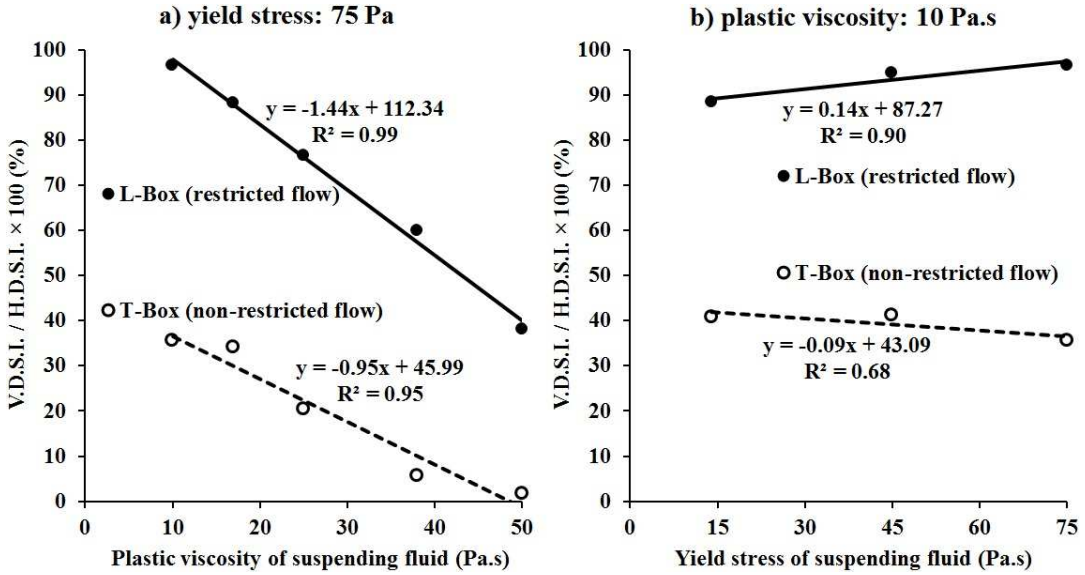

Figure 10. 5 The ratio of vertical dynamic segregation index to horizontal dynamic segregation index versus a) plastic viscosity (where τ_0 = 75 Pa), and b) yield stress (where μ_p = 10 Pa.s) of suspending fluid in L-Box and T-Box test set-ups

As can be observed in Fig. 10.5, both L-Box and T-Box tests exhibit higher dynamic segregation in the horizontal direction than the vertical one (i.e., V.D.S.I./H.D.S.I. < 100%). However, L-Box tests showed higher V.D.S.I./H.D.S.I. ratios than T-Box set-up. For example, for a given suspending fluid yield stress of 75 Pa and plastic viscosity of 10 to 50 Pa.s, values of dynamic segregation index in vertical direction are 38% to 97%, and 2% to 36% smaller than those obtained in the horizontal direction, in L-Box and T-Box set-ups, respectively. Therefore, L-Box test showed 36% to 61% higher V.D.S.I./H.D.S.I. ratios than T-Box test. On the other hand, for a given suspending fluid plastic viscosity of 10 Pa.s and yield stress values of 14 to 75 Pa, these differences are between 47% (i.e., 88% vs 41% for L-Box and T-Box set-ups, respectively) and 61% (i.e., 97% vs 36% for L-Box and T-Box set-ups, respectively). Therefore, it can be concluded that T-Box test is more appropriate to evaluate dynamic stability in horizontal

applications, such as long beam and slab elements, while L-Box test can be recommended for both horizontal and vertical applications, when dynamic stability and passing ability in both directions are interested to be evaluated (e.g., deep beams and slabs, and long wall elements).

CHAPTER 11 SUMMARY AND CONCLUSIONS

This study is mainly dedicated to analyze the flow performance of self-consolidating concrete (SCC) in workability tests and structural sections using analytical and numerical methods. The flow performance of the investigated SCC mixtures were analyzed as homogeneous and heterogeneous materials. The effect of rheological parameters, presence of reinforcing bars, coarse aggregate contents, and bar-particles coupled effect on flowability, passing ability, and dynamic stability properties of SCC were evaluated using a computational fluid dynamics (CFD) software (FLOW3D®). According to the results of each phase of the study, the following conclusions can be drawn.

11.1 Flow analysis of SCC as a homogeneous material

In the first part of the homogeneous analysis phase, the flow performance of SCC was modelled in the L-Box test set-up analytically and numerically considering SCC as a homogeneous single fluid material. In the second part, considering the same single fluid assumption, the flowability and passing ability properties of various SCC mixtures were evaluated during a casting process of a reinforced L-shaped beam. The theoretical predictions were also compared to the experimental results. The main concluding remarks for the homogeneous flow analysis are as follows:

11.1.1 Analytical modelling of flow of SCC in the L-Box test set-up

- A new analytical model is proposed to predict the flow performance of SCC in a modified L-Box set-up based on the Dam Break Theory [193]. The model considered the effect of rheological parameters of the mixtures using Bingham and Herschel-Bulkley models, density of the fresh SCC, and two different initial heights of the concrete in the vertical compartment of the apparatus.

- The proposed analytical model was shown to reproduce successfully the experimental profiles of several SCC mixtures with three different levels of static stability and three different waiting times.

- The Herschel-Bulkley model provided better estimation coefficients than the Bingham model.

- Since the analytical models neglected the effect of frictional and inertial forces, less accuracy was observed at the entrance of the horizontal channel, especially for the higher initial head of concrete.

11.1.2 Numerical modelling of flow of SCC in the L-Box test set-up

- Unlike the analytical models, CFD simulations take into account the effects of friction, inertia, and presence of reinforcing bars.

- Numerical predictions showed better agreement with experimental profiles than those obtained by the proposed analytical model, especially for higher initial head of SCC (corresponding to higher level of gravitational forces).

- According to the numerical results of flowability of SCC in L-Box set-up, a critical flow depth has been calculated. This corresponds to the zone with the highest risk of deformation, dynamic segregation, and blocking.

- The longer waiting times showed negative effects on the accuracy of the theoretical models reflected by the disturbed homogeneity of the mixtures. This can result in less precise approximation of the rheological parameters, especially for the yield stress values.

11.1.3 Numerical modelling of SCC casting of a full-scale reinforced L-shaped beam

- The results of numerical simulations of free surface flow profiles of SCC during casting in presence of longitudinal and vertical reinforcing bars along the horizontal channel of the beam were shown to have very good agreements ($R^2 > 0.96$) with experimental results.

- Effect of plastic viscosity of the concrete mixtures on free surface profile shapes, flow velocity, strain rate, and mass-average kinetic energy of SCC during beam casting process were evaluated successfully using CFD simulations. The results showed that for a given yield stress value, increasing the plastic viscosity results in decreasing the flowability of SCC in horizontal and vertical directions.

- Using the calculated values of flow velocity and shear rates, the critical thickness of segregation is estimated above the bottom row of horizontal bars in the reinforced cage. This critical depth indicates the zone of the highest potential of dynamic segregation. The flow performance of SCC in this zone is decisive to confirm the formwork filling quality demands.

- The numerical results exhibited lower flow velocity loss in the V-shaped sections in vertical direction compared to the simple rectangular sections. This result can be useful to better design the formworks and shapes of the structural sections, regarding workability and form filling ability aspects. Accordingly, the design of the current beam resulted in generating comparable flow rate magnitudes to those encountered in SCC pumping operations.

11.2 Flow analysis of SCC as a heterogeneous material

In the second phase of this study, the flow characteristic of SCC were evaluated as a heterogeneous suspension of coarse particles and a non-Newtonian suspending fluid. Shear-induced and gravitational dynamic segregation and blocking of the investigated suspensions were evaluated by comparing the particle contents in different horizontal and vertical sampling sections. The numerical simulations were carried out to simulate flow performance of SCC in the L-Box and T-Box test set-ups. These two workability tests can evaluate flowability, passing ability, and dynamic stability properties of SCC in presence, and in absence of reinforcing bar obstacles and in both horizontal and vertical directions. The main concluding remarks of the heterogeneous analysis phase can be summarized as follows:

11.2.1 Numerical simulation of heterogeneous flow of SCC in the L-Box test

1- Effect of rheological parameters of the suspending fluid:

CFD simulations can qualitatively predict the effect of rheological parameters and density of the suspending fluid on flow performance of SCC in L-Box set-up. The following conclusions can be pointed out:

- The numerical results showed that increasing plastic viscosity and yield stress can decrease the flowability, passing ability, and dynamic stability of the concrete suspension in the horizontal direction. However, this can increase the dynamic stability of SCC in the vertical direction.

- The plastic viscosity of the suspending fluid is shown to play the dominant role on heterogeneous properties of SCC during flow.

- According to the numerical simulations, the suspension with higher plastic viscosity of suspending fluid are more recommended for vertical applications, such as tall wall and

column elements. On the other hand, the lower viscosity SCC mixtures are found to be more appropriate for horizontal applications (e.g., long beam and slab elements).

- Increasing shear elasticity modulus of the suspending fluid resulted in decreasing flowability and vertical dynamic segregation of SCC. However, this results in increasing the risk of blocking.

- According to the numerical simulations, lower density of the suspending fluid compared to the coarse aggregates resulted in lower flowability and dynamic segregation in the horizontal direction. This results in more self-consolidating behavior than self-levelling properties.

- Suspending fluid density showed more dominant effect on gravitational induced dynamic segregation than plastic viscosity. Accordingly, less density of the suspending fluid can increase the vertical dynamic segregation.

- A new approach is proposed to classify the investigated SCC mixtures based on the filling ability. This consists a combination of flowability and passing ability properties. Accordingly, three levels of filling ability corresponding to low, medium, and high were defined. These levels correspond to the three $B.I._{max}$ (i.e., maximum blocking index) ranges of 100%-130% (high passing ability), 130%-160% (medium passing ability), and 160%-190% (low passing ability), respectively. As one of the main steps of the workability design procedure, the results of this classification can be used as a practical tool to optimize the rheology and mixture proportioning of SCC, with respect to the formwork filling ability properties in the reinforced areas of the formwork.

2- Coupled effect of reinforcing bars and coarse aggregate contents:

- According to the numerical results, a new approach is proposed to evaluate the bar-particles coupled effect on the horizontal dynamic stability and risk of blocking in three different interaction zones. These zones indicate parallel and opposite interactions

between bars and particles which affect the flow performance of the investigated suspensions.

- Increasing both the particle content of the concrete suspension and the number of bars in the L-Box horizontal section resulted in higher risk of blocking and dynamic segregation in the horizontal direction. Unlikely, this results in decreasing the vertical dynamic segregation. On the other hand, increasing the particle content can lead to an increase in the overall viscosity and yield stress values of the suspension. This can improve the dynamic stability of the mixture in the horizontal direction.

- The highest bar effect was observed in the middle of the horizontal channel, where the maximum horizontal dynamic segregation has also been obtained. Moreover, in the case of the highest number of obstacles and the maximum coarse aggregate content, the effect of particle contents and configurations of bars on passing ability and dynamic segregation of SCC are shown to be dominant in the middle horizontal sections.

- According to the numerical simulations, flow performance properties of SCC in the extreme sections located beneath the casting point and at the end of the formwork are found to depend mostly on the casting flow rate and length of formwork, respectively.

11.2.2 Numerical simulation of heterogeneous flow of SCC in the T-Box test

The results of the numerical simulation of flow of SCC in the T-Box set-up are found in qualitative agreement with those obtained experimentally by Esmaeilkhanian et al. [36-38]. According to the numerical results, the following conclusions can be drawn:

- Increasing both plastic viscosity and yield stress values of the suspending fluid can decrease flowability and dynamic segregation of SCC in both horizontal and vertical directions. However, the plastic viscosity showed more dominant effect than the yield stress.

- The heterogeneous characteristics of SCC flow in T-Box test for low and high viscosity suspensions were shown to be more affected by the initial flow energy provided by the initial flow cycles and higher numbers of flow cycles, respectively.

- Dynamic segregation of SCC in the T-Box test was found to be higher in the horizontal direction compared to the vertical one. Therefore, the T-Box test is more recommended for horizontal applications, such as casting of beam, long wall, and slab elements.

- A new definition and approach were proposed to classify the suspensions based on "non-restricted dynamic performability" as a result of the trade-off between flowability and dynamic stability properties in both the vertical and horizontal directions. Accordingly, the SCC suspensions were classified in three different zones of performability: zone 1 (low flowable, high dynamically stable), zone 2 (medium flowable, medium dynamically stable), and zone 3 (high flowable, low dynamically stable). This classification can be used as a practical tool in workability design procedure, in order to optimize the mixture proportioning, workability, and rheology, regarding flowability and dynamic stability aspects.

11.2.3 Comparison between flow performance of SCC in L-Box and T-Box set-ups

- The results of simulations showed that increasing both yield stress and plastic viscosity values of suspending fluid decrease flowability of SCC in both L-Box and T-Box set-ups. On the other hand, SCC mixtures exhibit higher flow velocity magnitudes in T-Box set-up, while higher values of strain rate and flow kinetic energy were obtained in the L-Box test.

- Plastic viscosity of suspending fluid showed more dominant effect on flow characteristics of SCC in both tests compared to the yield stress values.

- Rheological parameters showed opposite effects on dynamic stability of SCC in T-Box and L-Box set-ups. Indeed, increasing plastic viscosity of suspending fluid results in higher dynamic segregation in the L-Box set-up, while this decreased in the T-Box test.

- Numerical simulations showed that higher values of dynamic segregation in both vertical and horizontal directions were obtained in L-Box set-up compared to the T-Box test.

- Higher ratios of vertical to horizontal dynamic segregation indices were obtained in L-Box set-up compared to the T-Box test. Therefore, it can be concluded that T-Box test is more appropriate to evaluate dynamic stability in horizontal applications, such as long beam and slab elements, while L-Box test can be recommended for both horizontal and vertical applications, when dynamic stability and passing ability in both directions are of interest (e.g., deep beams and slabs, and long wall elements).

11.3 CONCLUSIONS (EN FRANÇAIS)

Cette étude se base principalement sur l'analyse des performances d'écoulement du béton autoplaçant (BAP) dans les essais de maniabilité et sur les sections structurales en utilisant des méthodes analytiques et numériques. La performance d'écoulement des mélanges du BAP étudiés ont été analysés en tant que matériaux homogènes et hétérogènes. L'effet des paramètres rhéologiques, présence de barres d'armature, des contenus des gros granulats, et l'effet couplé de deux derniers, la capacité de passage, et les propriétés de stabilité dynamique du BAP ont été évalués à l'aide d'un logiciel de mécanique des fluides numérique (MFN) nommé FLOW3D®. D'après les résultats de chaque phase de l'étude, les conclusions suivantes peuvent être tirées:

11.3.1 Analyse d'écoulement du BAP comme un matériau homogène

Dans la première partie de la phase d'analyse homogène, la performance d'écoulement du BAP a été modélisée dans l'essai de L-Box, analytiquement et numériquement considérant le BAP comme un fluide unique et homogène. Dans la deuxième partie, compte tenu de la même hypothèse du fluide unique, la fluidité et la capacité de passage des différents mélanges de BAP ont été évalués au cours d'un procédé de mise en place d'une poutre renforcée. Les prédictions théoriques ont également été comparés aux résultats expérimentaux. Les conclusions principales finales pour l'analyse d'écoulement homogène sont les suivantes:

1. Modélisation analytique de l'écoulement du BAP dans l'essai de L-Box :

- Un nouveau modèle analytique est proposé pour prédire la performance d'écoulement du BAP dans un L-Box modifié, basé sur la théorie de Dam Break [193]. Le modèle a examiné l'effet des paramètres rhéologiques des mélanges en utilisant des modèles de Bingham et Herschel-Bulkley, masse volumique du BAP à l'état frais, en considèrent deux hauteurs initiales différentes du béton dans le compartiment vertical du dispositif.

- Le modèle analytique proposé a reproduit avec succès les profils expérimentaux de plusieurs mélanges du BAP avec trois niveaux différents de stabilité statique et trois temps d'attente différents.

- Le modèle de Herschel-Bulkley fournit des meilleurs coefficients d'estimation que le modèle Bingham.

- Étant donné que les modèles analytiques négligent l'effet de friction et d'inertie, moins de précision a été obtenue au niveau de l'entrée du canal horizontal, en particulier pour la hauteur initiale du béton plus élevée.

2. La modélisation numérique de l'écoulement du BAP dans l'essai de L-Box :

- Contrairement aux modèles analytiques, simulations MFN considèrent les effets de la friction, l'inertie, et la présence de barres d'armature.

- Prédictions numériques ont montré un meilleur accord avec les profils expérimentaux que ceux obtenus par le modèle analytique proposé, en particulier pour la hauteur initiale du BAP plus élevée (correspondant à un niveau supérieur de gravité).

- Selon les résultats numériques de fluidité du BAP dans le dispositif de L-Box, une profondeur d'écoulement critique a été calculée, cela correspond à la zone avec le risque le plus élevé de déformation, la ségrégation dynamique, et le blocage.

- Les temps d'attente plus longs ont montré des effets négatifs sur la précision des modèles théoriques à cause de l'homogénéité perturbée des mélanges. Cela peut affecter la précision des valeurs des paramètres rhéologiques mesurés initialement, en particulier pour les valeurs de seuils de cisaillement.

3. Modélisation numérique de la mise en place du BAP dans une poutre renforcée :

- Les résultats des simulations numériques des profils de surface libre d'écoulement du BAP en présence de barres d'armature longitudinale, et verticale, dans le canal horizontal du poutre sont en accord avec des résultats expérimentaux (R^2> 0.96).

- L'effet de la viscosité plastique des mélanges de béton sur des formes de profil de surface libre, la vitesse d'écoulement, la taux de déformation, et l'énergie cinétique du BAP pendant du processus de la mise en place de la poutre ont été évaluées avec succès en utilisant des simulations MFN. Les résultats ont démontré que, pour une valeur donnée de seuil de cisaillement, augmentation des valeurs de viscosité plastique diminue la fluidité du BAP dans les directions horizontale et verticale.

- En utilisant les valeurs calculées de vitesse d'écoulement et des taux de cisaillement, la profondeur critique de la ségrégation est estimée au-dessus de la rangée inférieure de barres horizontales. Cette profondeur correspond à la zone du potentiel plus élevé de ségrégation dynamique (zone critique). La performance d'écoulement du BAP dans cette zone est décisive afin du valider la qualité de remplissage de coffrage.

- Les résultats numériques ont démontré une perte plus faible de la vitesse d'écoulement dans les sections en forme de V que dans la direction verticale par rapport aux sections rectangulaires simples. Ce résultat peut être utile pour une meilleure conception des coffrages ainsi que pour les formes des sections structurelles, concernant l'ouvrabilité et capacité de remplissage. Par conséquent, la conception de la poutre conduit à la génération des grandeurs des débits comparables à celles rencontrées dans les opérations de pompage du BAP.

11.3.2 Analyse d'écoulement du BAP comme un matériau hétérogène

Dans la deuxième phase de cette étude, les caractéristiques d'écoulement du BAP ont été évaluées comme une suspension hétérogène de grosses particules et un fluide non-Newtonien.

La ségrégation dynamique due par la gravité et cela induit par cisaillement ainsi que le blocage des suspensions étudiées ont été évaluées. Le comparant le contenue des particules dans des différentes sections d'échantillonnage horizontal et vertical a été réalisée. Les simulations numériques ont été réalisées pour simuler les performances d'écoulement du BAP dans les dispositifs des L-Box et T-Box. Ces deux tests de maniabilité peuvent évaluer la fluidité, la capacité de passage, et les propriétés de stabilité dynamique du BAP en présence et en l'absence de renforcement dans les directions horizontale et verticale. Les conclusions principales finales de la phase d'analyse hétérogène peuvent être résumées comme suit:

1. Simulation numérique d'écoulement hétérogène du BAP dans l'essai de L-Box :

1.a) L'effet des paramètres rhéologiques de la partie fluide de suspension

Les simulations MFN peuvent qualitativement prédire l'effet des paramètres rhéologiques et la masse volumique de la partie fluide de suspension sur la performance d'écoulement du BAP dans l'essai de L-Box. Les conclusions suivantes peuvent être tirées:

- Les résultats numériques ont montré que l'augmentation de la viscosité plastique et le seuil de cisaillement peuvent diminuer la fluidité, la capacité de passage, et la stabilité dynamique de la suspension de béton dans la direction horizontale. Cependant, ceci peut augmenter la stabilité dynamique du BAP dans la direction verticale.

- La viscosité plastique du fluide de suspension joue un rôle dominant sur les propriétés hétérogènes du BAP pendant l'écoulement.

- Selon les simulations numériques, la suspension avec la viscosité plastique plus élevée de la partie fluide de la suspension sont plus recommandé pour les applications verticales, par exemple les murs et colonnes et les éléments de grande taille. D'autre part, les mélanges avec la viscosité plastique moins élevée de la partie fluide de la suspension se trouvent être plus approprié pour les applications horizontales (par exemple, les poutres longues et les éléments de dalle).

- L'augmentation du module d'élasticité de cisaillement de la partie fluide de suspension a entraîné la diminution de la ségrégation dynamique verticale du BAP. Cependant, cela se traduit par l'augmentation du risque de blocage.

- Selon les simulations numériques, une masse volumique plus faible du fluide de suspension par rapport aux gros granulats diminue le fluidité et la ségrégation dynamique dans la direction horizontale. Cela se traduit par un comportement plus auto plaçant que des propriétés d'auto nivelant.

- La masse volumique de la partie fluide de la suspension démontrée un effet plus dominant sur la ségrégation dynamique induite par gravité que la viscosité plastique. Par conséquent, moins dense est la partie fluide de la suspension, plus la ségrégation dynamique verticale est à prévue.

- Une nouvelle approche est proposée pour classifier les mélanges du BAP en fonction de la capacité de remplissage. Celle-ci consiste d'une combinaison de fluidité et de la capacité de passage. Par conséquence, trois niveaux de capacité de remplissage correspondant à bas, moyen et élevé ont été définis. Ces niveaux correspondent aux trois $B.I._{max}$ (l'indice de blocage maximum) qui sont : 100% -130% (de capacité de passage élevée), 130% -160% (capacité de passage moyenne), et 160% -190% (capacité de passage faible), respectivement. Comme l'une des étapes principales du procédé de conception d'ouvrabilité, les résultats de cette classification peuvent être utilisés comme un outil pratique pour optimiser la rhéologie et dosage des mélanges du BAP, concernant les propriétés de capacité de remplissage de coffrage dans les zones renforcées.

1.b) L'effet couplé des barres d'armature et des contenus des gros granulats:

- Selon les résultats numériques, une nouvelle approche est proposée pour évaluer L'effet couplé des barres d'armature-gros granulats sur la stabilité dynamique horizontale et du risque de blocage dans trois zones d'interaction différentes. Ces zones indiquent des

effets parallèles et opposées entre les barres et les particules qui affectent la performance d'écoulement des suspensions étudiées.

- L'augmentation à la fois de la teneur en particules de la suspension du béton et le nombre de barres dans la section horizontale du L-Box a entraîné un risque plus élevé de blocage et de ségrégation dynamique dans la direction horizontale. Contrairement, il a entraîné une diminution de la ségrégation dynamique verticale. D'autre part, l'augmentation de la teneur de grosses particules peut augmenter la viscosité globale et le seuil de cisaillement de la suspension. Ceci peut améliorer la stabilité dynamique du mélange dans le sens horizontal.

- L'effet le plus élevée du nombre de barres a été observé dans le milieu du canal horizontal, où la ségrégation dynamique horizontale maximale a également été observée. D'autre part, dans le cas du plus nombre d'obstacles et de la teneur maximale des gros granulats, l'effet des contenus des granulats et des différents configurations de barres sur la capacité de passage et la ségrégation dynamique du BAP est dominant dans les sections horizontales du milieu.

- Selon les simulations numériques, les propriétés de performance d'écoulement du BAP dans les sections extrêmes situées sous le point de coulée et à la fin du coffrage se trouvent à dépendre principalement sur le débit de mise en place et de la longueur du coffrage, respectivement.

2. Simulation numérique d'écoulement hétérogène du BAP dans l'essai de T-Box :

Les résultats de simulation numérique de l'écoulement du BAP dans l'essais de T-Box se trouvent en accord qualitatif avec ceux obtenus expérimentalement par Esmaeilkhanian et al. [36-38]. Selon les résultats numériques, les conclusions suivantes peuvent être tirées:

- L'augmentation de la viscosité plastique et les seuils de cisaillement de la partie fluide de la suspension peut diminuer la fluidité et la ségrégation dynamique du BAP dans les

directions horizontale et verticale. Cependant, la viscosité plastique a démontré un effet plus dominant que le seuil de cisaillement.

- Les caractéristiques hétérogènes d'écoulement du BAP dans dispositifs de T-Box pour les suspensions avec des valeurs de la viscosité faible et élevé se sont révélés être plus affectés par l'énergie d'écoulement initial (fourni par les cycles d'écoulement initiaux) et du plus grand nombre de cycles d'écoulement, respectivement.

- La ségrégation dynamique du BAP dans l'essai de T-Box a été plus élevée dans la direction horizontale par rapport à la verticale. Par conséquent, l'essai de T-Box est plus recommandé pour les applications horizontales, par exemple la mise en place de poutre, les murs longs, et des éléments de dalle.

- Une nouvelle définition et l'approche ont été proposées pour classifier les suspensions à base de "performabilité dynamique non-renforcé" à la suite du compromis entre fluidité et stabilité dynamique dans les directions verticales et horizontales. Par conséquent, les suspensions du BAP ont été classées sur trois zones différentes de performabilité: Zone 1 (fluidité faible, stabilité dynamique haute), zone 2 (fluidité moyenne, stabilité dynamique moyenne), et la zone 3 (fluidité haute, stabilité dynamique bas). Cette classification peut être utilisée comme un outil pratique dans la conception d'ouvrabilité du BAP, afin d'optimiser le dosage de mélange, ouvrabilité et rhéologie, concernant les aspects de fluidité et de la stabilité dynamique.

3. Comparaison entre les performances d'écoulement du BAP dans les appareils des L-Box et T-Box:

- Les résultats des simulations ont démontré que l'augmentation des valeurs de seuil de cisaillement et de viscosité plastique de la partie fluide de la suspension diminue la fluidité du BAP dans les deux dispositifs des L-Box et T-Box. D'autre part, les mélanges du BAP présentent de vitesse d'écoulement plus élevés dans T-Box, tandis que des

valeurs plus élevées du taux de la déformation et d'énergie cinétique d'écoulement ont été obtenus dans l'essai de L-Box.

- La viscosité plastique de la partie fluide de suspension a démontré un effet plus important sur les caractéristiques d'écoulement du BAP dans les deux essais par rapport aux valeurs de seuil de cisaillement.

- Les paramètres rhéologiques ont démontré des effets opposés sur la stabilité dynamique du BAP dans les essais de T-Box et L-Box. En effet, l'augmentation de la viscosité plastique de la partie fluide de la suspension a augmenté la ségrégation dynamique dans l'essai de L-Box, alors qu'elle a diminué dans le T-Box.

- Des simulations numériques ont démontré que des valeurs plus élevées de ségrégation dynamique dans les deux directions verticales et horizontales ont été obtenus dans l'essai de L-Box par rapport à celui du T-Box.

- Des valeurs plus élevés de ratios des indices ségrégation dynamique vertical/horizontale ont été obtenus dans l'essai de L-Box comparativement à l'essai de T-Box. Par conséquent, on peut conclure que l'essai de T-Box est plus approprié pour évaluer la stabilité dynamique dans les applications horizontales, tell que éléments de poutre et dalles longues, tandis que l'essai de L-Box peut être recommandé pour les applications horizontales et verticales, lorsque la stabilité dynamique et la capacité de passage dans les directions sont d'intérêt (par exemple, des poutres et des dalles profondes, et des éléments de mur longues).

CHAPTER 12 FUTURE RESEARCHES

According to the results presented in this study, carried out on theoretical flow analysis of SCC, the following recommendations can be proposed for future researches:

12.1 Homogeneous flow analysis of SCC

12.1.1 Analytical predictions using Dam Break Theory

- Because of the similarity of the procedure of slump flow test to Dam Break Theory, it will be useful to apply the Dam Break Theory to model flow of SCC in the slump flow test.

- Predicting time dependent outputs of workability tests, such as $T_{50\ cm}$ in slump flow, $T_{20\ cm}$ and $T_{40\ cm}$ values in L-Box set-up using the Dam Break Theory is recommended.

- Applying other rheological models such as, modified Bingham model, to develop the proposed analytical model using Dam Break Theory

12.1.2 Numerical simulation of SCC as a homogeneous single fluid

- Evaluate the effect of rising rate of the sliding gate in the L-Box apparatus on flow profiles and the accuracy of the simulations.

- Study the effect of different coefficients of friction of formwork walls on flow performance of SCC.

- Using other power law rheological models, such as Herschel-Bulkley model, as well as shear rate dependent viscosity models, instead of simple Bingham model can improve

the accuracy of the simulations for prediction of flow behavior, especially for the shear-thinning or shear thickening mixtures under high shear rate regimes.

- Take into consideration the effect of time-dependent thixotropic behavior of concrete mixture in rheological models, especially for long casting periods.

- Carry out a comparison between hydrodynamics and hydrostatic formwork lateral pressure, based on the effect of rheological parameters of the mixtures during flow and thereafter at rest.

- Evaluate the effect of shear elasticity modulus of concrete on homogeneous behavior of SCC during casting process.

- Carry out a macro scale homogeneous approach study on elastic state of fresh SCC to develop an Elastometer and evaluate elastic properties of fresh concrete before beginning of viscous and plastic states.

- Apply empirical rheological models, considering time-dependent, shear history dependent, and temperature effects (thermodynamics), especially for simulation of long casting processes, or severe environmental casting conditions. This can lead to better workability design or modifying the empirical models for these special applications.

- Study the behavior of SCC flow in turbulent flow conditions, such as high pumping flow rates of very low viscosity SCC mixtures.

- Simulate the confined flows such as pumping or tremie pipes.

- Simulate multi-layers castings to evaluate effect of rheological parameters of different layers of concrete on formwork filling ability properties of each layer. This can help in proposing recommendations for multi-layer castings in different construction applications where one single layer casting is not executable.

- Classify SCC mixtures based on self-leveling and self-consolidating properties. This can be carried out by evaluation of rheological parameters on flow performance of SCC in different directions (horizontal, vertical, or combinatorial motions) using CFD simulations.

12.2 "Homo-Hetero"-geneous analysis of SCC flow: A transitional combination of homogeneous and heterogeneous analyses

- Verify of the properties of critical zones of segregation, blocking, and poor filling ability which were determined earlier by single fluid simulations using experimental workability tests. This can be carried out in small prototypes that can simulate the same velocity-shear rate conditions obtained in the homogeneous analysis of full-size casting.

- Carry out homogeneous analysis of casting static unstable mixtures, which were already segregated before beginning of the flow. This can be carried out using continuous multi-layer approach, following different rheological parameters in vertical direction of concrete profile thickness. New homogeneous/multi-layer rheological models can then be proposed to describe the rheological behavior of static unstable mixtures using CFD simulations. This can be useful for modification of rheometry measurement procedures for unstable SCC suspensions, in order to avoid the problems caused by migration of aggregates during the measurement which can affect negatively on the results.

12.3 Heterogeneous flow analysis of SCC

- Validate numerical results of heterogeneous analyses of SCC suspensions, presented in Chapters 7-10, by carrying experiments. This can help to modify the simplifications and assumptions of the carried out numerical models.

- Consideration of other rheological models, such as the Herschel-Bulkley model, for suspending fluids to evaluate non-linear behavior of suspending fluid in low/high shear rate zones between the particles, particles and reinforcing bars, and between particles and formwork walls.
- Simulate flow of SCC containing higher volumetric contents and different sizes of coarse aggregates.

- Develop experimental tests to measure coefficient of friction between fresh concrete and walls and reinforcing bars, between coarse aggregates and suspending fluid, as well as walls and reinforcing bars is highly recommended. This can lead to having better assumptions for the inputs of the numerical models.

- Study the wall effects on local segregation of aggregates beside formwork walls using CFD simulations and compare with experimental results.

- Simulate heterogeneous behavior of SCC mixtures in the elastic state, and taking into consideration wider ranges of shear elasticity modulus

- Evaluate the effect of particle migration on changing local rheology of concrete in segregated zones using numerical and experimental results.

- Evaluate the effect of water bleeding in changing of rheological parameters of SCC suspension, and consequently on the heterogeneous behavior of concrete during flow.

- Simulate the effect of reinforcing bars in vertical applications where the flow directions are mostly vertical, such as tall columns, pumping in high rise buildings, and tall deep concrete piles which are not accessible to be characterized experimentally. Higher free fall heights, as well as opposite direction of gravitational forces compared to the flow direction can be critical on flow performance of SCC in the vertical applications.

- Simulate the effect of internal or external vibrators on segregation and filling ability of semi-SCC mixtures in the casting process: Distribution, numbers, and necessary power of the vibrators can be predicted using the heterogeneous analysis of the casting process, carried out in the critical zones of poor formwork filling, dynamic segregation, and poor passing ability.
- Simulate the lattice effect of particles on static and dynamic segregation of SCC: The numerical results should be validated by experimental measurements.

- Simulate the effect of thixotropic behavior of suspending fluid on dynamic segregation of coarse particles, considering the effect of local shear rates between particles on thixotropic behavior of suspending fluids (i.e., cement paste and mortar matrix).

- Simulate heterogeneous behavior of SCC in confined flow conditions, such as pumping tubes, or complicated architectural elements.

- Combine VOF-CFD tools with particle based methods such as DEM and SPH, to increase capability of both methods, hence, can result in increasing accuracy of predictions and reduce the calculation times.

- In order to simulate huge full size casting problems, it is recommended to employ combination of homogeneous and heterogeneous approaches, using combination of mesh based and mesh less methods.

- Heterogeneous simulation of mixing process of concrete using CFD and DEM methods is also recommended to be carried out.

12.4. Numerical simulation of flow performance of fiber reinforced SCC (FRSCC)

- Characterize fresh properties of FRSCC for numerical models, in terms of rheological models and coefficient of frictions.

- Simulate the orientation of fibers during flow and thereafter at rest, by taking into consideration dynamic and static segregation of the aggregates.
- Evaluate the applicability of current workability tests of normal SCC to evaluate flow performance properties of FRSCC using CFD simulations.

- Characterize dynamic segregation patterns in FRSCC compared to normal SCC, to highlight the influence of fibers.

REFERENCES

[1] Nakashizuka, T., Iida, S., Suzuki, W., and Tanimoto, T. (1993). Seed dispersal and vegetation development on a debris avalanche on the Ontake Volcano, central Japan. *Journal of Vegetation Science*, 4(4), 537-542.

[2] Bartelt, P., and Brian, W. (2009). Granulometric investigations of snow avalanches. *Journal of Glaciology*, 55(193), 829-833.

[3] Liu, S. (1999). Particle dispersion for suspension flow. *Chemical Engineering Science*, 54(7), 873-891.

[4] Wiederseiner, S., Andreini, N., Épely-Chauvin, G., Moser, G., Monnereau, M., Gray, J.M.N.T., and Ancey, C. (2011). Experimental investigation into segregating granular flows down chutes. *Physics of Fluids*, 23, 013301.

[5] Gray, J.M.N.T., Gajjara, P., and Kokelaar, P. (2015). Particle-size segregation in dense granular avalanches. *Comptes Rendus Physique*, 16, 73-85.

[6] Kaur, P., Singh, S.K., Garg, V., Gulati, M., and Vaidya, Y. (2015). Optimization of spray drying process for formulation of solid dispersion containing polypeptide-k powder through quality by design approach. *Powder Technology*, 284, 1-11.

[7] Chimwani, N., Mulenga, F.K., and Hildebrandt, D. (2015). Ball size distribution for the maximum production of a narrowly-sized mill product. *Powder Technology*, 284, 12-18.

[8] Simons, T.A.H., Bensmann, S., Zigan, S., Feise, H.J., Zetzener, H., and Kwade, A. (2016). Characterization of granular mixing in a helical ribbon blade blender. *Powder Technology*, 293, 15-25.

[9] Zhaosheng, Y., Xueming, S., and Tanner, R. (2007). Dynamic simulation of shear-induced particle migration in a two-dimensional circular couette device. *Chinese Journal of Chemical Engineering*, 15(3), 333-338.

[10] Hacina, A., and Kamel, D. (2008). Indirect method of measuring dispersion coefficients for granular flow in a column of dihedrons. *International Journal of Food Engineering*, 4(7), Article 10.

[11] Simsek, E., Wirtz, S., Scherer, V., Kruggel-Emden, H., Grochowski, R., and Walzel, P. (2008). An experimental and numerical study of transversal dispersion of granular material on a vibrating conveyor. *Particulate Science and Technology*, 26(2), 177-196.

[12] Mewis, J., and Wagner, N. (2009). Current trends in suspension rheology. *Journal of Non-Newtonian Fluid Mechanics*, 157(3), 147-150.

[13] Christov, I.C., and Stone, H.A. (2014). Shear dispersion in dense granular flows. *Granular Matter*, 16(4), 509-515.

[14] Liao, C.-C., Lan, H.-W., and Hsiau, S.-S. (2016). Density-induced granular segregation in a slurry rotating drum. *International Journal of Multiphase Flow*, 84, 1-8.

[15] Leighton, D., and Arcrivos, A. (1987). The shear-induced migration of particles in concentrated suspensions. *Journal of Fluid Mechanics*, 181, 415-439.

[16] Gunes, D.Z., Scirocco, R., Mewis, J., and Vermant, J. (2008). Flow-induced orientation of non-spherical particles: Effect of aspect ratio and medium rheology. *Journal of Non-Newtonian Fluid Mechanics*, 155(1-2), 39-50.

[17] Huang, Q.-F., Zhan, M.-l., Sheng, J.-C., Luo, Y.-L., and Su, B.-Y. (2014). Investigation of fluid flow-induced particle migration in granular filters using a DEM-CFD method. *Journal of Hydrodynamics*, 26(3), 406-415.

[18] Murisic, N., Ho, J., Hu, V., Latterman, P., Koch, T., Lin, K., Mata, M., and Bertozzi, A.L. (2011). Particle-laden viscous thin-film flows on an incline: Experiments compared with a theory based on shear-induced migration and particle settling. *Physica D: Nonlinear Phenomena*, 240(20), 1661-1673.

[19] Yoon, S., Walkley, M.A., and Harlen, O.G. (2012). Two particle interactions in a confined viscoelastic fluid under shear. *Journal of Non-Newtonian Fluid Mechanics*, 185-186, 39-48.

[20] D'avino, G., and Maffettone, P.L. (2015). Particle dynamics in viscoelastic liquids. *Journal of Non-Newtonian Fluid Mechanics*, 215, 80-104.

[21] Jabbari, M., Spangenberg, J., and Hattel, J.H. (2016). Particle migration using local variation of the viscosity (LVOV) model in flow of a non-Newtonian fluid for ceramic tape casting. *Chemical Engineering Research and Design*, 109, 226-233.

[22] Naik, T.R. (2008). Sustainability of concrete construction. *Practice Periodical on Structural Design and Construction*, 13(2), 98-103.

[23] Daczko, J. and Khayat, K.H. (2007). *Self-consolidating concrete* (ACI 237R-07). American Concrete Institute Committee 237, Farmington Hills, USA, 91 p.

[24] Khayat, K.H. (1999). Workability, testing, and performance of self-consolidating concrete. *ACI Materials Journal*, 96(3), 346-353.

[25] EFNARC (2002). *The European Guidelines for Self-Compacting Concrete, Specification, Production and Use*, EFNARC, Norfolk, UK, ISBN: 0-9539733-4-4, 68 p.

[26] Khayat, K.H. and Mitchell, D. (2009). *Self-Consolidating Concrete for Precast, Prestressed Concrete Bridge Elements* (NCHRP Report 628). National Cooperative Highway Research Program, Transportation Research Board of the National Academies, Washington D.C., USA, 99 p.

[27] Roussel, N. (2012). *Understanding the Rheology of Concrete*, 1st edition, Woodhead Publishing, ISBN 9780857090287, Sawston, Cambridge, United Kingdom, 364 p.

[28] Roussel, N., (2006). A theoretical frame to study stability of fresh concrete. *Materials and Structures*, 39(1), 81-91.

[29] Thrane, L.N. (2007). *Form filling with self-compacting concrete*. Ph.D. thesis, Danish technological institute, Denmark, 295 p.

[30] Mehdipour, I., Vahdani, M., Amini, K., and Shekarchi, M. (2016). Linking stability characteristics to material performance of self-consolidating concrete-equivalent-mortar incorporating fly ash and metakaolin. *Construction and Building Materials*, 105, 206-217.

[31] Khayat, K.H. (1998). Use of viscosity-modifying admixture to reduce top-bar effect of anchored bars cast with fluid concrete. *ACI Materials Journal*, 95(2), 158-167.

[32] Sonebi, M., Grünewald, S., and Walraven, J. (2007). Filling ability and passing ability of self-consolidating concrete. *ACI Materials Journal*, 104(2), 162-170.

[33] Tanigawa, Y., and Mori, H. (1988). Toward the development of workability design of fresh concrete, *Cement & Concrete*, 501, 11-20 (in Japanese).

[34] Tanigawa, Y., and Mori, H., (1993). Toward the development of workability design of fresh concrete (continuation). *Cement & Concrete*, 551, 2-11 (in Japanese).

[35] Li, Z. (2007). State of workability design technology for fresh concrete in Japan. *Cement and Concrete Research*, 37(9), 1308-1320.

[36] Esmaeilkhanian, B. (2011). *Dynamic stability of self-consolidating concrete: Development of test methods and influencing parameters*. M.Sc. thesis, Université de Sherbrooke, Sherbrooke, Canada, 199 p.

[37] Esmaeilkhanian, B., Feys, D., Khayat, K.H., and Yahia, A. (2014). New test method to evaluate dynamic stability of self-consolidating concrete. *ACI Materials Journal*, 111(3), 299-308.

[38] Esmaeilkhanian, B., Khayat, K.H., Yahia, A., and Feys, D. (2014). Effects of mix design parameters and rheological properties on dynamic stability of self-consolidating concrete. *Cement & Concrete Composites*, 54, 21-28.

[39] Flatt, R.J., Larosa, D., and Roussel, N. (2006). Linking yield stress measurements: Spread test versus Viskomat. *Cement and Concrete Research*, 36(1), 99-109.

[40] Nguyen, T.L.H. and Roussel, N. (2006). Correlation between L-box test and rheological parameters of a homogeneous yield stress fluid. *Cement and Concrete Research*, 36(10), 1789-1796.

[41] Roussel, N. and Coussot, P. (2005). "Fifty cent rheometer" for yield stress measurements: From slump to spreading flow. *Journal of Rheology*, 49(3), 705-718.

[42] Roussel, N., Geiker, M.R., Dufour, F., Thrane, L.N., and Szabo, P. (2007). Computational modeling of concrete flow: General overview. *Cement and Concrete Research*, 37(9), 1298-1307.

[43] Yammine, J., Chaouche, M., Guerinet, M., Moranville, M., and Roussel, N. (2008). From ordinary rheology concrete to self compacting concrete: A transition between frictional and hydrodynamic interactions. *Cement and Concrete Research*, 38(7), 890-896.

[44] Roussel, N., Gram, A., Cremonesi, M., Ferrara, L., Krenzer, K., Mechtcherine, V., Shyshko, S., Skocec, J., Spangenberg, J., Svec, O., Thrane, L.N., and Vasilic, K. (2016). Numerical simulations of concrete flow: A benchmark comparison. *Cement and Concrete Research*, 79, 265-271.

[45] Shen, L., Struble, L., and Lange, D.A. (2009). Modeling dynamic segregation of self-consolidating concrete. *ACI Materials Journal*, 106(4), 375-380.

[46] Spangenberg, J., Roussel, N., Hattel, J.H., Stang, H., Skocek, J., and Geiker, M.R. (2012). Flow induced particle migration in fresh concrete: Theoretical frame, numerical simulations and experimental results on model fluids. *Cement and Concrete Research*, 42(4), 633-641.

[47] Spangenberg, J., Roussel, N., Hattel, J.H., Sarmiento, E.V., Zirgulis, G., and Geiker, M.R. (2012). Patterns of gravity induced aggregate migration during casting of fluid concretes. *Cement and Concrete Research*, 42(12), 1571-1578.

[48] Roussel, N. and Gram A. (2014). *Simulation of fresh concrete flow*. State of the Art Report of the RILEM Technical committee 222-SCF, Imprint: Springer, ISBN 978-94-017-8883-0, 147 p.

[49] Barnes, H.A., Hutton, J.F., and Walters, K. (1989). *An introduction to rheology*, Elsevier, Amsterdam, Netherlands, 199 p.

[50] Ferguson, J. and Kemblowski, Z. (1991). *Applied fluid rheology*, Springer, Netherlands, 323 p.

[51] Whorlow, R.W. (1992). *Rheological techniques*, Ellis Harwood, New York, USA, 460 p.

[52] Bartos, P. (1992). *Fresh Concrete: Properties and Tests*, Elsevier, 305 p.

[53] Tattersall, G.H. (1976). *The workability of concrete, A viewpoint Publication*, Cement & Concrete Association of Great Britain, 138 p.

[54] Yahia, A., and Khayat, K.H. (2001). Analytical models for estimating yield stress of high-performance pseudoplastic grout. *Cement and Concrete Research*, 31(5), 731-738.

[55] Atzeni, C., Massida, L., and Sanna, U. (1985). Comparison between rheological models for Portland cement pastes, *Cement and Concrete Research*, 15(3), 511-519.

[56] Herschel, W.H. and Bulkley, R. (1926). Consistency measurements of rubber benzene solutions. *Kolloid-Z*, 39, 291-300 (in German).

[57] Vom Berg, W. (1979). Influence of specific surface and concentration of solids upon the flow behavior of cement pastes. *Magazine of Concrete Research*, 31(109), 211-216.

[58] Jones, T.E.R. and Taylor, S. (1977). A mathematical model relating the flow curve of a cement paste to its water/cement ratio. *Magazine of Concrete Research*, 29(101), 207-212.

[59] Atzeni, C., Massida, L., and Sanna, U. (1985). Comparison between rheological models for Portland cement pastes. *Cement and Concrete Research*, 15(3), 511-519.

[60] Casson, W, (1959). A flow equation for pigment-oil suspensions of the printing ink type. In Mill, C.C., Editor, British Society of Rheology. *Rheology of disperse systems*, Pergamon press, New York, USA, p. 84.

[61] Yahia, A. and Khayat, K.H. (2003). Applicability of rheological models to high performance grout containing supplementary cementitious materials and viscosity enhancing admixtures. *Materials and Structures*, 36(6), 402-412.

[62] Struble, L.J. and Sun, G-K. (1995). Viscosity of Portland cement paste as a function of concentration. *Advanced Cement Based Materials*, 2(2), 62-69.

[63] Ish-Shalom, M. and Greenberg, S.A. (1960). The rheology of fresh Portland cement pastes, in Proceedings of *4th International Symposium on the Chemistry of Cement*, Monograph 43, volume 2. National Bureau of Standards, Washington DC, USA, p. 731-748.

[64] Bombled, J.P. (1970). A rheograph for studying the rheology of stiff pastes: application to cement setting. *Révue des Matériaux de Construction*, 673, 256-277.

[65] Casson, R.B.J., Domone, P.L.J., Scrivener, K., Jennings, H.M., Gillham, C.J., and Pratt, P.L. (1982). The measurement of early strength development in polymer modified cement pastes. in Skalny, J.P.: Editor, *Concrete rheology, Materials Research Society Symposium M*, Boston, USA, p. 66-75.

[66] Winnefeld, F. and Holzer, L. (2003). Monitoring early cement hydration by rheological measurements. In Justnes, H., Editor, Proceedings of *11th International Congress on the Chemistry of Cement*, Durban, South Africa, p. 330-339.

[67] Kellingray, D S., Greaves, C., and Dallimer, R.P. (1991). High temperature and high pressure rheology of oil well cement slurries. In Banfill, P.F.G., Editor, *Rheology of Fresh Cement and Concrete*, E &F N Spon, Liverpool, UK, p. 159-169.

[68] Domone, P.L.J. and Thurairatnam, H. (1988). The effect of water/cement ratio, plasticizers and temperature on the rheology of cement grouts. *Advances in Cement Research*, 1(4), 195-206.

[69] Petit, J.-Y., Wirquin, E., and Duthoit, B. (2005). Influence of temperature on yield value of highly flowable micromortars made with sulfonate based superplasticizers. *Cement and Concrete Research*, 35(2), 256-266.

[70] Grzeszczyk, S. and Kucharska, L. (1991). The influence of chemical composition of cement on the rheological properties. In Banfill, P.F.G., Editor, *Rheology of Fresh Cement and Concrete*, E &F N Spon, Liverpool, UK, p. 27-36.

[71] Ferraris, C.F., Obla, K.H., and Hill, R. (2001). The influence of mineral admixtures on the rheology of cement paste and concrete. *Cement and Concrete Research*, 31(2), 245-255.

[72] Park, C.K., Noh, M.H., and Park, T.H. (2005). Rheological properties of cementitious materials containing mineral admixtures. *Cement and Concrete Research*, 35(5), 842-849.

[73] Palomo, A., Banfill, P.F.G., Fernandez-Jiminez, A., and Swift, D.S. (2005). Properties of alkali-activated fly ashes determined from rheological measurements. *Advances in Cement Research*, 17(4), 143-151.

[74] Aïtcin, P.-C., Jolicoeur, C., and MacGregor, J.G. (1994). Superplasticizers: How they work and why they occasionally don't. *Concrete International*, 16(5), 45-52.

[75] Papo, A. and Piani, L. (2004). Effect of various superplasticizers on the rheological properties of Portland cement pastes. *Cement and Concrete Research*, 34(11), 2097-2101.

[76] Banfill, P.F.G. (2006). *Rheology of fresh cement and concrete, Rheology Reviews*, The British Society of Rheology, p. 61-130.

[77] Wallevik, O.H. (2003). Rheology – a scientific approach to develop self-compacting concrete. In Wallevik, O. and Nielsson, I., Editors, Self compacting concrete, Proceedings of the *3rd International RILEM Symposium, PRO33*, RILEM, Paris, France, p. 23-31.

[78] LaNier, M. (2003). *Interim Guidelines for the Use of Self-Consolidating Concrete in Precast/Prestressed Concrete Institute Member Plants* (TR-06-03), Precast/Prestressed Concrete Institute, Chicago, Illinois, USA, ISBN 0-937040-68-1, 165 p.

[79] Fernandez-Altable, V. and Casanova, I. (2006). Influence of mixing sequence and superplasticiser dosage on the rheological response of cement pastes at different temperatures. *Cement and Concrete Research*, 36(7), 1222-1230.

[80] ASTM C1611/C1611M-14 *Standard Test Method for Slump Flow of Self-Consolidating Concrete*, ASTM International, West Conshohocken, PA, 2014.

[81] ASTM C143/C143M-15a *Standard Test Method for Slump of Hydraulic-Cement Concrete*, ASTM International, West Conshohocken, PA, 2015.

[82] ASTM C1621/C1621M-14, *Standard test method for passing ability of self-consolidating concrete by J-Ring*, ASTM International, West Conshohocken, PA, Developed by Subcommittee: C09.47, Book of Standards 2014, V 04.02.

[83] Assaad, J., Khayat, K.H., and Daczko, J. (2004). Evaluation of static stability of self-consolidating concrete. *ACI Materials Journal*, 101(3), 207-215.

[84] ASTM C1610/C1610M-14, *Standard test method for static segregation of self-consolidating concrete using column technique*, ASTM International, West Conshohocken, PA, Developed by Subcommittee: C09.47, Book of Standards 2014, V 04.02.

[85] AASHTO PP 58-12, *Standard specification for static segregation of hardened self-consolidating concrete (SCC) cylinders*, 2015.

[86] Mesbah, H.A., Yahia, A., and Khayat, K.H. (2011). Electrical conductivity method to assess static stability of self-consolidating concrete. *Cement and Concrete Research*, 41(5), 451-458.

[87] ASTM C1712-14, *Standard test method for rapid assessment of static segregation resistance of self-consolidating concrete using penetration test*, ASTM International, West Conshohocken, PA, Developed by Subcommittee: C09.47, Book of Standards 2014, V 04.02.

[88] Shen, L., Jovein, H.B., and Li, M. (2014). Measuring static stability and robustness of self-consolidating concrete using modified Segregation Probe. *Construction and Building Materials*, 70, 210-216.

[89] Wang, X., Wang, K., Han, J., and Taylor, P. (2015). Image analysis applications on assessing static stability and flowability of self-consolidating concrete. *Cement and Concrete Composites*, 62, 156-167.

[90] Shen, L., Jovein, H.B., and Wang, Q. (2015). Correlating aggregate properties and concrete rheology to dynamic segregation of self-consolidating concrete. *Journal of Materials in Civil Engineering*, 28(1), 040150671-040150679.

[91] Shen, L., Jovein, H.B., Sun, Z., Wang, Q., and Li, W. (2015). Testing dynamic segregation of self-consolidating concrete. *Construction and Building Materials*, 75, 465-471.

[92] Turgut, P., Turk, K., and Bakirci, H. (2012). Segregation control of SCC with a modified L-box apparatus. *Magazine of Concrete Research*, 64(8), 707-716.

[93] Roussel, N. (2006). Correlation between yield stress and slump: Comparison between numerical simulations and concrete rheometers results. *Materials and Structures*, 39, 501-509.

[94] Mechtcherine, V., Gram, A., Krenzer, K., Schwabe, J-H., Shyshko, S., and Roussel, N. (2014). Simulation of fresh concrete flow using Discrete Element Method (DEM): theory and applications. *Materials and Structures*, 47(4), 615-630.

[95] Balmforth, N.J., Craster, R.V., Perona, P., Rust, A.C., and Sassi, R. (2007). Viscoplastic dam breaks and the Bostwick consistometer. *Journal of Non-Newtonian Fluid Mechanics*, 142(1-3), 63-78.

[96] Feys, D., Verhoeven, R., and De Schutter, G. (2008). Fresh self compacting concrete, a shear thickening material. *Cement and Concrete Research*, 38(7), 920-929.

[97] Feys, D., Verhoeven, R., and De Schutter, G. (2009). Why is fresh self-compacting concrete shear thickening?. *Cement and Concrete Research*, 39(6), 510-523.

[98] Petit, J-Y., Wirquin, E., Vanhove, Y., and Khayat, K.H. (2007). Yield stress and viscosity equations for mortars and self-consolidating concrete. *Cement and Concrete Research*, 37(5), 655-670.

[99] Coussot, P. (1997). *Mudflow Rheology and Dynamics*, 1st Edition. Taylor & Francis, ISBN 9789054106937, 272 p.

[100] Huang, X. and Garcia, M.H. (1997). A perturbation solution for Bingham-plastic mudflows. *Journal of Hydraulic Engineering*, 123(11), 986-994.

[101] Huang, X. and Garcia, M.H. (1998). A Herschel-Bulkley model for mud flow down a slope. *Journal of Fluid Mechanics*, 374(1), 305-333.

[102] Pinkerton, H. and Sparks, R.S.J. (1978). Field measurements of the rheology of lava. *Nature*, 276, 383-385.

[103] Balmforth, N.J., Burbridge, A.S., and Craster, R.V. (2000). Viscoplastic models of isothermal lava domes. *Journal of Fluid Mechanics*, 403, 37-65.

[104] Dent, J.D. and Lang, T.E. (1983). A biviscous modified Bingham model of snow avalanche motion. *Annals of Glaciology*, 4, 42-46.

[105] Kern, M., Tiefenbacher, F., and McElwaine J. (2004). The rheology of snow in large chute flows. *Cold Regions Science and Technology*, 39(2-3), 181-192.

[106] Iverson, R.M. (1997). The physics of debris flows. *Reviews of Geophysics*, 35(3), 245-296.

[107] Iverson, R.M. (2003). The debris-flow rheology myth. In Rickernmann, D. and Chen, C.L., Editors, Proceedings of the *3rd International Conference on Debris-Flow Hazards*

Mitigation: Mechanics, Prediction, and Assessment, Millpress, Davos, Switzerland, p. 303-314.

[108] Hogg, A.J. (2007). Two-dimensional granular slumps down slopes. *Physics of Fluids*, 19(9), 093301.

[109] Bingham, E.C. (1922). *Fluidity and plasticity*. Mc Graw-Hill, ISBN-13 9781432696757, New York, USA, 463 p.

[110] Bird, R.B., Dai, G.C., and Yarusso, B.J. (1983). The rheology and flow of viscoplastic materials. *Reviews in Chemical Engineering*, 1(1), 1-70.

[111] Balmforth, N.J. and Craster, R.V. (2002). Geophysical aspects of non-Newtonian fluid mechanics. In Blamforth, N.J. and Provenzale A., Editors, *Geomorphological Fluid Mechanics, Lecture Notes in Physics*, Gran Combin Summer School, Springer, p. 34-51.

[112] Ancey, C. (2007). Plasticity and geophysical flows: a review. *Journal of Non-Newtonian Fluid Mechanics*, 142(1-3), 4-35.

[113] Saramito, P. (2007). A new constitutive equation for elastoviscoplastic fluid flows. *Journal of Non-Newtonian Fluid Mechanics*, 145(1), 1-14.

[114] Saramito, P. (2009). A new elastoviscoplastic model based on the Herschel-Bulkley viscoplasticity. *Journal of Non-Newtonian Fluid Mechanics*, 158(1-3), 154-161.

[115] Liu, K.F. and Mei, C.C. (1990). Slow spreading of a sheet of Bingham fluid on an inclined plane. *Journal of Fluid Mechanics*, 207, 505-529.

[116] Piau, J-M. (1996). Flow of a yield stress fluid in a long domain. Application to flow on an inclined plane. *Journal of Rheology*, 40(4), 711-723.

[117] Piau, J-M. (2006). Consistometry slump and spreading tests: practical comments. *Journal of Non-Newtonian Fluid Mechanics*, 135(2-3), 177-178.

[118] Pashias, N., Boger, D.V., Summers, J., and Glenister, D.J. (1996). A fifty cent rheometer for yield stress measurements. *Journal of Rheology*, 40(6), 1179-1189.

[119] Schowalter, W.R. and Christensen, G. (1998). Toward a rationalization of the slump test for fresh concrete: comparisons of calculations and experiments. *Journal of Rheology*, 42(4), 865-870.

[120] Osmond, D.I. and Griffiths, R.W. (2001). The static shape of yield strength fluids slowly emplaced on slopes. *Journal of Geophysical Research*, 106(B8), 16241-16250.

[121] Chatzimina, M., Georgiou, G.C., Argyropaidas, I., Mitsoulis, E. and Huilgol, R.R. (2005). Cessation of Couette and Poiseuille flows of a Bingham plastic and finite stopping times. *Journal of Non-Newtonian Fluid Mechanics*, 129(3), 117-127.

[122] Balmforth, N.J., Craster, R.V., Rust, A.C., and Sassi, R. (2007). Viscoplastic flow over an inclined surface. *Journal of Non-Newtonian Fluid Mechanics*, 142(1-3), 219-243.

[123] Cochard, S. (2007). *Measurements of time-dependent free-surface viscoplastic flows down steep slopes*. Ph.D. Dissertation, Ecole Polytechnique Federale de Lausanne, Lausanne, Switzerland, 206 p.

[124] Cochard, S. and Ancey, C. (2009). Experimental investigation into the spreading of viscoplastic fluids onto inclined planes. *Journal of Non-Newtonian Fluid Mechanics*, 158(1), 73-84.

[125] Roquet, N. and Saramito, P. (2003). An adaptive finite element method for Bingham fluid flows around a cylinder. *Computer Methods in Applied Mechanics and Engineering*, 192(31-32), 3317-3341.

[126] Nikitin, K.D., Olshanskii, M.A., Terekhov, K.M., and Vassilevski, Y.V. (2011). Numerical method for the simulation of free surface flows of viscoplastic fluid in 3D. *Journal of Computational Mathematics*, 29(6), 605-622.

[127] Saramito, P., Smutek, C., and Cordonnier, B. (2013). Numerical modeling of shallow non-Newtonian flows: Part I. The 1D horizontal dam break problem revisited. *International Journal of Numerical Analysis and Modeling, Series B*, 1(1), 1-18.

[128] Bernabeu, N., Saramito, P., and Smutek, C. (2014). Numerical modeling of non-Newtonian viscoplastic flows: Part II. Viscoplastic fluids and general tridimensional topographies. *International Journal of Numerical Analysis and Modeling*, 11(1), 213-228.

[129] Murata, J. (1984). Flow and deformation of fresh concrete. *Matériaux et Constructions*, 98(2), 117-129.

[130] Christensen, G. (1991). *Modelling the Flow of Fresh Concrete: The slump test*. Ph.D. thesis, Princeton University, Princeton NJ, USA, 232 p.

[131] Clayton, S., Grice, T.G., and Boger, D.V. (2003). Analysis of the slump test for on-site yield stress measurement of mineral suspensions. *International Journal of Mineral Processing*, 70(1-4), 53-21.

[132] Saak, A.W., Jennings, H.M., and Shah, S.P. (2004). A generalized approach for the determination of yield stress by slump and slump flow. *Cement and Concrete Research*, 34(3), 363-371.

[133] Roussel, N., Stefani, C., and Leroy, R. (2005) From mini cone test to Abrams cone test: measurement of cement based materials yield stress using slump tests. *Cement and Concrete Research*, 35(5) 817-822.

[134] Chidiac, S.E. and Habibbeigi, F. (2005). Modelling the rheological behaviour of fresh concrete: An Elasto-Viscoplastic Finite Element approach. *Computers and Concrete*, 2(2), 97-110.

[135] Murata, J. and Kikukawa, H. (1992). Viscosity Equation for Fresh Concrete. *ACI Materials Journal*, 89(3), 230-237.

[136] Hu, C., De Larrard, F., Sedran, T., Boulay, C., Bosc, F., and Deflorenne, F. (1996). Validation of BTRHEOM, the new rheometer for soft-to-fluid concrete. *Materials and Structures*, 29(10), 620-631.

[137] Ferraris, C.F. and De Larrard, F. (1998). *Testing and modelling of fresh concrete rheology* (NISTIR 6094). Building and Fire Research Laboratory, National Institute of Standards and Technology, Gaithersburg, Maryland, USA, 71 p.

[138] Kurokawa, Y., Tanigawa, Y., Mori, H., and Komura, R. (1994). A study on the slump test and slump–flow test of fresh concrete. *Transactions of the Japan Concrete Institute*, 16.

[139] Domone, P. (1998). The slump flow test for high-workability concrete. *Cement and Concrete Research*, 28(2), 177-182.

[140] Chidiac, S.E., Habibbeigi, F., and Chan, D. (2006). Slump and slump flow for characterizing yield stress of fresh concrete. *ACI Materials Journal*, 103(6), 413-418.

[141] Murata, N., and Shitayama, Y. (1976). The deformation of fresh concrete under static load. *Annual Report of Cement Technology*, 30, 270-273 (in Japanese).

[142] Komura, R., Tanigawa, Y., Mori, H., and Kurokawa, Y. (1994). Rheological study on slumping behaviors of fresh concrete. *Journal of Structural and Construction Engineering*, 462, 1-10 (in Japanese).

[143] Kokado, T. And Hosoda, T. (1995). Method of evaluating yield value of fresh concrete with a Slump flow test. Proceedings of the *50th Annual Conference of JSCE*, Vol. V, p. 1002-1003.

[144] Helmuth, R.A., Hills, L.M., Whiting, D.A., and Bhattacharja, S. (1995). *Abnormal concrete performance in the presence of admixtures* (Report 2006). Portland Cement Association, Skokie, IL, USA, ISBN 0893121371, 94 p.

[145] Tregger, N., Ferrara, L., and Shah, S.P. (2008). Identifying viscosity of cement paste from mini-Slump-flow test. *ACI Materials Journal*, 105(6), 558-566.

[146] Coussot, P. and Ancey, C. (1999). *Rhéophysique des pâtes et des suspensions*. EDP Sciences, (in French), 264 p.

[147] Roussel, N. (2007). The LCPC BOX: a cheap and simple technique for yield stress measurements of SCC. *Materials and Structures*, 40(9), 889-896.

[148] Malvern, L.E. (1969). *Introduction to the Mechanics of Continuous Medium*. Prentice-Hall Inc., New Jersey, USA, 713 p.

[149] Mase, G. (1970). Schaum's Outline Series: *Theory and Problems of Continuum Mechanics*. McGraw-Hill Inc., USA, 221 p.

[150] Hirt C.W. and Nichols, B.D. (1981). Volume of fluid (VOF) method for the dynamics of free boundaries. *Journal of Computational Physics*, 39(1), 201-225.

[151] Kurokawa, Y., Tanigawa, Y., Mori, H., and Nishinosono, Y. (1996). Analytical study on effect of volume fraction of coarse aggregate on Bingham's constants of fresh concrete. *Transactions of the Japan Concrete Institute*, 18, 37-44.

[152] Thrane, L.N., Szabo, P., Geiker, M., Glavind, M., and Stang, H. (2005). Simulation and verification of flow in SCC test methods. In Shah. S., Editor, Proceedings of the *4th International RILEM Symposium on SCC*, Chicago, USA.

[153] Gram, A. (2009). *Numerical modelling of self-compacting concrete flow – discrete and continuous approach*. Licentiate Thesis, Royal Institute of Technology, Stockholm, Sweden, 74 p.

[154] Thrane, L.N., Szabo, P., Geiker, M., Glavind, and M., Stang, H. (2004). Simulation of the test method "L-Box" for self-compacting concrete. *Annual Trans. of the Nordic Rheology Society*, Reykjavik, Iceland, vol. 12, 47-54.

[155] Uebachs, S. and Brameshuber, W. (2005). Numerical simulation of the flow behaviour of self-compacting concretes using fluid mechanical methods. In Shah. S., Editor, Proceedings of the *4th International RILEM Symposium on SCC*, Chicago, USA.

[156] Waarde, F.V. (2007). *Formwork pressures when casting self-compacting concrete*. Master thesis, Technical Univeristy of Delft, Delft, Netherlands, 149 p.

[157] Bras, A. (2010). *Grout optimization for masonry consolidation*. Ph.D. Dissertation, Universidade Nova de Lisboa, Lisbon, Portugal, 250 p.

[158] Nguyen, V.H., Rémond, S., Galliad, J.L., Bigas, J.P., and Muller, P. (2006). Flow of Herschel-Bulkley fluids through the Marsh cone. *Journal of Non-Newtonian Fluid Mechanics*, 139(1-2), 128-134.

[159] Mori, H. and Tanigawa, Y. (1992). *Simulation methods for fluidity of fresh concrete*, Memoirs of the School of Engineering, Nagoya University, Nagoya, Japan, 44, 71-133.

[160] Kitaoji, H., Tanigawa, Y., Mori, H., Kurokawa, Y., and Urano, S. (1996). Flow simulation of fresh concrete cast into wall structure by viscoplastic divided space element method. *Transactions of the Japan Concrete Institute*, 16, 45-52.

[161] Ovarlez, G. and Roussel, N. (2006). A physical model for the prediction of lateral stress exerted by self-compacting concrete on formwork. *Materials and Structures*, 39(2), 269-279.

[162] Roussel, N., Staquet, S., D'aloia Schwarzentruber, L., Le Roy, R., Toutlemonde, F., (2007). SCC casting prediction for the realization of prototype VHPC-precambered composite beams. *Materials and Structures*, 40(9), 877-887.

[163] Roussel, N. and Cussigh, F. (2008). Distinct-layer casting of SCC: the mechanical consequence of thixotropy. *Cement and Concrete Research*, 38(5), 624-632.

[164] Krenzer, K. and Schwabe, J.-H. (2009). Calibration of parameters for particle simulation of building materials, using stochastic optimization procedures. In Wallevik, O.H., Kubens, S., and Oesterheld, S., Editors, Proceedings of the *3rd International RILEM Symposium on Rheology of Cement Suspensions such a Fresh Concrete*, RILEM Publications, Bagneux, Reykjavik, Iceland, p. 135-142.

[165] Shyshko, S. and Mechtcherine, V. (2010). Simulating fresh concrete behaviour – Establishing a link between the Bingham model and parameters of a DEM-based numerical model. In Brameshuber W., Editor, *International RILEM Conference on Material Science, HetMat Modelling of Heterogeneous Materials*, RILEM Publications SARL, p. 211-219.

[166] Mechtcherine, V. and Shyshko, S. (2007). Simulating the behaviour of fresh concrete using Distinct Element Method. In De Schutter, G. and Boel, V., Editors, Proceedings of the *5th International RILEM Symposium on Self-Compacting Concrete – SCC 2007*, RILEM Publications, Bagneux, Ghent, Belgium, p. 467-472.

[167] Mechtcherine, V. and Shyshko, S. (2009). Self-compacting concrete simulation using Distinct Element Method. In Wallevik, O.H., Kubens, S., and Oesterheld, S., Editors, Proceedings of the *3rd International RILEM Symposium on Rheology of Cement Suspensions such a Fresh Concrete*, RILEM Publications, Bagneux, Reykjavik, Iceland, p. 171-179.

[168] Gram, A. and Silfwerbrand, J. (2011). Numerical simulation of fresh SCC flow: applications. *Materials and Structures*, 44(4), 805-813.

[169] Noor, M.A. and Uomoto, T. (1999). Three-dimensional discrete element simulation of rheology tests of self-compacting concrete. In Skarendahl, Å. And Petersson, Ö., Editors, Proceedings of the *1st International RILEM Symposium on Self-Compacting Concrete*, Stockholm, Sweden, p. 35-46.

[170] Petersson, Ö. and Hakami, H. (2001). Simulation of SCC — laboratory experiments and numerical modeling of slump flow and L-box tests. Proceedings of the *2nd International RILEM Symposium on Self-Compacting Concrete*, Coms Engineering Corporation, Tokyo, Japan, p. 79-88.

[171] Petersson, Ö. (2003). Simulation of self-compacting concrete — laboratory experiments and numerical modeling of testing methods, J-Ring and L-box tests. In Wallevik, O. and Nielsson, I., Editors, Proceedings of the *3rd International Symposium on Self-Compacting Concrete*, Reykjavik, Iceland, p. 202-207.

[172] Cremonesi, M., Ferrara, L., Frangi, A., and Perego, U. (2010). Simulation of the flow of fresh cement suspensions by a Lagrangian Finite Element approach. *Journal of Non-Newtonian Fluid Mechanics*, 165(23-24), 1555-1563.

[173] Liu, G.R. and Liu, M.B. (2003). *Smoothed particle hydrodynamics: A Meshfree Particle Method*, World Scientific Printers CO. Pte. Ltd., Singapore, ISBN 981-238-456-1, 449 p.

[174] Zhu, H., Martys, N.S., Ferraris, C., and De Kee, D. (2010). A numerical study of the flow of Bingham-like fluids in two-dimensional vane and cylinder rheometers using a

smoothed particle hydrodynamics (SPH) based method. *Journal of Non-Newtonian Fluid Mechanics*, 165(7-8), 362-375.

[175] Deeb, R., Kulasegaram, S., and Karihaloo, B.L. (2014). 3D modelling of the flow of self-compacting concrete with or without steel fibres. Part I: slump flow test. *Computational Particle Mechanics*, 1(4), 373-389.

[176] Badry, F., Kulasegaram, S., and Karihaloo, B.L. (2016). Estimation of the yield stress and distribution of large aggregates from slump flow test of self-compacting concrete mixes using smooth particle hydrodynamics simulation, *Journal of Sustainable Cement-Based Materials*, 5(3), 117-134.

[177] Deeb, R., Karihaloo, B.L., and Kulasegaram, S. (2014). Reorientation of short steel fibres during the flow of self-compacting concrete mix and determination of the fibre orientation factor. *Cement and Concrete Research*, 56, 112-120.

[178] Abo Dhaheer, M.S., Kulasegaram, S., and Karihaloo, B.L. (2016). Simulation of self-compacting concrete flow in the J-ring test using smoothed particle hydrodynamics (SPH). Cement and Concrete Research, 89, 27-34.

[179] Deeb, R., Kulasegaram, S., and Karihaloo, B.L. (2014). 3D modelling of the flow of self-compacting concrete with or without steel fibres. Part II: L-box test and the assessment of fibre reorientation during the flow. *Computational Particle Mechanics*, 1(4), 391-408.

[180] Lashkarbolouk, H., Chamani, M.R., Halabian, A.M., and Pishevar, A.R., (2013). Viscosity evaluation of SCC based on flow simulation in the L-box test. *Magazine of Concrete Research*, 65(6), 365-376.

[181] Kulasegaram, S., Karihaloo, B.L., Ghanbari, A. (2011). Modelling the flow of self-compacting concrete. *International Journal for Numerical and Analytical Methods in Geomechanics*, 35(6), 713-723.

[182] Deeb, R. (2013). *Flow of Self-Compacting Concrete*. Ph.D. Thesis, School of Engineering, Cardiff University, Cardiff, UK, 256 p.

[183] Lashkarbolouk, H., Halabian, A.M., and Chamani, M.R. (2014). Simulation of concrete flow in V-funnel test and the proper range of viscosity and yield stress for SCC. *Materials and Structures*, 47(10), 1729-1743.

[184] Kim, J.M., Lee, S.G., and Kim, C. (2008). Numerical simulations of particle migration in suspension flows: Frame-invariant formulation of curvature-induced migration. *Journal of Non-Newtonian Fluid Mechanics*, 150(2-3), 162-176.

[185] D'Avino, G., Tuccillo, T., Maffettone, P.L., Greco, F., and Hulsen, M.A. (2010). Numerical simulations of particle migration in a viscoelastic fluid subjected to shear flow. *Computers & Fluids*, 39(4), 709-721.

[186] Villone, M.M., D'Avino, G., Hulsen, M.A., Greco, F., and Maffettone, P.L. (2011). Numerical simulations of particle migration in a viscoelastic fluid subjected to Poiseuille flow. *Computers & Fluids*, 42(1), 82-91.

[187] Mirbod, P. (2016). Two-dimensional computational fluid dynamical investigation of particle migration in rotating eccentric cylinders using suspension balance model. *International Journal of Multiphase Flow*, 80, 79-88.

[188] Whitham, G.B. (1955). The effects of hydraulic resistance in the dambreak problem. *Proceedings of the Royal Society A*, 227(1170), 399-407.

[189] Hunt, B. (1984). Dam-break solution. *Journal of Hydraulic Engineering*, 110(6), 675-686.

[190] Hunt, B. (1987). An inviscid dam-break solution. *Journal of Hydraulic Research*, 25(3), 313-327.

[191] Debiane, K. and Piau, J-M. (2001). Ecoulement genere par le lacher instantane d'un barrage retenant un fluide viscoplastique. *Les cahiers de rheologie*, 18(1), 45-54.

[192] Chanson, H., Jarny, S., and Coussot, P. (2006). Dam break wave of thixotropic fluid. *Journal of Hydraulic Engineering*, 132(3), 280-293.

[193] Matson, G.P. and Hogg, A.J. (2007). Two-dimensional dam break flows of Herschel–Bulkley fluids: the approach to the arrested state. *Journal of Non-Newtonian Fluid Mechanics*, 142(1-3), 79-94.

[194] Ancey, C. and Cochard, S. (2009). The dam-break problem for Herschel-Bulkley viscoplastic fluids down steep flumes. *Journal of Non-Newtonian Fluid Mechanics*, 158(1-3), 18-35.

[195] Ancey, C., Cochard, S., and Andreini, N. (2009). The dam-break problem for viscous fluids in the high-capillary-number limit. *Journal of Fluid Mechanics*, 624, 1-22.

[196] Hogg, A.J. and Matson, G.P. (2009). Slumps of viscoplastic fluids on slopes. *Journal of Non-Newtonian Fluid Mechanics*, 158(1-3), 101-112.

[197] Kevorkian, J. and Cole, J.D. (1996). *Multiple Scale and Singular Perturbation Methods*. Springer Sciences and Business Media, ISBN-13 9780387942025, 634 p.

[198] *FLOW-3D*, Flow Science Inc, www.flow3d.com.

[199] Uomoto, T. and Ozawa, K. (1999). *Recommendations for Self-Compacting Concrete*, Japan Society of Civil Engineers (JSCE), Tokyo, Japan.

[200] Parsons, J.D., Whipple, K.X., and Simoni, A. (2001). Experimental study of the grain-flow, fluid-mud transition in debris flows. *Journal of Geology*, 109(4), 427-447.

[201] Mei, C.C., Liu, K.F., and Yuhi, M. (2001). Mudflows – slow and fast. In Balmforth, N. and Provenzale, A., Editors, *Geomorphological Fluid Mechanics: Selected Topics in Geological and Geomorphological Fluid Mechanics*, Springer, 548-577.

[202] Alderman, N.J., Meeten, G.H., and Sherwood, J.D. (1991). Vane rheometry of bentonite gels. *Journal of Non-Newton Fluid Mechanics*, 39(3), 291-310.

[203] AASHTO T349-13, *Standard method of test for filling capacity of self-consolidating concrete using the Caisson test*, American Association of State and Highway Transportation Officials, 2013.

[204] Yahia, A., Khayat, K.H., and Sayed, M. (2012), Statistical modelling of the coupled effect of mix design and rebar spacing on restricted flow characteristics of SCC. *Construction and Building Materials*, 37, 699-706.

[205] Vanhove, Y. and Djelal, C. (2013). Friction mechanisms of fresh concrete under pressure. *International Journal of Civil Engineering and Technology (IJCIET)*, 4(6), 67-81.

[206] Feys, D. and Khayat, K.H. (2015). Recent developments in evaluating pumping behaviour of flowable and self-consolidating concretes. *Journal of Sustainable Cement-Based Materials*, 4(3-4), 238-251.

[207] Feys, D., Khayat, K.H., and Khatib, R. (2016). How do concrete rheology, tribology, flow rate and pipe radius influence pumping pressure?. *Cement and Concrete Composites*, 66, 38-46.

[208] Khayat, K.H., Assaad, J., Daczko, J. (2004). Comparison of field-oriented test methods to assess dynamic stability of self-consolidating concrete. *ACI Materials Journal*, 101(2), 168-176.

[209] Nepomuceno, M.C.S., Preira-de-Oliveira, L.A., Lopes, S.M.R., and Franco, R.M.C. (2016). Maximum coarse aggregate's volume fraction in self-compacting concrete for different flow restrictions. *Construction and Building Materials*, 113, 851-856.

[210] Körner, C., Thies, M., Hofmann, T., Thürey, N., and Rüde, U. (2005). Lattice Boltzman model for free surface flow for modeling foaming. *Journal of Statistical Physics*, 121(1),179-196.

[211] Man, H.-K. and van Mier, J.G.M. (2011). Damage distribution and size effect in numerical concrete from lattice analyses. *Cement and Concrete Composites*, 33(9), 867-880.

[212] Eliáš, J. and Stang, H. (2012). Lattice modeling of aggregate interlocking in concrete. *International Journal of Fracture*, 175(1), 1-11.